DIGITALCOMMONS
@WAYNESTATE

Wayne State University

Wayne State University Dissertations

January 2018

Carbohydrate-Based Inducers Of Cellular Stress For Targeting Cancer Cell Metabolism

Fidelis Ndombera
Wayne State University, fndombera@yahoo.com

Follow this and additional works at: https://digitalcommons.wayne.edu/oa_dissertations

Part of the Biochemistry Commons, Cell Biology Commons, and the Chemistry Commons

Recommended Citation

Ndombera, Fidelis, "Carbohydrate-Based Inducers Of Cellular Stress For Targeting Cancer Cell Metabolism" (2018). *Wayne State University Dissertations*. 1951.
https://digitalcommons.wayne.edu/oa_dissertations/1951

This Open Access Dissertation is brought to you for free and open access by DigitalCommons@WayneState. It has been accepted for inclusion in Wayne State University Dissertations by an authorized administrator of DigitalCommons@WayneState.

CARBOHYDRATE-BASED INDUCERS OF CELLULAR STRESS FOR TARGETING CANCER CELL METABOLISM

by

FIDELIS TOLOYI NDOMBERA

DISSERTATION

Submitted to the Graduate School

of Wayne State University,

Detroit, Michigan

in partial fulfillment of the requirements

for the degree of

DOCTOR OF PHILOSOPHY

2018

MAJOR: CHEMISTRY (Biochemistry)

Approved By:

……
Advisor Date

……

……..

…….

© COPYRIGHT BY

FIDELIS TOLOYI NDOMBERA

2018

All Rights Reserved

DEDICATION

This thesis is dedicated to my family; Julia Muthoni; my wife, Einstein Toloyi; my son and Maliya Toloyi; my daughter.

ACKNOWLEDGEMENTS

I acknowledge the support and advise of my advisor; Prof. Young-Hoon Ahn, who made me believe that I could learn any scientific concept and technique if I remained committed to it. His demand for excellence, wise counsel, persistence and focus were strong pillars in maintenance of my motivation. Additionally, am grateful to my principal investigator for providing me with independence of thought in solving research problems and providing numerous opportunity to present my findings in group meetings, seminars and conferences.

I also acknowledge the support of my thesis committee advisor; Prof. John SantaLucia, for his amiable counsel and advice. His valuable contributions throughout my graduate school as a student, teaching assistant and researcher was motivating and insightful. Additionally, I thank Prof. Jennifer Stockdill for the role she played in improving my organic chemistry knowledge as my teacher and mentor throughout graduate school. Finally, I thank Prof. Haidong Gu for her advice and contribution in biological experiments I performed in the final year of graduate school.

I sincerely thank my lab mates, Dr. Kusal Samarsinghe, Dr. Dilini Kekulandara, Danushka Munkanata Godage, Harshani Sewvandi, Adeleye Adewale, Maheeshi Abeywardana, Iftekar and Danushika for collegiality and support. Dr. Dilini Kekulandara validated western blot experiments of AMPK. I also specifically mention Garret Van Hecke who helped me in organic synthesis work with Shima Nagi and Ahmed Ayantayo. I also acknowledge Adam Schlichter, Mohammed Alzamani, Nirmeen Chouaib, Dhruvil Ashishkumar Patel for their participation in the Ahn lab research activities.

I am also thankful to my first-year lab mentor; Holly SantaLucia who helped me navigate the initial challenges of graduate school. I also thank Dr. Sue Dagher, Fang Chao Liu, Chris Smith who were helpful to me in the lab. I also thank the Chair of Chemistry Department, Prof. Mathew

Allen and graduate student services officer; Melissa Rochon for their support. The Wayne State University and the graduate school also deserves mention for funding of my studies. I sincerely also thank the BEST program and NOBCChE for career mentorship in my final years in graduate school.

Finally, I thank my dad; Joseph Ndombera, a veteran who believed that "Victory belongs to the most persevering" and my mom; Prisca Ndombera, who believed that daily prayers to God would protect and guide her son to success. I am grateful to my wife; Julia Muthoni who persistently reminded me that I was in graduate school by choice, since we left well-paying jobs for pursuit of an advanced degree, and so that our children, Einstein and Maliya, would aspire to emulate and out do their father. To my children, I thank them for providing the necessary breaks to replenish my energy and motivation for success!

FOREWORD

Intelligence is like hair, everyone has his/her own! Kenyan proverb.

TABLE OF CONTENTS

DEDICATION ii

ACKNOWLEDGEMENTS iii

FOREWORD v

TABLE OF CONTENTS vi

LIST OF ABBREVIATIONS xiii

LIST OF FIGURES xx

LIST OF SCHEMES xxvi

1.1 Cellular Stress 1

1.1.1 Metabolic Reprogramming in Cancer 1

1.2 Metabolic pathways involved in redox homeostasis 3

1.2.1 Glycolysis 3

1.2.2 Warburg effect 4

1.3 Pentose phosphate pathway (PPP) 5

1.4 TCA Cycle 6

1.5 Hexosamine biosynthetic pathway (HBP) 7

1.6 ER Stress, ROS and Unfolded Protein Response (UPR) 8

1.7 Targeting altered metabolism in cancer using carbohydrate-based small molecules 9

1.8 Sources of ROS in cancer 10

1.8.1 ASK-1-JNK Pathway 12

1.8.2 ASK-1-p38 pathway 13

1.8.3 AMPK-p53 pathway 13

1.9 Redox homeostasis in cancer 14

1.9.1 ROS Modulation as an anticancer strategy 15

1.9.2 2-Deoxy-D-glucose as an anticancer agent 16

1.9.3 Current dissertation work in examining carbohydrate-based inducers of cellular stress for targeting cancer cell metabolism 17

CHAPTER 2 DEVELOPMENT OF CARBOHYDRATE-BASED INDUCERS OF CELLULAR STRESS 19

2.1 Structural design of carbohydrate-based inducers of cellular stress 19

2.2 Approach on synthesis and characterization of carbohydrate-based small molecules 20

2.3 Results 22

2.3.1 Characterization of carbohydrate-based small molecules by LC-MS 22

2.3.1.1 K8A monoisotopic mass analysis by High resolution mass spectrometry 24

2.3.1 Characterization of K8 by NMR 25

2.3.1.1-^{1}H-NMR of K8 25

2.3.1.2 H-^{1}H COSY of K8 26

2.3.1.3 ^{1}H-^{13}C HSQC of K8 27

2.3.1.4 ^{13}C NMR of K8 28

2.3.1.5 ^{13}C HSQC of K8 showing chemical shift of anomeric carbon and proton 29

2.3.1.6 DEPT NMR of K8 30

2.3.2 Characterization of K8A by NMR 31

2.3.2.1 ^{1}H NMR of K8A 31

2.3.2.2 ^{13}C NMR of K8A (101 MHz, Methanol-d_4) 32

2.3.2.3 ^{1}H-^{1}H COSY of K8A 33

2.3.2.4 ^{1}H-^{13}C HSQC of K8A showing anomeric proton chemical shift 34

2.3.2.5 ^{1}H-^{13}C HSQC of K8A showing chemical shift of anomeric carbon and proton 35

2.4 Result and Discussion 36

2.5 Experimental procedures 37

2.5.1 Reagent/Materials 37

2.5.2 Synthesis of carbohydrate-based small molecules 38

2.5.3 Purification method of carbohydrate-based small molecules by semi-preparative HPLC .. 38

2.5.4 Protocol for characterization of carbohydrate-based small molecules by LC-MS 39

2.5.5 Chemical Synthesis of K8A 39

2.5.6 Chemical Synthesis of K8A analogs 40

2.6 Quantification of reactive oxygen species in mammalian cells 41

2.6.1 ROS Quantification using DCF Assay 41

2.6.2 Results 42

2.6.2.1 Optimization of DCF Assays using hydrogen peroxide and diamide 42

2.6.3 Evaluation of carbohydrates for ROS induction in H1299 cells 44

2.6.4 Carbohydrate-based small molecule evaluation for ROS induction in H1299 cells 45

2.6.5 ROS induction with serum starvation 46

2.6.6 Concentration-dependent evaluation of ROS induction by 1-naphthylamine- containing small molecules (8 series compounds) 47

2.6.7 Discussion on ROS evaluation 49

2.6.8 Experimental procedures 50

2.6.8.1 Cell culture 50

2.6.8.2 Protocol for quantification of ROS by DCF Assay 50

2.7 Cytotoxicity evaluation of small molecules in mammalian cells 51

2.7.1 Optimization of viability assay using MTT assay 51

2.7.2 Cytotoxicity screening of carbohydrate-based small molecules 53

2.7.3 Cytotoxicity evaluation of carbohydrates in mammalian cells 54

2.7.4 K8A cytotoxicity evaluation in mammalian cells 56

2.7.4.1 K8A is more potent than 2-DG in various mammalian cell lines 56

2.8 Evaluation of K8A in NCI-60 cell lines 65

2.8.1 Cytotoxicity evaluation of K8A analogues in mammalian cells 67

2.9 Discussion on cytotoxicity evaluation 70

2.10 Experimental procedures 72

2.11 MTT Assay 72

2.12 Trypan blue assay 72

2.13 Sulforhodamine B assay (SRB assay) 73

CHAPTER 3 ROS-INDUCED SIGNALING AND OXIDATIVE STRESS RESPONSE 74

3.1 Introduction 74

3.1.1 Nrf2-ARE pathway 74

3. 2 Results 76

3.2.2 K8A-induced NQO1 induction 76

3.2.3 K8A effect on ASK1-JNK and ASK1-p38 pathways 77

3.2.3 K8A induced AMPK-p53 apoptosis pathway 78

3.2.5 K8A induced ER stress in H1299, LNCaP and MDA-MB 231 cancer cells 79

3.2.6 Click chemistry reveals that K8A interferes with global glycosylation of proteins 80

3.3 Characterization and delineation of K8A glycosylation interference 82

3.3.1 OGT protein expression and purification 83

3.3.2 K8 does not interfere with protein O-GlcNAcylation *in vitro*. 83

3.3.3 OGT peptide synthesis 84

3.3.4 Mass spectrometry-based OGT assay reveal K8 does not interfere with peptide O-GlcNAcylation. 85

3.3.5 K8A induced O-GlcNAcylation in H1299 cells 87

3.4 Discussion 89

3.5 Experimental procedures 93

3.5.1 PEI Max mammalian cell OGT1 transfection 93

3.5.2 Mammalian cell lysis 93

3.5.4 SDS-PAGE 94

3.5.5 Coomassie staining 95

3.5.6 Western blot 95

3.5.7 Monitoring glycosylation by click chemistry 96

3.5.8 Monitoring glycosylation by mass spectrometry 96

3.5.9 OGT Peptide Synthesis 97

3.5.10 OGT isoforms 98

3.5.11 Bacterial cell stock storage 99

3.5.12 Bacterial cell transformation 99

3.5.13 DNA plasmid extraction with Miniprep Kit 100

3.5.14 Polymerase chain reaction (PCR) 100

3.5.15 Restriction digestion 101

3.5.16 Ligation 101

3.5.17 Bacterial protein expression and purification of sOGT 102

CHAPTER 4 METABOLOMIC STUDIES IN K8A-TREATED H1299 CANCER CELLS ... 103

4.1 Introduction 103

4.2 Metabolomics Approach 104

4.3 Results 106

4.3.1 Optimization of metabolite extraction 106

4.3.2 Metabolomics data analysis 107

4.3.3 Glycolytic metabolite levels in K8A-treated H1299 cells 108

4.3.4 Pentose phosphate pathway metabolite levels in K8A-treated H1299 cells 111

4.3.5 Hexosamine biosynthetic pathway metabolite levels in H1299 cells 113

4.3.6 Validation of HBP elevation by Western blot studies 115

4.3.7 Tricarboxylic Acid metabolite levels in H1299 cells treated with K8A 115

4.4 Amino acid levels in H1299 cells treated with K8A 118

4.5 Fatty acid levels in cells treated with K8A 120

4.6 Purine and Pyrimidine synthesis metabolite levels in H1299 cells treated with K8A 121

4.7 Discussion 122

4.8 Experimental procedure 127

4.8.1 Sample preparation and metabolic profiling 127

Conclusion and future directions 127

APPENDIX A: LC-MS Data 130

APPENDIX A (continued): LC-MS Data 131

APPENDIX B: HPLC CHROMATOGRAMS OF A1 & A2 132

APPENDIX C: NMR Data 133

APPENDIX D: OGT Cloning and bacterial expression 152

APPENDIX E: K8A potentially blocks N-glycosylation of proteins 153

APPENDIX F: COPYRIGHT PERMISSIONS: NRF2-ARE PATHWAY 154

APPENDIX G: COPYRIGHT PERMISSIONS: PENTOSE PHOSPHATE PATHWAY 155

APPENDIX H: COPYRIGHT PERMISSIONS: CANCER METABOLISM 156

APPENDIX F: COPYRIGHT PERMISSIONS: REDOX HOMEOSTASIS..... 157

REFERENCES 158

ABSTRACT..... 199

AUTOBIOGRAPHICAL STATEMENT..... 200

LIST OF ABBREVIATIONS

1,3BPG-1,3-Bisphospho glycerate

2-DG-2-deoxy-D-glucose

2PG-2-phospho glycerate

3PG-3-phospho glycerate

ACC-acetyl CoA carboxylase

AIF- apoptosis-inducing factor

AMA-Antimycin A

AMP-Adenine monophosphate

AMP-Adenosine monophosphate

AMPK-AMP-activated kinase

APS-Ammonium persulphate

ARE-Antioxidant response elements

ASK1- Apoptosis signal-regulating kinase 1

ATF6-Activating transcription factor 6

ATP-Adenosine triphosphate

Ac4GlcNAl -NN-(4-pentynoyl)-glucosamine tetraacylated

BSA-Bovine serum albumin

Bak-Bcl-2 antagonist/killer

Bax- bcl-2-like protein 4

Bcl-2-B-cell lymphoma 2

CHOP-CCAAT/enhancer-binding protein (C/EBP)-homologous protein

COSY-Homonuclear correlation spectroscopy

DCF-Dichloro flourescein

DCFH-DA-2,7-dichlorodihidroflourescein diacetate

DCM-Dichloromethane

DEPT-Distortionless enhancement by polarization transfer

DHAP-Dihydroxyacetone phosphate

DMEM-Dulbecco's Modified Eagle's Medium

DMF-Dimethyl formamide

DMSO-Dimethyl sulfoxide

DNA-Deoxyribonucleic acid

DTT-Dithiothreitol

E4P-erythrose-4-phosphate

EDTA-Ethylene diamine tetra acetic acid

ER-Endoplasmic reticulum

EROα1- Endoplasmic reticulum oxireductin 1

ESI-Electrospray ionization

ETC-Electron transport chain

F-2,6-BP-fructose-2,6-bisphosphate

F6P-Fructose-6-phosphate

FADH2-Flavin adenine dinucleotide

FBP-Fructose-1,6-bisphosphate

FBS-Fetal bovine serum

G3P-Glyceraldehyde-3-phosphate

G6P-Glucose-6-phosphate

G6PD-Glucose-6-phosphate dehydrogenase

GAPDH-Glyceraldehyde 3-phosphate dehydrogenase

GCL-γ-glutamyl-cysteine-ligase

GDP-Guanine diphosphate

GFAT1- Glutamine: fructose-6-phosphate aminotransferase 1

GLS2- glutaminase 2

GLUT-1-Glucose transporter 1

GMP-Guanine monophosphate

GPX3-Glutathione peroxidase 3

GR-Glutathione reductase

GRP78-Glucose regulated protein 78

GS-Glutathione synthetase

GSH-Glutathione

GSSG-Oxidized glutathione

GST-Glutathione synthetase

GalNAI- N-(4-pentynoyl)-galactosamine tetraacylated (Ac4GalNAl)

HBP-Hexosamine biosynthetic pathway

HBTU- 2-(1H-benzotriazol-1-yl)-1,1,3,3-tetramethyluronium hexafluorophosphate

HEK 293-Human embryonic kidney 293 cells

HIF-1-Hypoxia inducible factor

HILIC-Hydrophilic liquid chromatography

HKII-Hexokinase II

HPLC-High performance liquid chromatography

HSF1-Heat shock factor 1

HSP-90-Heat shock protein 90

HSQC-Heteronuclear single quantum coherence

IAM-Iodoacetamide

IDH1-Isocitrate dehydrogenase 1

IMP-Inosine monophosphate

IPTG-Isopropyl-1-thio-β-D-galactopyranoside

IRE1- inositol-requiring enzyme 1

JNK- c-Jun N-terminal kinases

KRAS- Kirsten rat sarcoma virus

Keap-1-Kelch-like ECH-associated protein 1

LB-Luria Broth

LC-MS-Liquid chromatography-mass spectrometry

LC-QTOF-Liquid Chromatography Quadrupole time-of-flight mass spectrometry

MCF7-Michigan cancer foundation-7 breast cancer cell line

MCT1-Monocarboxylate transporter 1

ME1-Malic enzyme 1

MRM-Multiple reaction monitoring

MTT- (3-(4,5-Dimethylthiazol-2-yl)-2,5-Diphenyltetrazolium Bromide.

NADH-Nicotinamide adenine dinucleotide hydrate

NADPH-Nicotinamide adenine dinucleotide phosphate hydrate

NMR-Nuclear Magnetic Resonance

NMR-Nuclear magnetic resonance

NOS-Nitric oxide synthase

NOX-NADPH Oxidase

NQO1- NAD(P)H: quinone oxidoreductase1

Nrf2- nuclear factor erythroid 2 (NFE2)-related factor 2

OAA-oxaloacetate

OGT-O-GlcNAc Transferase

OXPHOS-oxidative phosphorylation

PBS-Phosphate buffered saline

PCR-Polymerase chain reaction

PDI-Protein Disulfide isomerase

PDK2- pyruvate dehydrogenase kinase 2

PEI-Max-Polyethylenimine

PEP-Phospho enol pyruvate

PERK-protein kinase RNA-like ER kinase

PET- positron emission tomography

PFK1-Phosphofructokinase 1

PGAM-phosphoglycerate mutase

PGI-Phosphoglucose isomerase

PKM2-Pyruvate kinase isoform 2

POX-proline oxidase

PPP-Pentose phosphate pathway

R-5-P/R5P-Ribose-5-phosphate

RAC- Rho family of GTPases

RFU-Relative fluorescence unit

RIPA-Radioimmunoprecipitation assay buffer

RNS-Reactive nitrogen species

ROS-Reactive oxygen species

RPMI- Roswell Park Memorial Institute medium

RSDs-Relative standard deviations

S7P-Sedoheptulose-7-phosphate

SCO2-synthesis of cytochrome c oxidase assembly 2

SDS-PAGE-Sodium dodecyl sulfate polyacrylamide gel electrophoresis

SMAD4- Mothers against decapentaplegic homolog 4

SOD-Superoxide dismutase

SREBP-1- Sterol regulatory element-binding transcription factor 1

TALDO- transaldolase

TBS-Tris-buffered saline

TBTA- Tris[(1-benzyl-1H-1,2,3-triazol-4-yl) methyl] amine

TCA-Tricarboxylic acid

TCEP-Tris(2-carboxyethyl) phosphine

TEMED- N, N, N’, N’-tetramethylenediamine

THPTA-Tris(3-hydroxypropyltriazolyimethyl) amine

TIGAR- TP53 Induced Glycolysis Regulatory Phosphatase

TKT-transketolase

TRX-Thioredoxin

UDP-GlcNAc-UDP-N-acetylglucosamine

UDP-N-acetylglucosamine (UDP-GlcNAc)

UDP-glucuronosyltransferases (UGT)

UPR-Unfolded protein response

UTP-Uridine triphosphate

XBP1-X-box binding protein 1

XO-Xanthine oxidase

Xu5P/X-5-P -Xylulose-5-phosphate

p38-mitogen activated protein-38

LIST OF FIGURES

Figure 1-Metabolism of glucose for redox homeostasis, cellular energetics and protein glycosylation 2

Figure 2-The pentose phosphate pathway. Figure adapted with permission from Patra, K. C.; Hay, N., The pentose phosphate pathway and cancer. Trends in biochemical sciences **2014**, 39 (8), 347-354..... 5

Figure 3-NADPH & NADH generating pathways in a cancer cell. Adapted from DeBerardinis, R. J.; Chandel, N. S., Fundamentals of cancer metabolism. Science Advances **2016,** 2 (5). 7

Figure 4-Major sources and types of ROS in the ER of mammalian cells. Adapted with permission from Zeeshan, H.; Lee, G.; Kim, H.-R.; Chae, H.-J., Endoplasmic Reticulum Stress and Associated ROS. International journal of molecular sciences **2016,** 17 (3), 327. 8

Figure 5- ROS-ER stress signaling pathways 10

Figure 6-Major **s**ources and types of ROS from a mammalian cell (Adapted with permission from Wang, K.; Zhang, T.; Dong, Q.; Nice, E. C.; Huang, C.; Wei, Y., Redox homeostasis: the linchpin in stem cell self-renewal and differentiation. Cell Death &Amp; Disease **2013,** 4, e537.) 11

Figure 7-Major **s**ources and types of ROS in the mitochondrion in a mammalian cell[110]. Adapted with permission from Li, X.; Fang, P.; Mai, J.; Choi, E. T.; Wang, H.; Yang, X.-f., Targeting mitochondrial reactive oxygen species as novel therapy for inflammatory diseases and cancers. Journal of Hematology & Oncology **2013,** 6 (1), 19. 12

Figure 8- ROS signaling pathways that may lead to apoptosis. 12

Figure 9-Redox homeostasis is a balance between ROS and antioxidants..... 15

Figure 10-Therapeutic window for design and development of ROS-inducing anticancer drugs 16

Figure 11- Carbohydrate-based small molecule scaffold (R^1 & R^2 as in scheme 1). 20

Figure 12- HPLC spectrum of K8 at a detection wavelength of 214nm 22

Figure 13-LC spectrum of K8 at a detection wavelength of 254nm..... 22

Figure 14- MS spectrum of K8 23

Figure 15-LC spectrum of K8A at 254nm 23

Figure 16- MS spectrum of K8A 23

Figure 17-Monoisotopic mass analysis for K8A. 24

Figure 18 ^{1}H-NMR of K8..... 25

Figure 19- ^{1}H-^{1}H COSY of K8 26

Figure 20-^{1}H-^{13}C HSQC of K8 27

Figure 21- ^{13}C NMR of K8 28

Figure 22-^{13}C HSQC of K8..... 29

Figure 23-DEPT NMR of K8 30

Figure 24-^{1}H NMR of K8A 31

Figure 25- ^{13}C NMR of K8A..... 32

Figure 26- ^{1}H-^{1}H COSY of K8A..... 33

Figure 27- ^{1}H-^{13}C HSQC of K8A 34

Figure 28- ^{1}H-^{13}C HSQC of K8A showing anomeric carbon and proton..... 35

Figure 29- DCF Assay work flow..... 42

Figure 30-ROS levels generated in H1299 cells treated separately with hydrogen peroxide and diamide..... 43

Figure 31-Comparison of ROS levels generated by various ROS inducers. 44

Figure 32-ROS levels generated by D-glucose and D-galactose in H1299 cells. 44

Figure 33-ROS levels generated by L-arabinose and D-mannose in H1299 cells. 45

Figure 34-ROS induction screening of carbohydrate-based small molecules in H1299 cells..... 45

Figure 35-ROS levels generated by H8 and K8 with and without serum starvation..... 46

Figure 36-ROS levels generated by D-arabinose (H), D-xylose (K), A8 and G8. 47

Figure 37-ROS levels generated by C8, L8, H8 and K8 in H1299 cells. 48

Figure 38-ROS levels generated by K8A and 2-DG in H1299 cells. 48

Figure 39-Diamide and hydrogen peroxide cytotoxicity in A549 and H1299 cells. 52

Figure 40-Sulforaphane cytotoxicity in H1299 cells overexpressing KRAS. 53

Figure 41-Carbohydrate-based small molecule cytotoxicity screening in H1299 cells 53

Figure 42-K8 and H8 cytotoxicity in H1299 cells 54

Figure 43-D-xylose, D-arabinose, D-galactose, D-mannose, D-fructose and 2-deoxy-D-glucose cytotoxicity in H1299 cells. 55

Figure 44-K8A cytotoxicity in A549, LNCaP, MDA-MB 231 and MDA-MB 231 cells 57

Figure 45-KA, K8A, 2DGA and 2DG8A cytotoxicity in H1299 cells 59

Figure 46-KA, K8A, 2DGA and 2DG8A cytotoxicity in MDA-MB 231 cells 60

Figure 47-KA, K8A, 2DGA and 2DG8A cytotoxicity in LNCaP cells 61

Figure 48-KA, K8A, 2DGA and 2DG8A cytotoxicity in DU145 cells 62

Figure 49-K, KA, K8 and K8A cytotoxicity in Hela cells 63

Figure 50-K, KA, K8 and K8A cytotoxicity in A549 cells 64

Figure 51-K8A and 2DG8A cytotoxicity in MCF7 cells 64

Figure 52-K8A cytotoxicity in Raji and Daudi cells 65

Figure 53-K8A cytotoxicity in NCI-60 cancer cell lines 66

Figure 54-A9A, C9A, G9A and L9A cytotoxicity in H1299 cells 68

Figure 55-C8A and L8A cytotoxicity in H1299 cells 68

Figure 56-A9A, G9A, K9A and C8A cytotoxicity in Hela cells 69

Figure 57-K9A, K10A, K11A and K12A cytotoxicity in H1299 cells 70

Figure 58-Nrf2-ARE response pathway in stimulated and unstimulated conditions 75

Figure 59-K8A effect on Nrf2-ARE pathway in H1299 and LNCaP cells 76

Figure 60-K8A and 2-DG effect on Nrf2-ARE pathway in H1299 cells 77

Figure 61-K8A and 2-DG effect on ASK1-JNK pathway in H1299 cells transfected with ASK1 77

Figure 62-K8A and 2-DG effect on JNK expression in H1299 cells 78

Figure 63-K8A effect on p38 expression in H1299 and LNCaP cells..... 78

Figure 64-K8A and 2-DG effect on AMPK-p53 pathway in HEK 293 and H1299 cells 79

Figure 65-K8A and 2-DG effect on ER-stress induced grp78 in H1299, LNCaP and MDA-MB 231 cells. 80

Figure 66-Concentration-dependent K8A-induced disruption of global protein glycosylation in H1299 cells monitored with GlcNAI vs GalNAI. 81

Figure 67-Comparison of 2-DG, 2DGA and K8A-induced disruption of global protein glycosylation in H1299 cells monitored with GlcNAI. 82

Figure 68-SDS-PAGE for purified His-tagged Hsp-90. 83

Figure 69-sOGT-catalyzed *in vitro* Hsp-90 O-GlcNAcylation. 83

Figure 70-K8 effect of Hsp-90 O-GlcNAcylation 84

Figure 71-Mass spectrum of OGT peptide. 85

Figure 72-Work flow for mass-spectrometry based glycosylation assay 86

Figure 73-Monitoring peptide glycosylation by mass spectrometry in various conditions(a-d). . 87

Figure 74-K8A and 2-DG induced O-GlcNAcylation in H1299 cells. 88

Figure 75- K8A induced O-GlcNAcylation in H1299 cells transfected with full-length Flag-tagged OGT. 88

Figure 76-AMPK-p53 pathway 90

Figure 77-O-GlcNAcylation in glycolysis, PPP, TCA pathways[274] (Adopted with permission from reference 207)..... 92

Figure 78-Workflow for OGT transfection in H1299 cells 93

Figure 79-Overall structure of human OGT complexed to UDP (a), Schematic of OGT domain architecture with the TPR units shown in gray, the transitional helix (H3) in purple, the N-Cat domain in blue, the Int-D domain in green, and the C-Cat domain in red. The native isoforms of OGT (sOGT, mOGT, and ncOGT) and the crystallization construct differ only in the number of TPRs, as shown. (b), Overall fold of OGT from the OGT-UDP complex in a ribbon representation. The coloring is the same as the schematic in a. The UDP is shown in cyan. The N-Cat domain helices unique to OGT are indicated as H1 and H2.[275] Adapted with permission

from Lazarus, M. B.; Nam, Y.; Jiang, J.; Sliz, P.; Walker, S., Structure of human O-GlcNAc transferase and its complex with a peptide substrate. *Nature* **2011,** *469*, 564. 99

Figure 80-Metabolomics work flow. 105

Figure 81-Mass spectrum for C^{12}-C^{13}-glucose from cell extract showing M/Z^{Na+} =203, 209 peaks 106

Figure 82-Optimization of collision energies for LC/MSMS molecular transition of C-13 glucose. 107

Figure 83-Protein levels of metabolite extracts from H1299 cells 107

Figure 84-Glycolytic metabolite levels in K8A-treated H1299 cells 110

Figure 85-Glycerol-3-phosphate levels in K8A-treated H1299 cells 110

Figure 86-Dihydroxy-acetone phosphate levels in K8A-treated H1299 cells 111

Figure 87-Phosphoenol pyruvate levels in K8A-treated H1299 cells; unsure of what is the statistical analysis in these data..... 111

Figure 88- Pentose Phosphate pathway metabolite levels in K8A-treated H1299 cells..... 112

Figure 89-NADPH/NADP ratio in K8A-treated H1299 cells 113

Figure 90-Hexosamine biosynthetic pathway metabolites in K8A-treated H1299 cells..... 114

Figure 91-UTP, UDP and N-acetyl-glucosamine-1-phosphate levels in H1299 cells..... 114

Figure 92-UDP-glucose and UDP-D-glucuronate levels in K8A-treated H1299 cells 115

Figure 93-TCA metabolite levels in K8A-treated H1299 cells 116

Figure 94-NAD^+/NADH levels in K8A-treated cells 116

Figure 95-ADP and AMP levels in K8A-treated H1299 cells..... 117

Figure 96-UTP, UDP, UMP, GDP and GMP levels in K8A-treated H1299 cells. 118

Figure 97-Amino acid levels in K8A-treated H1299 cells 119

Figure 98-Aspartate levels in K8A-treated H1299 cells..... 120

Figure 99-Arginine and citrulline levels in K8A-treated H1299 cells..... 120

Figure 100-Oleic acid, palmitic acid and stearic acid levels in K8A-treated cells 121

Figure 101-Inosine and IMP levels in H1299 cells 122

Figure 102-Hypoxanthine and xanthine levels in H1299 cells 122

Figure 103-TCA cycle shift under oxidative stress conditions 125

Figure 104-K8A mechanism of action model 129

LIST OF SCHEMES

Scheme 1: Chemical synthesis of carbohydrate-based small molecules……....21

Scheme 2: Chemical synthesis of K8…….38

Scheme 3: Chemical synthesis of K8A analogs with aniline derivative variation…….40

Scheme 4: Chemical synthesis of K8A analogs with sugar derivative variations……...40

LIST OF TABLES

Table 1**:** Cytotoxicity of various carbohydrate-based small molecules in various cancer cell lines 60

Table 2**:** Cytotoxicity of various K8A analogues in cancer cell 67

Table 3**:** SDS-PAGE separating layer recipe 97

Table 4**:** SDS-PAGE stacking layer recipe 97

Table 5**:** Mass of protected amino acids used for 9-mer OGT-peptide synthesis 98

Table 6: PCR cycles program for OGT gene amplification 101

CHAPTER 1 INTRODUCTION

1.1 Cellular Stress

Cancer cells are susceptible to physiologic stresses such as oxidative stress[1-2], nutrient stress, endoplasmic reticulum (ER) stress[3], and proteotoxic stress[4-9] because of their high metabolic rates. In general, cells can modify their genetic, metabolic, transcriptional and translational landscape in response to these stresses. Additionally, posttranslational and signaling pathways modulate metabolic flux to promote survival, a phenomenon called "cellular stress response". Cancer cells adopt diverse mechanisms to cope with these stresses to survive and enhance proliferation[10]. Cancer cells invoke mechanisms such as Warburg effect, oxidative stress response and the unfolded protein response (UPR), to mitigate against impending cell death[11-12,13-15]. The example includes the use of oncogenes in alteration of metabolism that provides cancer cells with unique stress response mechanisms and growth advantage over non-transformed cells[16]. Uncontrolled increase in cellular stress in cancer cells, beyond protective thresholds, leads to metabolic stress and induction of cell death mechanisms[17]. These death mechanisms include apoptosis, necrosis, and autophagy[17-19]. Importantly, use of small molecules that disrupt the altered metabolism to augment stress have therapeutic potential[20]. Arguably, small molecules that modulate reactive oxygen species (ROS) have potential to disrupt metabolic reprogramming in cancer[20-27].

1.1.1 Metabolic Reprogramming in Cancer

Metabolic reprogramming is a hallmark of cancer that provides cancer cells with a growth advantage over non-transformed cells[28]. In metabolic reprogramming, glucose modulates redox homeostasis control, cellular energetics and protein glycosylation[28]. Cancer cells are therefore programmed by oncogenes to increase glucose uptake. Additionally, the increased glycolytic metabolites, are directed to the pentose phosphate pathway (PPP) and hexosamine biosynthetic

pathway (HBP) (Figure 1.1), to produce NADPH and UDP-N-acetylglucosamine (UDP-GlcNAc) and other metabolites that promote cell proliferation[29]. NADPH and UDP-GlcNAc produced by the above pathways is essential for protection against reactive oxygen species (ROS)[30-31]. Importantly, this metabolic reprogramming is essential for maintenance of redox homeostasis, of which disruption can lead to cancer cell death.

Glucose flux into glycolysis, PPP and HBP thrive in cancer cells, partly due to mutations of tumor suppressors such as p53, which regulate levels of glucose transporters, glycolytic and HBP enzymes[16, 32]. In recent years, therapeutic strategies are shifting from targeting these oncogenes towards the glucosome[33] and modulation of nutrients to disrupt altered metabolism in cancer[32, 34-36]. For example, glycolytic inhibition with 2-deoxy-D-glucose[37-39] and blocking glycosylation of G6PD using small molecules reduced PPP flux and NADPH levels, increased ROS, disrupted metabolism and diminished cancer cell proliferation[40]. Additionally, recent connection between oncogenes and altered metabolism has stimulated work on various cancer cell metabolism targets that include glycolysis, PPP, TCA cycle and HBP (Figures 1 & 2)[41].

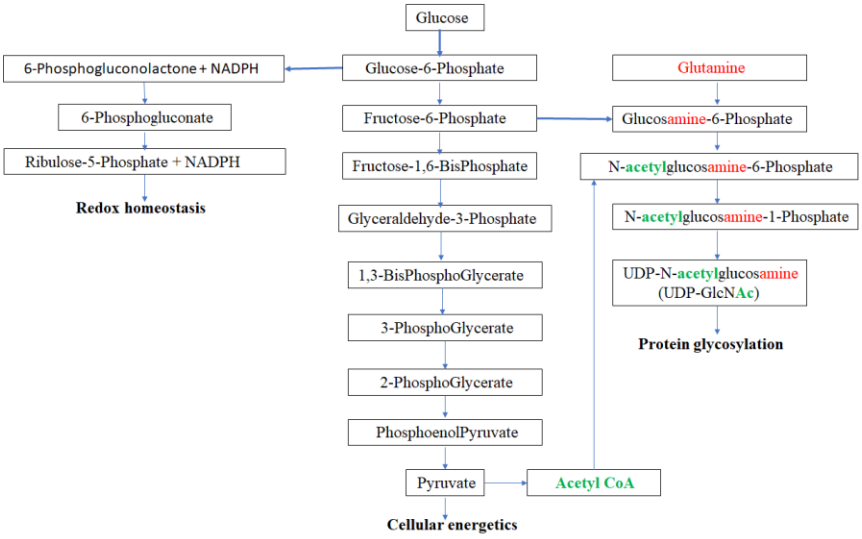

Figure 1-Metabolism of glucose for redox homeostasis, cellular energetics and protein glycosylation

1.2 Metabolic pathways involved in redox homeostasis

1.2.1 Glycolysis

A common feature of cancer cells is upregulation of aerobic glycolysis due to increased glucose consumption; a phenotype observed by positron emission tomography (PET)[42-43]. Cancer cells prefer aerobic glycolysis over mitochondrial oxidation because glucose turnover is increased resulting in greater ATP production. Aerobic glycolysis generates ATP at a higher rate but in lower ATP yields than oxidative phosphorylation[44]. ATP formed through glycolysis is sufficient for cancer growth.

Additionally, glycolytic enzymes that include HKII, PFKI, GAPDH and PKM2 are involved in redox homeostasis[45-48]. GAPDH catalyzes the first glycolytic step that generates NADH required in oxidative phosphorylation. Importantly, GAPDH can reverse flux under oxidative stress via the catalytic cysteine residue that when oxidized lowers GAPDH enzyme activity[49-50]. In this way, glycolytic flux is reversed towards the PPP with prolonged ROS exposure leading to GAPDH-induced apoptosis. In a similar way, other glycolytic enzymes such as HKII, PFK1 and PKM2 redirect metabolites towards PPP under oxidative stress conditions[50]. Indeed, inhibiting HKII[51] and other glycolytic enzymes causes cancer cell death. Notably, non-metabolic roles of Nrf2-HKII are emerging as coactivators of xanthine oxidoreductase (XOR), that place HKII in direct ROS modulatory function in cancer cells[52]. The change of flux by the glycolytic enzymes and cancer cell reliance on the Warburg effect is a defense mechanism that promotes tumorigenesis and malignancy progression. Conversely, targeting these cytoprotective enzymes has therapeutic potential.

1.2.2 Warburg effect

Otto Warburg reported that tumor cells consume glucose at high rates compared to normal cells with production of lactate, a phenomenon known as the ‘‘Warburg effect’’[53]. In Warburg effect, lactate is extruded by monocarboxylate transporters to the cancer cell environment[54]. On the other hand, normal cells metabolize glucose into pyruvate that is contained within cells, partly because of suppression of monocarboxylate transporter 1 (MCT1) by p53[54]. Inhibiting MCT1 is therefore beneficial to normal cells[55] because pyruvate is metabolized to acetyl CoA. Acetyl CoA enters the Krebs cycle that generate antioxidant intermediates such as citrate, malate, NADH and $FADH_2$. This enhances antioxidant capacities of normal cells, while cancer cells exhibiting Warburg effect may be deprived of this protection, and will be more susceptible to oxidative stress.[56] To explain this observation, Warburg proposed that tumor cells have a permanent loss of oxidative metabolism leading to a compensatory increase in glycolytic flux. However, various studies have shown that although mitochondrial dysfunction in cancer cells can disrupt energy metabolism, many tumor cells demonstrate normal mitochondrial function with oxidative phosphorylation[57-58].

Later, it was demonstrated that the high glycolytic rate provides a growth advantage for rapidly proliferating cancer cells. Warburg effect allows cells to use glucose to produce ATP at higher rates than through oxidative phosphorylation, even though the yield of ATP per glucose consumed is low[58]. Additionally, glucose provides cells with intermediates needed for biosynthetic pathways, including ribose for nucleotides; citrate for lipids and, NADPH for ROS detoxification[59-60]. Furthermore, Warburg effect regenerates NAD+ during conversion of pyruvate to lactate[61]. Of note, glycolytic intermediates, G6P and F6P, are the key regulatory branch points in glycolysis that apportion metabolites into the PPP and HBP.

1.3 Pentose phosphate pathway (PPP)

The Warburg effect is directly involved in regulation of redox homeostasis by controlling glucose flux into the PPP. The PPP is involved in synthesis of NADPH that maintains cellular antioxidants such as glutathione (GSH) in its reduced state[62-63](Figure 1.1.1). In normal cells, PPP is regulated partly by nutrient uptake and energy needs of the cell.

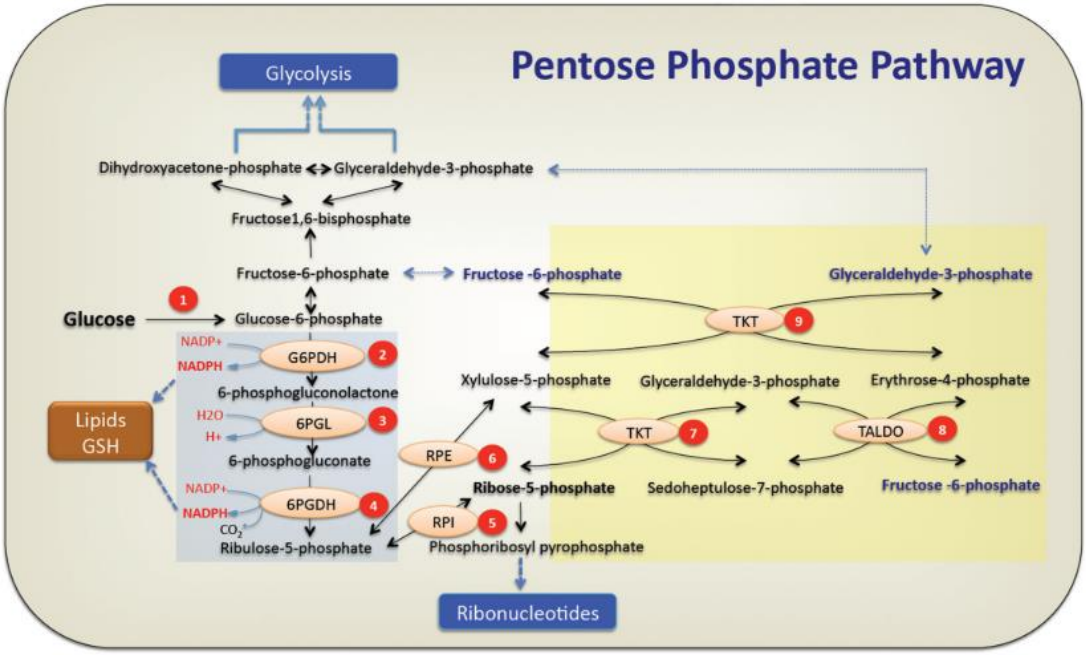

Figure 2-The pentose phosphate pathway. Figure adapted with permission from Patra, K. C.; Hay, N., The pentose phosphate pathway and cancer. Trends in biochemical sciences **2014**, 39 (8), 347-354.

However, in cancer cells, PPP is controlled by oncogenes that alter nutrient uptake accompanied by change of flux to redirect metabolites to biomass synthetic pathways[64]. G6PDH catalyzes the critical rate limiting step of the PPP by converting G6P to 6-phosphoglucono-δ-lactone and NADPH[65] (Figure 1.1.1). High G6PDH activity results in an increase in DNA and fatty acid biosynthesis, necessary for cell proliferation. 6-Phosphogluconate is subsequently converted to ribulose-5-phosphate (Ru5P), carbon dioxide and NADPH by 6-phosphogluconate dehydrogenase

(6PGDH)[63-64]. 6PGDH, like G6PDH, controls redox homeostasis by increasing the production of NADPH. Additionally, genetic changes of signaling pathways affect the PPP directly and indirectly[63].

Reversible enzymes in PPP, transketolase (TKT) and transaldolase (TALDO), mediate the nonoxidative PPP[66]. During oxidative stress, TKT converts ribose-5-phosphate (R5P) and xylulose-5-phosphate (Xu5P) to produce G3P and S7P[67]. Another TKT reaction occurs between Xu5P and E4P to generate F6P and G3P. On the other hand, TALDO truncates and transfers a three-carbon unit from S7P to G3P to form E4P and F6P[67]. F6P is then converted back to G6P to generate more NADPH. G3P re-enters glycolysis and eventually the TCA cycle. Overall, cancer cells predominantly employ the nonoxidative PPP to generate ribonucleotides required cancer cell division and growth[68].

1.4 TCA Cycle

In most cancer cells, the TCA cycle provides intermediates in the synthesis of lipids, proteins and nucleic acids, with reduced production of oxidizable intermediates required for ATP synthesis[69]. Importantly, the TCA cycle intricately maintains NADH and NADPH levels from multiple sources that are required for cellular energetics, redox homeostasis and anabolism (Figure 1.1.2). For example, to synthesize lipids, cancer cells transfer mitochondrial citrate out to the cytosol to be converted to oxaloacetate (OAA) and the lipogenic precursor acetyl-CoA[69-71]. Additionally, p53 inhibition of PDK2 expression results in increased conversion of pyruvate to mitochondrial acetyl-CoA[72]. To regulate mitochondrial metabolism, p53 enhances the expression of SCO2 and AIF, two factors that control assembly of complexes of the electron transport chain (ETC)[72]. p53 also downregulates PDK2 and upregulates GLS(2) to facilitate entry of metabolites such as glutamine into the TCA cycle[73]. Additionally, TCA cycle intermediates such as citrate can

be exported into the cytosol from the mitochondrion, where ME or IDH1 use them to generate reducing power in the form of NADPH[74-75]. On the other hand, IDH1 generate NADPH in the mitochondrion. Equally important in redox homeostasis is the concerted roles of SHMT1/2 and MTHFD1/2 in maintaining NADPH in the mitochondrion and cytosol (Figure 3).

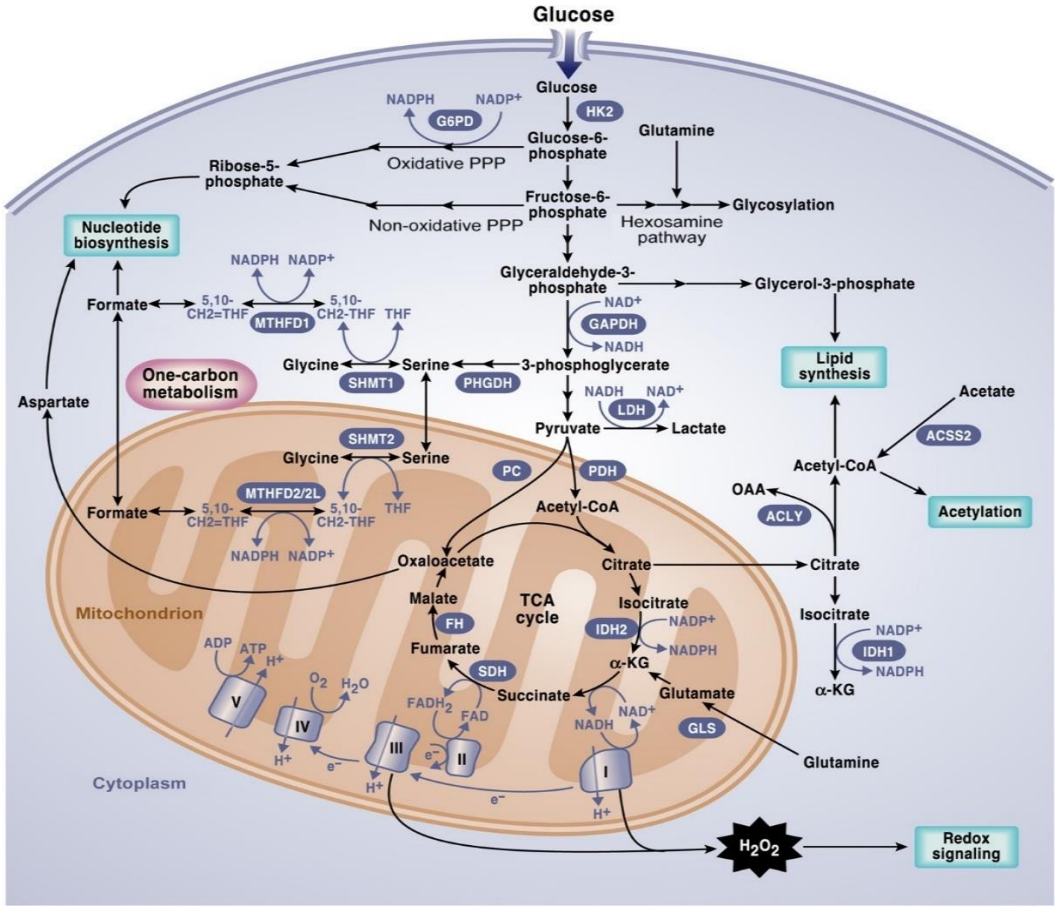

Figure 3-NADPH & NADH generating pathways in a cancer cell. Adapted from DeBerardinis, R. J.; Chandel, N. S., Fundamentals of cancer metabolism. Science Advances **2016,** 2 (5).

1.5 Hexosamine biosynthetic pathway (HBP)

High glucose uptake in cancer cells increase flux via the HBP to induce *O*-GlcNAcylation and modulate redox homeostasis and cellular energetics[76]. Metabolic and glycolytic enzymes such as PFK1[77] and PKM2[78-79] undergo *O*-GlcNAcylation to promote change of flux into the PPP[80] during oxidative stress. *O*-GlcNAc modification of proteins is dependent on the concentration of UDP-

GlcNAc, which is a donor substrate of *O*-GlcNAc transferase (OGT). UDP-GlcNAc synthesis require glutamine, acetyl-coenzyme A, uridine, and ATP, making it a biomarker of cellular energetics[31, 76]. UDP-GlcNAc is used in modification of various proteins by *O*-GlcNAc and for biosynthesis of extracellular N- and O-glycans. Importantly, HBP and *O*-GlcNAc modification allow cells to link cellular metabolism to the regulation of cellular processes, such as oxidative stress response[31].

1.6 ER Stress, ROS and Unfolded Protein Response (UPR)

Disruption of the equilibrium between protein synthesis and protein folding capacity observed in cells causes oxidative and ER stress[15]. Additionally, protein folding by disulfide bond formation using protein disulfide isomerase (PDI) lead to ROS generation[81] (Figure 4).

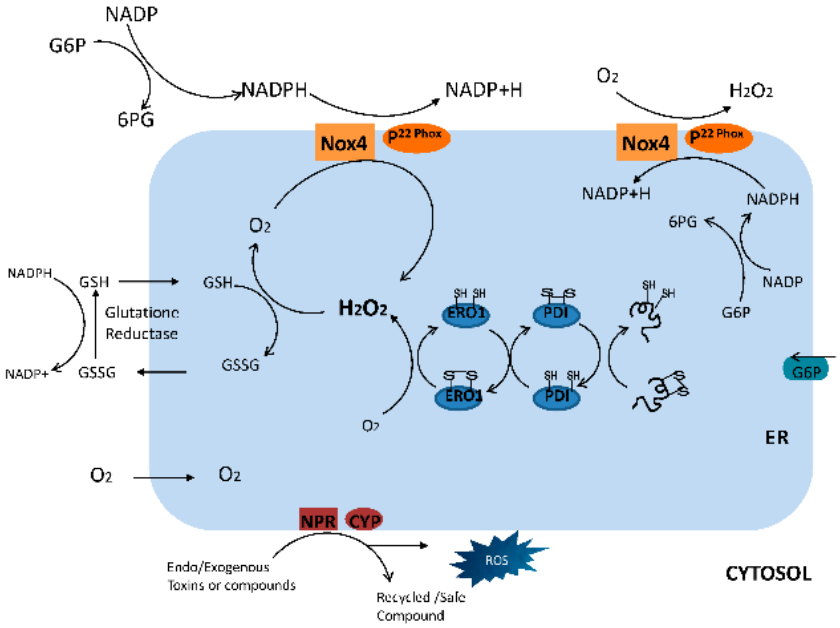

Figure 4-Major sources and types of ROS in the ER of mammalian cells. Adapted with permission from Zeeshan, H.; Lee, G.; Kim, H.-R.; Chae, H.-J., Endoplasmic Reticulum Stress and Associated ROS. International journal of molecular sciences **2016,** 17 (3), 327.

PDI is maintained in its reduced form by EROα1 which require oxygen[82-83]. This latter reaction produces hydrogen peroxide in the ER[83]. Overall, electron transfer from PDI to molecular oxygen and EROα1 uses a FAD-dependent reaction. Additionally, under stressed conditions, Nox4

expression is increased and generate ROS[84]. Nox4 associated with p22phox uses NADH or NADPH for oxygen reduction to produce a superoxide anion. Other sources of ROS in the ER include NADPH-p450 reductase (NPR) and the microsomal monooxygenase system (MOO)[81].

The capacity of the ER to respond to protein misfolding, changes in ROS and nutrient status makes it an effective early sensor of cellular stress. The ER can sense dramatic drops in cellular glucose levels using ER-resident GRP78 protein[85-87]. The UPR signals cellular stress through three distinct stress sensors located at the ER membrane, that include PERK, IRE1 and ATF6[87-88]. Subsequently, to restore favorable folding of proteins, IRE1 is phosphorylated to induce ER stress response chaperones such as GRP78[88]. GRP78 dissociates from IRE1 to assist in protein folding and forestall cell death. However, prolonged GRP78 activation triggers apoptosis[89].

IRE1 can also recruit ASK1 that activates JNK (Figure 5) and p38 pathways[90-91]. Phosphorylated JNK translocate to nuclei to phosphorylate and transactivate c-Jun that is involved in transcription of proapoptotic genes[91]. Additionally, IRE1-mediated activation of JNK contributes to cell death by phosphorylating and inactivating the anti-apoptotic regulator Bcl-2[92]. Concertedly, the transcription factor CCAAT/enhancer-binding protein (C/EBP)-homologous protein (CHOP) down-regulates Bcl-2 expression[93]. Furthermore, in oxidative stress conditions, PERK phosphorylates Nrf2 that induce ROS detoxifying enzymes[94]. Lately, ROS and ER stress have been linked to protein glycosylation[95-96] (Figure 5). Thus, the ER as a sensor of cellular stress is critical for maintaining cellular redox homeostasis.

1.7 Targeting altered metabolism in cancer using carbohydrate-based small molecules

Broad utilization and differential rate of monosaccharide uptake in cancer cells compared to normal cells has been used in positron emission tomography (PET) and in cancer therapeutics. In PET, 2-[18F]-2-Deoxy-D-glucose (FDG) is used in imaging and locating tumor metastases.

Concomitantly, 2-deoxy-D-glucose is used as an anticancer agent[97-99]. Broad specificity and high monosaccharide uptake by glucose transporter 1 (GLUT-1) is used in targeting cancer cell metabolism[59]. Indeed, substitution at various positions on the glucose moiety is well tolerated by GLUT-1[100]. Anticancer drugs such as 2-deoxy-D-glucose exploit GLUT-1 substrate promiscuity to target cancer cells which have enhanced glucose uptake to fuel their metabolism. High 2-deoxy-D-glucose uptake induce ROS production. Furthermore, there is an emerging interest in the roles of glucose-deprivation[101], 2-deoxy-D-glucose and glycoconjugate anticancer agents, in ROS elevation, ROS-apoptosis signaling and cancer cell metabolism[100].

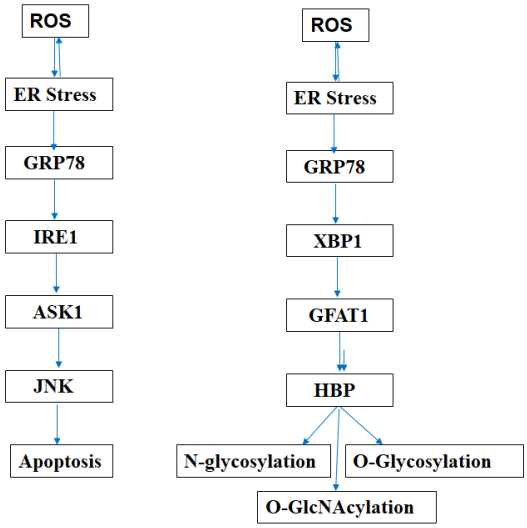

Figure 5- ROS-ER stress signaling pathways

1.8 Sources of ROS in cancer

Cells maintain a constant redox internal environment to survive, partly because ROS are a major threat faced by cells[102]. Major ROS include the superoxide anion ($O_2^{\bullet-}$), and hydroxyl radical ($OH^{\bullet}$) that is involved in Fenton reaction[103]. Other ROS include hypochlorous species (HOCl), peroxynitrite anion ($ONOO^-$), nitric oxide ($NO^{\bullet}$) and hydrogen peroxide (H_2O_2)[4,104]. There are multiple enzyme sources of ROS that include superoxide dismutases (SODs), EROα1, nitric oxide synthase (NOS) and NADPH oxidase (NOX)[105-106]. Organelle sources of ROS include the

endoplasmic reticulum, peroxisomes and the mitochondria (Figure 6 and 7). The mitochondria are at the nexus of redox homeostasis, bioenergetics and metabolic pathways that regulate ATP synthesis, ROS generation, signaling and cell death.

Electron flow from metabolites to the ETC chain in the mitochondrion may generate the superoxide anion at any of the complexes I, II and III (Figure 7) under conditions that include nutrient deprivation and hypoxia[107]. The superoxide anion is the major form of ROS that is converted to hydrogen peroxide by SOD1, SOD2 and SOD3[108]. Another ROS form, nitric oxide, generated by nitric oxide synthase from arginine, may react with the superoxide anion to generate the peroxynitrite anion ($ONOO^-$). Concomitantly, hydrogen peroxide may undergo the Fenton reaction to form the highly reactive hydroxyl radical. Cells endeavor to remove hydrogen peroxide by use of enzymes that include catalase, glutathione peroxidase (GPX) and peroxiredoxin (PRX). These redox enzymes convert hydrogen peroxide to harmless water.

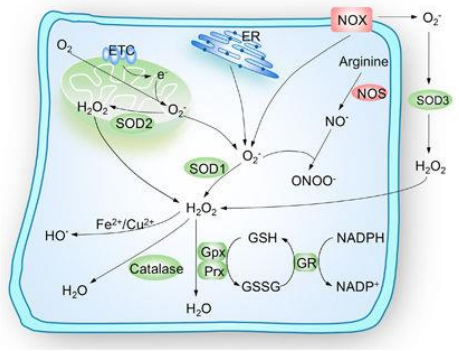

Figure 6-Major **s**ources and types of ROS from a mammalian cell (Adapted with permission from Wang, K.; Zhang, T.; Dong, Q.; Nice, E. C.; Huang, C.; Wei, Y., Redox homeostasis: the linchpin in stem cell self-renewal and differentiation. Cell Death &Amp; Disease **2013,** 4, e537.)

Additionally, mitochondrial dehydrogenases that include glycerol-3 phosphate dehydrogenase, glycerol-3 phosphate dehydrogenase, alpha ketoglutarate dehydrogenase[73] and pyruvate dehydrogenase modulate ROS production.

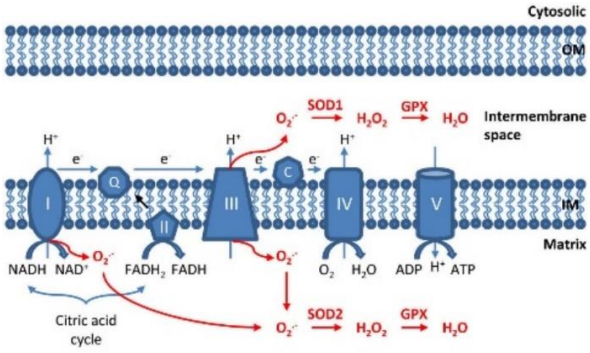

Figure 7-Major **s**ources and types of ROS in the mitochondrion in a mammalian cell[110]. Adapted with permission from Li, X.; Fang, P.; Mai, J.; Choi, E. T.; Wang, H.; Yang, X.-f., Targeting mitochondrial reactive oxygen species as novel therapy for inflammatory diseases and cancers. Journal of Hematology & Oncology **2013,** 6 (1), 19.

Cancer cells have high ROS because they have high metabolic activity than non-transformed cells. Oncogene-driven high sugar uptake and altered metabolism concertedly generate and mitigate ROS levels. Additionally, mitochondrial dysfunction and overexpression of reactive oxygen species modulator 1 (Romo1) has been associated with mitochondrial generation of ROS[111-112]. High levels of ROS may induce signaling and apoptotic pathways that include JNK-ASK1 pathway, p38 pathway and AMPK-p53 pathway (Figure 8).

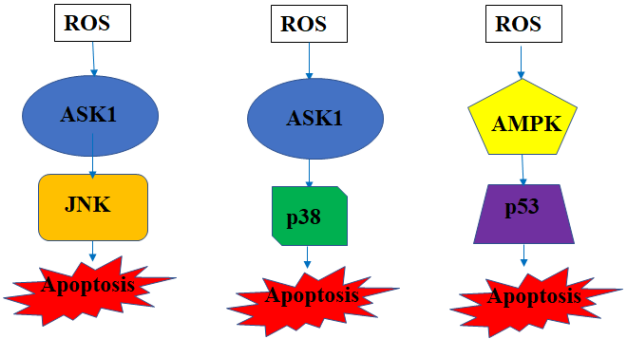

Figure 8- ROS signaling pathways that may lead to apoptosis.

1.8.1 ASK-1-JNK Pathway

Under cellular stress conditions, ASK-1 activates multiple pathways that include JNK and p38 pathways[90]. JNK activation occurs through double phosphorylation of threonine (Thr) and tyrosine (Tyr) residues within a Thr-Pro-Tyr motif. JNK modifies the activity of many proteins in

the mitochondria and nucleus[113]. Downstream targets include c-Jun, p53, ATF2, SMAD4, and HSF1[113]. Additionally, after activation by ROS, JNK translocates to mitochondrion and activate apoptotic proteins such as Bax and Bak[114]. In addition, ROS may activate JNK indirectly by inducing release of ASK-1 from binding TRX and GST which are ROS detoxifying enzymes[113]. In inactivated cells, TRX binds to ASK-1, but ROS convert TRX to the active oxidized form[115]. In this way, JNK activity regulates important cellular functions including redox homeostasis, cell growth and apoptosis.

1.8.2 ASK-1-p38 pathway

Another mitogen activated protein kinase is p38 that is equally sensitive to ROS and activates apoptosis. p38 is also subject to activation by ASK-1 and other upstream MAP3Ks[90, 116]. ROS oxidizes TRX to dissociate from ASK-1 for its activation, leading to the activation of both JNK and p38 pathways (Figure 8). Notably, ASK-1-deficient cells show reduced activations of JNK and p38 MAPK pathways[117]. p38 mechanism of apoptosis involves phosphorylation of Bcl-2 family of proteins, release of cytochrome c from the mitochondria, and caspase activation[118].

1.8.3 AMPK-p53 pathway

p53 is a tumor suppressor and transcription factor that regulates glucose metabolism, cell survival, DNA repair, apoptosis and senescence[72]. Loss of wild-type p53 and mutations occur in more than 50% of all human cancers with severe impact on cellular metabolism[16]. Normally, p53 lowers the glycolytic rate by directly downregulating GLUT 1 and GLUT 4 and by indirectly inhibiting GLUT3[16]. p53 regulates glycolytic enzymes including HKII, PFK1 and PGAM[71, 119]. p53 upregulates TIGAR which reduces F-2,6-BP and consequently PFK1 activity. This leads to the diversion of G6P into the PPP. Notably, p53 alters the activity of G6PD that catalyzes the rate-limiting step of PPP, effectively limiting production of NADPH[120]. Importantly, p53 plays a major

role in redox homeostasis and ROS-mediated apoptosis. Overexpression of p53 induces activation of p53-inducible genes (PIGS) that encode ROS producing enzymes such as NQO1 and proline oxidase[121]. Additionally, p53 suppress the expression of antioxidant enzymes such as SOD2 leading to increase in mitochondrial ROS and apoptosis[122].

p53 undergoes multiple posttranslational modifications under oxidative stress such as phosphorylation by ROS-sensitive p38. Recently, changes in O-GlcNAcylation homeostasis was shown to stabilize p53[123] and mediate apoptosis[124]. Modulation of O-GlcNAc levels triggers p53 pathway activation in response to stress[123]. Indeed, p53 O-GlcNAcylation at serine 149 reduced its ubiquitination and abrogated its proteolysis[123].

1.9 Redox homeostasis in cancer

Redox homeostasis is an intricate and dynamic balance between ROS and antioxidants in mammalian cells (Figure 9). Previous studies have shown that ROS are often increased in cancer cells relative to normal cells, and they contribute to initiation, progression and metastases of cancer. Multiple factors cause the elevation of ROS in cancer cells, including metabolic reprogramming, oncogene activation, and cellular hypoxic conditions. For example, oncogene activation of MYC and KRAS facilitates generation of glycolytic metabolites, which flux into various biochemical pathways that promote cell proliferation while generating high ROS[125]. Additionally, RAS transformation activates *RAC* that regulates membrane-associated NADPH oxidase which produce O_2^-.[126] In addition, mitochondrial DNA mutations in cancer enhance ROS production and tumorigenesis. Respiratory complexes are coded by mitochondrial DNA of which mutation may significantly affect the respiratory activity in mitochondria[127]. Moreover, mitochondrial DNA mutation may be enhanced due to proximity to the site of ROS production within mitochondria, thus increasing its vulnerability to ROS-induced damage.

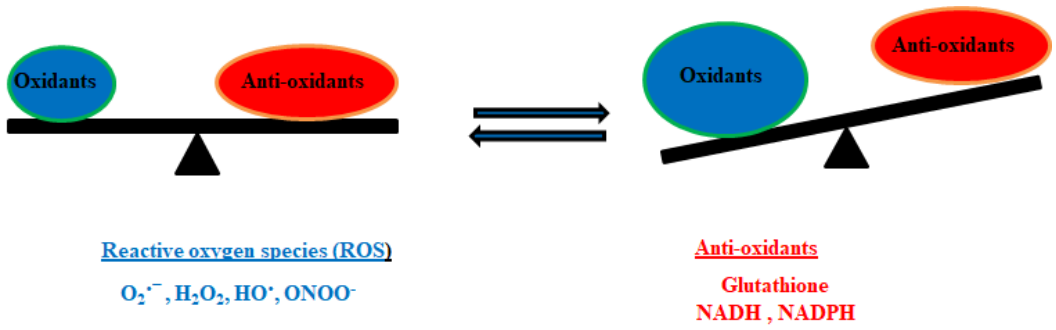

Figure 9-Redox homeostasis is a balance between ROS and antioxidants.

Overall, multiple mechanisms contribute to the elevation of ROS in cancer cells. Consequently, cancer cells enhance their anti-oxidant mechanisms to maintain ROS within a certain threshold level (Figure 10) that affords their survival without detrimental damages. This suggests that the redox system in cancer cells is finely tuned, and any insult or stress that further increase ROS beyond a certain antioxidant protective threshold (Figure 1.6) causes cancer cell death. Numerous studies have characterized the increased vulnerability or sensitivity of cancer cells toward ROS and the consequence of ROS-induced cancer cell death[128-130]. For example, ROS-induced death has partly been attributed to loss of superoxide dismutase (SOD3), catalase (CAT) and glutathione peroxidase 3 (GPX3)[131]. SOD3, CAT and GPX3 gene expression was examined in 1,981 tumors covering 19 cancer types, showing that these antioxidant enzymes are differentially downregulated between cancer and normal cells[131]. It is therefore emerging that an elevation of ROS by using ROS-inducing compounds aggravates cancer cell vulnerability to ROS and could be a viable strategy of killing them[132].

1.9.1 ROS Modulation as an anticancer strategy

Emerging studies indicate that disruption of cancer cell metabolism and increasing ROS beyond cancer cell antioxidant protective threshold is an effective strategy of selective killing of cancer cells[24, 133]. A therapeutic window exists for ROS modulation using small molecules and combination therapies for cancer treatment[134-135]. Notably, cancer chemotherapeutic agents, such

as cisplatin, induce apoptosis partially via ROS generation by directly reacting with glutathione[136], and thus provide vital mechanistic insights[137].

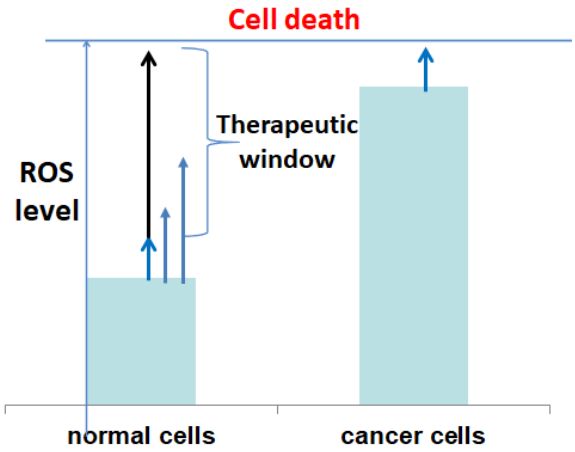

Figure 10-Therapeutic window for design and development of ROS-inducing anticancer drugs

1.9.2 2-Deoxy-D-glucose as an anticancer agent

2-DG is a glucose analog without the C-2 hydroxyl group. 2-DG competes with glucose for uptake via glucose transporters such as GLUT-1[26]. 2-DG is also a competitive inhibitor of hexokinase (HK). Phosphorylation of 2-DG by HK sequesters it within the cytoplasm thus abrogating the glycolytic pathway. This reduces availability of PPP metabolites such as NADPH. NADPH is involved in generation of reducing equivalents such as glutathione. The net effect of 2-DG is an increase in ROS. In this way, 2-DG is a ROS modulator that is cytotoxic in many cancer cell types[138-144]. 2-DG also mimics glucose-deprivation through AMPK activation, mTOR inactivation and cell cycle arrest[26].

Many studies have demonstrated 2-DG cytotoxicity and increase in ROS that is ablated by thiol anti-oxidants such as N-acetylcysteine[145]. Accumulation of phosphorylated 2-DG kills the cancer cell because 2-DG augments generation of ROS. Of note is a new metabolic fate of 2-DG in cancer involving G6PD(H) within the ER and utilizing NAD^+ and $NADP^+$ that has recently been reported[146-147]. 2-deoxyglucose uptake can be regulated by nicotinamide

phosphoribosyltransferase (NAMPT) that synthesize NAD+[146]. Notably, 2-DG uptake increased in Nampt knockdown cells[146].

The mechanisms being studied to explain 2-DG cytotoxicity include increased oxidative and ER stress, disruption of cellular energetics, interference with N-linked glycosylation[148], and induction of death receptor-mediated apoptosis, autophagy, necrosis and mitotic catastrophe[142, 149-154]. Apoptosis is a form of cell death promoted by caspases which degrade cellular substrates without extracellular cytoplasmic spillage. Conversely, necrosis involves rupture of the plasma membrane and cell death. The use of 2-DG is however limited by high-dose systemic toxicity because high concentrations are required to out-compete intracellular glucose concentrations.[153, 155]Additionally, 2-DG activates numerous pro-survival pathways[155] and thus provides a rationale for alternative carbohydrate-based cancer therapies.

1.9.3 Current dissertation work in examining carbohydrate-based inducers of cellular stress for targeting cancer cell metabolism

We hypothesized that carbohydrate-derivatives can be used to make a library to find ROS-inducing small molecules that are more potent than 2-deoxy-D-glucose in cancer cell lines. Therapeutic design of the small molecule exploited the enhanced sugar-uptake phenotype and elevated ROS levels in cancer cells. A simple synthetic strategy was selected that would enable generation of many small molecules in a short time as well as utilizing structure-activity relations envisaged with GLUT-1.

N-aryl glycosides were favorable candidates partly because they are less prone to hydrolysis by glycosidases than O-glycosides[156-157]. Subsequently, N-aryl glycosides were synthesized from simple unprotected monosaccharides and aniline derivatives as described in Chapter 2. Initial screening revealed discovery of a N-naphthyl-β-D-xylose (K8) that induced oxidative and ER stress in H1299 lung cancer cell line. In this study, acetylated N-naphthyl-β-D-xylose (K8A) was

tested for cytotoxicity and disruption of redox homeostasis in cancer cell lines. In Chapter 3, the effect of K8A on redox signaling pathways that include ASK1-JNK, ASK1-p38, AMPK-p53 pathways and ER stress signaling was evaluated. Additionally, we demonstrated using click chemistry in H1299 cells, that K8A interferes with glucose metabolism by disrupting global protein glycosylation. To delineate various forms of glycosylation, we evaluated O and N-glycosylation with antibodies. Importantly, we used metabolomics in Chapter 4 to characterize changes in redox-sensitive metabolic pathways that include glycolysis, pentose phosphate pathway and TCA cycle.

CHAPTER 2 DEVELOPMENT OF CARBOHYDRATE-BASED INDUCERS OF CELLULAR STRESS

2.1 Structural design of carbohydrate-based inducers of cellular stress

The design of the structure of the small molecule was based on studies that have demonstrated that cancer cells have greater cytotoxic sensitivity to 2-deoxy-D-glucose and glucose deprivation[145, 158-159]. Additionally, since absolute glucose deprivation cannot be achieved *in vivo*, it has been demonstrated that 2-deoxy-D-glucose mimics glucose deprivation to inhibit glucose metabolism[145]. Such small molecules selectively kill cancer cells by oxidative stress and metabolic inhibition[20, 24]. We therefore designed the structure of the small molecules with a sugar moiety to explore carbohydrate-induced-cytotoxicity in cancer cells.

The inclusion of a monosaccharide moiety was meant to streamline targeting cancer cells with phenotypes that bear enhanced sugar uptake and high intracellular ROS levels[135, 160-161]. Moreover, most cancer cells overexpress glucose transporter 1(GLUT-1) and other sugar transporters to facilitate enhanced cellular sugar entry[162]. GLUT-1 is up-regulated partly by mutant p53 and other oncogenes[16]. We therefore hypothesized that our monosaccharide-containing small molecules would enter cancer cells aided by sugar transporters and by simple diffusion. Moreover, substitution at the anomeric carbon (C1), carbon 2 (C2) and carbon 6 (C6) of glucose is tolerated by GLUT-1 and has been demonstrated with some glycoconjugate anticancer agents[161, 163]. Subsequently, we ensured a majority of the designed sugar-conjugated small molecules maintained these vital structure-activity relationships.

Our small molecules had a basic N-glycoside structure (Figure 11) that consists of a sugar building block in scheme 1 (glycone, R_2), with various substituent groups (R_1) covalently conjugated to an aromatic amine (aniline derivatives in scheme 1)[164].

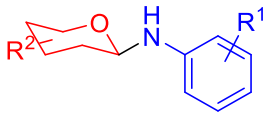

Figure 11- Carbohydrate-based small molecule scaffold (R^1 & R^2 as in scheme 1).

2.2 Approach on synthesis and characterization of carbohydrate-based small molecules

Synthetic chemists are continuously examining sets of robust chemical reactions that can generate the full complement of glycoside linkages. Furthermore, synthesis of N-glycosides from unprotected sugars is less explored, partly because conjugation of nitrogen scaffolds at the anomeric position remains a difficult task. Moreover, a systematic study involving formation and characterization of N-glycosides using one-step synthetic strategy is yet to be fully understood. More importantly, biological and therapeutic potential of glycosides[165] prompted us to pursue one-step synthesis methodologies to streamline generation of a library of compounds

Bridiau and his coworkers synthesized *β*-*N*-aryl-glycosides from equimolar amounts of unprotected sugars with aniline derivatives in aqueous media, at pH 6.5 and about 40˚C-70˚C [157] for 5 hours. However, higher sugar equivalents and longer reaction times of up to six days were used without success in optimization of the reaction. The condensation reaction was however largely stereoselective and was partly controlled by steric effects with most compounds being β-products. The *N*-aryl-glycosides were obtained in variable yields (30-50%) depending on the reactivity of the aniline derivatives. We modified and optimized Bridiau method to include 20% DMSO in phosphate buffer at pH 6.5 and higher temperature (50-70˚C) for 10-16 hours (Scheme 1). The 20% DMSO in PBS conditions enabled solubility of aniline and heterocyclic derivatives thus expanding the scope of this reaction. Purification by HPLC was done after removal of unreacted charred starting material by filtration over cotton wool using a syringe. HPLC peaks of products and reactants were clearly resolved as in the example in Appendix B. Initial

characterization was by LC-MS (Appendix A) and therefore stereochemistry at the anomeric carbon could not be determined at this stage.

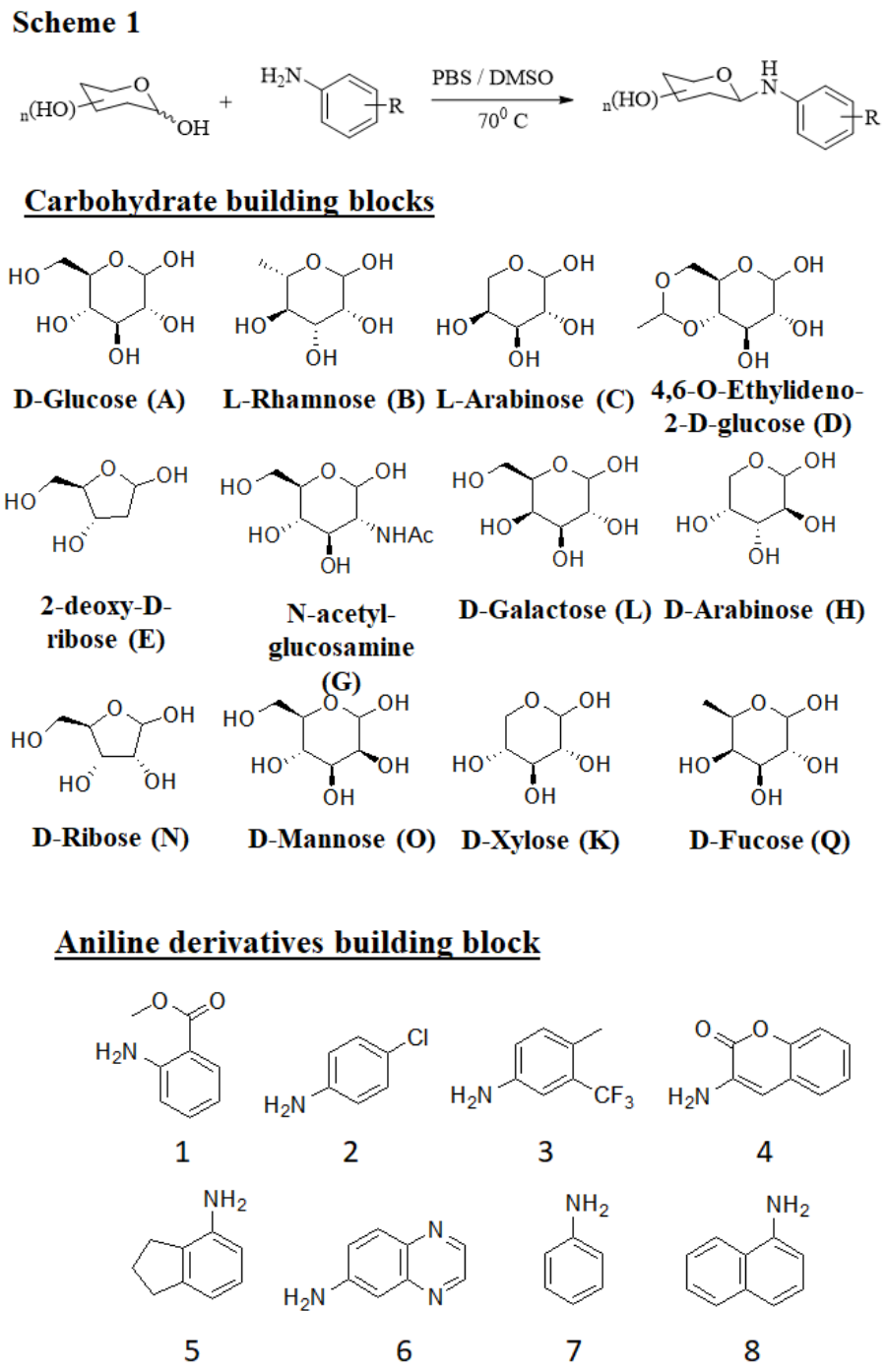

Scheme 1. Chemical synthesis of carbohydrate-based small molecules.

2.3 Results

2.3.1 Characterization of carbohydrate-based small molecules by LC-MS

After reaction of individual carbohydrate (A–L) and aniline derivatives (1–8) (Scheme 1) in a ratio of 16:1 in 20% DMSO/phosphate buffer (pH 6.5), the mixture was directly injected to a semi-preparative HPLC column for purification of products. After LC-MS analysis of individual products, compounds that had a high purity (>90%) (Appendix A) out of 96 compounds made were selected for subsequent ROS screening in cancer cells. After this initial screening, 8-series compounds (with 1-naphthylamine aglycone) were re-synthesized, including A8, C8, H8, and K8, for further evaluation. After re-synthesis, we were able to determine the anomeric configuration of compounds by NMR analysis. HPLC (Figure 12), LC-MS (Figure 13, 14, 15, & 16) and NMR spectra (Figures 18-2) of the hit compound K8 and the acetylated form (K8A) is shown.

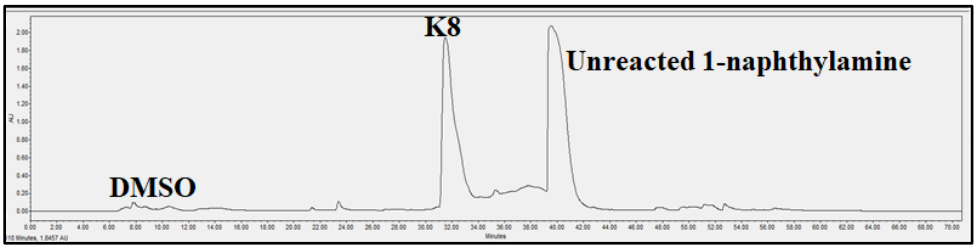

Figure 12- HPLC spectrum of K8 at a detection wavelength of 214nm.

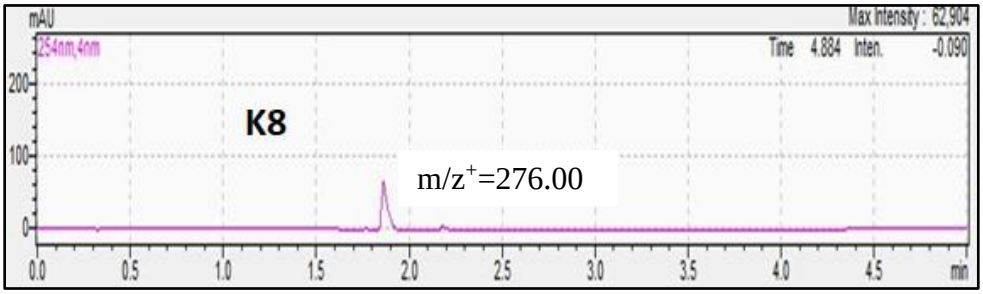

Figure 13-LC spectrum of K8 at a detection wavelength of 254nm.

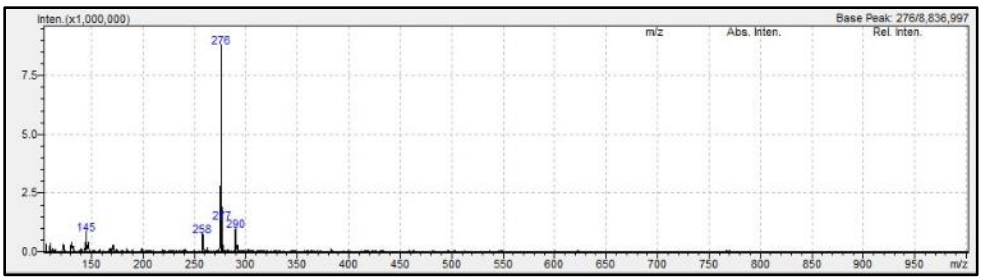

Figure 14- MS spectrum of K8

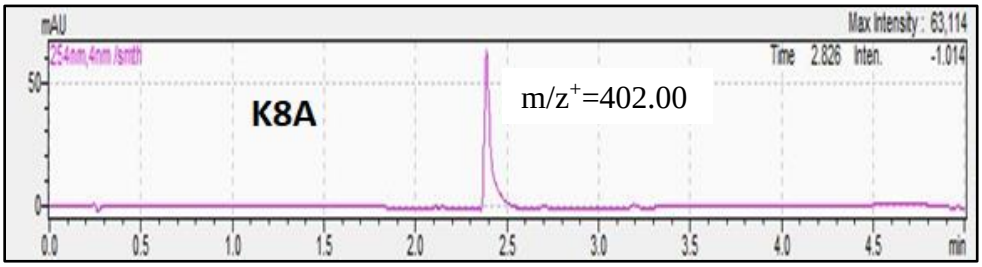

Figure 15-LC spectrum of K8A at 254nm

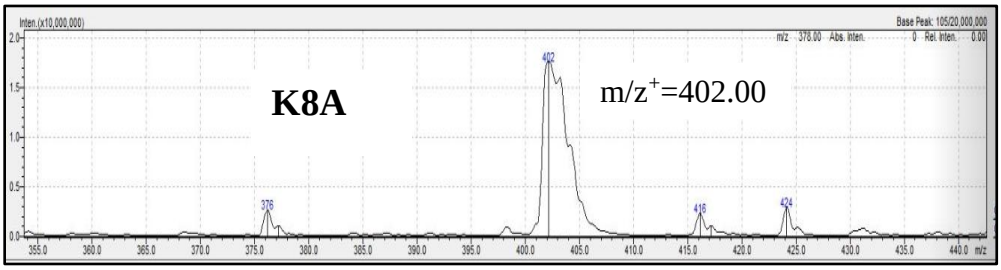

Figure 16- MS spectrum of K8A

2.3.1.1 K8A monoisotopic mass analysis by High resolution mass spectrometry

Elemental Composition Report

Single Mass Analysis
Tolerance = 5.0 PPM / DBE: min = -1.5, max = 50.0
Element prediction: Off
Number of isotope peaks used for i-FIT = 3

Monoisotopic Mass, Even Electron Ions
85 formula(e) evaluated with 3 results within limits (all results (up to 1000) for each mass)
Elements Used:
C: 15-25 H: 15-25 N: 0-5 O: 1-10 Na: 0-1
PON-CHECK-hrsm

2018_0228_117 43 (0.918)

LCT Premier
1: TOF MS ES+
3.58e+003

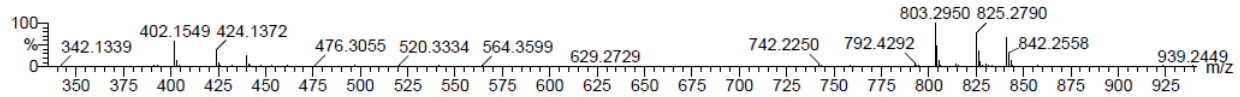

Minimum:				-1.5			
Maximum:		5.0	5.0	50.0			
Mass	Calc. Mass	mDa	PPM	DBE	i-FIT	i-FIT (Norm)	Formula
424.1372	424.1356	1.6	3.8	9.5	7.8	0.5	C18 H22 N3 O9
	424.1372	0.0	0.0	10.5	8.2	1.0	C21 H23 N O7 Na
	424.1386	-1.4	-3.3	15.5	10.9	3.6	C22 H19 N5 O3 Na

Figure 17-Monoisotopic mass analysis for K8A.

2.3.1 Characterization of K8 by NMR

2.3.1.1-^{1}H-NMR of K8

K8

^{1}H NMR (600 MHz, CD_3OD) δ 8.10 – 8.05 (m, 1H), 7.76 – 7.72 (m, 1H), 7.40 (dt, J = 6.3, 3.6 Hz, 2H), 7.31 – 7.25 (m, 2H), 6.84 (d, J = 7.2 Hz, 1H), 4.67 (d, J = 8.2 Hz, 1H), 3.90 (td, J = 11.2, 10.7, 5.8 Hz, 1H), 3.61 – 3.54 (m, 2H), 3.49 (t, J = 8.7 Hz, 1H), 3.39 (t, J = 10.7 Hz, 1H).

fc_p13_1hnmr
fc_p13_1hnmr

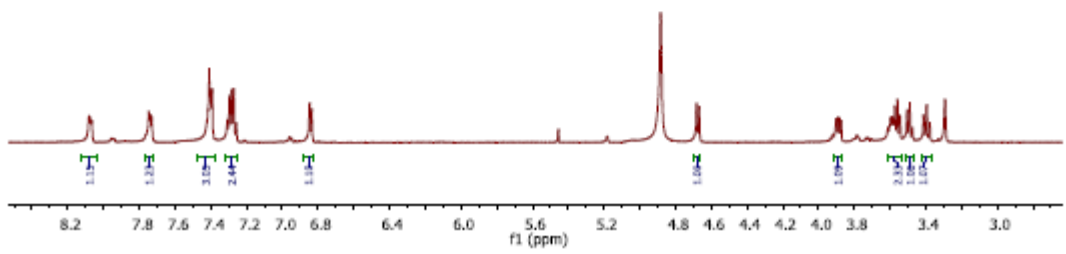

Figure 18 ^{1}H-NMR of K8

2.3.1.2 H-^{1}H COSY of K8

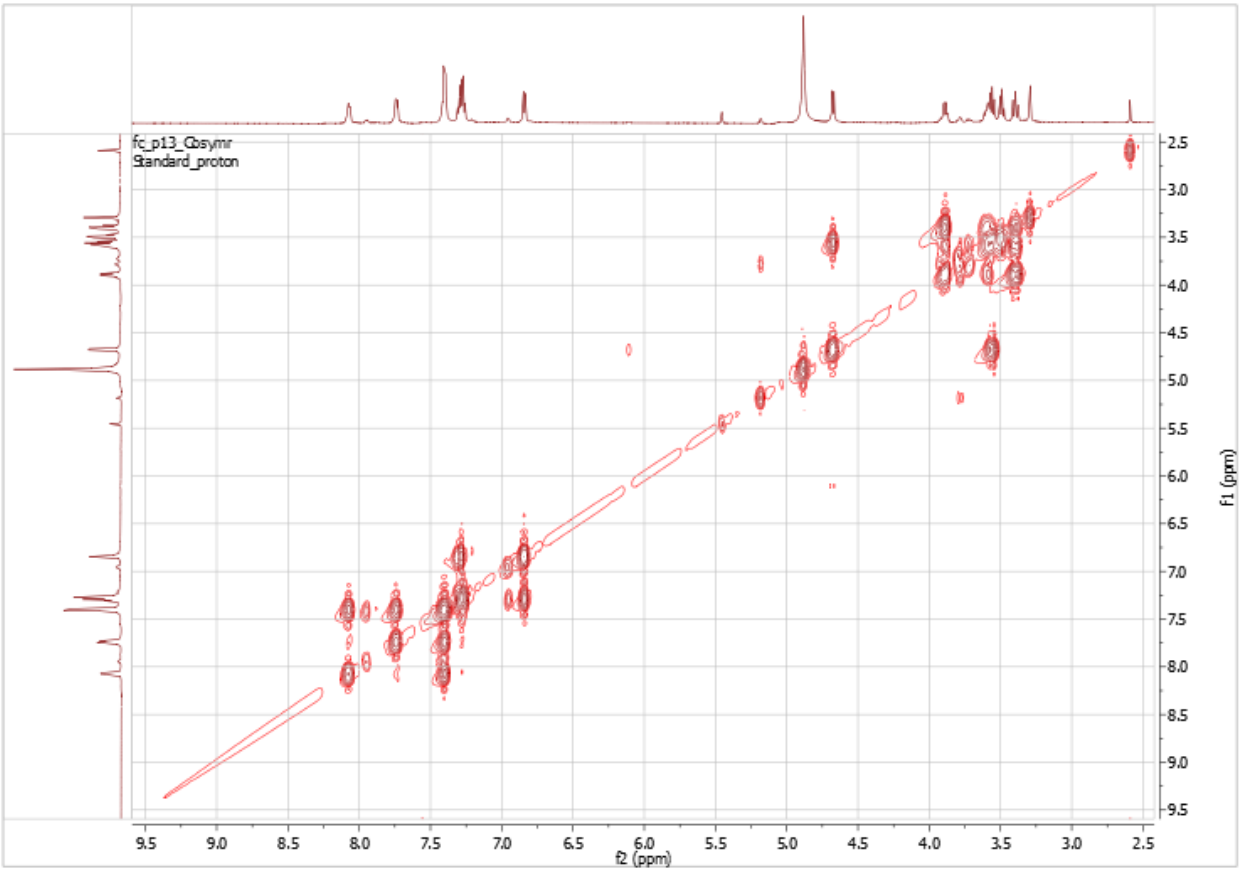

Figure 19- ^{1}H-^{1}H COSY of K8

2.3.1.3 ^{1}H-^{13}C HSQC of K8

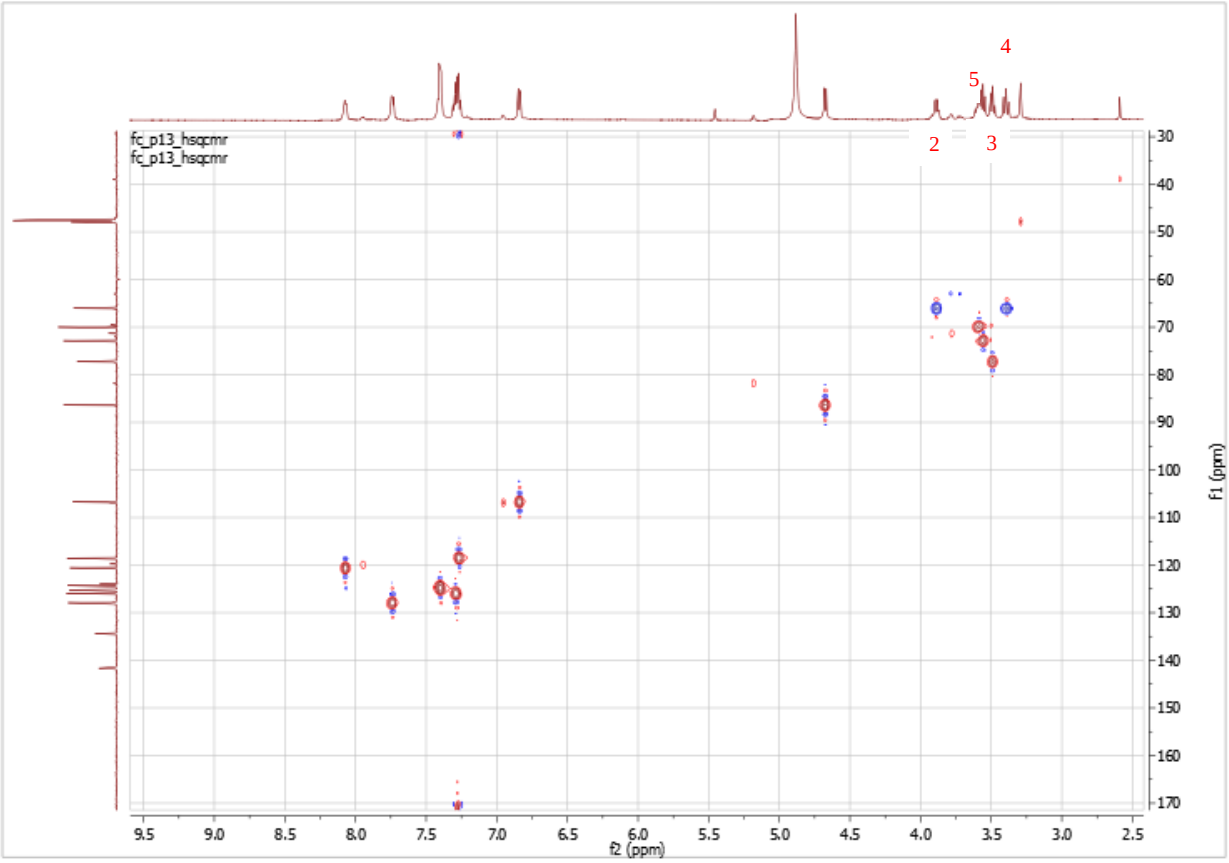

Figure 20-^{1}H-^{13}C HSQC of K8

2.3.1.4 ^{13}C NMR of K8

^{13}C NMR (151 MHz, CD3OD) δ 141.65, 134.39, 128.10, 125.97, 125.93, 124.04, 123.99, 123.80, 118.55,106.74, 86.39, 77.26, 72.89, 71.99, 66.04.

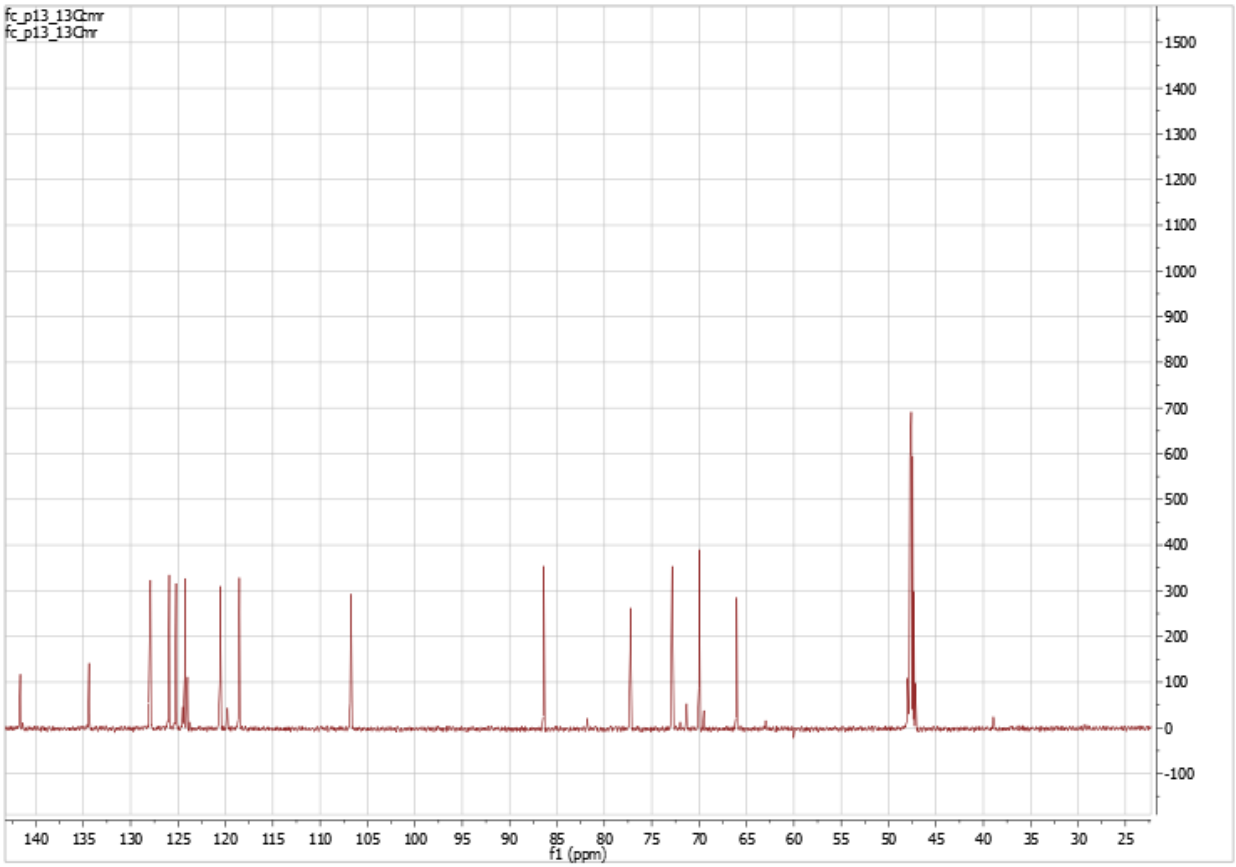

Figure 21- ^{13}C NMR of K8

2.3.1.5 ^{13}C HSQC of K8 showing chemical shift of anomeric carbon and proton

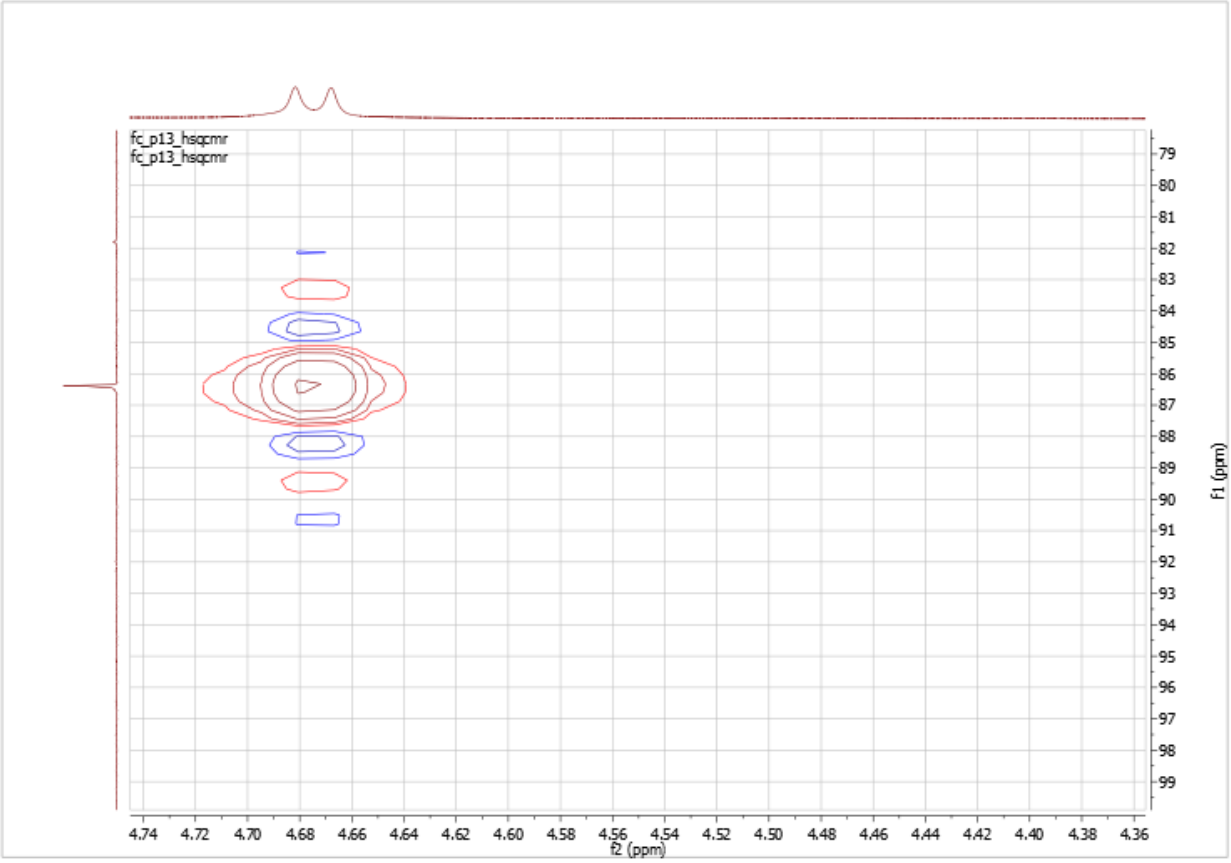

Figure 22-^{13}C HSQC of K8

2.3.1.6 DEPT NMR of K8

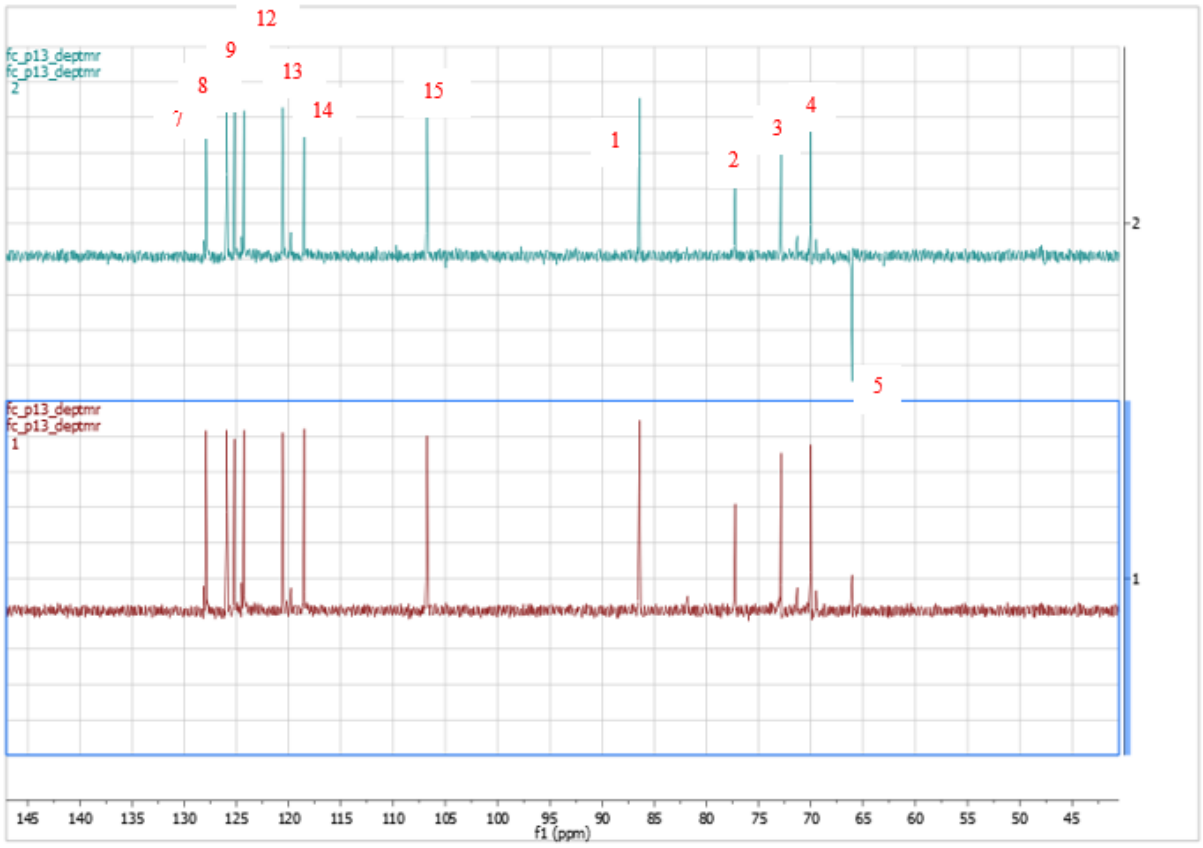

Figure 23-DEPT NMR of K8

2.3.2 Characterization of K8A by NMR

2.3.2.1 ^{1}H NMR of K8A

^{1}H NMR (400 MHz, CD_3OD) δ 7.90 – 7.82 (m, 1H), 7.80 – 7.70 (m, 1H), 7.46 – 7.38 (m, 2H), 7.35 – 7.26 (m, 2H), 6.89 – 6.83 (m, 1H), 5.44 (t, *J* = 9.5 Hz, 1H), 5.25 (t, *J* = 9.2 Hz, 1H), 5.05 (ddd, *J* = 10.6, 9.5, 5.6 Hz, 1H), 5.00 (d, *J* = 8.9 Hz, 1H), 4.07 (dd, *J* = 11.3, 5.6 Hz, 1H), 3.63 (t, *J* = 10.9 Hz, 1H), 2.05 (s, 3H), 2.03 (s, 3H), 1.99 (s, 3H).

^{13}C NMR (101 MHz, CD_3OD) δ 171.05, 170.28, 170.19, 140.84, 134.36, 127.93, 125.80, 125.33, 124.57, 120.51, 119.29, 107.52, 84.62, 72.92, 71.46, 69.47, 62.89, 19.32, 19.24, 19.16. $[\alpha]D^{RT}$-45.9 (*c*,0.5, methanol).

^{1}H NMR (400 MHz, CD_3OD)

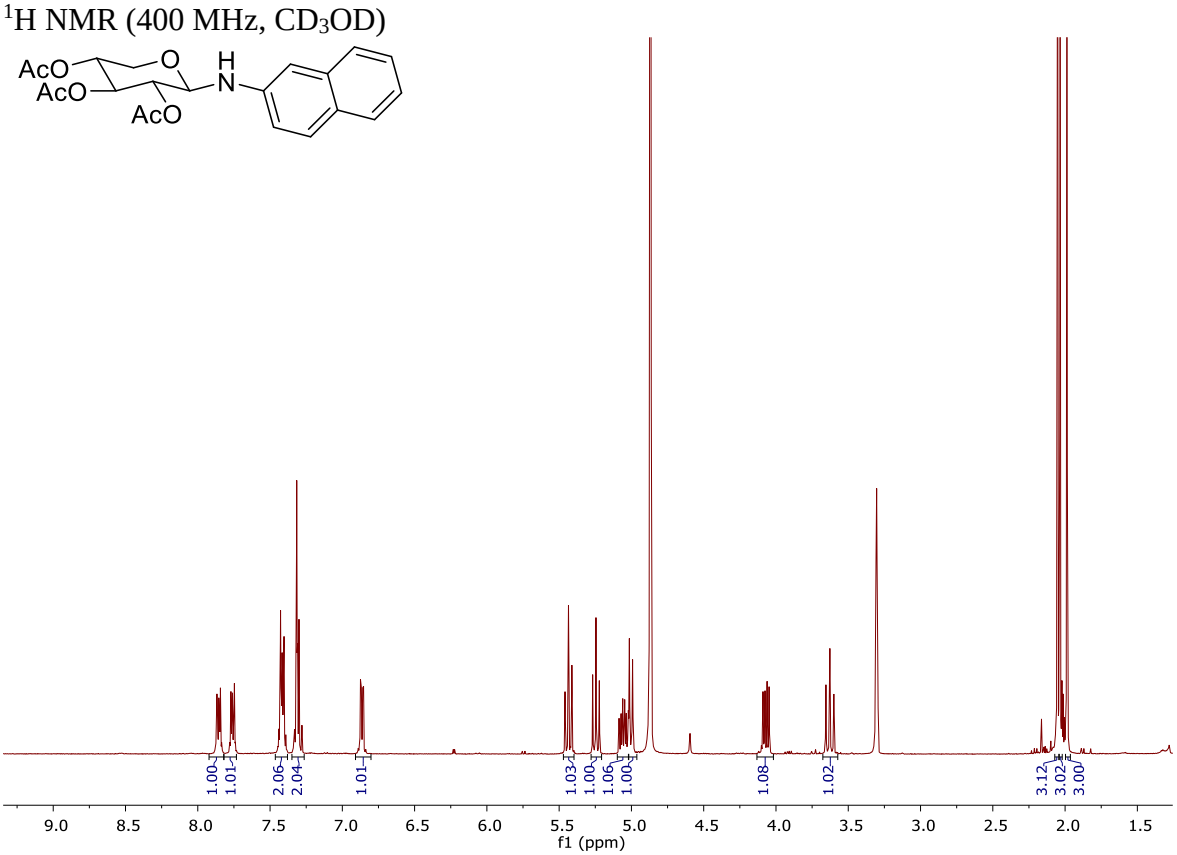

Figure 24-^{1}H NMR of K8A

2.3.2.2 ^{13}C NMR of K8A (101 MHz, CD_3OD)

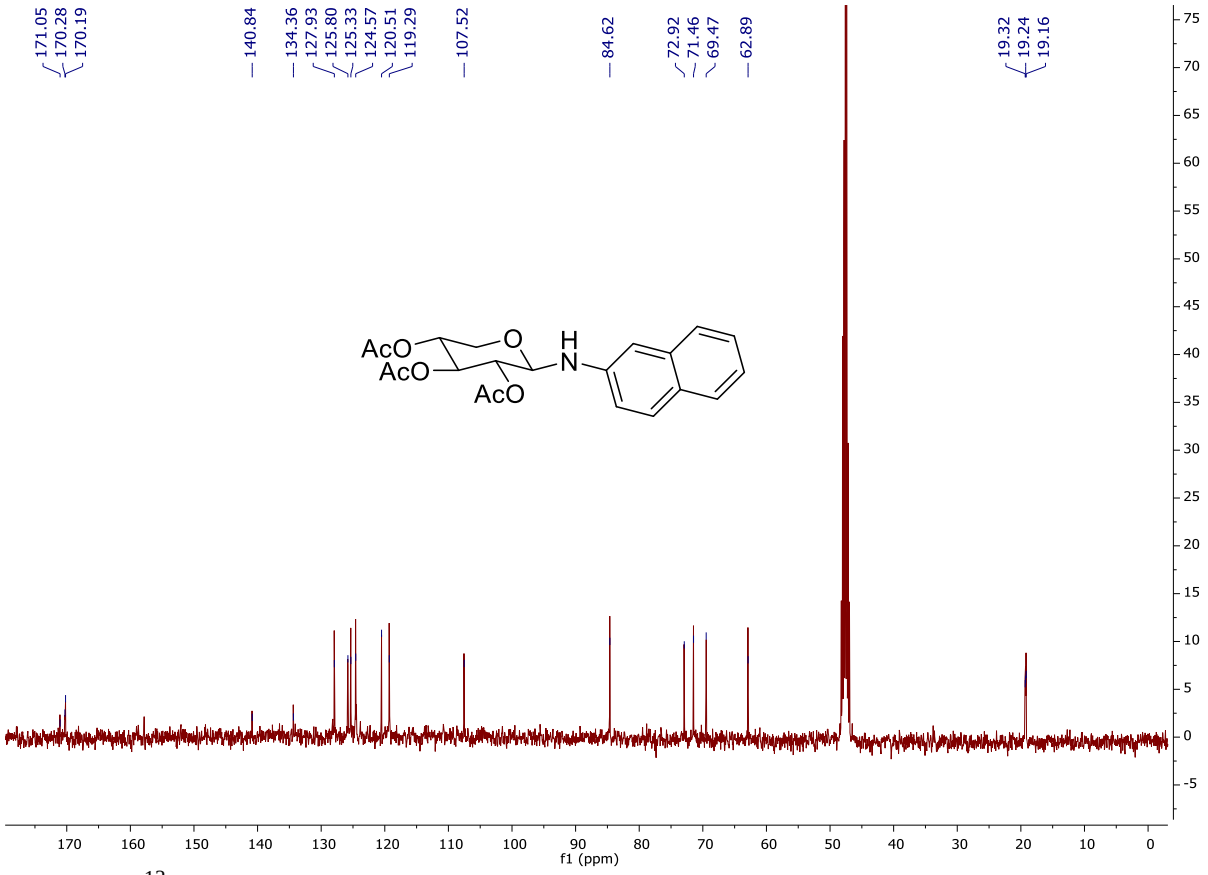

Figure 25- ^{13}C NMR of K8A

2.3.2.3 ^{1}H-^{1}H COSY of K8A

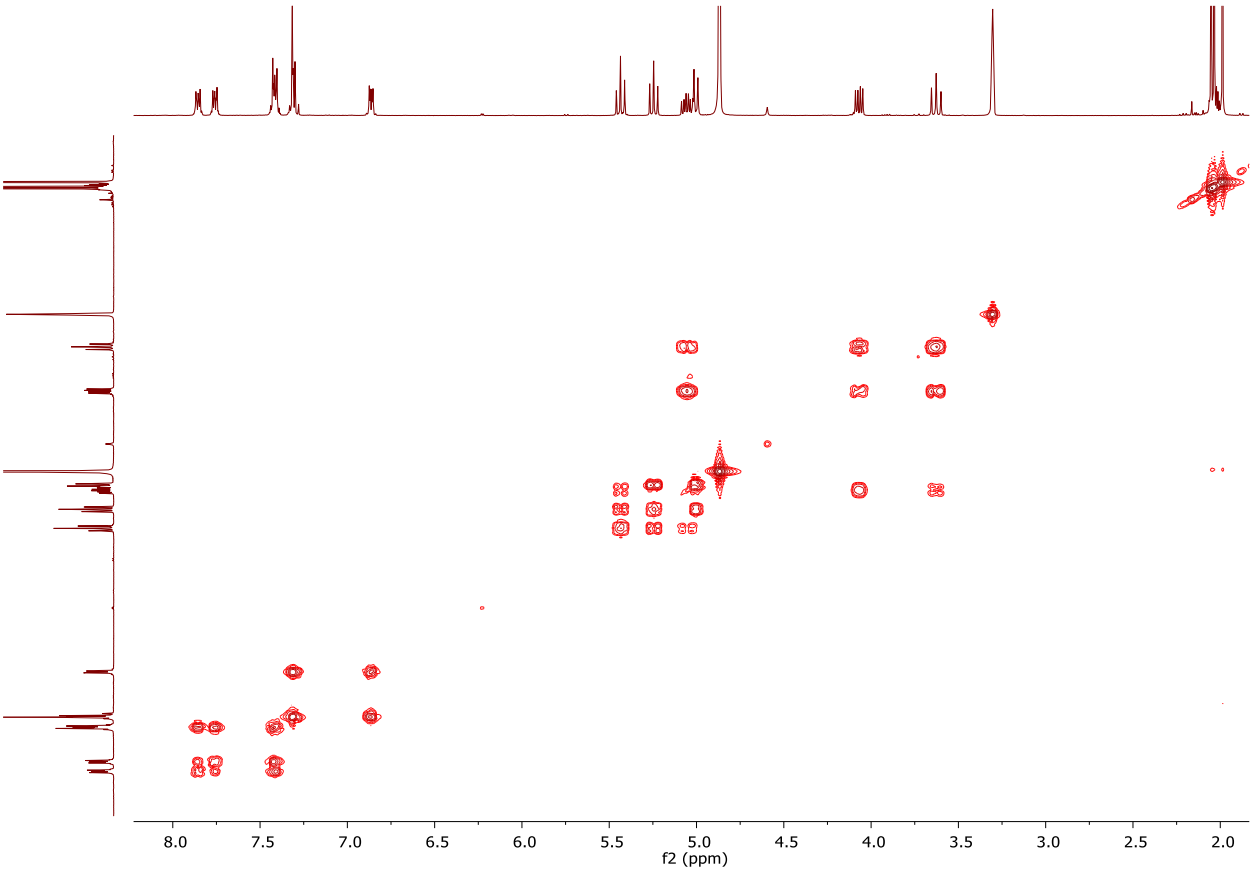

Figure 26- ^{1}H-^{1}H COSY of K8A

2.3.2.4 ^{1}H-^{13}C HSQC of K8A showing anomeric proton chemical shift

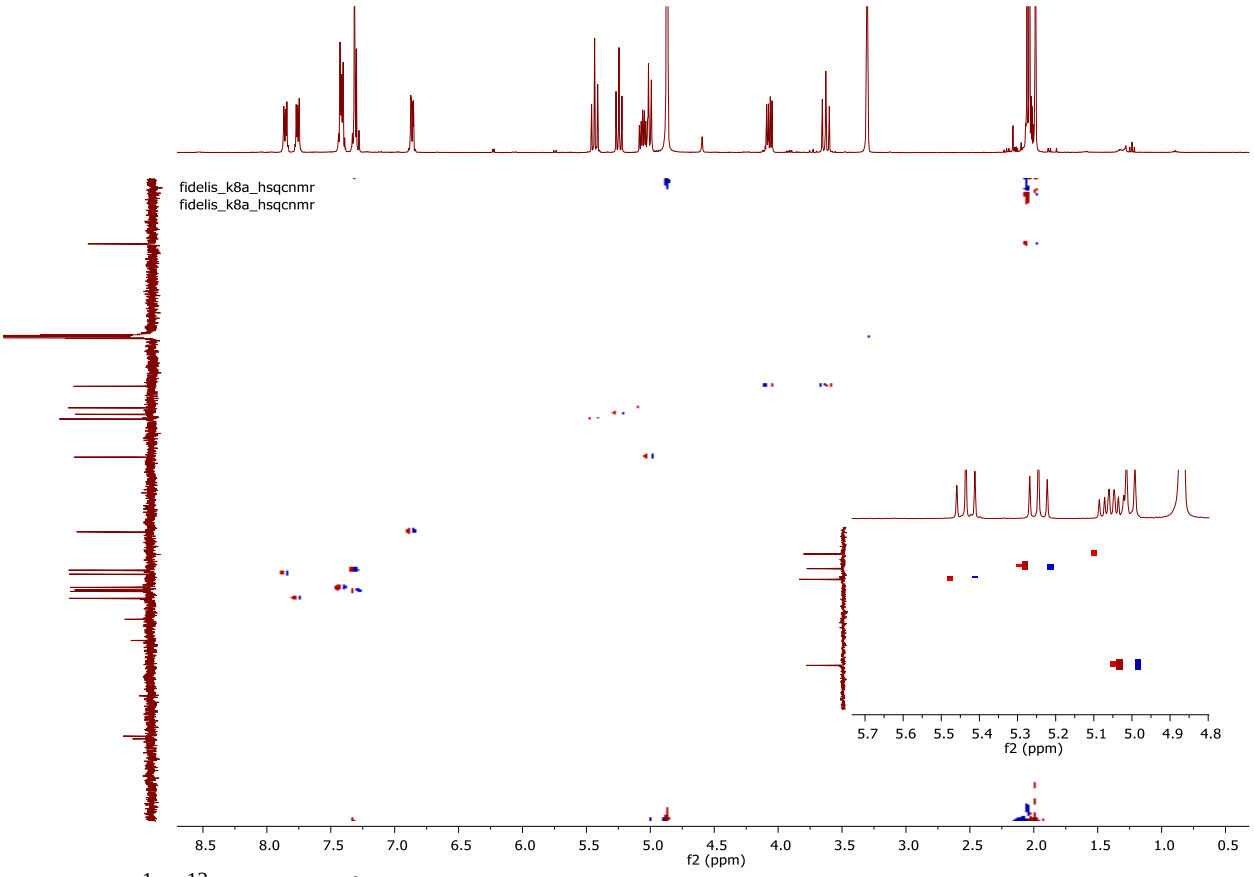

Figure 27- ^{1}H-^{13}C HSQC of K8A

2.3.2.5 ^{1}H-^{13}C HSQC of K8A showing chemical shift of anomeric carbon and proton

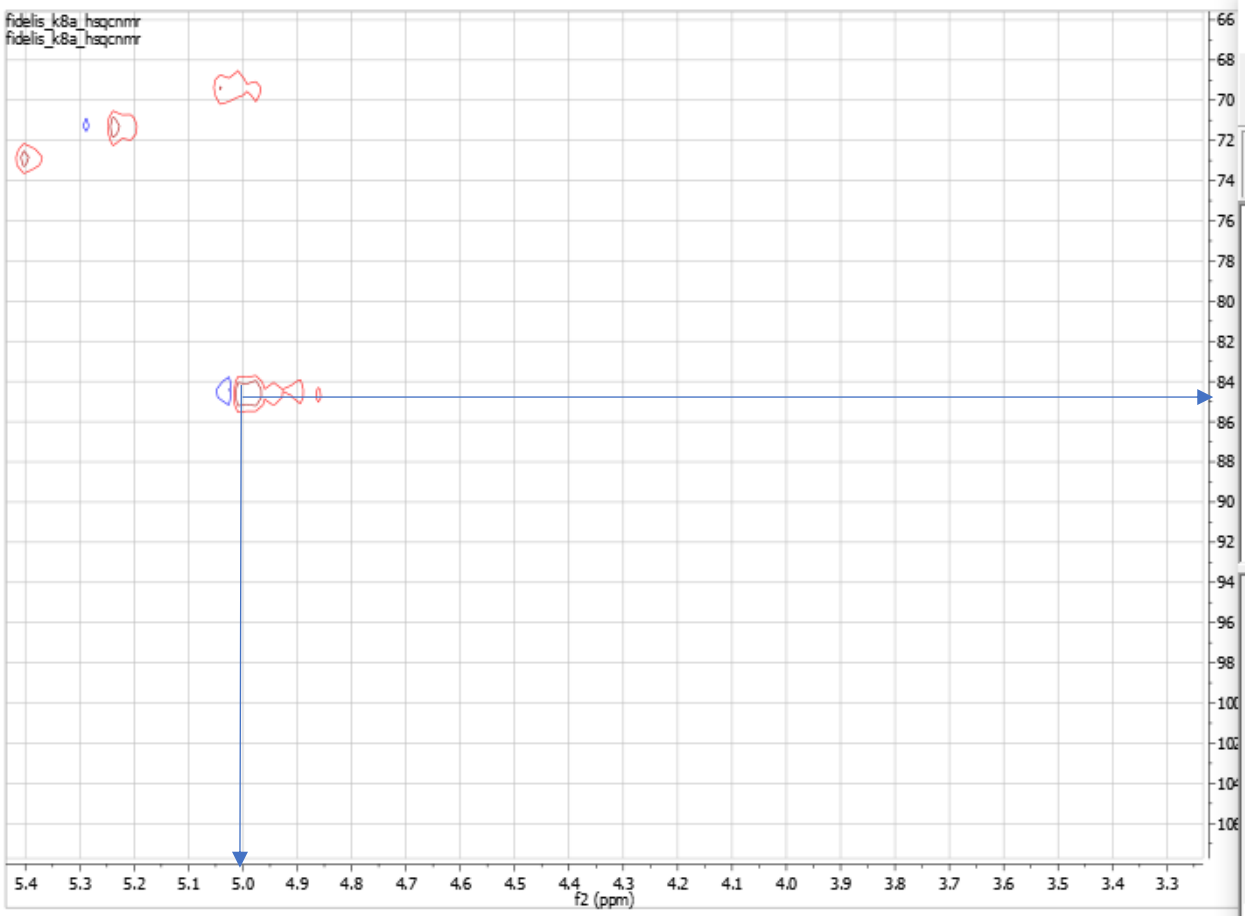

Figure 28- ^{1}H-^{13}C HSQC of K8A showing anomeric carbon and proton

2.4 Result and Discussion

For some carbohydrate-based small molecules, HPLC chromatograms at 214 nm and 254 nm showed the presence of at least three peaks for each of the reaction mixtures (Figure 2.2). The first peak at around 8 to 14 minutes was due to elution of DMSO used to dissolve the aromatic amine and unreacted sugar (Figure 2.2). The second peak was due to the reaction product eluted at around 18-35 minutes (Figure 2.2). This variation in elution time was likely due to hydrophobicity of the substituent groups on the aglycone and hydroxyl groups on the glycone. Some reaction products appeared as two peaks possibly due to presence of the alpha and beta monomers of the monosaccharide. The final peak was due to the unreacted aromatic amine (Appendix). The LC-MS analysis indicated that the products corresponded to a m/z ratio of molecular ion +1 (MH^+).

Bioactive compounds K8 and K8A were fully characterized by LC-MS, ^{1}H NMR, ^{13}C NMR, HSQC, COSY and DEPT experiments (Figures 2.3-2.15). The m/z ratio for K8 (M.W. 275) was 276.00 with LC indicating about a high purity denoted by a single peak. K8A (M.W. 401) m/z ratio was 402.00 and the single LC peak indicated a high purity. Importantly, K8A monoisotopic mass analysis was 424.1372 for m/z, was equal to the addition of one sodium atom. The m/z ratio for other carbohydrate-based molecules are as in the appendix A. For K8, the proton at anomeric carbon (H-1) coupled to (H-2) with a chemical shift 4.67 ppm (d, J= 8.2 Hz, 1H) allowed us to characterize K8 with β-configuration. ^{1}H spectra of carbohydrates enable identification of anomeric protons at known chemical shifts[166], typically 4.4-5.5[167-168]. Anomeric configurations may also be assigned $J_{H\text{-}H}$ coupling that enable determination of stereochemistry. $J_{H1\text{-}H2}$ values of 7–9 Hz for the diaxial coupling are assigned a β-configuration[169]. $J_{H1\text{-}H2}$ values of 2–4 Hz due to equatorial–axial coupling denotes α-anomeric structure[169]. Exceptions exist for sugars like D-mannose, which has an equatorial H-2, with $J_{H1\text{-}H2}$ values set at about 1.6 Hz due to coupling

between diequatorial protons and about 0.8 Hz for the axial–equatorial coupling of the β-anomer[169].

The ^{13}C NMR chemical shift of carbon atoms in sugars range between 68-77 ppm[169]. Additionally, in ^{13}C NMR, glycosylation leads to high frequency shifts of 4-10 ppm for the carbons at the anomeric and linked positions[169-170]. The anomeric carbon and protons in K8 were identified using ^{13}C NMR (86 ppm) and HSQC (^{1}H NMR; 4.68 ppm, ^{13}C NMR; 86.5 ppm). Additionally, DEPT confirmed the seven CH bonds of the aglycone (1-naphthylamine), one CH_2 bond of the glycone (D-xylose) and its four CH bonds. In a similar way, the anomeric carbon in K8A (acetylated K8) was identified by ^{1}H NMR of anomeric proton at chemical shift (4.98 d, J = 9.2 Hz, 1H), HSQC (^{1}H NMR; 4.98ppm, ^{13}C NMR; 84.6ppm). The acetyl groups were identified by ^{1}H NMR (2.07- 1.98 (m, 9H) and ^{13}C NMR (19.32, 19.24, 19.16). The pure compounds were stored in DMSO in -80°C freezer for future cell-based assays.

2.5 Experimental procedures

2.5.1 Reagent/Materials

Unless otherwise stated, all reactions were carried out under an atmosphere of dry nitrogen in oven dried glassware. Indicated reaction temperatures refer to those of the reaction bath, while room temperature is noted as 25 °C. All solvents were anhydrous quality purchased from Sigma-Aldrich Chemical Co. (Saint Louis, MO) and were used as received. Commercially available starting materials and reagents were purchased from Sigma-Aldrich Chemical Co or TCI America and were used as received.

2.5.2 Synthesis of carbohydrate-based small molecules

One-step synthesis of **(K8)** (Scheme 2) is described here to illustrate the reaction scheme and protocols used in making the glycoconjugate small molecules in our library.

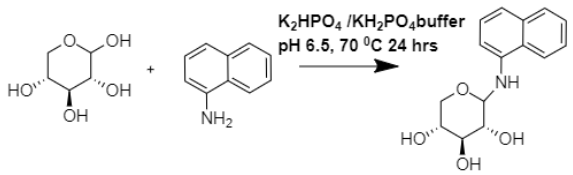

Scheme 2: Chemical synthesis of K8.

To react D-xylose (337.5 mg, 249.8 mmol) with 1-naphthylamine (18.9 mg, 14.67 mmol) (Scheme 2), a reaction mixture of 1 equivalent amine in dimethyl sulfoxide (DMSO) and 17 equivalents of preheated carbohydrate in potassium phosphate buffer (pH=6.5) was prepared in a 4 mL glass vial and incubated in a sand bath at 70 ^{o}C for 24 hours. The reaction-product mixture was filtered twice using cotton wool to remove any solid particles and charred sugar debris. Centrifugation at low speed ensured any solid particles are removed and only clear solution was drawn in a syringe.

2.5.3 Purification method of carbohydrate-based small molecules by semi-preparative HPLC

Products formed were purified by using a semi-preparative high-pressure liquid chromatography (HPLC) system (Waters Co). A HPLC system was used with a gradient elution method that consists of a mobile phase composition of 95% water and 5% acetonitrile, a flow rate of 10 mL/min, injection volume of 3-4 mL, run time of 40-75 minutes and detection wavelengths of 214 nm and 254 nm. Separation of products and reactants were obtained using a C-18 reverse phase column. This method was used for identification of product fractions for further analysis by LC-MS. Product fraction elution occurred at retention times between 20-35 minutes and collected in 50 ml falcon tubes, flash-frozen in liquid nitrogen and lyophilized under vacuum until the

product appeared to be completely dry. Upon removal, the products were dissolved in 1 mL of 50% acetonitrile/water mixture and transferred to a pre-weighed 1.5 ml Eppendorf tube and re-lyophilized until completely dry. The products were then stored in -80 ^{0}C freezer.

2.5.4 Protocol for characterization of carbohydrate-based small molecules by LC-MS

About 0.1 mg of the separated and lyophilized reaction products were dissolved in 50 µL of 50% acetonitrile/water mixture. Samples were injected into a Shimadzu Triple-quadruple liquid chromatography-mass spectrometer (LC-MS) in a positive ion mode at a flow rate of 0.45 mL/min using a 30 mm C-18 reverse-phase column at a scan wavelength between 190-500 nm and pressure range of 2000-2300 psi. The LC 5-minute gradient-elution-method consisted of 95% water/5% acetonitrile (0-1 minute), acetonitrile gradient, 5-100% (1-4 minutes) and 100-5% acetonitrile (4-5 minutes). LC Chromatograms were obtained using a photo diode array detector at 254 nm and 280 nm.

2.5.5 Chemical Synthesis of K8A

To prepare K8A (Scheme 3), D-xylose (500 mg, 3.33 mmol) and 1-naphthylamine (525 mg, 3.66 mmol) was refluxed in ethanol for 8 hours to obtain brown sparkly crystalline solid (730 mg). The reaction was monitored by thin layer chromatography. The crystalline solid obtained (500 mg) was reacted with acetic anhydride (8.17 mmol) in pyridine (0.79 mL, 9.81 mmol) in an ice bath for 3 hours and in the cold room for another 13 hours. The reactant mixture was then quenched by pouring into ice/water, extracted, washed with aqueous sodium bicarbonate, water and brine, and purified by column chromatography (1:4 ethyl acetate/hexane solvent conditions). After purification, a yellow solid K8A (622 mg, 1.55 mmol) was obtained and it was further recrystallized from ethanol to provide the white K8A crystals.

2.5.6 Chemical Synthesis of K8A analogs

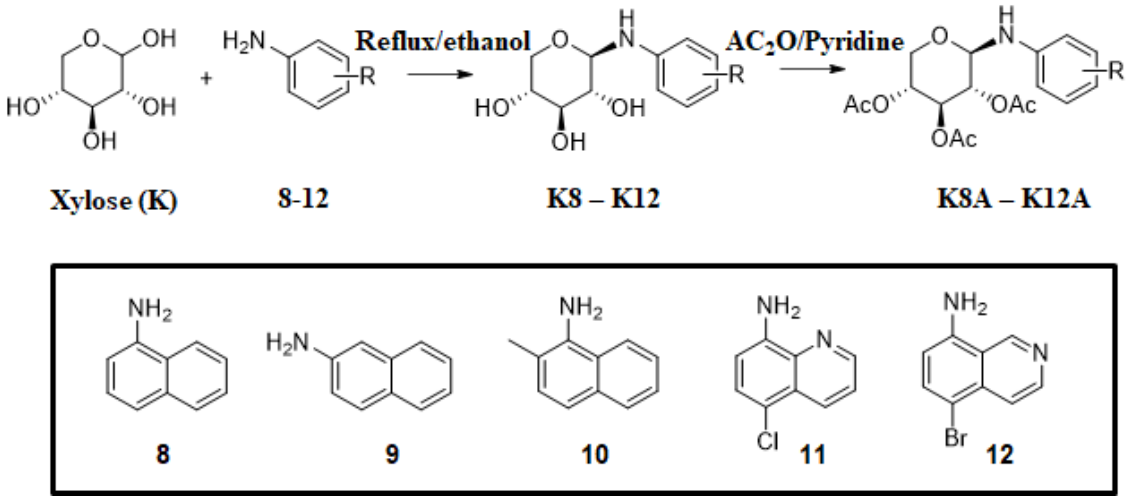

Scheme 3: Chemical synthesis of K8A analogs with aniline derivative variation.

To further explore cytotoxicity of K8A, synthesis of K8A analogs (Scheme 4) of diverse sugars was done with 2-naphthylamine instead of 1-naphthylamine (Figure 1) to generate 9 series compounds that include 2-naphthylamine and L-arabinose (C9A), D-arabinose (H9A), D-xylose (K9A), D-galactose (L9A), D-ribose, I9A and D-fucose (Q9A). Additionally, the aniline moiety was varied to generate K10, K11 and K12. Other 8-series compounds C8A, H8A and L8A were also synthesized. A8A occurred as an inseparable mixture possibly of the α and β anomers.

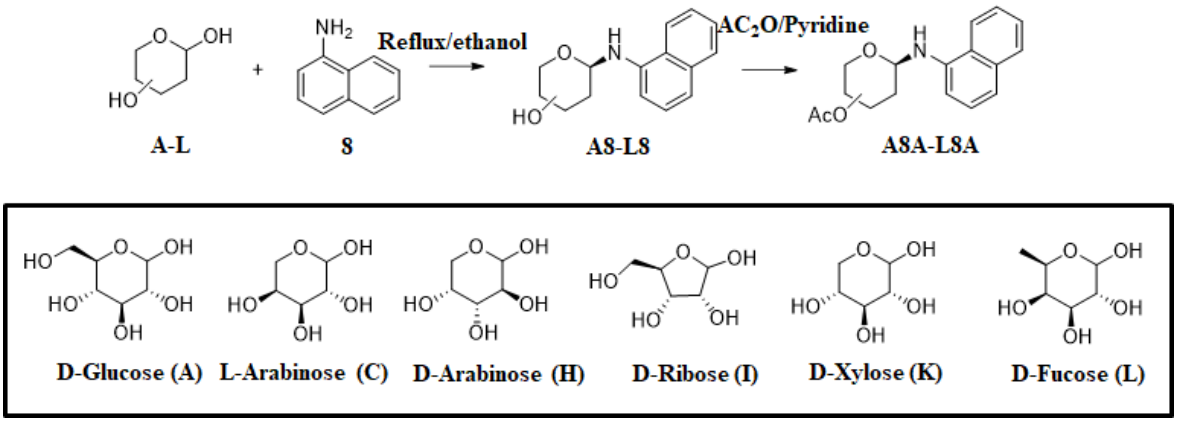

Scheme 4: Chemical synthesis of K8A analogs with sugar derivative variations.

2.6 Quantification of reactive oxygen species in mammalian cells

2.6.1 ROS Quantification using DCF Assay

Oxidative stress can be quantified indirectly by measuring the products of oxidative damage, such as lipid peroxides[171], protein carbonyl content[172] and DNA adduct formation[173]. Additionally, oxidative stress can be measured by evaluating oxidative stress response in various forms that include thiol-redox status[174], O-GlcNAcylation[175], and evaluation of antioxidant enzymes. However, a more direct and sensitive method of oxidative stress quantification is the dichlorodihydroflourescein (DCF) Assay[176](Figure 29). 2’7’-dichlorodihydroflourescin diacetate (DCFH-DA) readily cross membranes and is deacetylated by intracellular esterases to non-fluorescent 2’7’-dichlorodihydroflourescein (DCFH). Deacetylation ensures specific labeling of intracellular contents, and thus excludes staining of ROS in the extracellular medium. In the presence of hydrogen peroxide and ROS; DCFH is oxidized into highly fluorescent dichloroflourescein (DCF) (Figure 29)[177]. DCF is detected by fluorescence spectroscopy on a plate reader with maximum excitation and emission wavelengths of 485 nm and 535 nm, respectively.

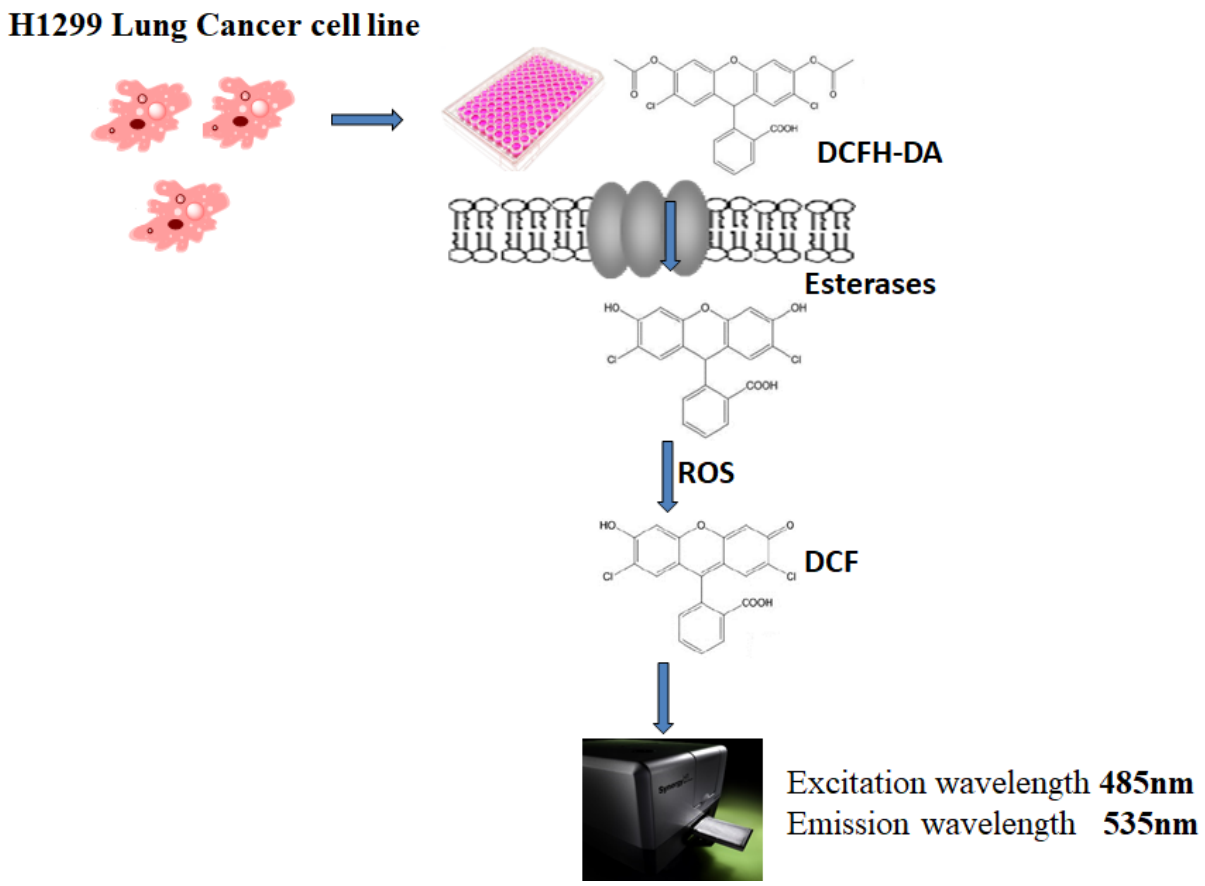

Figure 29- DCF Assay work flow.

2.6.2 Results

2.6.2.1 Optimization of DCF Assays using hydrogen peroxide and diamide

DCF assay was optimized using hydrogen peroxide and diamide in H1299 lung cancer cell line (Figure 29). Intracellular ROS levels were initially measured 5 minutes after cells were treated with various concentrations of hydrogen peroxide. This was repeated periodically after 30 minutes, 1 hour and 4 hours. The fluorescence signals showed time- and concentration-dependent change. The fluorescence signals, generated by 500 µM hydrogen peroxide, were increased by over 2-fold in 4 hours (Figure 30). On the other hand, the fluorescence signals were increased by 2-fold in 3 hours and 6-fold upon incubation of 300 µM and 1 mM diamide, respectively (Figure 31). Diamide concentrations beyond 2 mM did not induce further increase in ROS (Figure 30). Additionally,

glycolytic inhibitor 2-deoxy-D-glucose (10mM) was evaluated and compared for fluorescence signals generated on treatment of cells with hydrogen peroxide (25 µM), and diamide (500 µM) (Figure 31). These low concentrations of hydrogen peroxide and diamide induced higher ROS levels than 2-deoxy-D-glucose (10 mM).

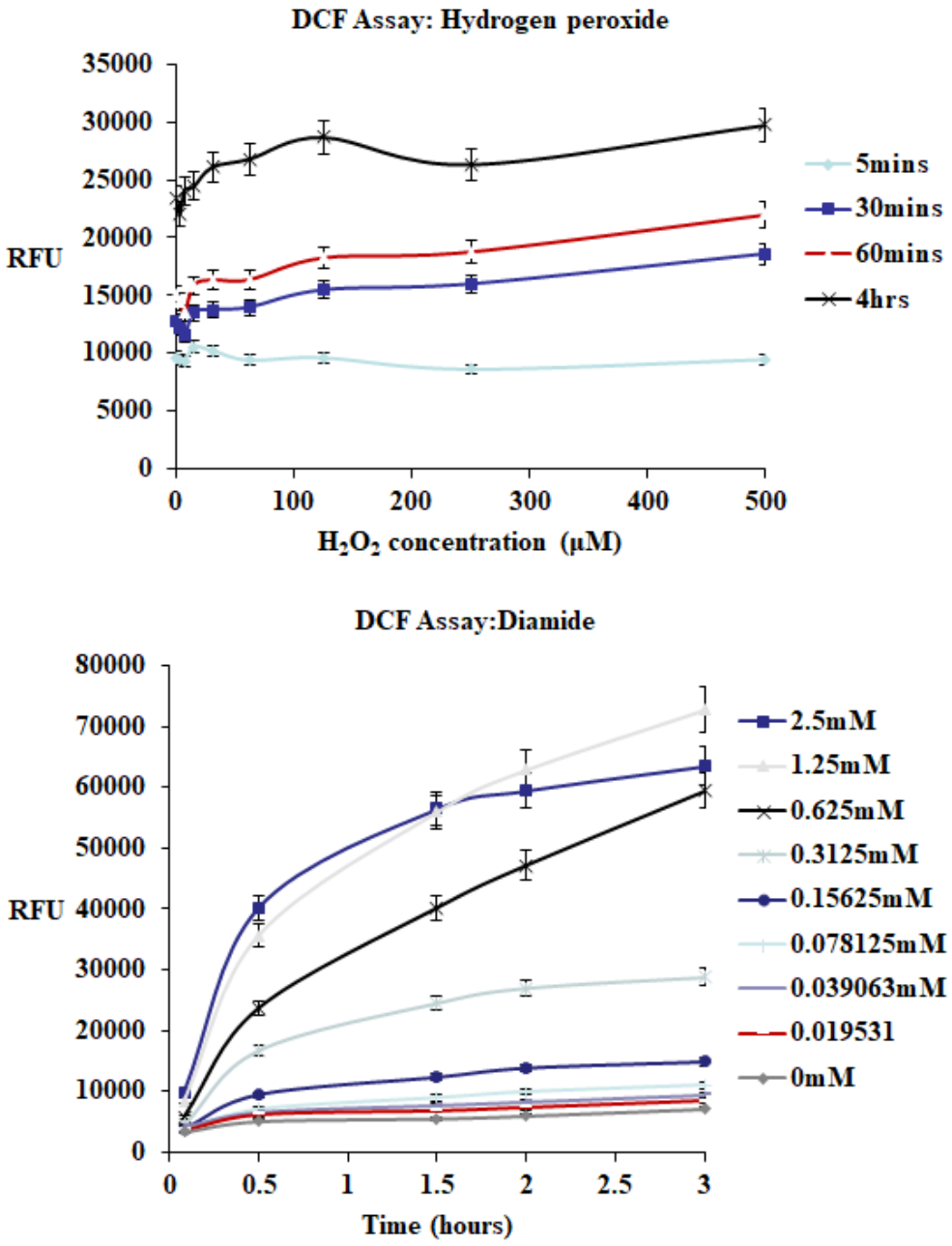

Figure 30-ROS levels generated in H1299 cells treated separately with hydrogen peroxide and diamide.

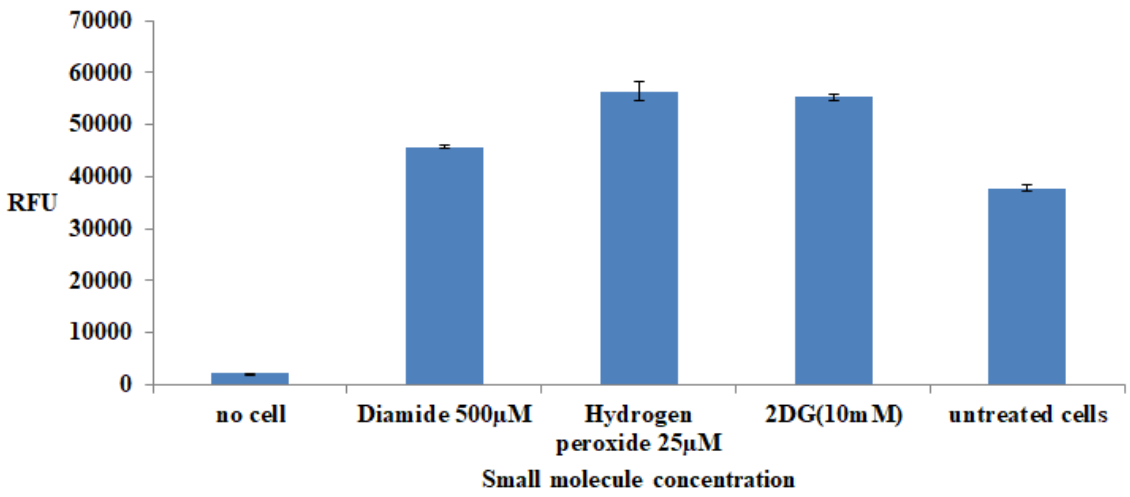

Figure 31-Comparison of ROS levels generated by various ROS inducers.

2.6.3 Evaluation of carbohydrates for ROS induction in H1299 cells

Various carbohydrates were evaluated for ROS induction in H1299 cells using the DCF assay at 4 hours post treatment. Monosaccharides, including D-glucose, D-galactose, D-mannose, D-xylose, D-arabinose and L-arabinose did not induce any significant change of ROS levels (Figure 32-33, 36).

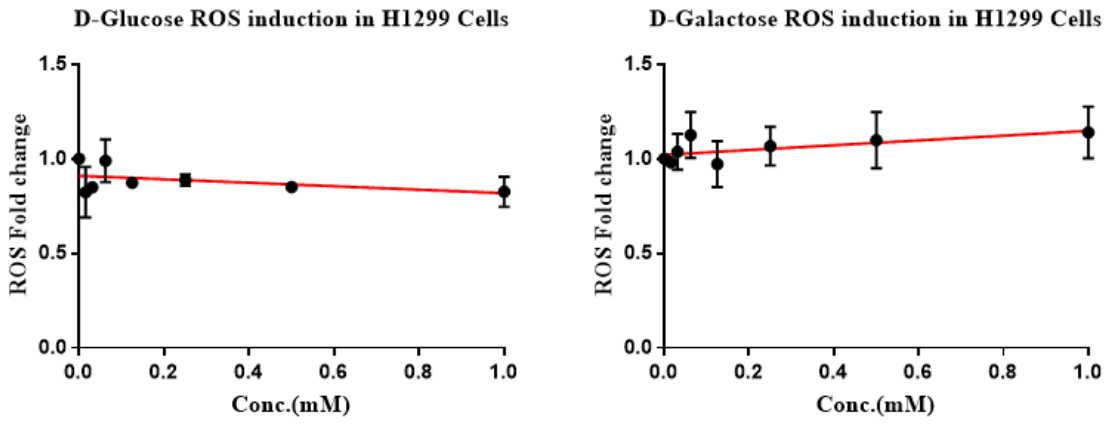

Figure 32-ROS levels generated by D-glucose and D-galactose in H1299 cells.

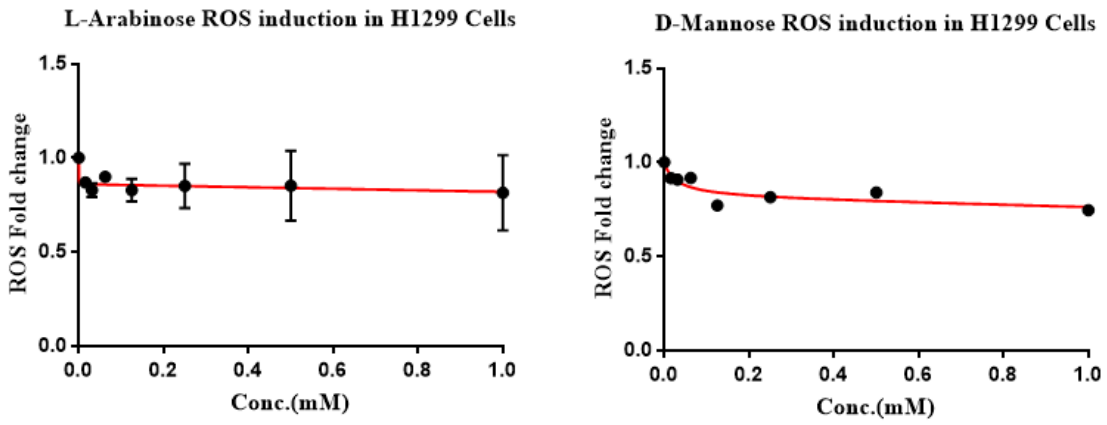

Figure 33-ROS levels generated by L-arabinose and D-mannose in H1299 cells.

2.6.4 Carbohydrate-based small molecule evaluation for ROS induction in H1299 cells

The DCF assay of the small molecule library revealed that most of these molecules did not induce generation of ROS at levels higher than untreated controls (Figure 34). However, 13 molecules induced ROS generation at levels that were 50% higher than the untreated cells. Of note, were small molecules that contained the 1-naphthylamine moiety (denoted as 8 series) that induced ROS at levels 2-fold higher than the untreated controls. These 8-series molecules were later evaluated for ROS-induction in a concentration-dependent manner.

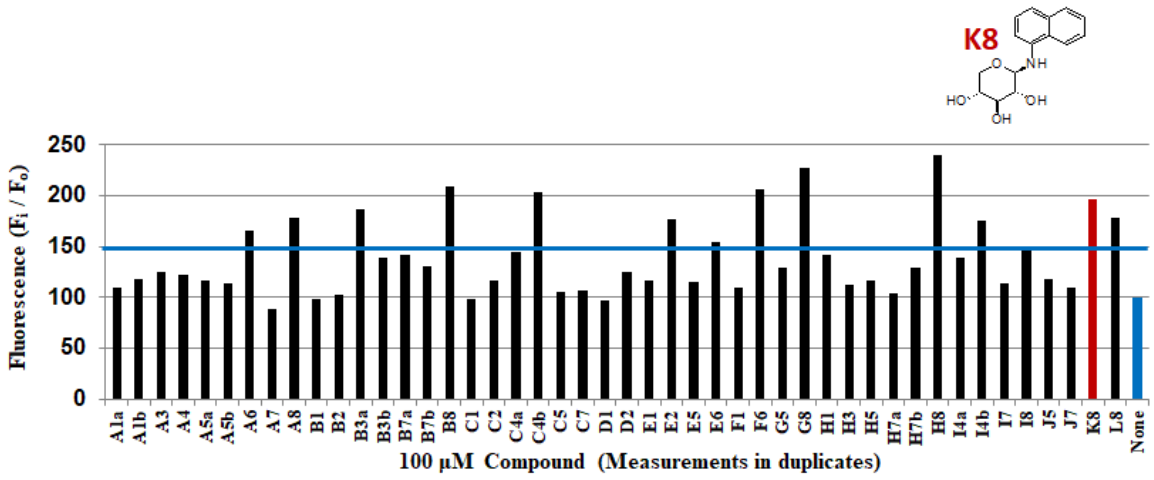

Figure 34-ROS induction screening of carbohydrate-based small molecules in H1299 cells.

2.6.5 ROS induction with serum starvation

H8 and K8 was evaluated for ROS-induction with and without serum (Figure 35). Higher ROS levels were generated with serum starvation prior to compound treatment. Subsequently, other experiments were performed without serum. H8 with serum starvation showed over 3-fold increase in ROS, more than H8 with serum at 100 µM. On the other hand, K8 at 100 µM with serum starvation showed over 6-fold increase in ROS induction than K8 with serum in six hours.

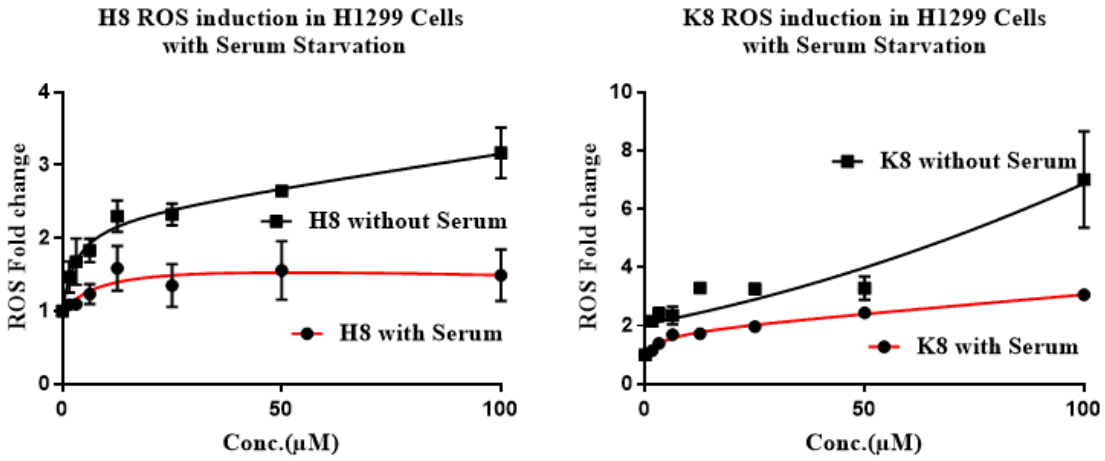

Figure 35-ROS levels generated by H8 and K8 with and without serum starvation

Fetal bovine serum (FBS) is added to mammalian cell growth media to provide key growth promoting ingredients needed for cell proliferation. It contains growth factors, hormones, attachment and spreading factors, minerals, trace elements, lipids, and various other factors that are necessary for cell growth, differentiation, transport, attachment, spreading, pH maintenance, and protease inhibition[178-179]. Importantly, these ingredients in serum modulate ROS[180-181]. The ROS data obtained with H8 and K8 molecules are consistent with the foregoing observations, and subsequently, serum was excluded in all ROS measurements.

2.6.6 Concentration-dependent evaluation of ROS induction by 1-naphthylamine-containing small molecules (8 series compounds)

Concentration-dependent evaluation of ROS induction was done on A8, C8, L8, H8, and K8 (Figure 36-37). Most of these molecules (A8, C8, G8 and L8) showed a small increase of ROS induction. Of note is the correlation of ROS levels to the structure of compounds. For example, A8 (glucose conjugate) and G8 (galactose conjugate) which are epimers, differ only in sugar stereochemistry at carbon-4, and had similar ROS induction pattern. Of interest were H8, K8 and K8A, which showed up to 2-fold increase in ROS within 100 µM in H1299 cells (Figure 37). H8 and K8 have similar structure with different stereochemistry at carbon position 2 and 3 on the sugar. Importantly, K8A generated higher ROS levels than glycolytic inhibitor 2-DG.

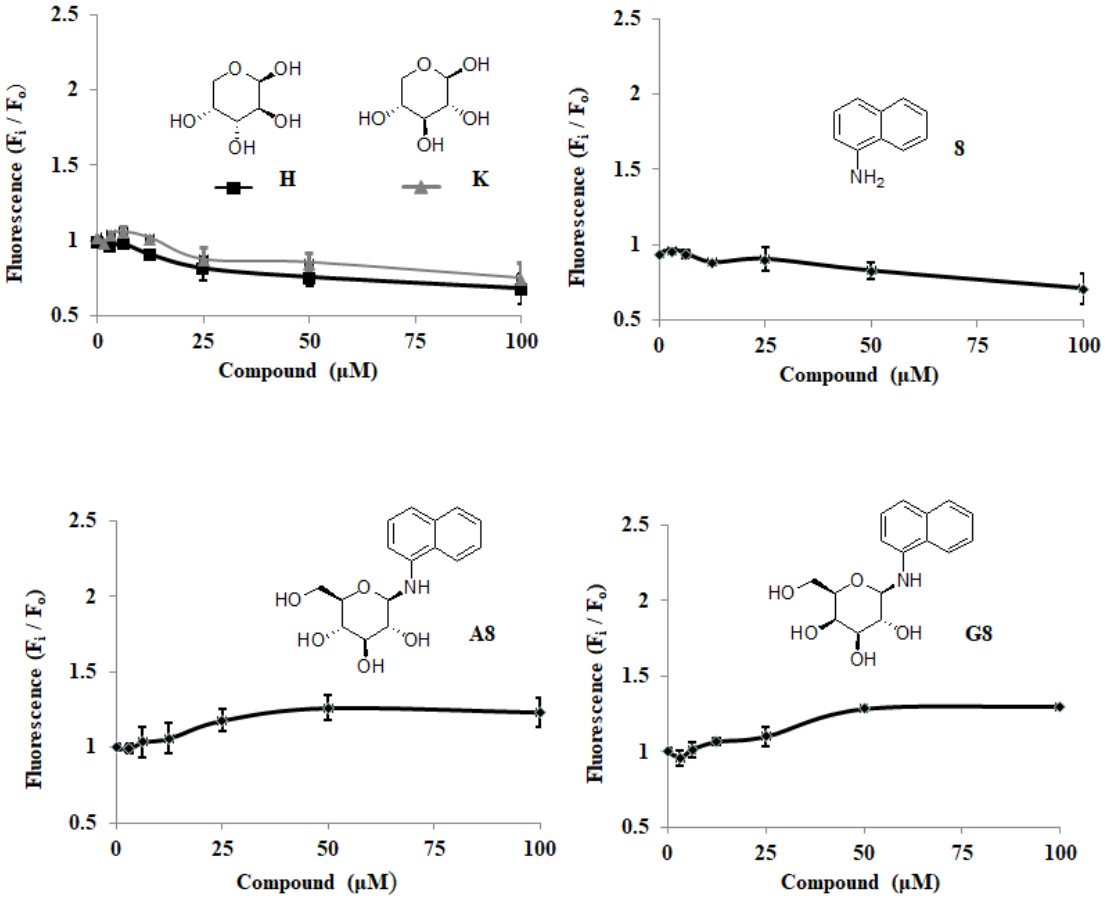

Figure 36-ROS levels generated by D-arabinose (H), D-xylose (K), A8 and G8.

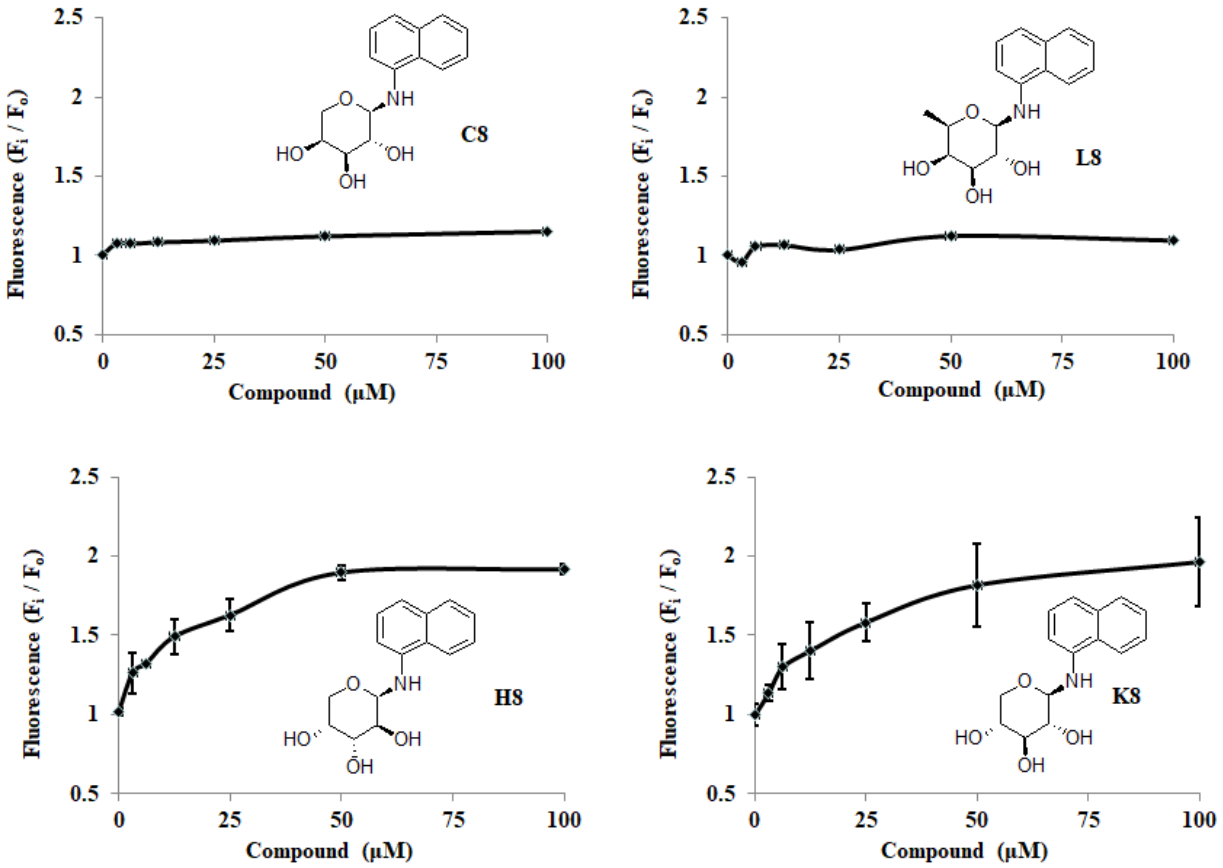

Figure 37-ROS levels generated by C8, L8, H8 and K8 in H1299 cells.

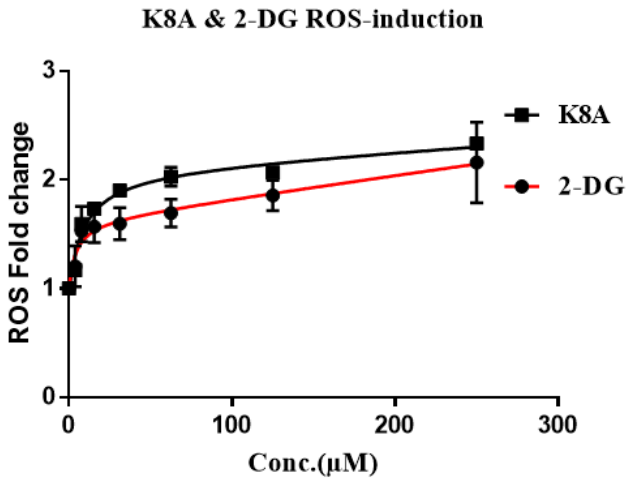

Figure 38-ROS levels generated by K8A and 2-DG in H1299 cells.

2.6.7 Discussion on ROS evaluation

Glucose and other monosaccharides are major precursors of NADPH biosynthesis that is important for maintaining redox homeostasis in cells. NADPH is also produced by malic enzyme 1 (ME1), isocitrate dehydrogenase 1 (IDH1), hexose-6-phosphate dehydrogenase and by one-carbon metabolism[182-184]. Conversely, glucose deprivation induces ROS production and oxidative stress due to low levels of NADPH in a cell. Glucose and other hexoses reduce ROS and reverse oxidative stress induced by glucose deprivation[185-187].

Expectedly, our data indicate that D-glucose, D-mannose, D-xylose, D-arabinose, and L-arabinose do not disrupt redox homeostasis or induce ROS at low concentrations. Exceptionally, glycolytic inhibitors, such as 2-DG, deprives cells of NADPH by blocking phosphorylation of glucose to reduce glucose flux to NADPH-producing PPP. Of note is the small molecule library screening that revealed ROS generation by N-naphthyl-D-arabinose (H8), N-naphthyl-D-xylose (K8) and acetylated N-naphthyl-D-xylose (K8A). Importantly, K8A induced ROS at higher levels than 2-DG.

Structurally, H8 and K8 contain a similar monosaccharide with D-arabinose (H) and D-xylose (K), respectively, which are pentoses with a reversed stereochemistry at 2-OH and 3-OH positions. Additionally, there was no increase of ROS by C8 that contain L-arabinose, showing the differential effect of the stereochemistry of D-arabinose in H8 versus L-arabinose in C8. On the other hand, A8 and C8 did not induce a significant increase of ROS level, suggesting that hexoses are less effective for ROS production. Additionally, C8 (L-arabinose conjugate) and L8 (D-fucose conjugate) had identical ROS induction patterns. Together, these ROS data suggest that the methyl or hydroxymethyl group at the fifth position of a hexopyranose may not be important for ROS induction, whereas 1-naphthylamine moiety contributes to ROS induction.

2.6.8 Experimental procedures

2.6.8.1 Cell culture

H1299 cells were cultured as monolayers at 37 ºC in a humidified incubator with 95% air and 5% CO_2 in RPMI media supplemented in 10% FBS and penicillin (mg/mL) and streptomycin (µg/mL). A549, LNCaP, MDA-MB 231, MDA-MB 453, and MCF7, Hela cells were separately cultured as monolayers at 37 ºC in a humidified incubator with 95% air and 5% CO_2 in DMEM supplemented in 10% FBS and penicillin (mg/mL) and streptomycin (µg/mL). Cells were maintained in sterile conditions and split in new media every 3-4 days. The cells were trypsinized, counted using a hemocytometer, and diluted to ensure 10,000 cells per well in a 96-well plate. The cells were then left overnight to attach on the bottom surface before DCF or MTT assay.

2.6.8.2 Protocol for quantification of ROS by DCF Assay

The DCF assay was optimized in a series of conditions using hydrogen peroxide and diamide. About 10,000 cells were seeded per well and incubated at 37 ºC, 5% CO_2 for 24 hours for attachment on 96-well black plates with transparent bottom. Cells were then washed with warm PBS. 25 µM of DCFH-DA was then added, and cells were incubated in the same conditions for 45 minutes. Cells were then washed with RPMI medium without phenol-red, followed by duplicate addition and serial dilution of small molecules. The ROS signal was compared with that of untreated cells. Fluorescence emission scan was done at wavelengths between 520 nm and 580 nm after excitation at 485 nm. This was periodically done at various time points. ROS levels were recorded as relative fluorescent units (RFU) and plotted as mean RFU for various concentrations and time points.

2.7 Cytotoxicity evaluation of small molecules in mammalian cells

Cell viability of adherent cells was measured by using the 3-(4,5-dimethylthiazol-2-yl)-diphenyl tetrazolium bromide (MTT) assay, which is based on the conversion of MTT to formazan by mitochondrial and cytosolic dehydrogenases[188]. Solubilized formazan is detected by measuring ultra-violet (UV) absorbance at 490-570 nm. MTT assay is therefore effective in determining viable cells and is widely used in drug screening tests. Viability of suspension cells (Daudi and Raji) was measured using the Trypan blue assay and an automated cell counter[189-190]. Additionally, the NCI-60 human tumor cell lines screen was also used to screen the hit compound K8A in 60 different human tumor cell lines, that include leukemia, melanoma, colon, lung, ovary, brain, prostrate, breast, and kidney cancer.

2.7.1 Optimization of viability assay using MTT assay

Optimization of MTT assay was done using L744832, PD18352 and sulforaphane (Figure 2.26). L744832 is a farnesyl transferase inhibitor that is highly toxic to cancer cells[191]. PD184352 is an ATP non-competitive mitogen-activated protein kinase kinase (MEK1/2) inhibitor[192]. Sulforaphane [1-isothiocyanato-4-(methylsulfinyl) butane] is a highly potent inducer of phase 2 cytoprotective enzymes with anticancer activity[193]. Additionally, cell viability of two ROS-generating molecules (hydrogen peroxide and diamide) were evaluated in two lung-cancer cell lines, H1299 and A549. H1299 cells is an immortalized human non-small cell lung carcinoma cell line with a homozygous partial deletion of the *TP53* gene[194]. H1299 cells do not express the tumor suppressor p53 protein. A549 cells are adenocarcinoma lung cancer cells[195] that express p53.

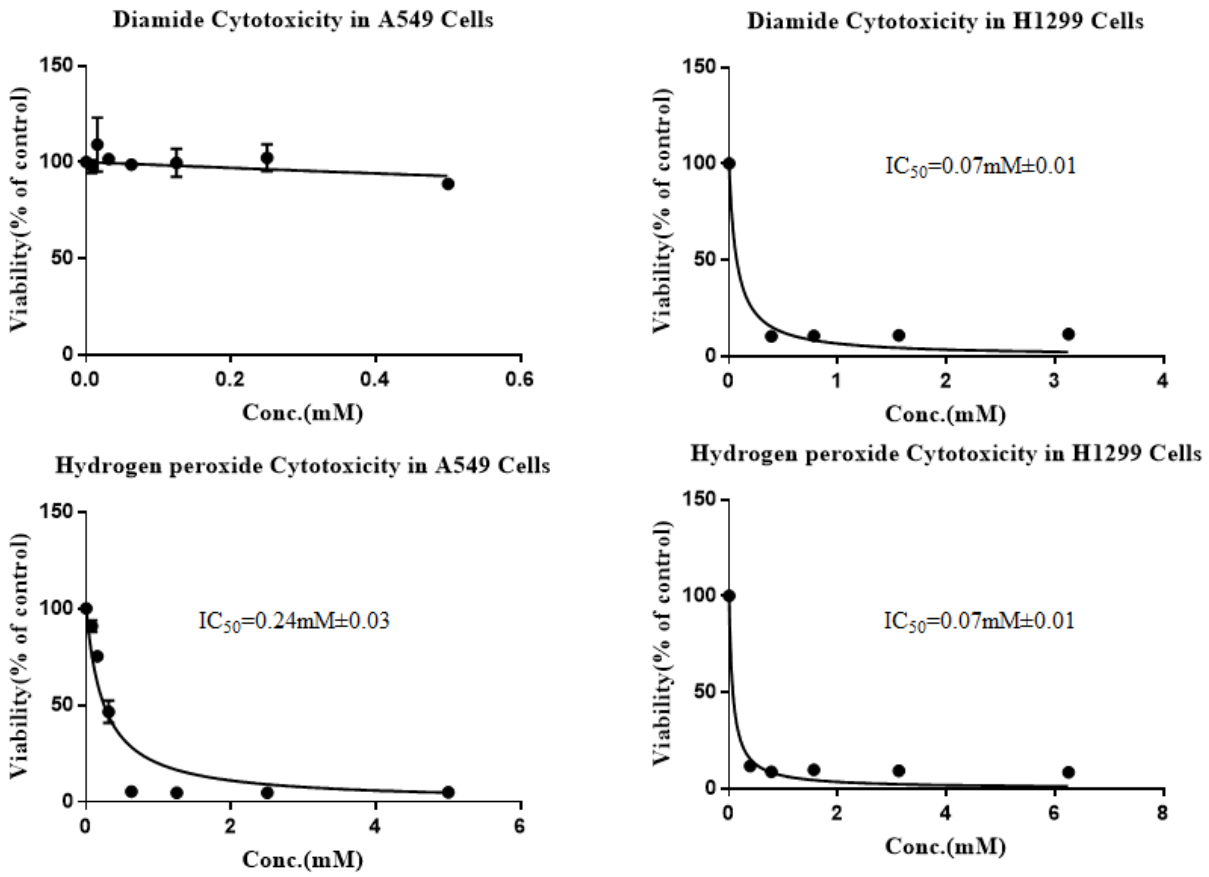

Figure 39-Diamide and hydrogen peroxide cytotoxicity in A549 and H1299 cells.

L744832 (IC_{50} = 2.25µM), PD18352(IC_{50} = 3.86µM) and sulforaphane (IC_{50} = 10.9µM) potency in H1299 cells was comparable to reported IC_{50} values. For example, sulforaphane had an IC_{50} of 9.52±1.23µM in H1299[196] cells and 10.2 ±0.12 µM in A549 cells in recent studies[197]. Additionally, the decreased potency of sulforaphane (IC_{50}=21.3±2.05µM) was shown in KRAS-stable H1299 cells (Figure 40), and other cell lines as reported previously[196, 198]. Furthermore, cytotoxicity hydrogen peroxide and diamide in A549 and H1299 lung cancer cells was consistent with literature reports on similar assays[199-200]. Diamide is a strong thiol oxidizing agent that causes accumulation of ROS[201-202].

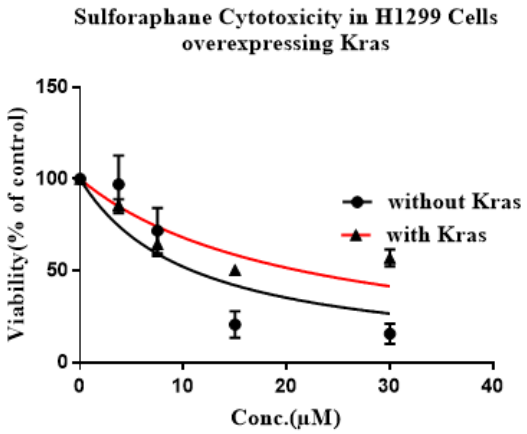

Figure 40-Sulforaphane cytotoxicity in H1299 cells overexpressing KRAS.

2.7.2 Cytotoxicity screening of carbohydrate-based small molecules

The cytotoxicity screening (Figure 41) of the carbohydrate-based small molecules revealed that K8 (40% viability at 100 µM) and H8 (20% viability at 100 µM) were the most potent cytotoxic molecules in H1299 cells that generated the highest levels of ROS and were eligible candidates for subsequent assays (Figure 2.29). Concentration-dependent cytotoxicity was observed with H8 and K8 in the same cell line.

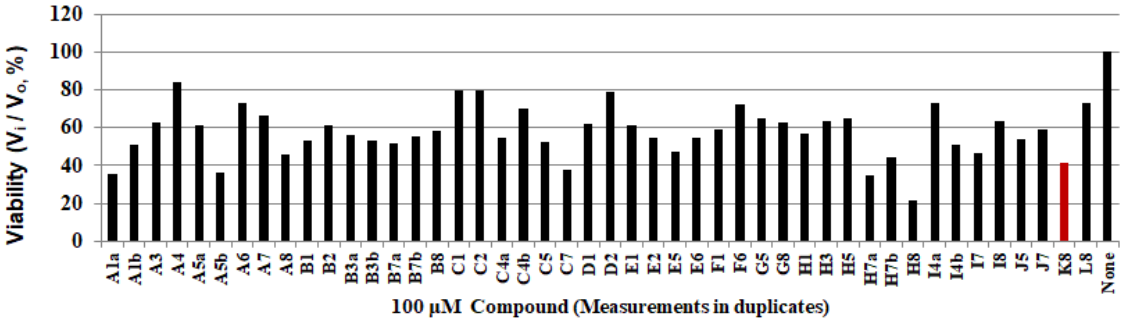

Figure 41-Carbohydrate-based small molecule cytotoxicity screening in H1299 cells

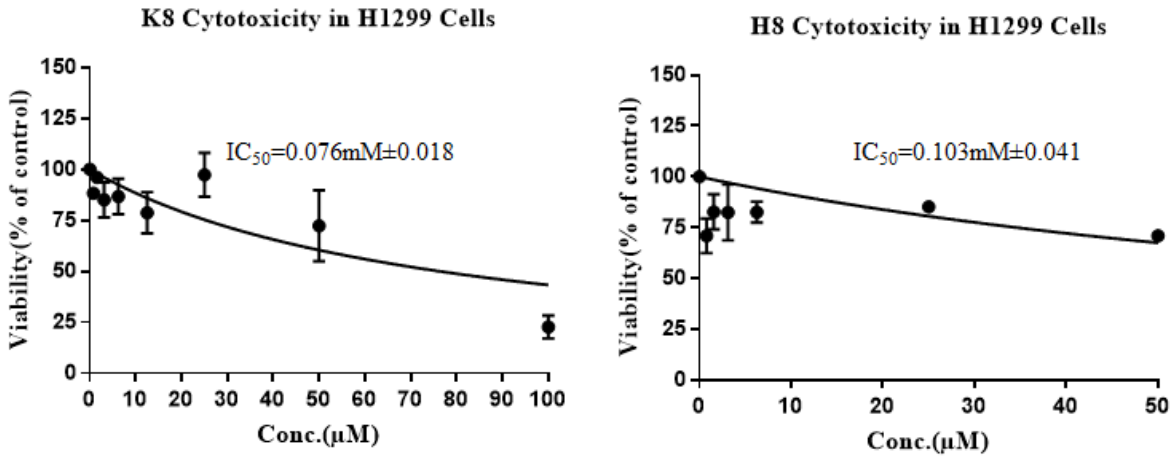

Figure 42-K8 and H8 cytotoxicity in H1299 cells

2.7.3 Cytotoxicity evaluation of carbohydrates in mammalian cells

Evaluation of various monosaccharides revealed that many sugars had no or low cytotoxicity in H1299 cells at the concentrations tested (Figure 43). The IC_{50} values of 2-DG was approximately 0.79mM, which was the most cytotoxic monosaccharide in the H1299 lung cancer cell line. The observed 2-DG IC_{50} in H1299 cells is consistent with literature values in similar cell lines[37].

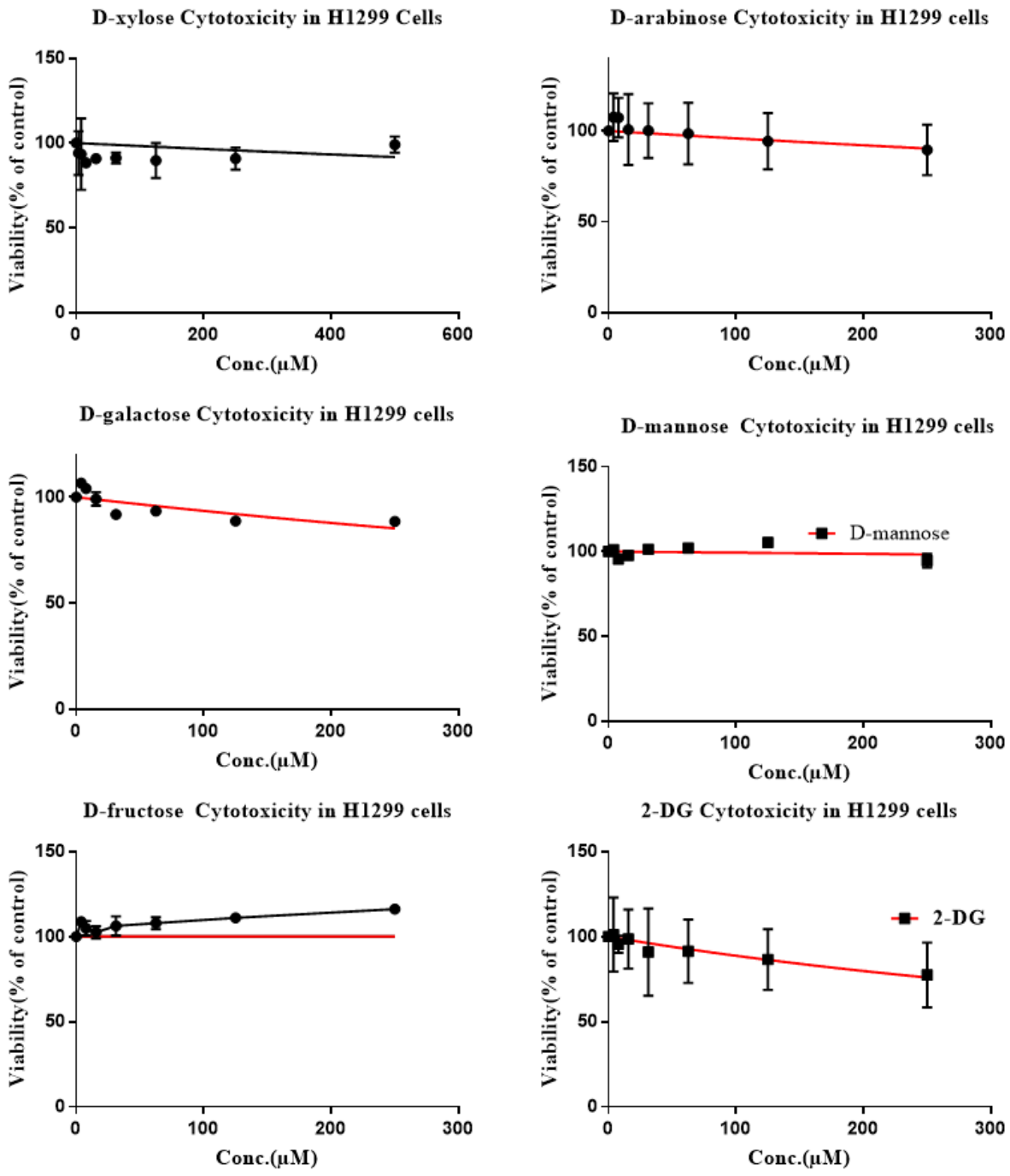

Figure 43-D-xylose, D-arabinose, D-galactose, D-mannose, D-fructose and 2-deoxy-D-glucose cytotoxicity in H1299 cells.

2.7.4 K8A cytotoxicity evaluation in mammalian cells

2.7.4.1 K8A is more potent than 2-DG in various mammalian cell lines

K8A was more potent than 2-DG in H1299, A549, MDA-MB 231 and LNCaP cell lines (Figure 44). The IC_{50} values of 2-DG were in the range of 0.7-3 mM and was more than 10-fold higher than the IC_{50} of K8A in cancer cell lines. K8A IC_{50} were in the range 0.05mM-0.15mM (50-150µM) in H1299 (IC_{50} = 0.045 mM), A549 (IC_{50} = 0.029 mM), MDA-MB 231 (IC_{50} = 0.137 mM), Raji (IC_{50} =0.03mM) and Daudi (IC_{50} =0.08mM) (Figure 44). K8A IC_{50} was low in a prostate cancer cell line, LNCaP. Additionally, K8A was more potent than the acetylated form of 2-deoxy-D-glucose (2DGA) in H1299 (Figure 45), MDA-MB 231(Figure 46), LNCaP (Figure 47), DU145 cell lines (Figure 48), Hela cells (Figure 49) and A549 (Figure 50) (Table 1). Notably, K8A was more potent than 2DG8A in most cells including MCF7 (Figure 51), which is a glycoconjugate of acetylated 2-deoxy-D-glucose and 1-naphthylamine and is therefore structurally like K8A.

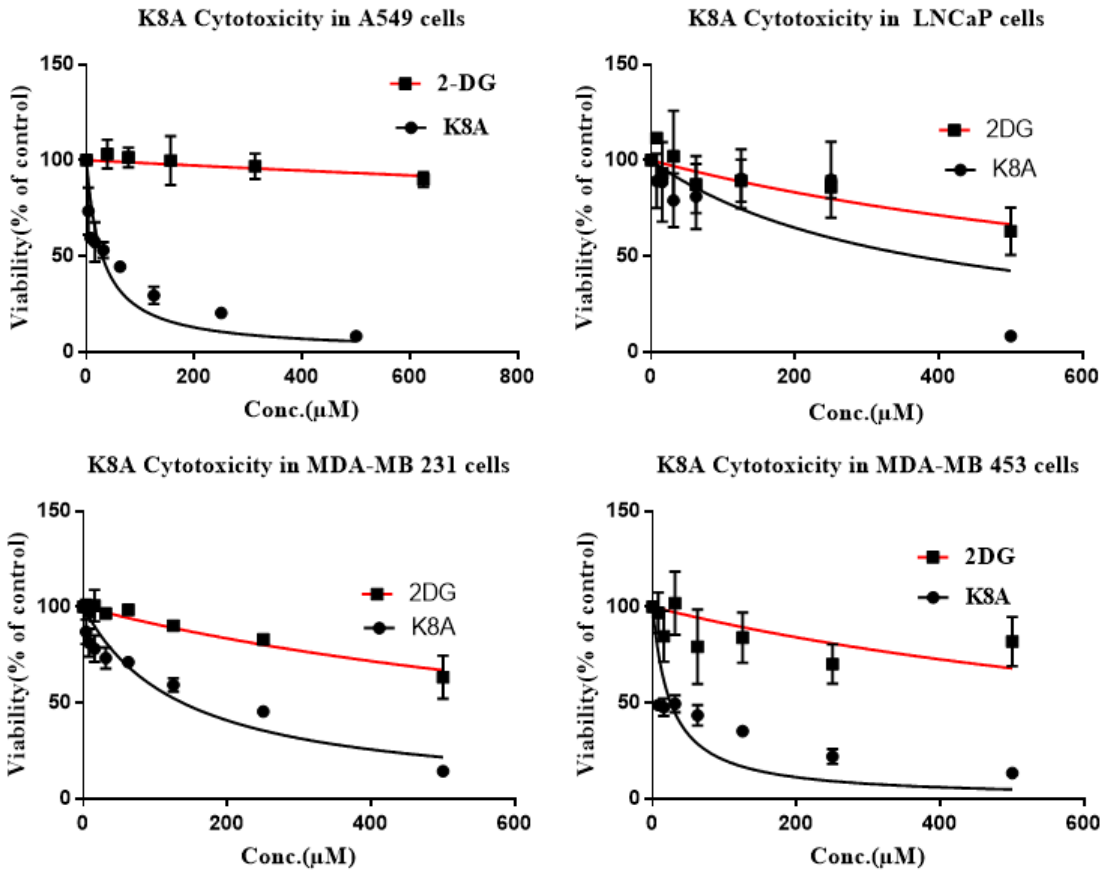

Figure 44-K8A cytotoxicity in A549, LNCaP, MDA-MB 231 and MDA-MB 231 cells

Table 1**:** Cytotoxicity of various carbohydrate-based small molecules in various cancer cell lines

Cell line	**Cell type**	**K (mM)**	**KA (mM)**	**K8 (mM)**	**K8A (mM)**	**2DG (mM)**	**2DGA (mM)**	**2DG8A (mM)**
H1299	Lung	~5.54	~2.51	0.076±0.19	0.045±0.003	0.79±0.32	0.145±0.032	0.151±0.027
A549	Lung	~2.95	~7.96	0.122±0.26	0.029±0.005	3.87±0.58	ND	ND
231	Breast	ND	0.19.1±0.03	ND	0.138±0.019	1.01±0.11	0.146±0.026	0.205±0.047
453	Breast	ND	ND	ND	0.024±0.004	1.06±0.36	ND	0.019±0.003
MCF7	Breast	ND	ND	ND	0.049±0.01	ND	ND	0.95±0.013
DU145	Prostrate	ND	0.52±0.12	ND	0.072±0.007	ND	0.228±0.037	0.12±0.014
LNCaP	Prostrate	ND	ND	ND	0.365±0.135	0.995±0.25	ND	0.635±0.295
Hela	Cervical	ND	0.86±0.25	0.103±0.02	0.104±0.013	ND	ND	ND
Daudi	lymphoma	ND	ND	ND	~0.08	ND	ND	ND
Raji	lymphoma	ND	ND	ND	~0.03	ND	ND	ND

ND: Not determined

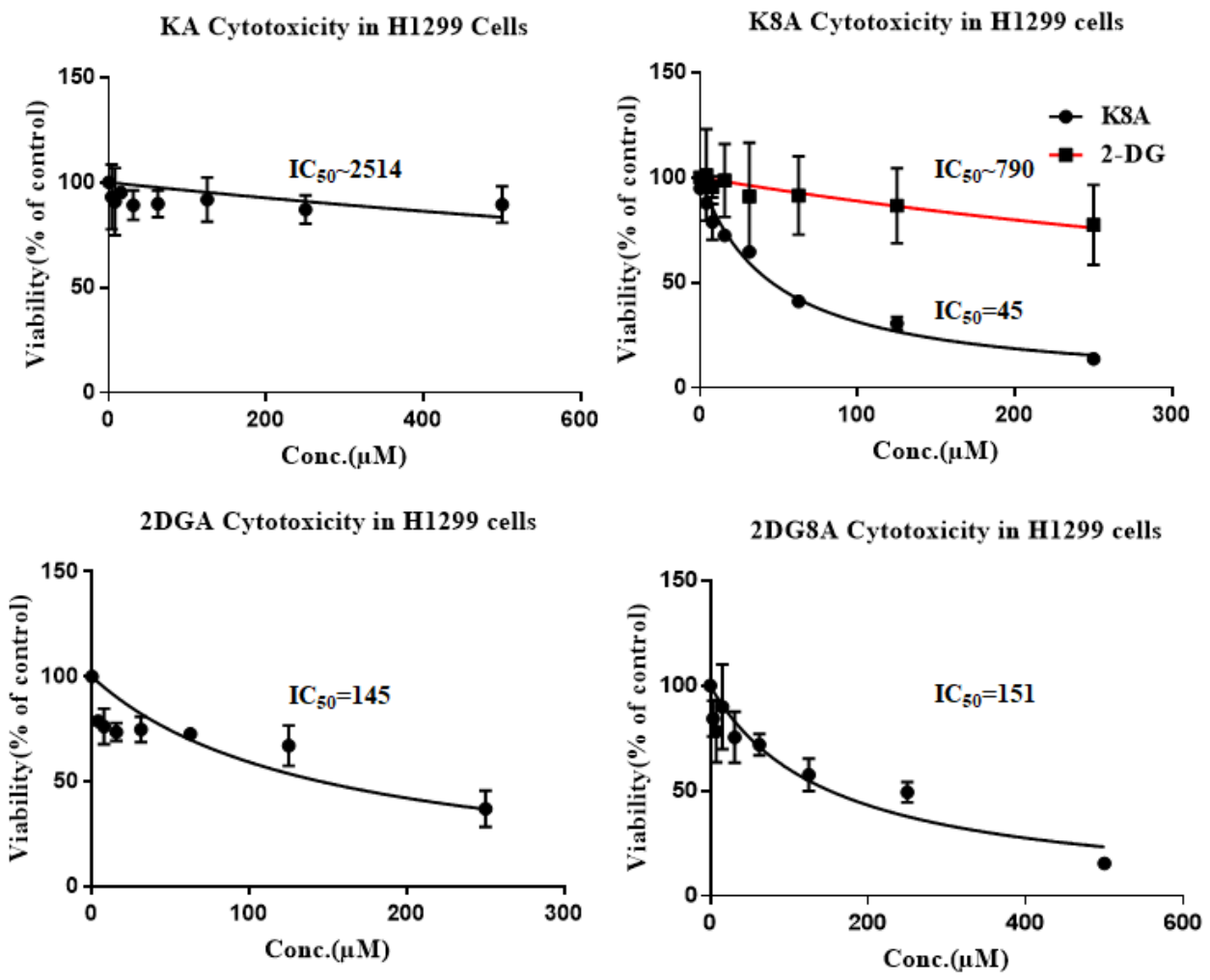

Figure 45-KA, K8A, 2DGA and 2DG8A cytotoxicity in H1299 cells

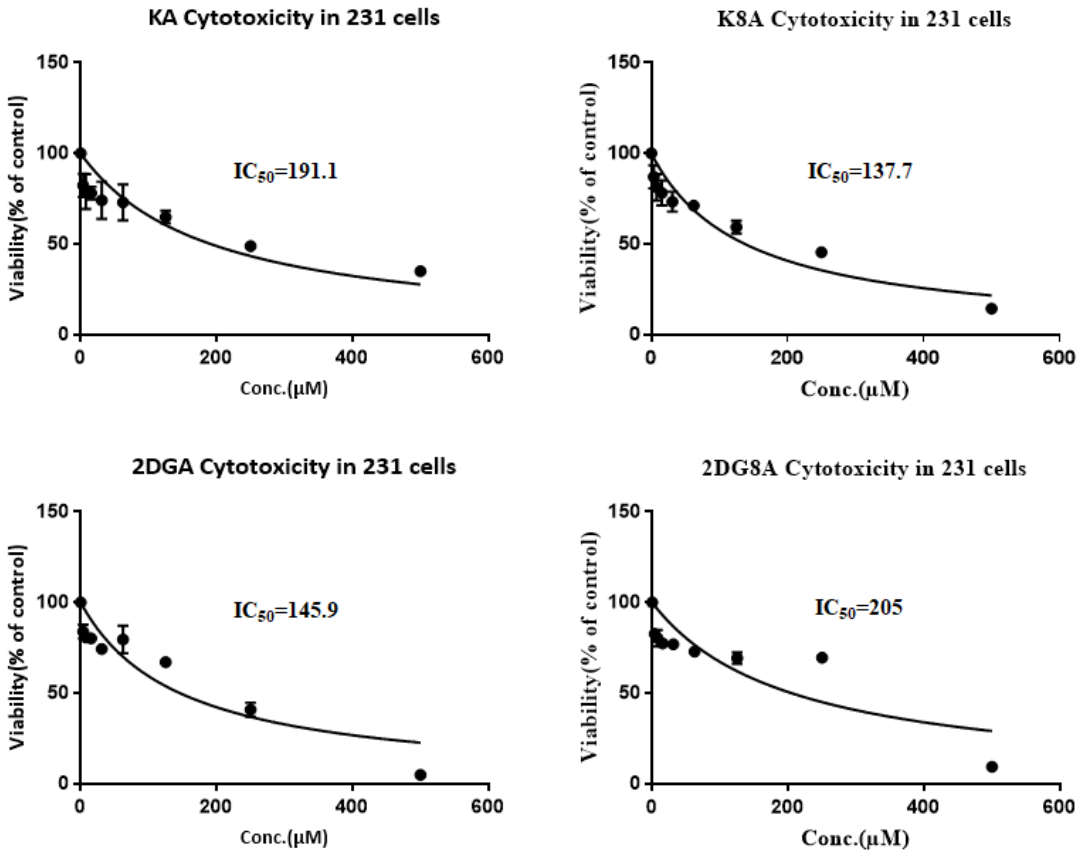

Figure 46-KA, K8A, 2DGA and 2DG8A cytotoxicity in MDA-MB 231 cells

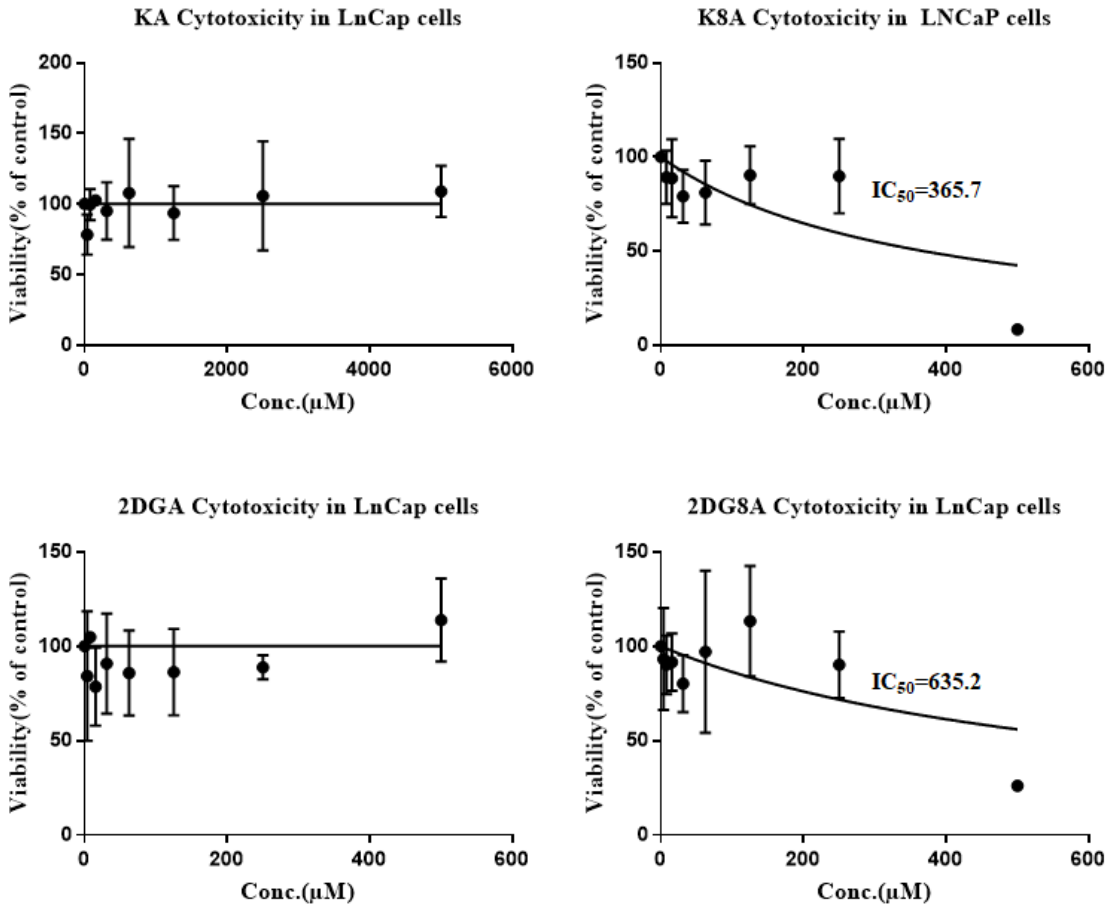

Figure 47-KA, K8A, 2DGA and 2DG8A cytotoxicity in LNCaP cells

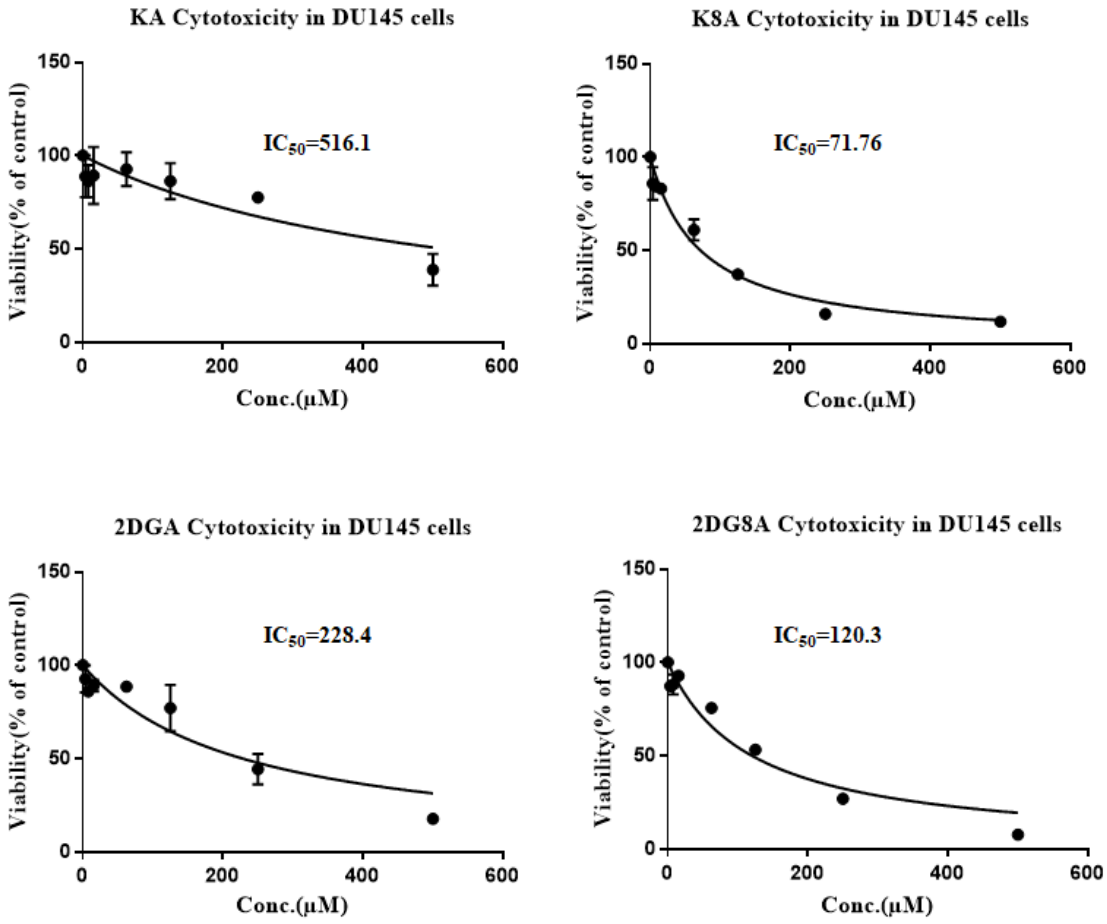

Figure 48-KA, K8A, 2DGA and 2DG8A cytotoxicity in DU145 cells

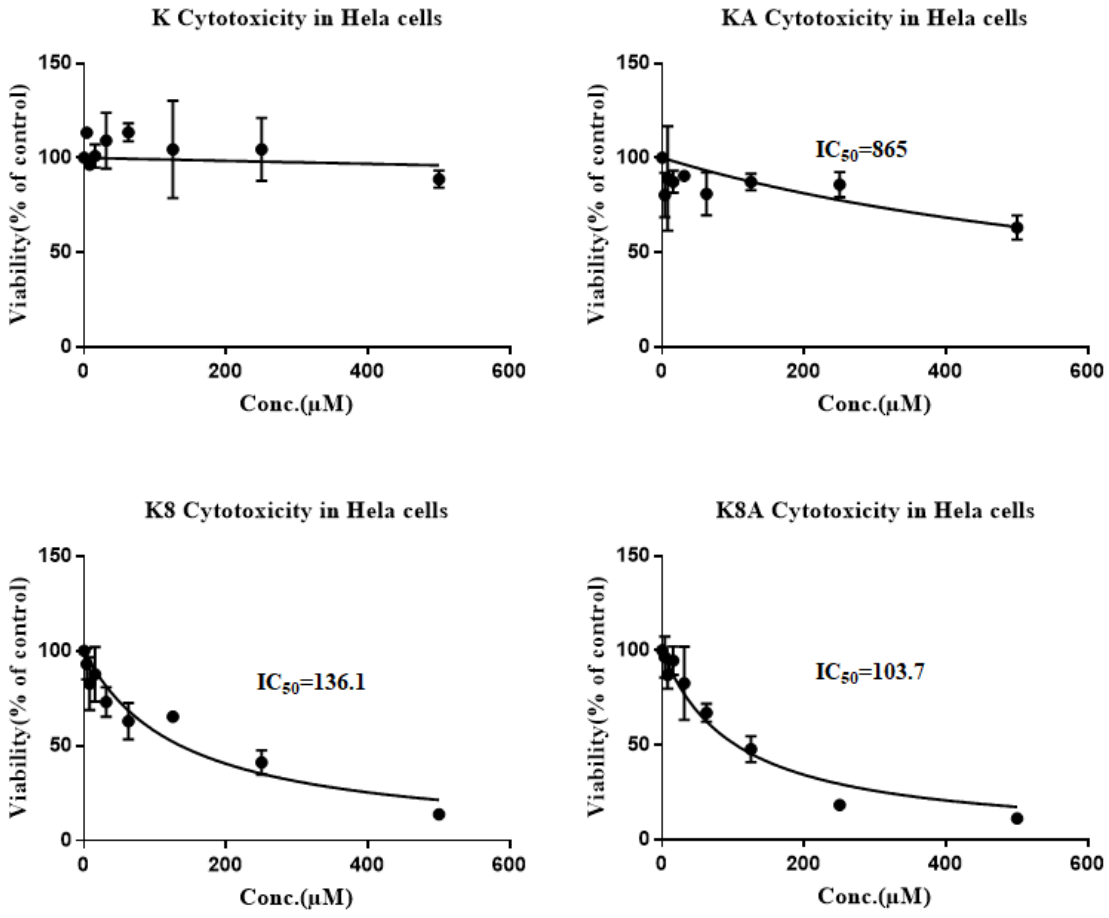

Figure 49-K, KA, K8 and K8A cytotoxicity in Hela cells

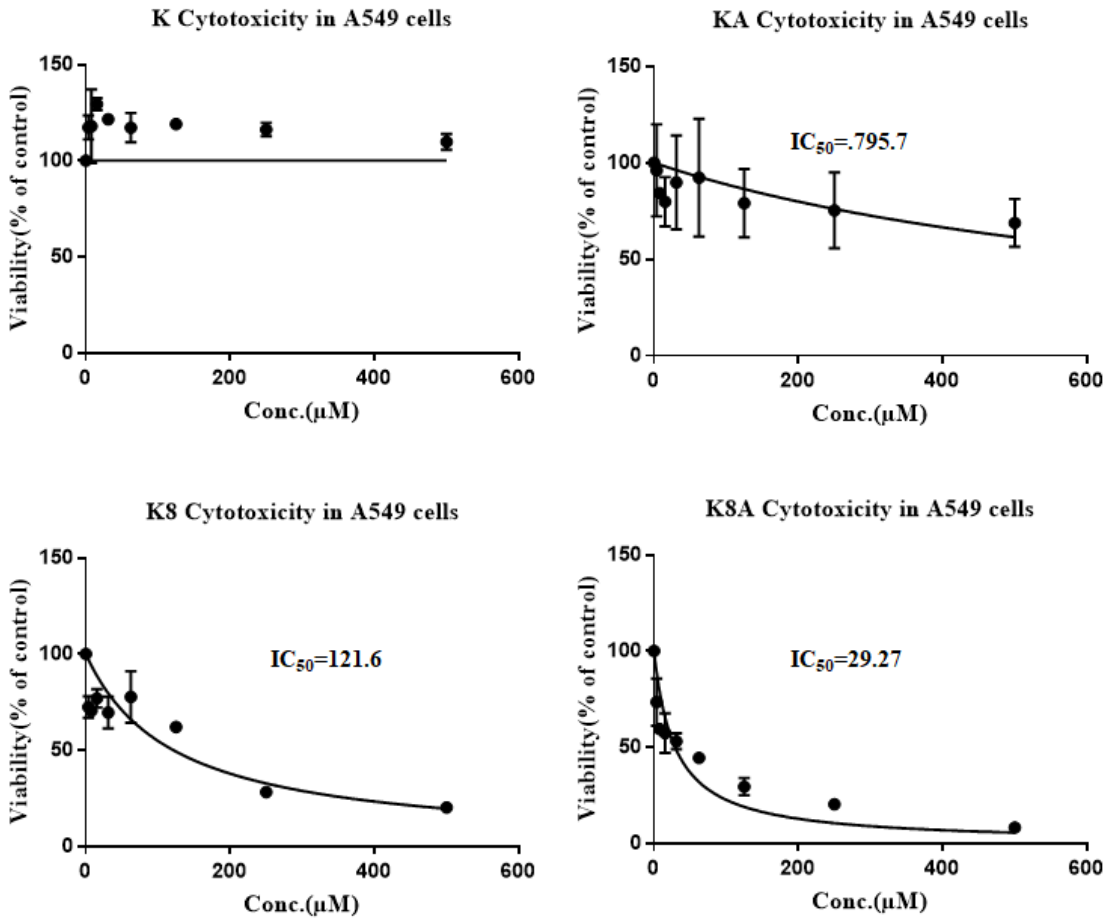

Figure 50-K, KA, K8 and K8A cytotoxicity in A549 cells

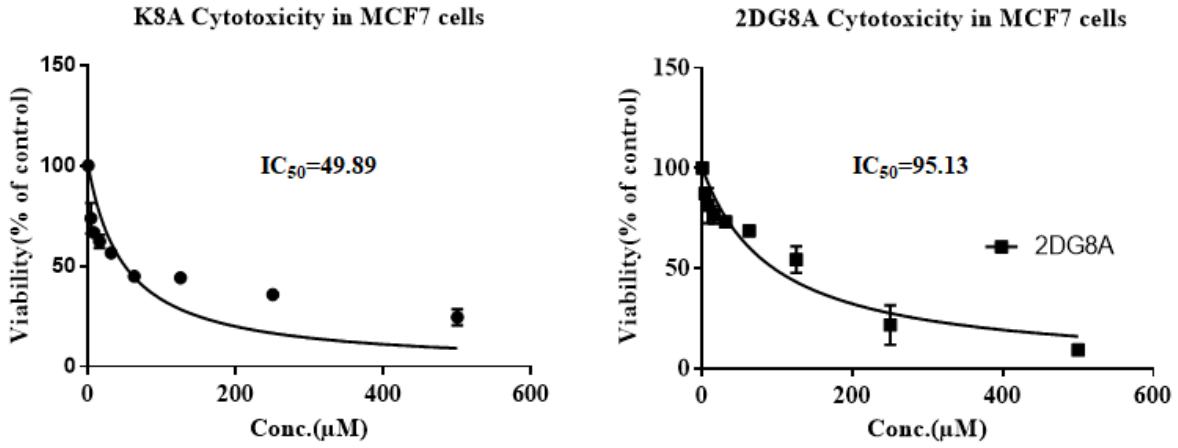

Figure 51-K8A and 2DG8A cytotoxicity in MCF7 cells

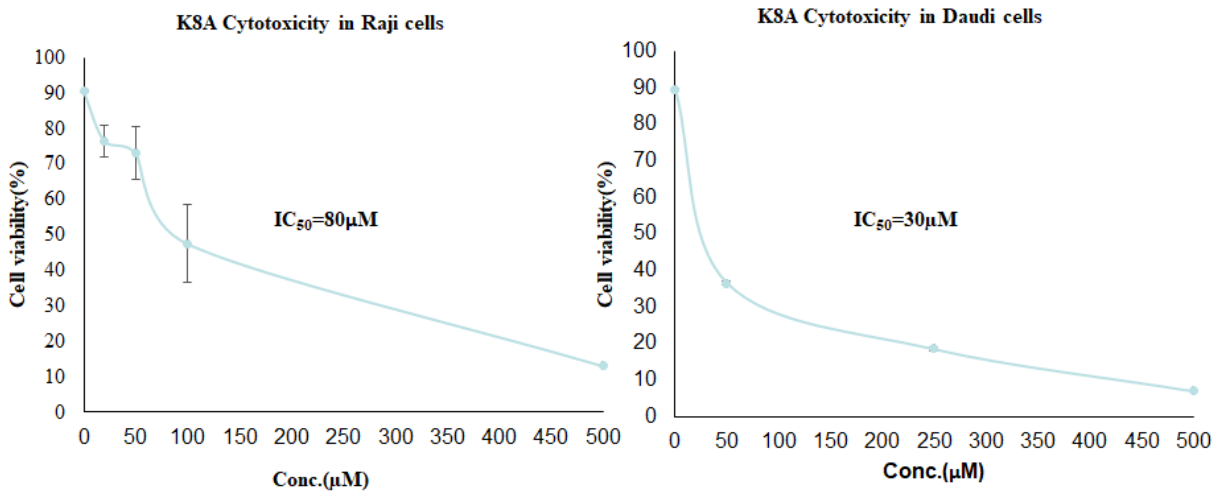

Figure 52-K8A cytotoxicity in Raji and Daudi cells

2.8 Evaluation of K8A in NCI-60 cell lines

To increase the scope of cancer cells potentially targeted by K8A, the compound was evaluated in NCI-60 cell lines with a sulforhodamine assay, showing growth inhibition of K8A in various cancer cell lines at a concentration of 10 µM (Figure 53). The data include growth inhibition (values between 0 and 100) and lethality (values less than 0). For example, a value of 0 means no net growth and a value of 100 means no growth inhibition over the course of the experiment (48 hours). NCI data revealed that K8A (10µM) had cytotoxicity in three cell lines, CCRF-CEM (Leukemia), NCI-H522 (Non-small lung cancer) and UO-31 (Renal cancer). The growth percent in CCRF-CEM, NCI-H522 and UO-31 was 71.71, 69.31 and 62.41 respectively at 10µM of K8A. This information is available for comparative analysis on NCI website (NSC D-793207/1).

Developmental Therapeutics Program

One Dose Mean Graph

NSC: D-793207 / 1	Conc: 1.00E-5 Molar	Test Date: Sep 12, 2016
Experiment ID: 1609OS82		Report Date: Sep 28, 2016

Panel/Cell Line	Growth Percent
Leukemia	
CCRF-CEM	71.71
RPMI-8226	87.94
Non-Small Cell Lung Cancer	
A549/ATCC	102.27
EKVX	99.79
HOP-62	94.05
HOP-92	104.42
NCI-H226	97.19
NCI-H23	94.81
NCI-H322M	94.36
NCI-H460	98.04
NCI-H522	68.31
Colon Cancer	
COLO 205	99.66
HCC-2998	94.22
HCT-15	93.98
HT29	84.24
KM12	84.16
SW-620	98.41
CNS Cancer	
SF-268	83.07
SF-295	94.49
SF-539	90.20
SNB-19	104.79
SNB-75	93.93
U251	104.81
Melanoma	
LOX IMVI	88.81
MALME-3M	86.87
M14	99.57
MDA-MB-435	101.77
SK-MEL-2	82.31
SK-MEL-28	109.76
SK-MEL-5	103.22
UACC-257	103.03
UACC-62	97.21
Ovarian Cancer	
IGROV1	97.93
OVCAR-3	95.69
OVCAR-4	103.24
OVCAR-5	99.99
OVCAR-8	101.82
NCI/ADR-RES	95.88
SK-OV-3	104.78
Renal Cancer	
786-0	107.14
A498	100.93
ACHN	98.76
RXF 393	105.20
SN12C	94.33
TK-10	115.23
UO-31	62.41
Prostate Cancer	
PC-3	90.76
DU-145	100.46
Breast Cancer	
MDA-MB-231/ATCC	88.99
HS 578T	96.31
BT-549	89.09
T-47D	86.64
MDA-MB-468	104.28
Mean	95.31
Delta	32.90
Range	52.82

Mean Growth Percent - Growth Percent

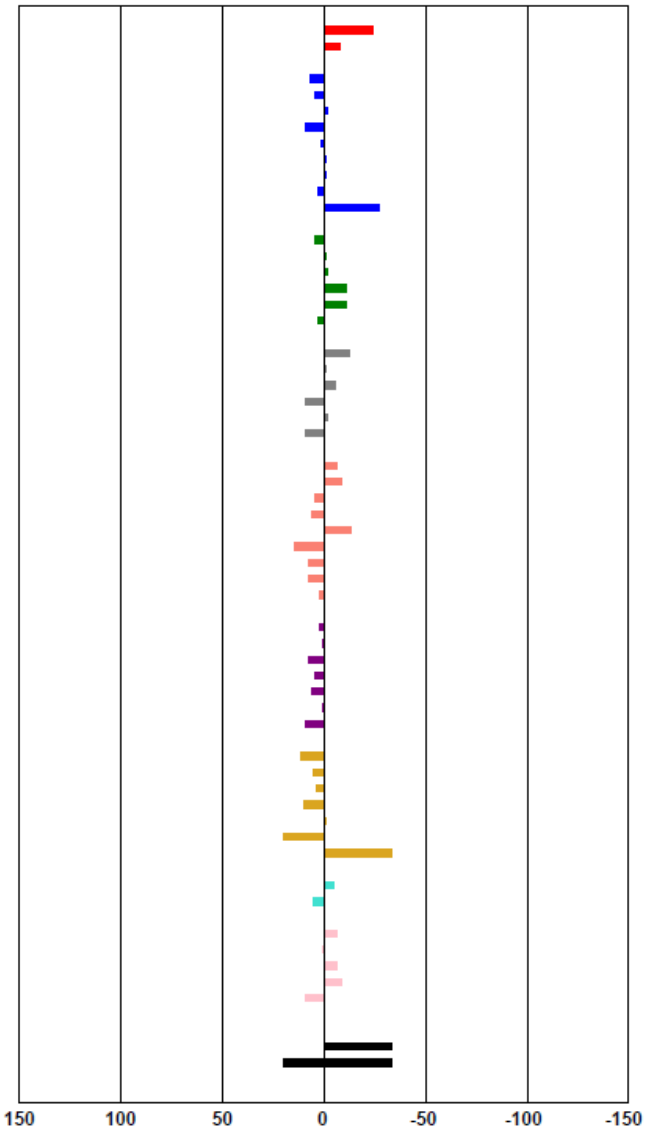

Figure 53-K8A cytotoxicity in NCI-60 cancer cell lines

2.8.1 Cytotoxicity evaluation of K8A analogues in mammalian cells

We evaluated acetylated N-naphthyl-β-D-xylose (K8A) and K8A analogs cytotoxicity using MTT assay in p53-null H1299 lung cancer cell (Figure 54, 57), p53-mutant expressing MDA-MB 231 breast cancer cell, and p53 wild-type expressing LNCaP prostate cancer, A549 lung cancer, MDA-MB 453 breast cancer, DU145 prostate cancer, and Hela cervical cancer cell lines (Figure 56) (Table 2). Previously, K8A showed cytotoxicity in H1299 cells with p53 activation in HEK 293 cells. (K8A) was more potent for cytotoxicity than 2-DG in all cell lines.

Table 2**:** Cytotoxicity of various K8A analogues in cancer cell.

Cell line	**Cell type**	**A9A (mM)**	**C9A (mM)**	**C8A (mM)**	**G9A (mM)**	**K9A (mM)**	**L8A (mM)**	**L9A (mM)**	**K10A (mM)**	**K11A (mM)**	**K12A (mM)**
H1299	Lung	0.443±0.053	0.430±0.094	~1.15	0.456±0.032	0.390±0.096	~7.41	0.140±0.039	0.118±0.019	0.0547±0.003	0.162±0.018
231	Breast	ND	ND	ND	ND	ND	ND	ND	0.344±0.061	0.198±0.029	ND
453	Breast	ND	ND	ND	ND	ND	ND	ND	0.501±0.096	0.220±0.038	0.278.4±0.043
LNCaP	Prostrate	ND	ND	ND	ND	ND	ND	ND	0.443±0.057	0.219.7±0.038	0.222±0.037
Hela	Cervical	0.152±0.027	ND	0.352±0.114	0.352±0.114	0.235±0.066	ND	ND	ND	ND	ND

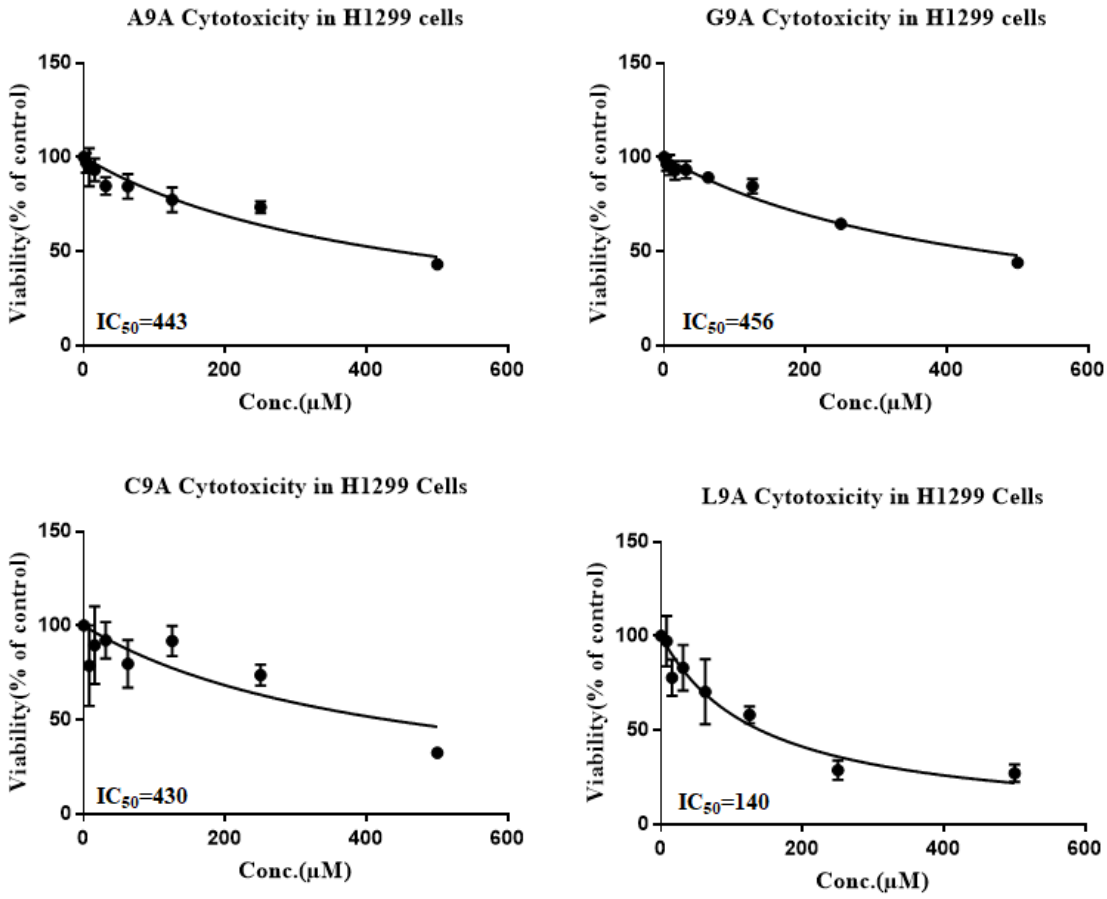

Figure 54-A9A, C9A, G9A and L9A cytotoxicity in H1299 cells

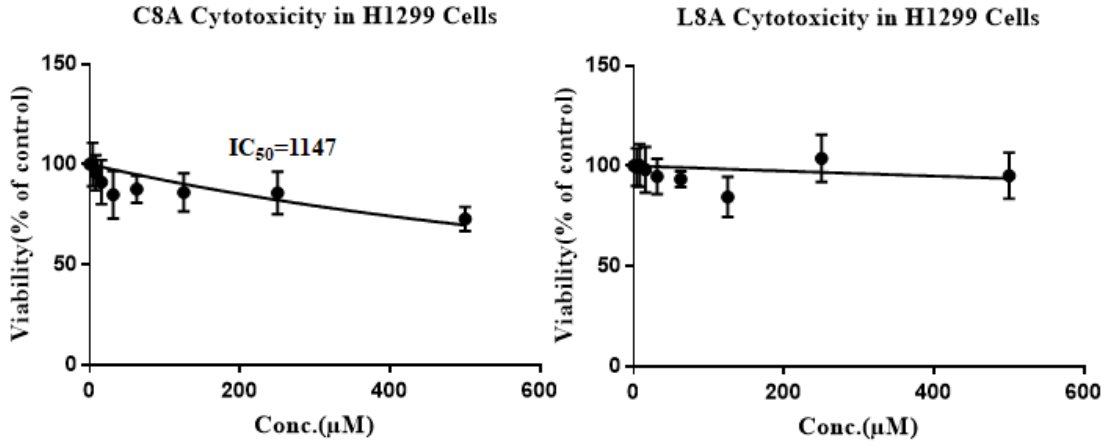

Figure 55-C8A and L8A cytotoxicity in H1299 cells

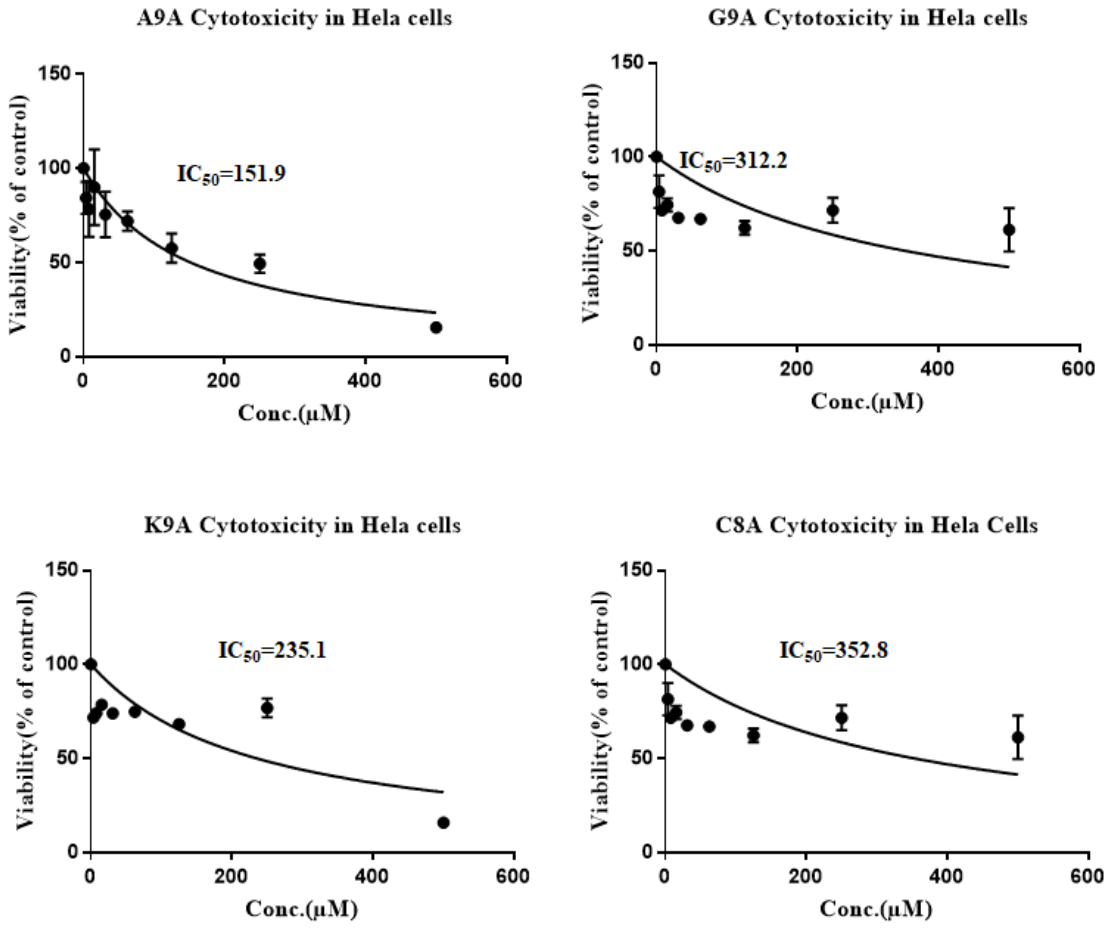

Figure 56-A9A, G9A, K9A and C8A cytotoxicity in Hela cells

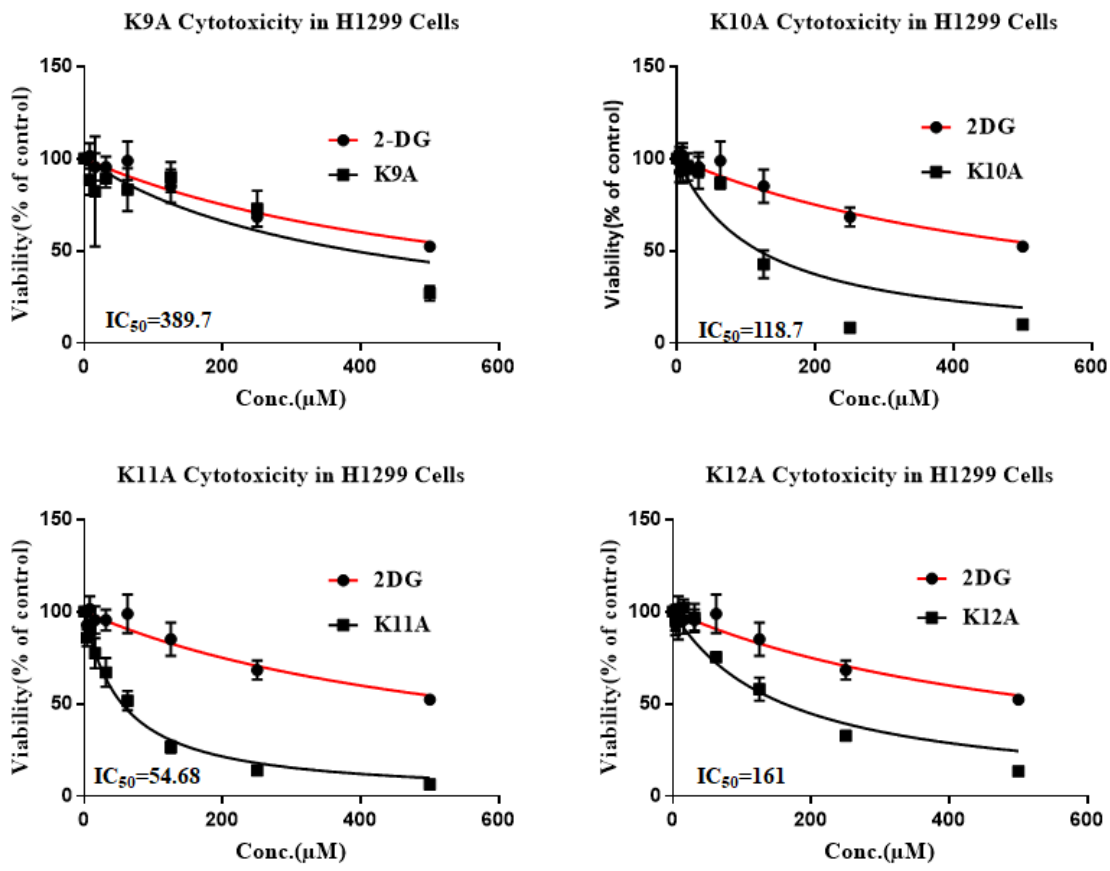

Figure 57-K9A, K10A, K11A and K12A cytotoxicity in H1299 cells

2.9 Discussion on cytotoxicity evaluation

The sensitivity of cancer cells to glycolytic inhibition and glucose deprivation provides a therapeutic strategy for control of cancer cell proliferation[158]. Additionally, enhanced monosaccharide uptake and overexpression of glucose transporters underscore the importance of sugars in cancer cell growth[203]. Evaluation of H1299 cancer cell growth inhibition showed that D-galactose, D-mannose, D-arabinose and D-xylose showed minimal growth inhibition at low concentrations. These carbohydrates did not generate appreciable levels of ROS. Of note are reports that show that D-galactose (>25 mM) generate ROS[204] and activate p38 in lens epithelial cells[205]. In our study, D-galactose (<1 mM) showed a small increase (about 10% within 1 mM) of ROS levels in H1299 cells. However, D-fructose did not affect H1299 cancer cell growth at these

low concentrations. Notably, D-arabinose (IC_{50} = 0.85 mM) and 2-deoxy-D-glucose (IC_{50} = 0.79 mM) showed comparable cytotoxicity. 2-deoxy-D-glucose is a ROS inducer and glycolytic inhibitor in clinical trials for treatment of various types of cancer[206-210].

The cytotoxicity screening of the carbohydrate-based small molecules in H1299 cells and other cell lines revealed that N-naphthyl-D-xylose (K8, IC_{50} =0.076 mM) were among the most potent from the library. Importantly, K8 induced the highest levels of ROS thus drawing a correlation between cytotoxicity and ROS generation. Additionally, cytotoxicity data for D-arabinose (H, IC_{50} = 0.85mM) and D-xylose (K, IC_{50}~5.5 mM) underscored importance for conjugation with 1-naphthylamine. Independently, 1-naphthylamine did not induce ROS (Figure 2.23) and is not cytotoxic nor carcinogenic[211]. Of note is enhanced potency with sugar acetylation (KA, IC_{50}= 2.5 mM) and (K8A, IC_{50} = 0.045 mM) in H1299 cells. A similar pattern was observed in other cell lines (Table 2). K8A is likely to be deacetylated by non-specific intracellular esterases to generate bioactive K8. K8A generated similar levels of ROS to K8, but it was more potent than K8, probably due to increased lipophilicity conferred by acetyl groups. Notably, xylosides have anticancer potential in various cancer cell lines[212-214].

Structural modification of K8A revealed that both N-naphthyl group and β-D-xylose are important in maintenance of high potency (Table 2). Additionally, 2-naphthylamine conjugate (K9A, IC_{50} = 0.39 mM) had about 10-fold lower cytotoxicity in H1299 cells compared to 1-naphthylamine conjugate (K8A), suggesting importance of 1-naphthylamine moiety. Expectedly, 2-naphthylamine glycosides (A9A, C9A, G9A and L9A) had lower cytotoxicity in various cell lines tested (Table 2). Alkylated-N-Naphthyl-β-D-Xylose (K10A, IC_{50}=0.12mM) (Figure 57) had 2-fold lower cytotoxicity than K8A, underscoring importance of non-substituted 1-naphthylamine moiety in reduced cell proliferation observed in H1299 cells. The cytotoxicity observed with K8A

was lost with bigger halogens, such as bromine (K12A, IC_{50} = 0.17 mM). Of note is the enhanced potency of K8A; an N-naphthyl-conjugate of acetylated xylose in various cell lines. Importantly, most of the carbohydrate-based N-1-naphthyl-conjugates were more potent than 2-deoxy-D-glucose (2-DG) and acetylated 2-deoxy-D-glucose (2-DGA) (Table 1 & 2). Furthermore, a conjugate of acetylated 2-deoxy-D-glucose (2DG8A, IC_{50}=0.15mM) was less potent than K8A in H1299 cells and other cell lines.

2.10 Experimental procedures

2.11 MTT Assay

About 10,000 cells were seeded per well and incubated at 37 ºC, 5% CO_2 for 24 hours on 96 well transparent plates for attachment. Cells were then dosed with known concentrations of the small molecules in triplicate and incubated for 24 hours in the same conditions. Media was then removed, and cells incubated with 100 µL of MTT solution (5mg/ml) for 4 hours at 37 ºC. The MTT solution was removed, and 200 µL of DMSO was added to each well to dissolve formazan. The absorbance of the cultures was measured using a multi-well spectrophotometer (Hybrid H1) at a wavelength of 550 nm. Cell viability was expressed as OD values and calculated as the percentage of absorbance in the control cultures (untreated cells).

2.12 Trypan blue assay

For suspension cells, Raji and Daudi cells, cytotoxicity was evaluated using the trypan blue assay[215]. Trypan blue solution was sterile filtered to remove any particles in the solution that would interfere with the counting process. Cells were harvested by centrifugation in a 15 mL falcon tube. The supernatant was removed by aspiration. The cells were resuspended in 1 mL of DMEM and dilution was done at 1:1 ratio with Trypan Blue dye (0.4% solution). About 10 µL was transferred

to fill the hemocytometer chamber before placement in the automated cell counter (TC20 automated cell counter).

2.13 Sulforhodamine B assay (SRB assay)

The hit compound K8A was evaluated by the National Cancer Institute using SRB assay[216]. K8A was dissolved in DMSO and stored frozen prior to use. The 60 human cancer cell lines were grown in RPMI 1640 medium with 5% FBS and 2 mM L-glutamine. The cells were inoculated into 96 well plates in 100 μL at plating densities ranging from 5,000 to 40,000 cells per well depending on the growth rates of individual cell lines. The cells were then incubated at 37° C, 5 % CO_2, 95 % air and 100 % relative humidity for 24 hours prior to dosage with K8A. During dosage, an aliquot of frozen K8A in DMSO was thawed and diluted to twice the desired final maximum test concentration (10 μM) with complete medium containing 50 μg/ml gentamicin. After 24 hours, two plates of each cell line were fixed *in situ* with trichloroacetic acid, to represent a measurement of the cell population for each cell line at the time of drug dosage (Tz). After drug dosage, the plates are incubated for an additional 48 hours at 37 °C, 5 % CO_2, 95 % air, and 100 % relative humidity. For adherent cells, the assay is terminated by the addition of cold TCA. Cells were fixed by addition of 50 μL of cold 50 % (w/v) TCA (final concentration, 10 % TCA) and incubated for 60 minutes at 4°C. For suspension cells, the assay is terminated by fixing settled cells at the bottom of the wells by gently adding 50 μL of 80 % TCA (final concentration, 16 % TCA). The supernatant was removed, and the plates washed with water. Sulforhodamine B (SRB) solution (100 μL) at 0.4 % (w/v) in 1 % acetic acid was added to each well and incubated for 10 minutes at room temperature. The plates were then washed with 1% acetic acid to remove unbound stain. Bound stain was then dissolved in 10 mM trizma base, and the absorbance at a wavelength of 515 nm was read on a plate reader. Percentage growth inhibition was then computed.

CHAPTER 3 ROS-INDUCED SIGNALING AND OXIDATIVE STRESS RESPONSE

3.1 Introduction

Cells maintain the redox environment by various mechanisms. The ROS detoxification systems are controlled by enzymes regulated by various antioxidant response pathways, that include the Nrf2-ARE pathway [217]. Additionally, ROS may induce other pathways that include ASK1-JNK pathway[90], ASK1-p38 pathway[218], AMPK-p53 pathway[219] and protein glycosylation pathways[220]. Glycosylation of proteins is dependent on the concentration of carbohydrate donor substrates, including UDP-GlcNAc

UDP-GlcNAc is used in enzymatic post-translational modification of many cytosolic and nuclear proteins by *O*-linked β-*N*-acetylglucosamine (*O*-GlcNAc). Additionally, UDP-GlcNAc metabolite is required for the biosynthesis of extracellular N-linked and O-linked glycans[221-222]. Importantly, HBP and O-GlcNAc modification allows cells to link nutrient availability and cellular metabolism to the regulation of oxidative stress response and cell death[220]. In N-linked glycosylation, two N-acetyl glucosamine residues are attached to an asparagine residue of a protein followed by mannose residues. In O-linked glycosylation, N-acetyl galactosamine is attached to a serine or threonine residue of proteins followed by other glycans such as galactose and sialic acid[222]. K8A was evaluated for potential roles in ASK1-JNK pathway, ASK1-p38 pathway, AMPK-p53 apoptotic pathway and HBP pathway.

3.1.1 Nrf2-ARE pathway

Nrf2 is a redox-sensitive transcription factor in which Keap1 functions as Nrf2-specific adaptor that is crucial in redox homeostasis (Figure 58). Previously, small molecules blocked Nrf2-antioxidant response to increase ROS levels in A549 and H1299 cell lines[223-225]. p53-null H1299 cells with low basal Nrf2 levels had high ROS levels than A549 cells that have high basal Nrf2

levels[225]. Keap1 is a regulator of Nrf2, acting as a sensor of ROS. In absence of ROS, Nrf2 is degraded through the proteasome pathway. Keap1 has cysteine residues that require oxidation to detach and release Nrf2, which translocate to the nucleus. In the nucleus, Nrf2 binds to antioxidant response elements (ARE) leading to transcription of antioxidant and xenobiotic enzymes[226]. Transcription factors that bind to the human NQOl ARE include Nrf1, Nrf2, c-Jun, c-Fos, Jun-D, Jun-B, and Fral[227-228]. Nrf2 target genes include NQO1, HO-1, glutathione peroxidase and glutathione S-transferases (GSTs) such as GSTO1[229]. Additionally, UDP-glucuronyl transferases (UDPGTs) involved in conjugation of hydrophobic metabolites to D-glucuronic acid are considered phase II detoxification enzymes[230].

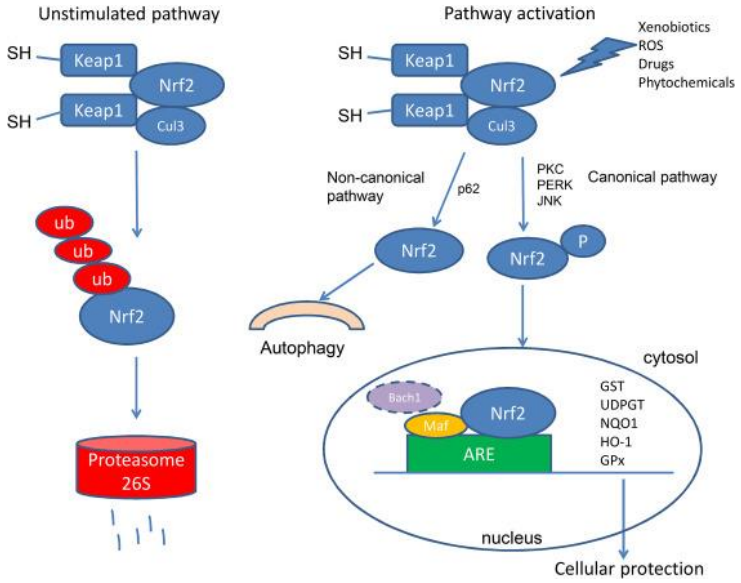

Figure 58-Nrf2-ARE response pathway in stimulated and unstimulated conditions

GSTs catalyze the conjugation of reduced glutathione (GSH) to xenobiotics for detoxification. Of note, is Nrf2 activation of genes that encode the catalytic and regulatory subunits of gamma-glutamyl-cysteinyl-ligase (GCL), a rate-limiting enzyme of glutathione synthesis[231]. Additionally, Nrf2 activates many PPP enzymes including NADPH producing enzymes such as G6PD, TKT,

TALDO and ME1[231-232]. Thus, Nrf2 activates both the oxidative and nonoxidative PPP to increase NADPH and nucleotide production. Notably, Nrf2 is involved in autophagy via stabilization by p62; a binding partner of Keap 1.[233] On the other hand, NQO1 is involved in detoxification of quinones to hydroquinone by utilizing NADPH to generate $NADP^{+}$[234].

3. 2 Results

3.2.2 K8A-induced NQO1 induction

K8A induced downstream effects on Nrf2-ARE pathway in H1299 cells without altering Nrf2 levels. Western blot studies revealed NQO1 induction in a concentration dependent manner when H1299 cells were treated with K8A (Figure 59-60). The level of GSTO1, which is another Nrf2-ARE pathway antioxidant enzyme, remained unchanged in H1299 cells.

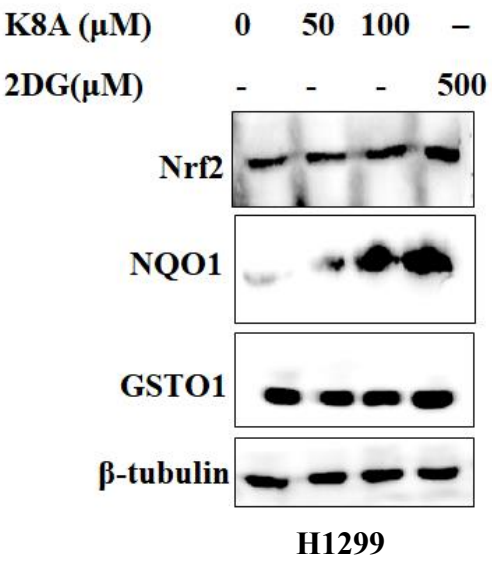

Figure 59-K8A effect on Nrf2-ARE pathway in H1299 and LNCaP cells

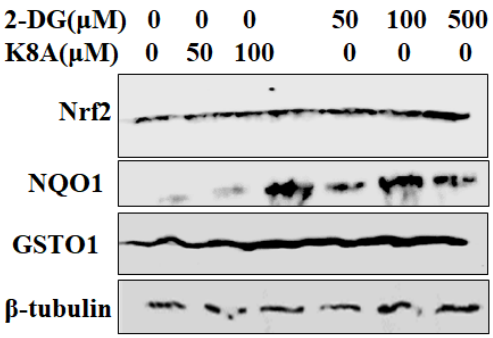

Figure 60-K8A and 2-DG effect on Nrf2-ARE pathway in H1299 cells

3.2.3 K8A effect on ASK1-JNK and ASK1-p38 pathways

ASK1 is a serine-threonine kinase in the c-Jun N-terminal kinase/stress-activated protein kinase (JNK) and p38 MAPK signaling cascades. ASK1 cysteine 250 is oxidized by ROS to facilitate JNK activation[235]. Additionally, ROS-induced activation of ASK1 may involve phosphorylation of its threonine 838 leading to activation of downstream JNK[114, 235] and p38 pathways. K8A did not induce concentration-dependent ASK1 activation within 100 μM in both ASK1-transfected and non-transfected H1299 cells (Figure 61). Additionally, p38 was not activated by K8A in H1299 and LNCaP cell lines (Figure 63)

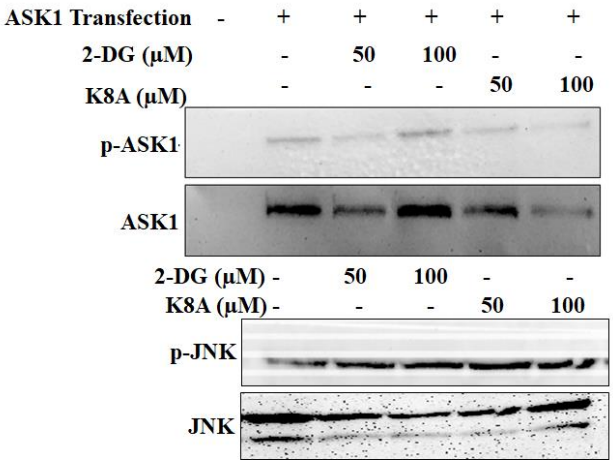

Figure 61-K8A and 2-DG effect on ASK1-JNK pathway in H1299 cells transfected with ASK1

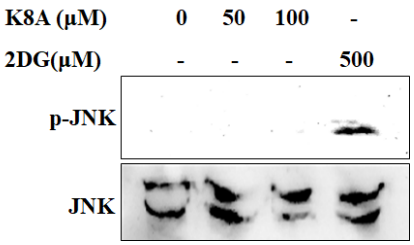

Figure 62-K8A and 2-DG effect on JNK expression in H1299 cells

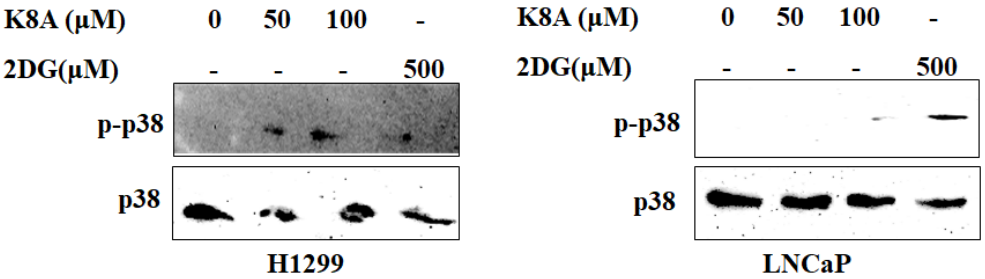

Figure 63-K8A effect on p38 expression in H1299 and LNCaP cells

3.2.3 K8A induced AMPK-p53 apoptosis pathway

AMPK is sensitive to changes in the cellular AMP/ADP to ATP ratio[236]. The increase of the cellular ADP/ATP ratio denotes an imbalance between ATP production and ATP utilization processes[237]. Additionally, AMPK may sense changes in intracellular glucose levels independent of adenine nucleotide levels such as ATP[237]. Cellular energetic changes lead to accumulation of AMP and ADP levels, resulting in the binding of AMP and ADP to AMPK. K8A induced AMPK activation within 100 μM in H1299 and HEK 293 cells (Figure 64). Under oxidative stress, AMPK induce phosphorylation of tumor suppressor protein p53 at serine 15, which mediates AMPK-dependent cell cycle arrest[238].

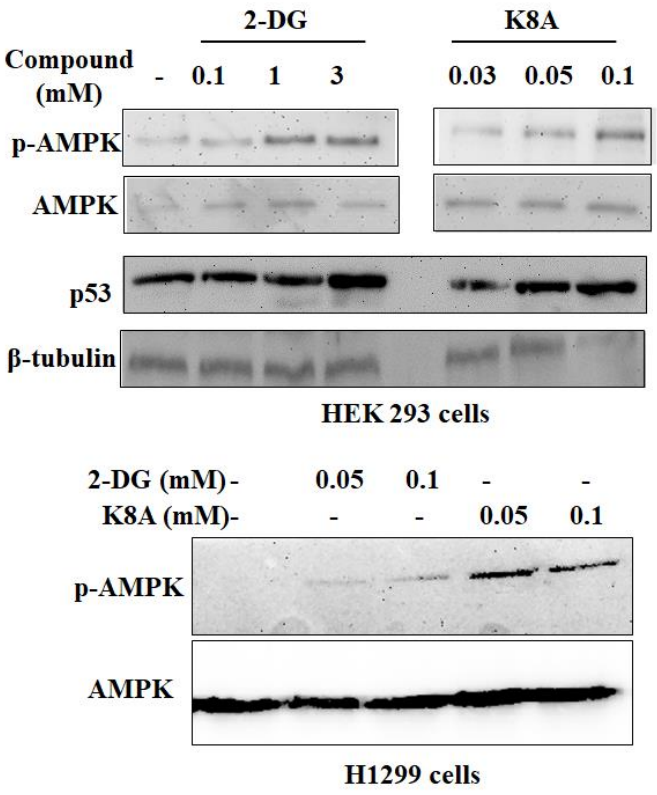

Figure 64-K8A and 2-DG effect on AMPK-p53 pathway in HEK 293 and H1299 cells

3.2.5 K8A induced ER stress in H1299, LNCaP and MDA-MB 231 cancer cells

ER stress occurs when misfolded and unfolded proteins accumulate in cells[239]. Prolonged accumulation of misfolded proteins activates the UPR. UPR involves formation of disulfide bonds between cysteine residues of misfolded and unfolded proteins. This disulfide bond formation is catalyzed by various enzymes that include PDI[240]. ROS generation occurs when endoplasmic reticulum oxidoreductin 1(EROα1) reduce oxidized PDI by electron transfer to molecular oxygen[241].

Additionally, ER-stress activate molecular chaperones that include grp78[242]. Grp78 is considered a gate-keeper of UPR. Notably, grp78 is a cellular stress sensor that responds to dramatic decreases of glucose and increases of ROS in the ER[243]. In this study, K8A induced increase of grp78 expression in H1299, LNCaP and MDA-MB 231 cells (Figure 65).

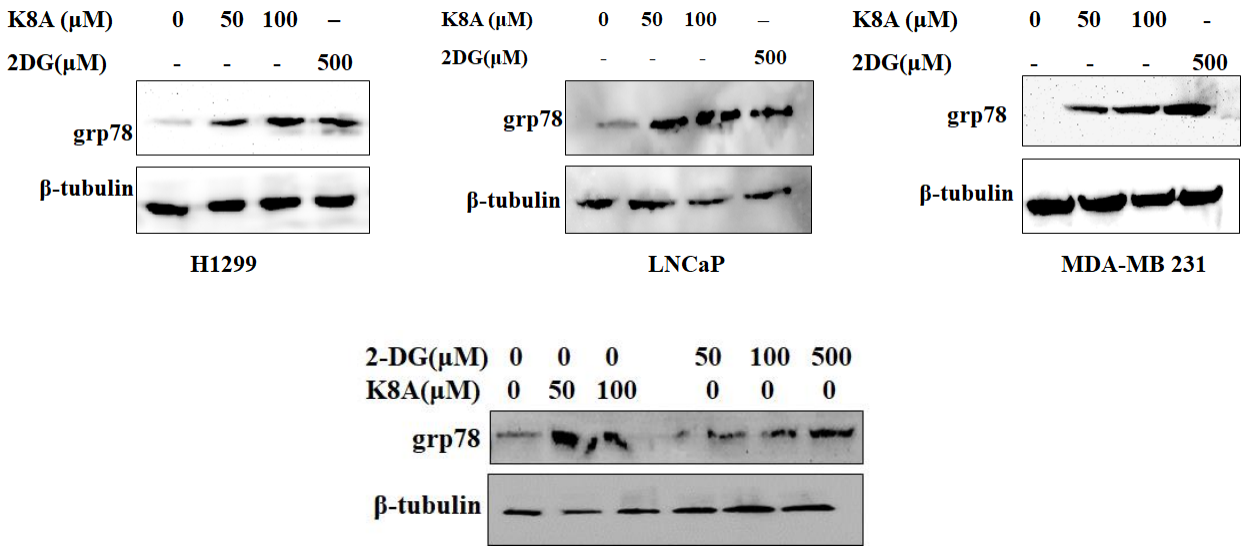

Figure 65-K8A and 2-DG effect on ER-stress induced grp78 in H1299, LNCaP and MDA-MB 231 cells.

3.2.6 Click chemistry reveals that K8A interferes with global glycosylation of proteins

Protein glycosylation may be monitored by metabolic labelling by use of unnatural sugars containing bioorthogonal azide or alkyne groups[244-246]. Metabolic labelling occurs because N-acetylglucosamine (GlcNAc) can be installed on proteins via an alternative HBP called salvage HBP[247]. This salvage pathway is initiated by GlcNAc kinase and facilitates delivery of abiotic moieties that contain clickable handles on the N-acyl group of GlcNAc[248]. We therefore labelled glycoproteins in H1299 cells using N-(4-pentynoyl)-glucosamine tetraacylated (Ac_4GlcNAl). Ac_4GlcNAl provides a robust two-step technique that enabled us monitor glycosylation of proteins, known to be elevated in H1299 cells. The alkyne-modified proteins from cell lysate were chemoselectively labeled by click chemistry and detected with fluorescent Cy5 azide after running on SDS PAGE gels.

We incubated Ac4GlcNAI or Ac4GalNAI to label glycosylated proteins, while examining the effect of K8A on the glycosylation. Upon addition of Ac4GlcNAl or Ac4GalNAI, there were many

bands that correspond to glycosylated proteins after click reaction with Cy5-azide. When K8A was co-incubated, protein glycosylation was decreased significantly (Figure 66) with Ac_4GlcNAl protein labelling, but not with Ac_4GalNAl protein labelling. In comparison to K8A, neither 2-DG (50 μM) nor acetylated 2-DG (100 μM) effectively interfered with global protein glycosylation (Figure 66-67).

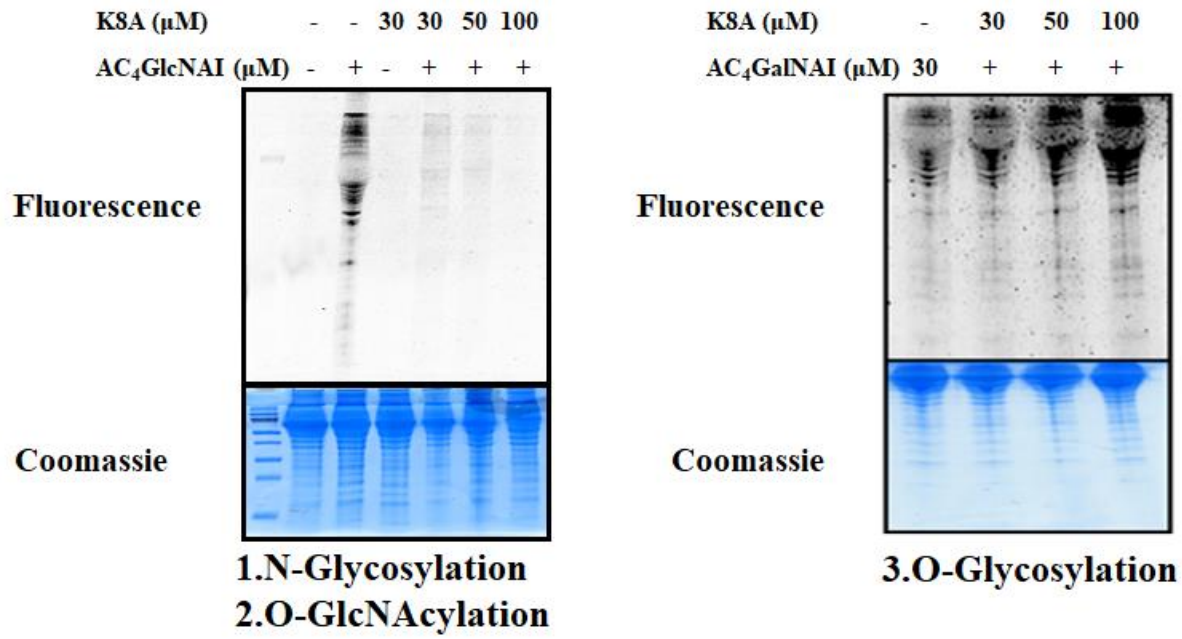

Figure 66-Concentration-dependent K8A-induced disruption of global protein glycosylation in H1299 cells monitored with GlcNAI vs GalNAI.

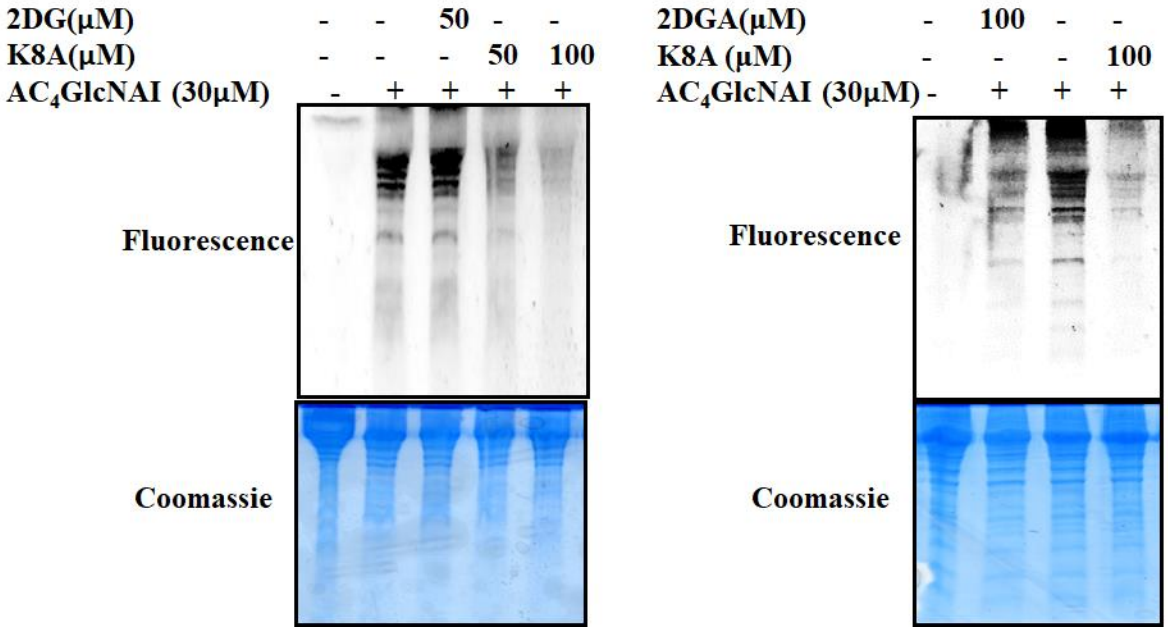

Figure 67-Comparison of 2-DG, 2DGA and K8A-induced disruption of global protein glycosylation in H1299 cells monitored with GlcNAI.

3.3 Characterization and delineation of K8A glycosylation interference

To characterize K8A glycosylation interference *in vitro*, OGT enzyme[249] was cloned, expressed and purified. Additionally, OGT substrates[250-252] (OGT-peptide and Hsp 90) were synthesized and purified respectively**.** The peptide sequence was YSESPSTST and varied slightly with the OGT peptide YSDSPSTST[253] that is widely used in glycosylation experiments. Previously replacement of aspartic acid with acidic amino acid residues did not change glycosylation of this peptide.[253] Additionally, the peptide sequence is based on the common amino acid sequence at glycosylation site of Nup62 protein that is glycosylated *in vivo*[254]. Mass spectrometry and gel-based assays were then used to evaluate K8A glycosylation interference of the peptide and Hsp90 protein, respectively.

3.3.1 OGT protein expression and purification

Truncated OGT(sOGT)[255] was cloned and expressed in bacteria and purified on a His-tag column (Figure 68). sOGT was used because purification of full length OGT is difficult with low yields. Additionally, the catalytic domains are preserved in Sogt

that retains enzyme activity as full-length OGT.

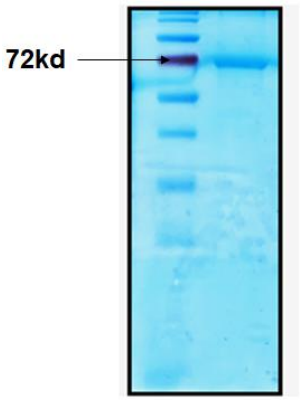

Figure 68-SDS-PAGE for purified His-tagged Hsp-90.

3.3.2 K8 does not interfere with protein O-GlcNAcylation *in vitro*.

OGT enzyme activity was validated using Hsp90, a molecular chaperone that is known to be glycosylated[246]. Incubation of UDP-GlcNAc with OGT and Hsp90 yielded glycosylated Hsp90 that was monitored by O-GlcNAc specific antibody known as CTD 110.6[256]. The Coomassie stained SDS PAGE gel was used to monitor the protein levels. The purified OGT enzyme was found to be active because O-GlcNAc modification on Hsp 90 was detected by Western blot (Figure 69).

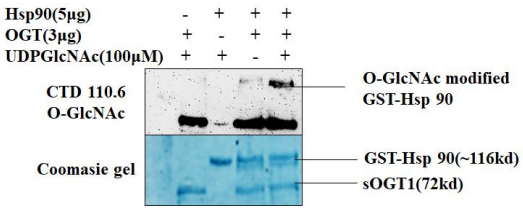

Figure 69-sOGT-catalyzed *in vitro* Hsp-90 O-GlcNAcylation.

K8 did not inhibit OGT since O-GlcNAc modification on Hsp 90 (Figure 70). Additionally, autoglycosylation of OGT was observed (Figure 70).

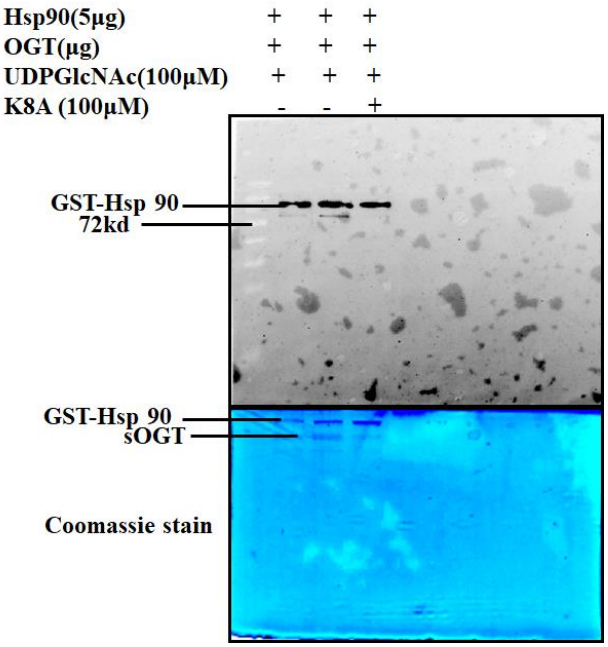

Figure 70-K8 effect of Hsp-90 O-GlcNAcylation

3.3.3 OGT peptide synthesis

OGT peptide (YSDSPSTST) from Nup62 glycosylation site studies[253] was synthesized on Wang resin using Fmoc-solid phase peptide chemistry[257]. The mass of the peptide was confirmed using ESI mass spectrometry and the 9-mer peptide mass confirmed as in the spectrum below (Figure 71). The spectrum shows m/z+ values of the 9-mer peptide fragments;857.47, 669.19,485, 238.97 and 195.94 (Figure 71).

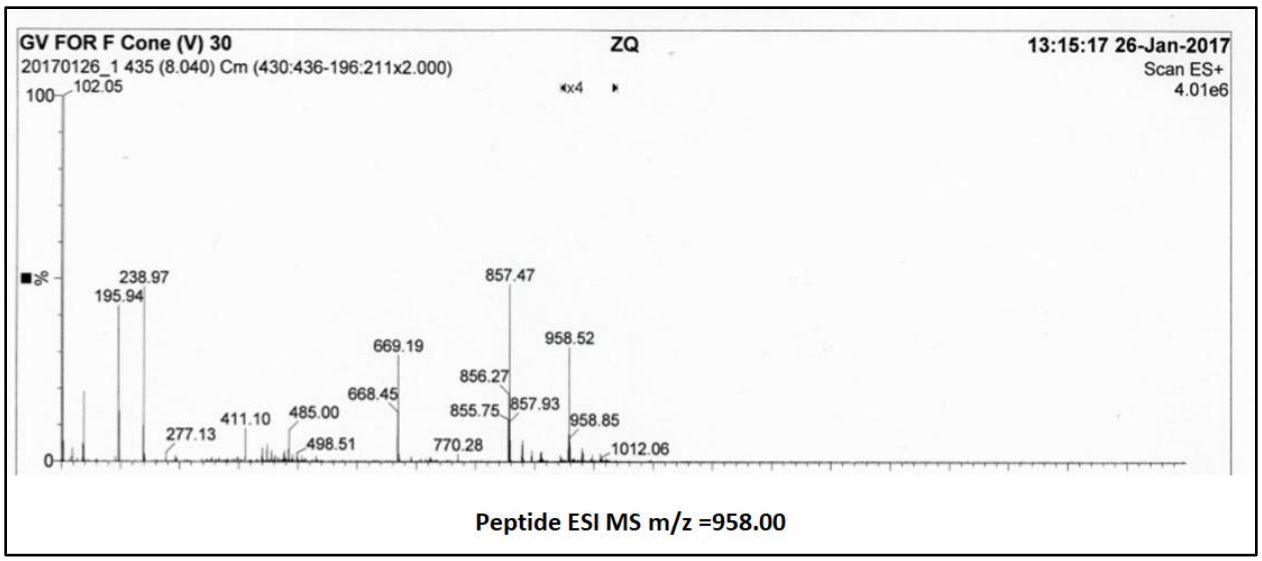

Figure 71-Mass spectrum of OGT peptide.

3.3.4 Mass spectrometry-based OGT assay reveal K8 does not interfere with peptide O-GlcNAcylation.

Protein glycosylation was monitored *in vitro* (Figure 71,73) using a synthetic peptide and purified His-tag OGT enzyme. The mass of glycosylated peptide was monitored by LC-MS after removal of the protein using a molecular weight cutter. Incubation of the peptide in presence of K8 did not inhibit OGT and the peak of the glycosylated peptide was still observed (Figure 73). In this assay, after injection of the sample to LC-MS, the *O*-GlcNAc modification of peptide was evaluated. We did not observe any difference in intensity of the extracted mass peak (m/z^{2+}=589.00) corresponding to the modified peptide between K8 treated samples and untreated samples. Additionally, K8 mass peak (m/z^{+}= 276.00) remained unchanged. This suggests that K8A does not inhibit OGT, and that it possibly acts through a different mechanism. UDP-GlcNAc substrate, UDP and GlcNAc products being highly hydrophilic eluted early as shown in the LC data.

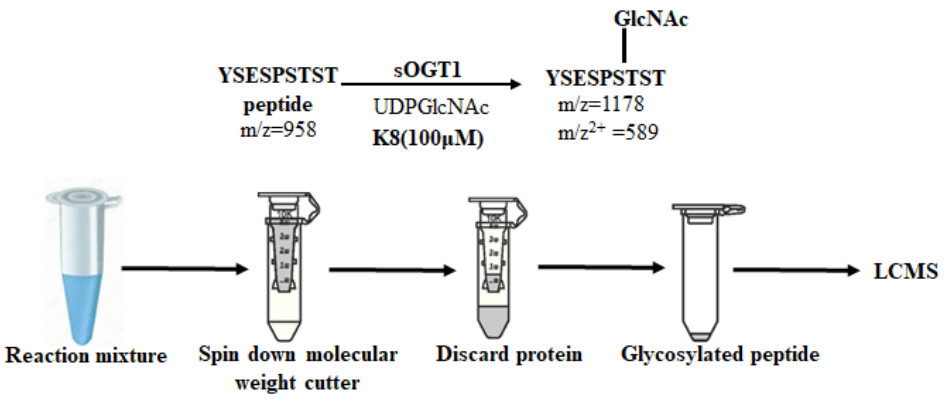

Figure 72-Work flow for mass-spectrometry based glycosylation assay

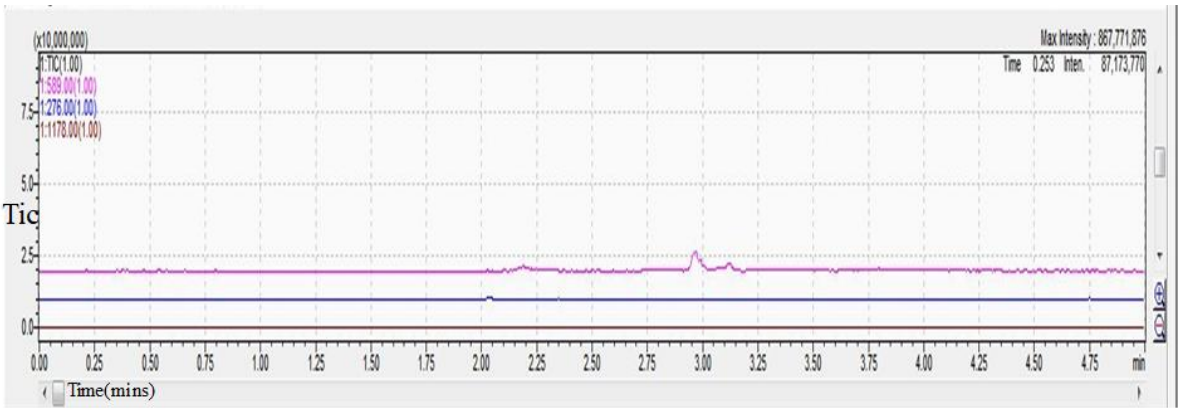

a) No OGT enzyme No K8 control MS assay

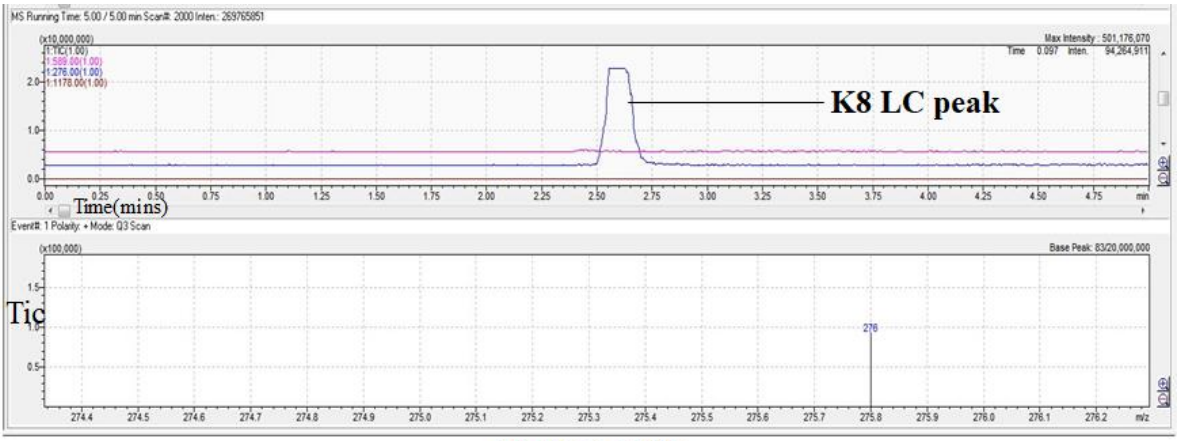

b) K8 LCMS

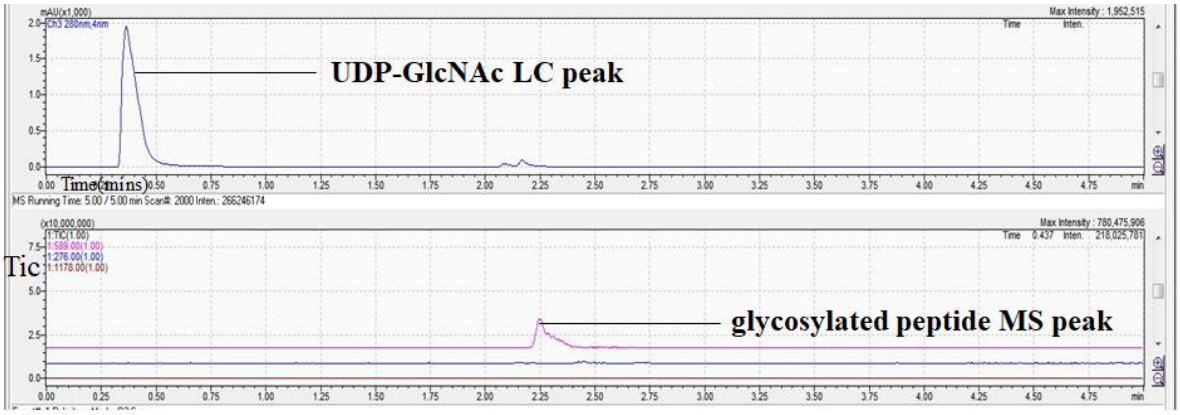

c)OGT enzyme MS assay without K8

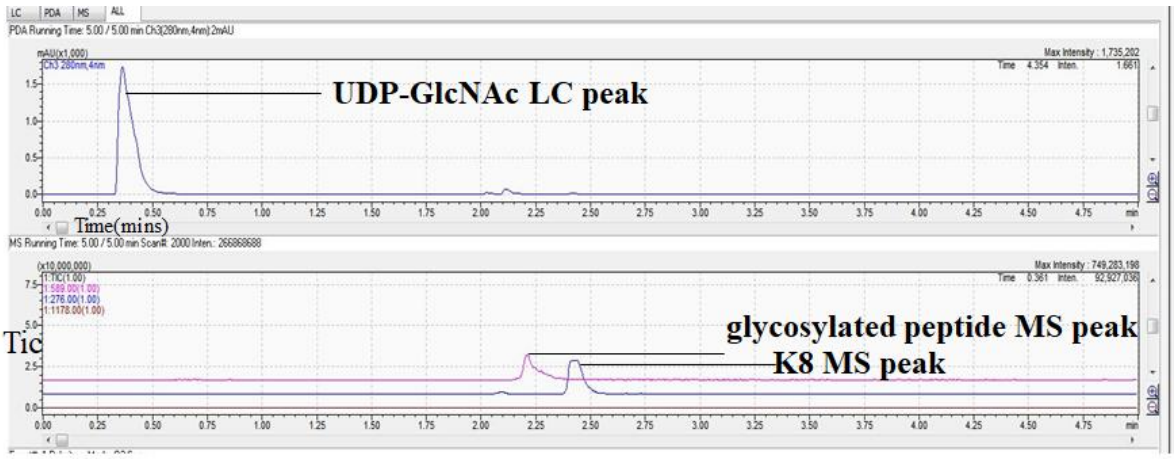

d) OGT enzyme MS assay with K8

Figure 73-Monitoring peptide glycosylation by mass spectrometry in various conditions(a-d). (a) Mass spectrum of control experiment without OGT and K8 (b) Mass spectrum of K8 (inhibitor) (c) Mass spectrum of glycosylation experiment without K8. (d) Mass spectrum of glycosylation experiment in presence of K8.

3.3.5 K8A induced O-GlcNAcylation in H1299 cells

O-GlcNAcylation is increased in response to many stresses that include oxidative and ER stress[258]. In this study, K8A induced O-GlcNAcylation of global proteins in H1299 cells comparable to induction by 2-DG (Figure 74). Of note is the high level of OGT expression induced

by 2-DG treatment to H1299 cells (Figure 74). Additionally, metabolomics revealed a huge increase in free UDP-GlcNAc in the same cell type.

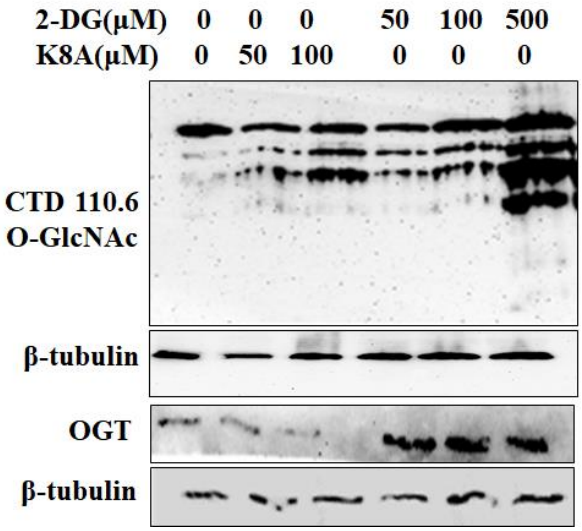

Figure 74-K8A and 2-DG induced O-GlcNAcylation in H1299 cells.

Validation of K8A-induced O-GlcNAcylation was done by checking expression levels in Flag-tagged OGT transfected cells (Figure 75). OGT transfected cells showed higher levels of O-GlcNAc modification of global proteins compared to non-transfected ones.

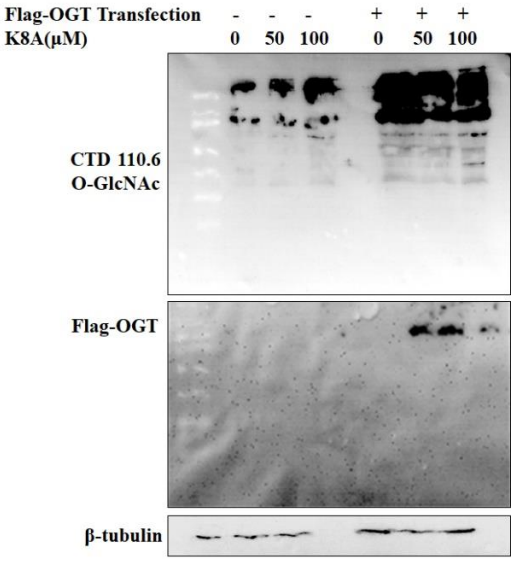

Figure 75- K8A induced O-GlcNAcylation in H1299 cells transfected with full-length Flag-tagged OGT.

3.4 Discussion

K8A induced NQO1 expression in H1299 and LNCaP cells. However, Nrf2 which is upstream of NQO1 remained unaltered in H1299 cells. Nrf2 is stabilized by Keap1 that promotes Nrf2 degradation when O-GlcNAcylated[259]. Notably, K8A induced global O-GlcNAcylation and likely is responsible for low Nrf2 levels.

NQO1 is a phase II detoxifying enzyme that require NADPH to catalyze the two-electron reduction of quinones, quinone imines and nitrogen oxides[234]. Phase II enzymes promote the conjugation of phase I products with endogenous cofactors such as glutathione and glucuronic acid to produce water soluble products which are easily excreted. Glutathione is generated by GST and glucuronic acid by UDP-glucuronosyltransferases (UGT)[260-261]. Additionally, NQO1 regulate the stability of p53 and directly influence apoptosis[262]. p53 is a tumor suppressor gene that regulates cellular growth and cause cell cycle arrest (Figure 76). Additionally, prolonged increase in NQO1 expression consume large amounts of NADPH to generate lethal ROS[263]. Interestingly, overexpression of p53 may lead to upregulation of p53-induced genes that include NQO1 and proline oxidase (POX) which generate ROS that cause apoptosis[264]. Additionally, p53 suppress expression of antioxidant enzymes such as manganese superoxide dismutase (Mn SOD)[265].

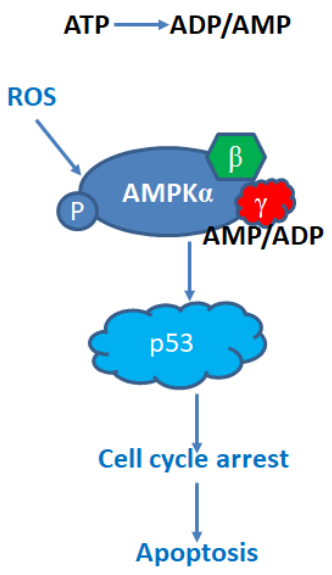

Figure 76-AMPK-p53 pathway

In addition, p53 may be stabilized by AMPK[266] and by O-GlcNAcylation[124]. In response to cellular energetic stress and increase in the ratio of ADP to ATP, adenylate kinase converts two molecules of ADP into ATP and AMP[238]. From a metabolic standpoint, AMPK promotes ATP conservation under conditions of metabolic stress. Notably, AMPK is activated in cells in response to ROS generation, glucose withdrawal and 2-DG treatment. ROS induce AMPK activity to regulate glucose metabolism. ROS also directly oxidize AMPK on cysteine 299 and 304 to activate it in a process that involves S-glutathionylation[267]. Other ROS-sensitive metabolic pathways such as ASK1-JNK-apoptosis and p38 pathways were not activated, albeit existence of AMPK-p38-PGC-1α pathway[268]. Previously, O-GlcNAcylation impaired JNK activation in cancer cells and stabilized p53[124, 269].

In response to low ATP levels, AMP binds to AMPK to activate its phosphorylation and downstream signaling that include p53 activation and apoptosis. Additionally, AMPK phosphorylate and regulate expression of metabolic enzymes involved in various pathways that include glycolysis and lipid synthesis[270]. Once AMPK activity increases, energy-consuming

pathways such as lipogenesis are inhibited, while energy-producing pathways such as glucose uptake and fatty acid oxidation are upregulated. AMPK suppresses expression of lipogenesis-associated genes such as fatty acid synthase, pyruvate kinase and acetyl CoA carboxylase (ACC). Interestingly, our metabolomics data in Chapter 4 reveal that fatty acid levels were unaltered and corroborate AMPK inhibition of fatty acid synthesis. Additionally, AMPK phosphorylates PFK2 to increase the glycolytic rate[268].

ER stress sensor grp78 induces signaling effects that involve UPR. In response to ER stresses, the unfolded protein response (UPR) is activated. UPR activate the HBP through X-box binding protein 1 (Xbp1)-dependent transcriptional induction of GFAT1, ATF4 and other key enzymes involved in the HBP, glycosylation and carbohydrate metabolism[271]. GFAT1 upregulation lead to increase in UDP-GlcNAc levels and increase in O-GlcNAcylation. To detect O-GlcNAc modification, CTD 110.6 antibody was used[247]. CTD 110.6 was used because it recognizes a wider range of *O*-GlcNAcylated proteins than RL-2. CTD 110.6 antibody is less dependent on protein structure than RL-2. CTD 110.6 is raised against the epitope of an O-GlcNAc–modified C-terminal domain of the RNA polymerase II large subunit and RL2 is raised against the epitope of an *O*-GlcNAc–modified nuclear pore (NP62) protein.

O-GlcNAcylation protects cells from oxidative stress. Metabolic enzymes of glycolysis, PPP and TCA are glycosylated to promote ROS detoxification. Interestingly, HKII, PFK1 and PKM2 are regulated by O-GlcNAcylation to promote glycolytic change of flux to PPP and HBP. Previously, PFK1 was O-GlcNAcylated at serine 529 to inactivate it leading to accumulation of F6P that is directed to HBP and PPP[50]. Additionally, PKM2 was O-GlcNAcylated at two residues (threonine 405 and serine 406) to reduce its activity, leading to accumulation of PEP[272]. Western blot data and metabolomics data indicated that O-GlcNAcylation of proteins was induced by K8A

in p53 null H1299 cells (Figure 77). Importantly, O-GlcNAcylation protects cells from oxidative, ER and other forms of cellular stress. Remarkably, O-GlcNAcylation is high in p53 null cells than wild-type expressing cells[124] further suggesting a prominent role of this modification in cytoprotection. Of note are reports of the decrease in ATP levels in H1299 cells overexpressing OGT[273] which partly corroborates our findings on effects of K8A-induced O-GlcNAcylation in the same cell line.

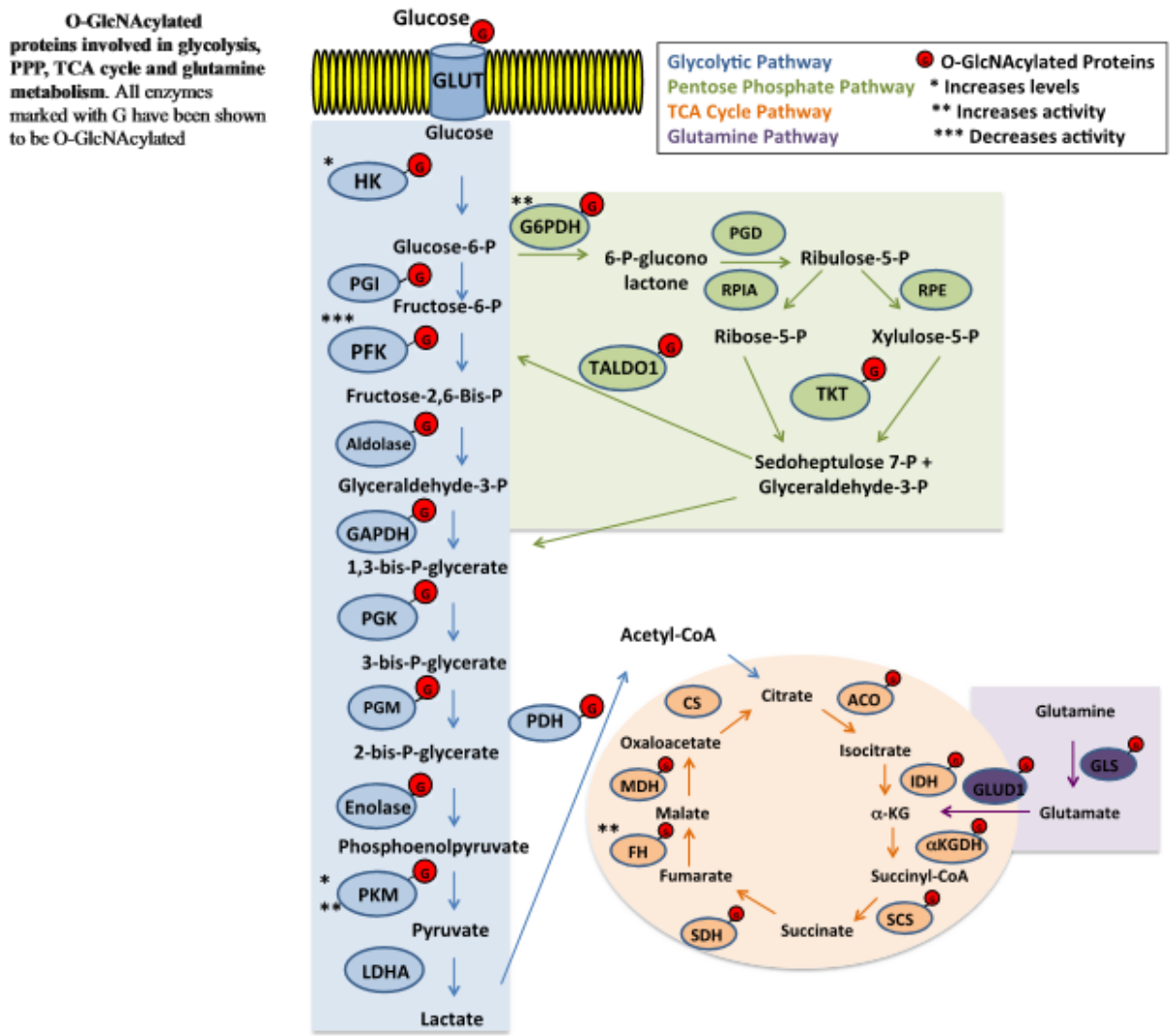

Figure 77-O-GlcNAcylation in glycolysis, PPP, TCA pathways[274] (Adopted with permission from reference 207)

3.5 Experimental procedures

3.5.1 PEI Max mammalian cell OGT1 transfection

Transfection of PRK5-Flag OGT1 plasmid into H1299 cells (Figure 78) was done at 80-90% confluency at 37 °C by using PEI Max (Life Technologies, Grand Island, NY) according to manufacturer's protocol. PEI-Max stock solution consisted of 100 mg PEI Max dissolved in 10 mL of deionized water and slightly vortexed. The working solution was sterile filtered and kept at a concentration of 1 mg/mL. 9 µg of PEI 'Max' and 3 µg of DNA were diluted separately into 250 µL of serum free DMEM medium without antibiotics and kept at room temperature for 15 minutes in the biosafety hood. The diluted PEI 'Max' was then added to the diluted DNA and incubated at room temperature for another 15 minutes. The mixture was added to cells pre-washed with PBS and incubated at 37 °C. The medium was changed at 6 hours after transfection, and cell lysates were prepared 48 hours after transfection. Transformation efficiency was checked by Western blot.

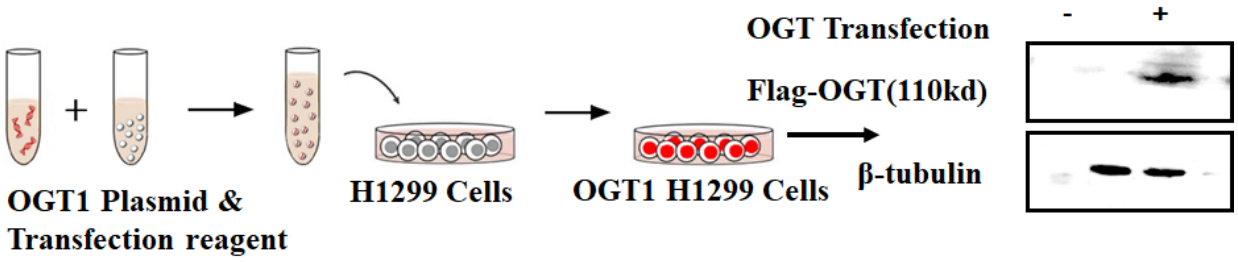

Figure 78-Workflow for OGT transfection in H1299 cells

3.5.2 Mammalian cell lysis

Mammalian cells were lysed with 350 µL RIPA buffer following removal of medium and washing with ice-cold PBS. The cells were scrapped off the 6 cm dishes, transferred to an eppendorf tube, and rotated in the cold room. The lysates were centrifuged at 13,000 rpm for 20 minutes to remove cell debris. The supernatant protein concentration was estimated by using Bradford assay.

3.5.3 Determination of protein concentration using Bradford assay

200 μL of Bradford reagent was added to each well on a 96-well plate containing various concentrations of BSA (1, 0.5, 0.25, 0.125 mg/mL) to make a standard curve. BSA was serially diluted from a 10 mg/mL stock solution. 10 μL of the BSA dilutions were added to the Bradford reagent. UV absorbance was read at 595 nm. Separately, 10 μL of appropriate protein or cell lysate was added separately and to the 200 μL of 1X Bradford reagent and absorbance determined at 595 nm. A standard calibration curve of BSA was constructed and used to compute the protein concentration of cell lysate or pure His/GST-tagged protein.

3.5.4 SDS-PAGE

SDS-PAGE gel consists of a separating layer and a stacking layer. The SDS-PAGE separating buffer was made for different types of gel by mixing the components from stock solutions as in the table below.

Table 3**:** SDS-PAGE separating layer recipe

Stock Solution	**7%**	**10%**	**12%**
1M Tris pH 8.8	3.75ml	3.75ml	3.75ml
20% SDS	0.05ml	0.05ml	0.05ml
40% Acrylamide (Biorad 37:1)	1.73ml	2.50ml	3ml
H_2O	4.40ml	3.73ml	3.2ml
10% Ammonium persulfate	100 μL	100 μL	100 μL
TEMED (Sigma)	10 μL	10 μL	10 μL

Table 4**:** SDS-PAGE stacking layer recipe

The SDS-PAGE stacking buffer was made by mixing the following components from stock solutions. SDS-PAGE stacking buffer recipe	
1M Tris pH 6.8	0.63ml
20% SDS	0.05ml
40% Acrylamide	0.83ml
H_2O	3.4ml
10% Ammonium persulfate	50 μL
TEMED	5 μL

The SDS-PAGE separating layer was made by adding onto glass plates mounted on a Biorad gel making rack. A drop of isopropanol was added over the separating layer to ensure complete removal of bubbles and facilitate formation of an even surface. Upon solidification, the isopropanol was removed, and the stacking layer added using a pipetteman with a 10-well or 15-well comb slid between the glass plates. Upon solidification, the comb was removed and transferred to the SDS-PAGE running container with SDS-running buffer (1x; 0.025M Tris; 0.05M glycine, 0.5% SDS). The SDS-PAGE was run for 1-2 hours at 150-200 V. The gel was then removed, washed with water before imaging, staining or transfer to Western blot.

3.5.5 Coomassie staining

SDS-PAGE gels were stained in staining solution (0.1% Coomassie Brilliant Blue R-250 in 50% methanol and 10% glacial acetic acid) for 2 hours with shaking. Destaining was done by draining off the stain, followed by destaining solution (40% methanol and 10% glacial acetic acid) for 10-20 hours. The gel was then scanned.

3.5.6 Western blot

Western blot evaluation was done with different concentrations of K8A. After washing cells with PBS, cells were lysed with RIPA buffer (50 mM Tris, pH 7.4, 1% NP-40, 0.25% sodium deoxycholate, 150 mM NaCl) containing protease inhibitors (Roche). Lysates were centrifuged at 13,000 rpm for 15 minutes, and supernatant was collected. Protein concentrations were determined with Bradford assay. Cell lysate (50 μg) was resolved in 10% SDS-PAGE gel, transferred to PVDF membrane and immunoblotted with the indicated antibodies. All antibodies used in this study were obtained from Cell signaling Technologies. After transferring to PVDF membrane, the membrane was blocked with 5% BSA in TBST (50 mM Tris-HCl, 150 mM NaCl, 0.1% Tween) and incubated with primary antibodies (1:1000 dilution) in 5% BSA in TBST at 4 ^{o}C overnight. After washing

with TBST, the blot was incubated with secondary antibody for 2 hours at room temperature. After washing, chemiluminescence was used to visualize expression levels of p53, ASK1, JNK, OGT, β-tubulin, GRP78, Nrf2, NQO1, CTD110.6 in H1299, MDA-MB 231 and LNCaP cells upon incubation with various concentrations of 2-DG, and K8A.

3.5.7 Monitoring glycosylation by click chemistry

For glycosylation competition experiments, cells were incubated with different concentrations of K8A, Ac_4GlcNAl or both for 20 hours. After washing with PBS, cells were then lysed with RIPA buffer (50 mM Tris, pH 7.4, 1% NP-40, 0.25% sodium deoxycholate, 150 mM NaCl) containing protease inhibitors (Roche). Lysates were centrifuged at 13,000 rpm for 15 minutes, and supernatant was collected. Protein concentrations were determined with Bradford assay. Cell lysates (0.2 ml, 2 mg/mL protein concentration) were treated with stock solutions of rhodamine azide (final 200 μM) and tris(2-carboxyethylphosphine) (TCEP) (final 2 mM) prepared in water, TBTA (final 1mM) prepared in t-butanol/DMSO (4/1, vol/vol), and $CuSO_4$ (final 2 mM) prepared in water. After incubation at 37 ^{o}C for 1 hour, cell lysates were diluted with a loading buffer and separated on SDS-PAGE gel. Resolved proteins were imaged for fluorescence.

3.5.8 Monitoring glycosylation by mass spectrometry

In a reaction buffer (50 mM Tris–HCl, pH 7.4, 1 mM DTT, and 12.5 mM $MgCl_2$), 6 μg OGT (0.85 μg/μL), 0.25 mM OGT peptide, 0.5 mM UDP GlcNAc were added and incubated for 30 minutes at room temperature. The reaction was quenched by boiling. The proteins were removed by filtration with 30, 000 MW protein column and centrifuged at 13,000 rpm for 20 minutes. The supernatant was collected and injected to LC-MS (SHIMADZU 8040 Triple Quadrupole). The enzyme assay was repeated in the presence of K8 inhibitor at 100 μM.

3.5.9 OGT Peptide Synthesis

OGT peptide YSESPSTST, was synthesized using Fmoc chemistry and purified by reverse phase HPLC and dissolved in water at a stock solution of 10 mM. To sythesize the 9-mer peptide, 100 mg (0.087 mmol) of Wang resin was weighed and transferred to a column and washed with 1 column volume of DMF. After draining, the bottom was capped. Separately, Fmoc-Thr(tBu)-OH and 140 mg HBTU (0.37 mmol/g) was weighed and transferred to a vial containing 2 mL of base (5% DIPEA in DMF) and slightly vortexed. The mixture was transferred to the column which was inverted severally with occasional release of pressure. The column was rotated in a 3-hour coupling reaction. The column was then drained and washed with 5 column volumes DMF, 5 column volumes DCM and another 5 column volumes of DMF. After draining, a second coupling with the same Fmoc-Thr(tBu)-OH and HBTU was repeated and with washing in a similar way. Deprotection was done using 3 mL of deprotection solution (20% piperidine in DMF) in a rotator for 45 minutes, followed by washing in a similar way. The coupling, washing and deprotection steps were repeated for all the amino acids as in the table below. The remaining protection groups were cleaved off with a cleavage cocktail (90% TFA, 5% phenol, 2.5% water, 2.5% thioanisole). The supernatant was drained, concentrated in liquid nitrogen and precipitated with ether solution. The crude peptide was dissolved in 3 mL of water and purified in a reverse phase HPLC column. Characterization was done by LC-MS and ESI mass spectrometry.

Table 5**:** Mass of protected amino acids used for 9-mer OGT-peptide synthesis

Name and sequence of peptide					
OGT Peptide (TSTSPSESY)					
Name of resin			**[loading level]**	**Amount of resin**	**[mmol]**
Wang			0.87 mmol/g	100 mg	0.087
Amino acids					
	AA	**MW**	**mmol**	**mg**	
Thr	1	397.5	0.348	138.33	
Ser	2	383.4	0.348	133.4232	
Thr	3	397.5	0.348	138.33	
Ser	4	383.4	0.348	133.4232	
Pro	5	337.4	0.348	117.4152	
Ser	6	383.4	0.348	133.4232	
Glu	7	425.5	0.348	148.074	
Ser	8	383.4	0.348	133.4232	
Tyr	9	459.6	0.348	159.9408	

3.5.10 OGT isoforms

There are three known isoforms of OGT, all of which share an identical catalytic domain, but differ in the number of tetratricopeptide repeat motifs found at the N-terminus (Figure 79)[250, 275]. The longest form of OGT is found in the nucleus and cytoplasm (ncOGT; 116 kD), with the next longest isoform found in the mitochondria (mOGT; 103 kD). The shortest form of OGT (sOGT; 70 kD) is both nuclear and cytoplasmic. sOGT shares common carboxy-terminal catalytic domains with full length ncOGT, but they differ in length owing to variable numbers of amino-terminal tetratricopeptide repeats (TPRs).

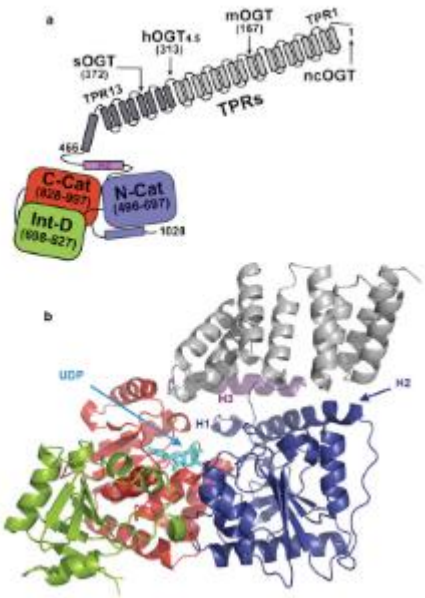

Figure 79-Overall structure of human OGT complexed to UDP (a), Schematic of OGT domain architecture with the TPR units shown in gray, the transitional helix (H3) in purple, the N-Cat domain in blue, the Int-D domain in green, and the C-Cat domain in red. The native isoforms of OGT (sOGT, mOGT, and ncOGT) and the crystallization construct differ only in the number of TPRs, as shown. (b), Overall fold of OGT from the OGT-UDP complex in a ribbon representation. The coloring is the same as the schematic in a. The UDP is shown in cyan. The N-Cat domain helices unique to OGT are indicated as H1 and H2.[275] Adapted with permission from Lazarus, M. B.; Nam, Y.; Jiang, J.; Sliz, P.; Walker, S., Structure of human O-GlcNAc transferase and its complex with a peptide substrate. *Nature* **2011,** *469*, 564.

3.5.11 Bacterial cell stock storage

A single colony was picked by a sterile tip and inoculated in 5 mL of LB media and incubated for 20 hours in a shaker with a rotator at 37ºC. 750 µL of this solution was then mixed with 250 µL of autoclaved 60% glycerol in a 1.5 mL eppendorf tube, flash frozen in liquid nitrogen and stored at -80 ºC freezer.

3.5.12 Bacterial cell transformation

A 50 µL aliquot of DH5α glycerol stock was thawed in ice for 10 minutes after which 50 ng of plasmid DNA was added and left on ice for about 20 minutes. The cells were then heat-shocked for 45 seconds at 42 ºC and quickly transferred on ice for another 2 minutes. The cells were then

mixed with 450 µL of super optimal (SOC) medium and incubated for 1 hour with rotation shaking at 37 ºC. The bacterial cells were then evenly spread on agar plates containing appropriate antibiotic and incubated at 37 ºC for 20 hours.

3.5.13 DNA plasmid extraction with Miniprep Kit

About 1 µL of bacterial cell stock containing appropriate plasmid was inoculated in 5 mL of LB media with appropriate antibiotic and incubated at 37 ºC with rotation for 20 hours. The DNA was extracted using the QIAGEN miniprep kit. The overnight culture solution was centrifuged at 5,000 rpm for 10 minutes and the supernatant was disposed. The cell pellet was resuspended in 250 µL of buffer P1 (50mM Tris-HCl, pH 8.0, 10 mM EDTA, 100 µg/mL RNAse). 250 µL of a lysis buffer P2 (200 mM sodium hydroxide, 1% SDS) was then added and the tube was gently shaken 6 times, followed by 350 µL neutralization buffer N3 (3.0 M potassium acetate, pH 5.5) with gentle shaking 6 times. The mixture was then centrifuged at 13,000 rpm for 10 minutes. The supernatant was transferred to a spin column that allows DNA binding, followed by centrifugation at 13,000 rpm twice. The flow through was discarded and the spin column with bound DNA washed twice with 500 µL of a wash buffer. Bound DNA was eluted with 30 µL water by centrifugation at 13,000rpm for 2 minutes. The DNA concentration was determined by UV at 260 and 280 nm.

3.5.14 Polymerase chain reaction (PCR)

OGT gene encoding short OGT was amplified from PRK5-OGT vector by PCR using a thermocycler (Eppendorf Master Cycler Gradient). The PCR reaction mixture consisted of 50 ng of a template plasmid with OGT gene, 1 µL each of forward and reverse primers from 10 µM stock solution, 5 µL of ultra pfu buffer and 2 µL of dNTPs from a 10 mM stock of nitrogen bases. The final reaction mixture was 50 µL with addition of deionized water and 1 µL of pfu enzyme. The

thermocycler was programmed as in the table below. The PCR product was checked by agarose gel electrophoresis.

Table 6: PCR cycles program for OGT gene amplification

Cycle type	Temperature (°C)	Time	Number of cycles
Initial denaturation	95	5minutes	1
Denaturation	95	1minute	35
Annealing	55	1minute	35
Extension	72	1minute	35
Final extension	72	10minutes	1

3.5.15 Restriction digestion

A construct encoding short human OGT1 cDNA was cloned into PET28a vector (Novagen Catalogue number-698643) after double restriction digestion with BamH1 and Not1. PCR product was digested by incubating in 1 µL BamH1 enzyme and 1 µL Not1 enzyme and 5µL 10x Cutsmart NEB buffer and 1 µL of BSA (from 10 mg/ml BSA stock) in a 50 µL aqueous solution. Digestion was done in an incubator at 37°C for 2 hours. The digested PCR product size was checked by running an agarose gel (90 V for 40 minutes).

3.5.16 Ligation

Ligation was carried out at 16 °C for 20 hours in 20 µL volume. The ligation mixture consisted of double digested pET28a vector and OGT1 gene in 1:5 ratio, 1 µL from T4 DNA ligase enzyme (400,000 units/mL) and deionized water. The PCR clean-up protocol was performed on the ligation mixture after which it was put on ice for 20 minutes (PCR cleanup is not necessary). Transformation was carried out as described above and plated on agar plates with Kanamycin (50 µg/mL). After 20 hours, a single colony was picked from the plate and used to inoculate 5 mL LB

culture media with 50 μg/mL Kanamycin. DNA extraction was done as above, and concentration determined by the Nanodrop UV absorbance meter. The gene construct was confirmed by DNA sequencing.

3.5.17 Bacterial protein expression and purification of sOGT

pET28a containing sOGT gene construct was transformed into *E. coli* BL21(DE3) bacterial strain. BL21 cells were grown at 37 ºC in Luria broth containing Kanamycin (50 μg/mL) to an OD_{600} of 0.8 and induced with 1 mM isopropyl β-D-1-thiogalactopyranoside (IPTG). Cells were further grown at 18 ºC for 20 hours, then harvested by centrifugation for 20 minutes at 5,000 rpm and resuspended in a lysis buffer (100 mM Tris-HCl pH 7.4, 125 mM NaCl, 10 mM imidazole, 250 μM DTT). Lysates were prepared by passing cell suspension through a chilled French press twice at 1,500 psi. The cell lysates were centrifuged at 14,000 rpm and the supernatant was loaded on and incubated with prewashed nickel beads for 3 hours. After draining the flow through, the nickel beads were washed with a wash buffer (pH 7.4, 125 mM NaCl, 50 mM imidazole, 250 μM DTT) and the protein was eluted with an elution buffer (100 mM Tris-HCl, pH 7.4, 125 mM NaCl, 250 mM imidazole, 250 μM DTT. The fractions containing pure His-tagged protein were determined from SDS PAGE, combined and dialyzed with a dialysis buffer (100 mM Tris-HCl pH=7.4, 125 mM NaCl, 12 mM $MgCl_2$). The protein was concentrated, and the concentration was determined by Bradford Assay (Bio-Rad)

CHAPTER 4 METABOLOMIC STUDIES IN K8A-TREATED H1299 CANCER CELLS

4.1 Introduction

The fate of glucose in cancer cells include cellular energetic pathways such as glycolysis, tricarboxylic acid cycle and mitochondrial electron transport chain. Glucose is also the major source of NADPH generated by the pentose phosphate pathway (PPP). NADPH maintains redox homeostasis by maintaining antioxidants such as glutathione in their reduced state. Additionally, the hexosamine biosynthetic pathway (HBP) contributes to redox homeostasis by generation of UDP-GlcNAc that is important for O-GlcNAcylation of proteins. Protein modifications such as glutathionylation and O-GlcNAcylation protect proteins from oxidative stress. Metabolite flux in glycolysis, the PPP, TCA and HBP are intricately controlled in cancer cells for survival, proliferation and ROS detoxification. For these reasons, cancer cells have evolved coping mechanisms that include metabolic reprogramming and alternative signaling cascades to regulate levels of ROS that are elevated in most cancer cells.

Small molecules that disrupt glucose metabolism elevate ROS and cause cancer cell death. The glucose metabolism inhibitors, such as 2-deoxy-D-glucose, bromopyruvate[276] and lonidamine[277], induce ROS and selectively target cancer cells. Additionally, glucose deprivation induced ROS and cell death of diverse cancer types[158]. Of note is the disruption of cellular energetics by reduction of energy storage compounds, such as ATP with elevation of AMP by these glycolytic inhibitors[26]. Elevation of AMP activates AMPK that acts as the energy sensor of the cell[266]. AMPK has multiple targets, including p53. Wild type p53 is a tumor suppressor protein that regulates cell cycle growth and induce apoptosis[266, 278].

Importantly, the PPP and HBP enzymes respond to elevation of ROS generated by glycolytic inhibitors to protect the cell. Under oxidative stress, glycolytic flux reverses to feed the PPP and

HBP that provide NADPH and UDP-GlcNAc[29, 63]. NADPH and UDP-GlcNAc are precursors to glutathione and O-GlcNAcylation. Additionally, oxidative stress induces ER stress and the UPR to maintain proteostasis[9]. Glycolytic inhibitors such as 2-DG induce ER stress, block N-glycosylation and elevate O-GlcNAcylation. ER stress is detected initially by elevation of grp78[279]. grp78 is an ER resident protein that senses a dramatic drop in glucose levels in a cell and provide the direct link between nutrient status of a cell, oxidative stress and protein folding[280].

Targeting cancer cell metabolism provides a multipronged approach of induction of metabolic stress that lead to overall cellular stress. Carbohydrate-based molecules that target cell metabolism hold therapeutic potential because cancer cells show phenotypes that enhance selectivity. Elevated sugar-uptake and high ROS in cancer cells is a dual phenotype that was exploited to target cancer cell metabolism. To test this hypothesis, an N-aryl glycoside (K8A) was first evaluated for ROS induction in H1299 cells and found to generate 2-fold ROS levels compared to the control. Additionally, K8A activated AMPK in both HEK 293 and H1299 cells, compelling this work to evaluate metabolite levels involved in cellular metabolism in glycolysis, PPP and TCA cycles via the metabolomics approach.

4.2 Metabolomics Approach

To investigate whether K8A disrupted metabolism, a metabolomics approach[281-282] was used to quantify metabolites at a fixed metabolic state in H1299 lung cancer cells. The goal of metabolomics studies was to identify significantly altered metabolite levels and altered biochemical pathways upon treatment of K8A. The cells were grown to about 80% confluency before treatment with 100 μM K8A for 20 hours. Metabolomics involved metabolites of various pathways that include glycolysis, PPP and TCA cycle using a method previously optimized[283]. LC-MS detection involved a one-step liquid-liquid organic solvent extraction of cultured H1299

cells and separation on a 1 mm x150 mm HILIC specific column in a 35-minute separation cycle. The metabolite detection was compared with untreated controls with the same protein concentration. All metabolites with the internal standards were measured by ESI ionization on a LC-QTOF mass spectrometer.

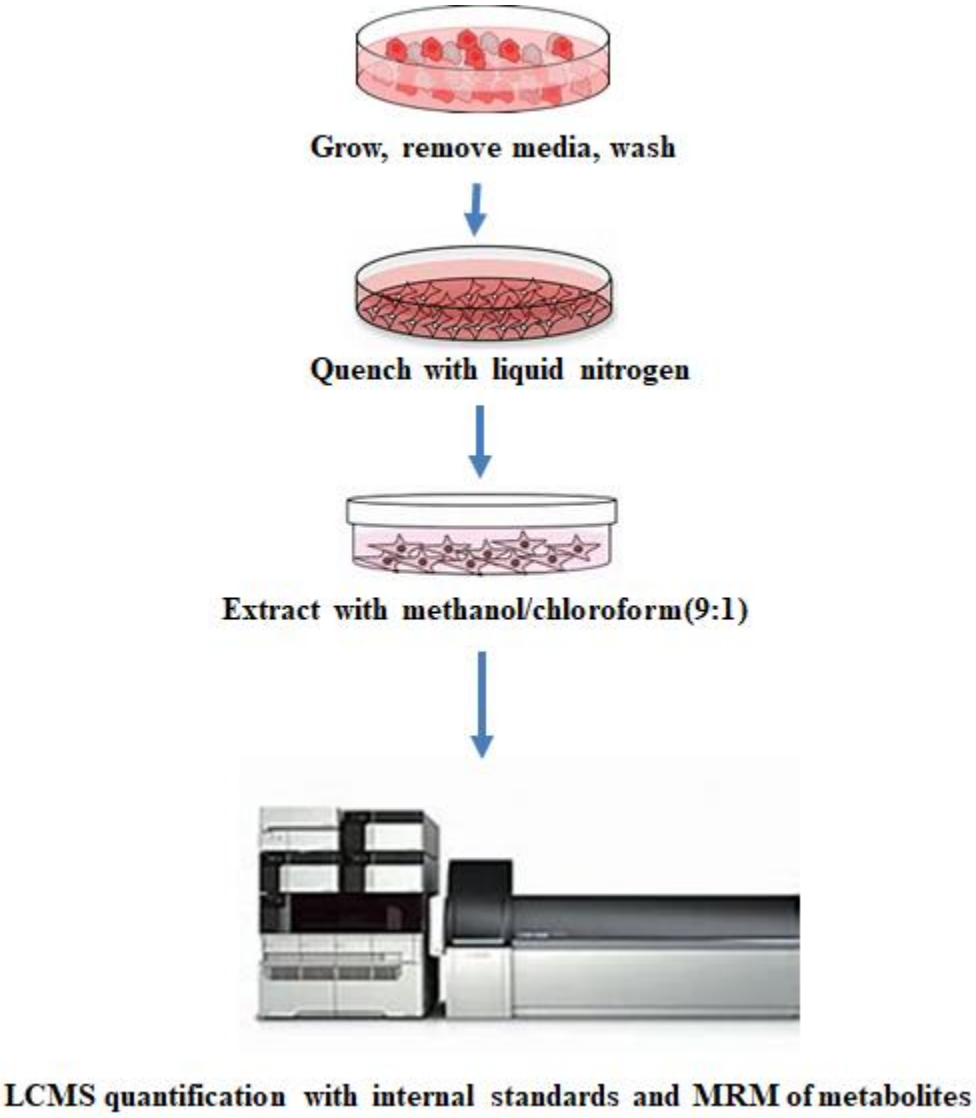

Figure 80-Metabolomics work flow.

4.3 Results

4.3.1 Optimization of metabolite extraction

H1299 cell metabolism was quenched using liquid nitrogen in ice conditions and stored in -80 ^{0}C freezer. Metabolites were extracted using 80% methanol without cell lysis from cells pretreated with C-12 and C-13 glucose. Previously, trypsinization, physical removal, centrifugation and filtration prior to quenching significantly altered the metabolite profile[284-285]. The mixture of metabolite solution was injected into a LC-MS (SHIMADZU 8040) with an optimized multiple reaction monitoring for glucose. The sodium adducts for C-12 and C-13 were then extracted from the mass spectrum (Figure 81). The data revealed that the metabolite extraction method was reliable and robust. Additionally, the LC/MS/MS instrument was optimized to run on negative ion mode at a collision energy of 15.0 volts and the C-13 glucose molecular transition 185 to 91 was observed (Figure 82). The cells were then lysed with PBS and protein concentration quantified by Bradford assay. To quantify metabolites, a LC-QTOF mass spectrometer was used as previously described.

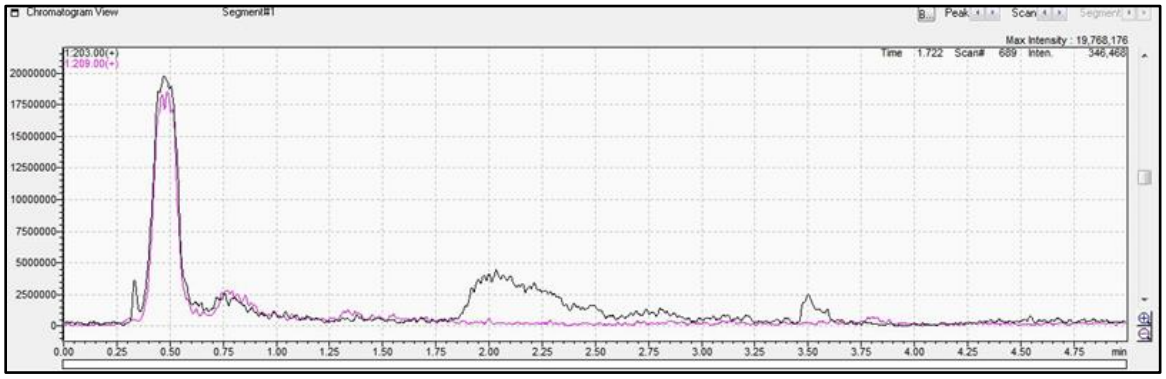

Figure 81-Mass spectrum for C^{12}-C^{13-}glucose from cell extract showing M/Z^{Na+} =203, 209 peaks

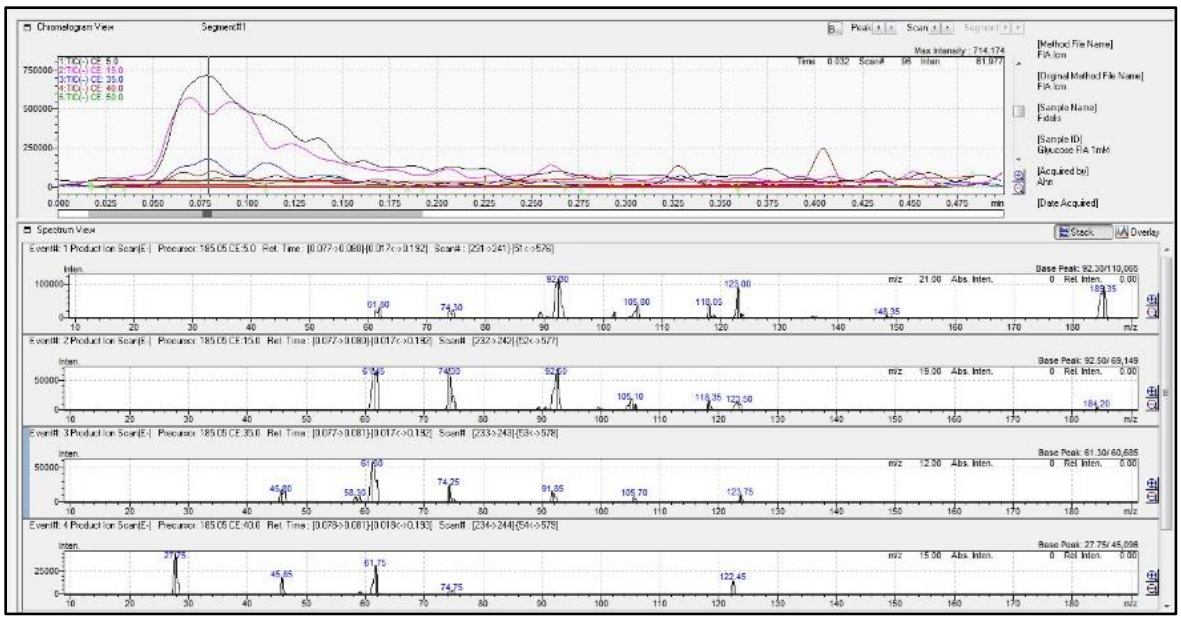

Figure 82-Optimization of collision energies for LC/MSMS molecular transition of C-13 glucose.

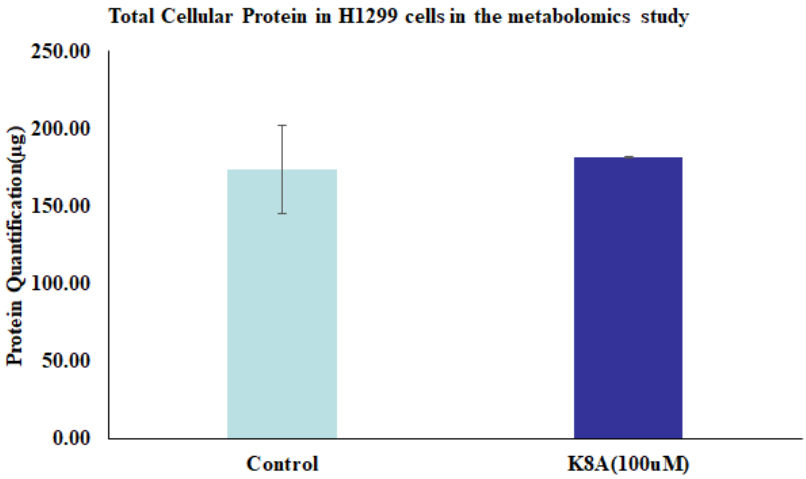

Figure 83-Protein levels of metabolite extracts from H1299 cells

4.3.2 Metabolomics data analysis

The protocol and data analysis were done at the University of Michigan Metabolomics core and contained two different forms of data: one is Gly-TCA-quantitative, the other is TCA-plus. The difference between them is that for the quantitative report, there was a full calibration curve, so

the values were reported as μM or μmol/μg protein, depending on the normalization to the protein content of the H1299 cells (Figure 83). These data set was converted to picomoles.

For the TCA-plus, the data is semi-quantitative, so the areas normalized to an internal standard were used. Additionally, although it is important to normalize when there are large differences in the number of cells produced under control and treatment conditions, we used the non-normalized data because the protein content of the treated and untreated samples showed very minimal cell number differences. In terms of data quality, the pools served as the primary quality check. of the pool indicates the extract from each of our samples. This pool is injected multiple times over the course of the analysis. Thus, if the data for the pools looks consistent, this tells us not only that the instrument is running well, but that the data quality (peak shape and area) are good enough that the data analysis software can successfully integrate them. The data for the pools for each compound can be found on the Raw data appendix. The RSDs for the pools averaged around 2-5%. The quantitative and semiquantitative metabolite data was grouped and graphed into various metabolic pathways.

4.3.3 Glycolytic metabolite levels in K8A-treated H1299 cells

Glycolytic metabolites were evaluated at 100 μM K8A treatment with untreated controls in triplicate. Although glycolysis is a step-wise sequence of ten enzyme-catalyzed reactions, the intermediates provide entry points to glycolysis[286]. The first five phases constitute the investment phase because ATP is consumed, whereas the final five steps constitute the payoff phase because ATP is produced[282]. We determined levels of G6P, F6P, FBP, 2PG, 3PG, DHAP, G3P and PEP. Glucose is converted to glucose-6-phosphate by hexokinase and then isomerized to F6P by hexose phosphate isomerase. In the third step, PFK1 expends ATP energy to phosphorylate F6P to FBP.

FBP is then cleaved by an aldolase into DHAP, and G3P. In the fifth step, triose phosphate isomerase interconverts DHAP and G3P.

In the payoff phase, G3P is converted to 1,3BPG with production of NADH. In the next step, 1,3BPG provide a phosphate to ADP that generate ATP and 3PG. 3PG is converted to 2PG which produce PEP. PEP provides the second ATP with release of pyruvate. DHAP when converted to G3P, is processed by the glycolytic enzymes in a similar way.

Metabolomics revealed that G6P/F6P pair of metabolites increased more than 2-fold with treatment of 100 μM K8A compared to untreated controls (Figure 84). G6P and F6P being isomers had similar molecular transitions during MRM in the metabolomics analysis. There was an insignificant decrease in FBP levels with K8A treatment. DHAP and G3P levels were however unchanged with this treatment (Figure 85, 86). There was no significant difference in metabolite levels 2PG/3PG between treated and untreated controls. 2PG and 3PG are isomers and had the same indistinguishable product ion masses. G6P and F6P are at the branch points of PPP and HBP respectively and elevation of these metabolites point to oxidative response induced by K8A. Notably, K8A induced a five-fold increase in PEP (Figure 87) consistent with ROS induced elevation of PEP recently reported[282].

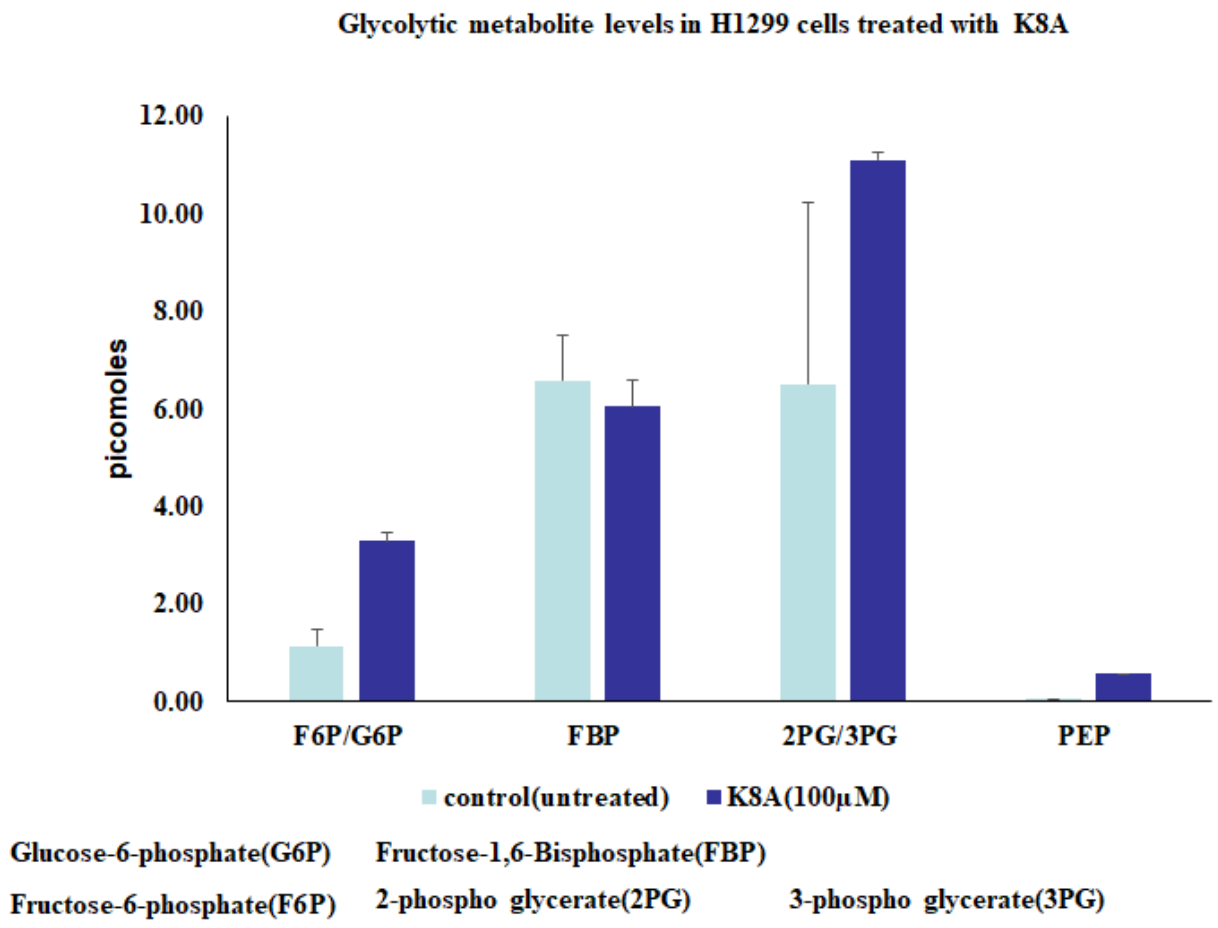

Figure 84-Glycolytic metabolite levels in K8A-treated H1299 cells

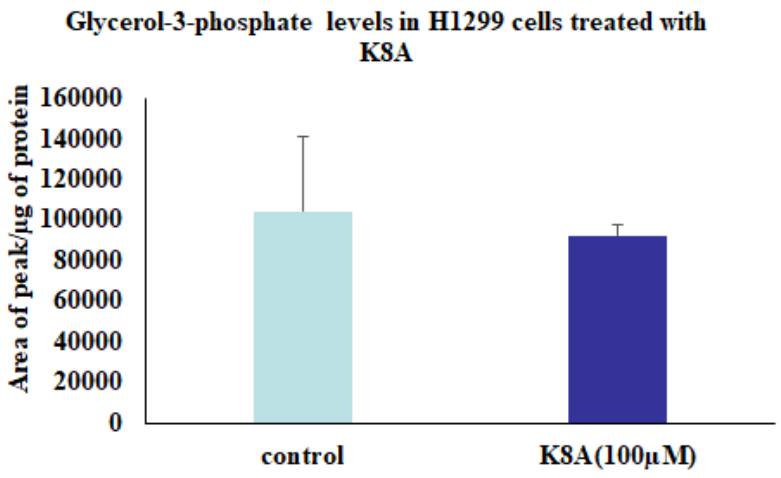

Figure 85-Glycerol-3-phosphate levels in K8A-treated H1299 cells

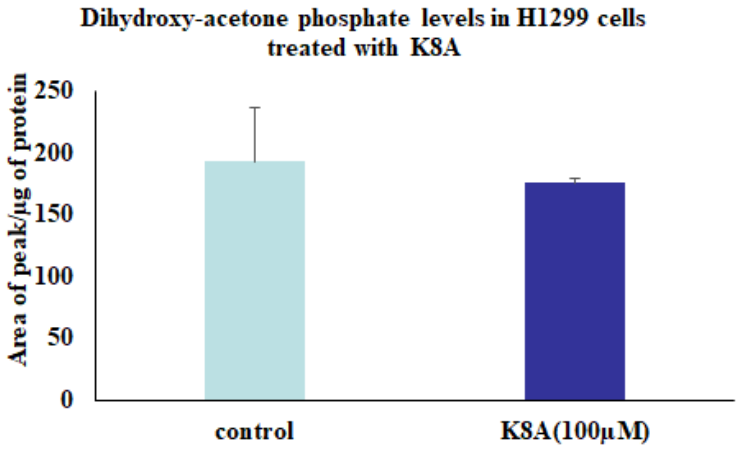

Figure 86-Dihydroxy-acetone phosphate levels in K8A-treated H1299 cells

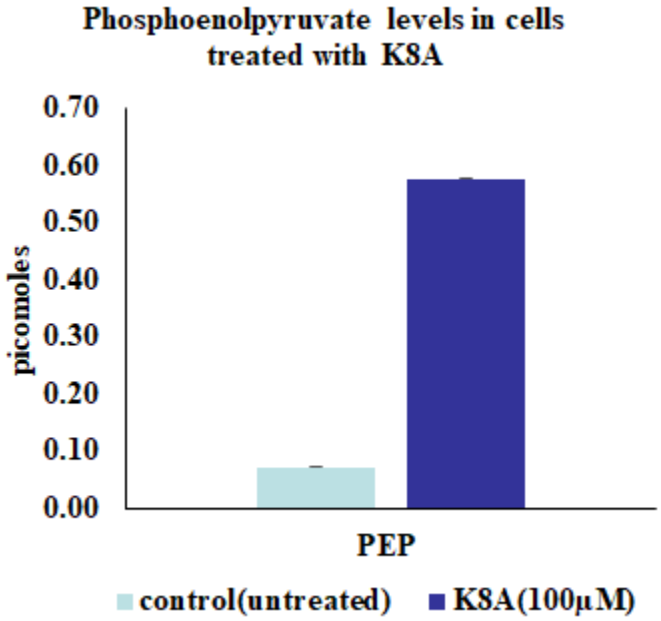

Figure 87-Phosphoenol pyruvate levels in K8A-treated H1299 cells; unsure of what is the statistical analysis in these data.

4.3.4 Pentose phosphate pathway metabolite levels in K8A-treated H1299 cells

The PPP generates NADPH in the oxidative phase and pentoses in the non-oxidative phase. NADPH utility includes ROS detoxification and fatty acid synthesis. R5P is used in nucleotide synthesis and E4P is used in synthesis of aromatic amino acids. The glycolysis-PPP branchpoint

metabolite G6P was increased with K8A treatment as mentioned above. Further metabolomics revealed about fivefold increase in R5P and E4P with 100 µM treatment of H1299 cells (Figure 88). Additionally, a non-significant increase of 6PG and NADP was observed with unchanged NADPH levels (Figure 88, 89). Overall, the PPP was elevated but notably the NADPH/NADP ratio was dramatically reduced in K8A treated cells compared to the untreated controls (Figure 89).

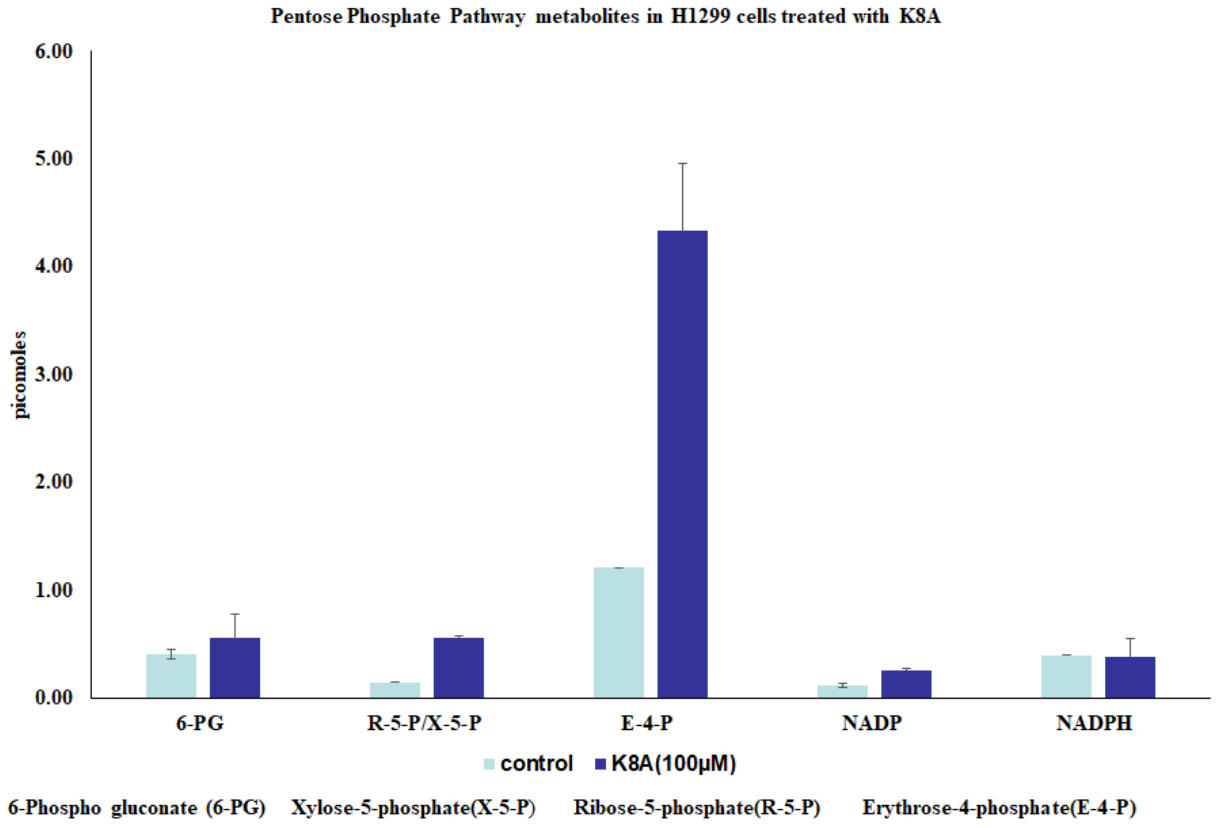

Figure 88- Pentose Phosphate pathway metabolite levels in K8A-treated H1299 cells

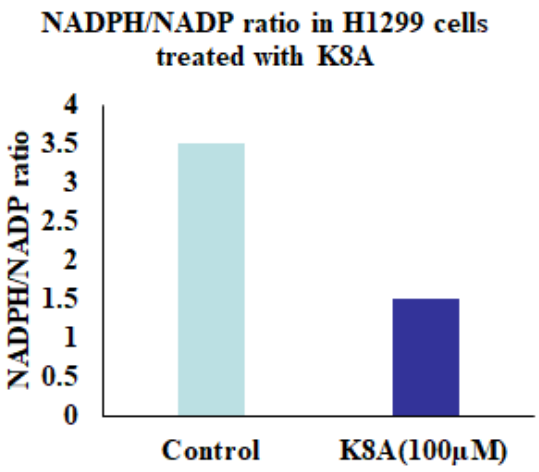

Figure 89-NADPH/NADP ratio in K8A-treated H1299 cells

4.3.5 Hexosamine biosynthetic pathway metabolite levels in H1299 cells

HBP relies on multiple substrates to synthesize UDP-GlcNAc that include glucose, glutamine, acetyl CoA and UTP. The glycolytic-HBP branchpoint F6P requires glutamine for conversion to glucosamine-6-phosphate. GlcN-6P is then acetylated by acetyl CoA to form GlcNAc-6P. GlcNAc-6P is isomerized to GlcNAc-1P which is then activated by UTP to generate UDP-GlcNAc.

Metabolomics revealed 10-fold increase in UDP-GlcNAc levels indicating dramatic upregulation of HBP by K8A (Figure 90). HBP substrate analysis revealed unchanged levels of hexoses and acetyl CoA and marginal increase in glutamine uptake with 100 μM K8A treatment of H1299 cells. Of note is 2-fold reduction of UTP levels and 2-fold increase of UDP levels (Figure 91). These changes are likely reflected by the final step of UDP-GlcNAc synthesis. Additionally, there was a 2-fold increase in N-acetyl glucosamine-1-phosphate levels (GlcNAc-1P) that is activated by UTP at this stage to produce UDP-GlcNAc. UDP-glucose and UDP-glucuronate levels (Figure 92) also increased 2-fold with K8A treatment in H1299 cells. UDP-glucose and NAD^+ are substrates for UDP-glucose dehydrogenase that generate UDP-glucuronate. UDP-

glucuronate are precursors for synthesis of various polysaccharides that include glycogen, glycosaminoglycans and proteoglycans.

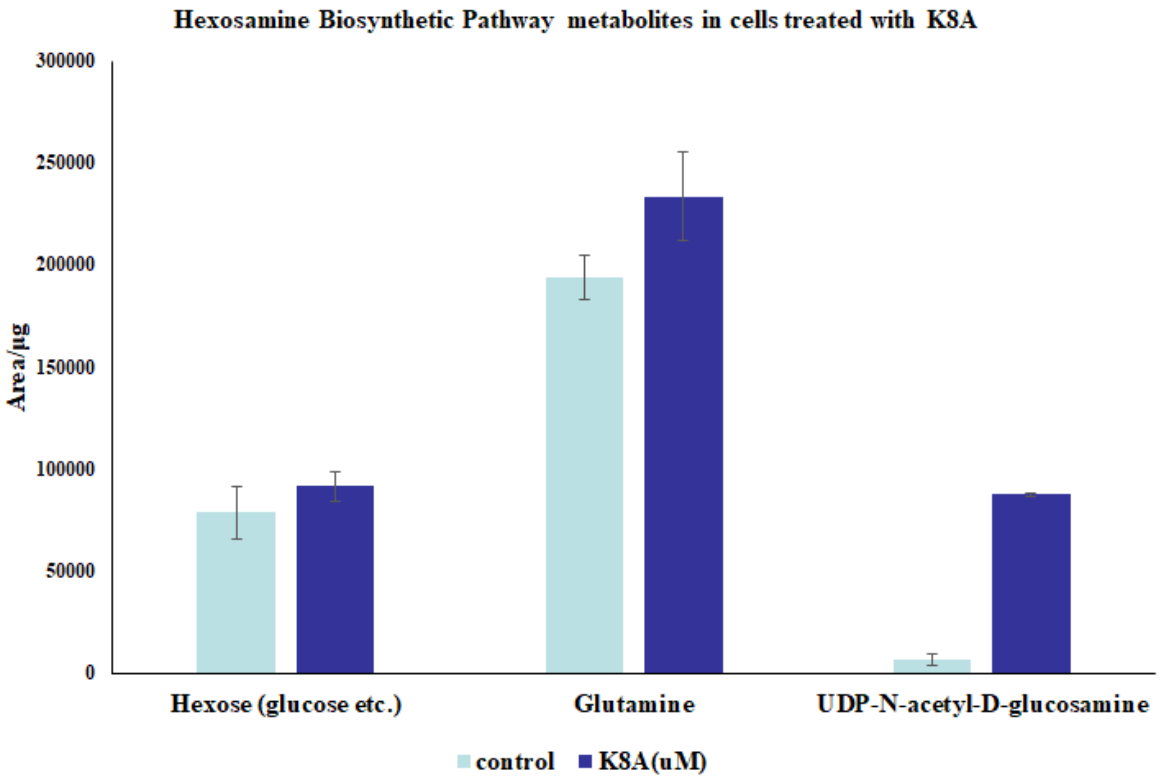

Figure 90-Hexosamine biosynthetic pathway metabolites in K8A-treated H1299 cells

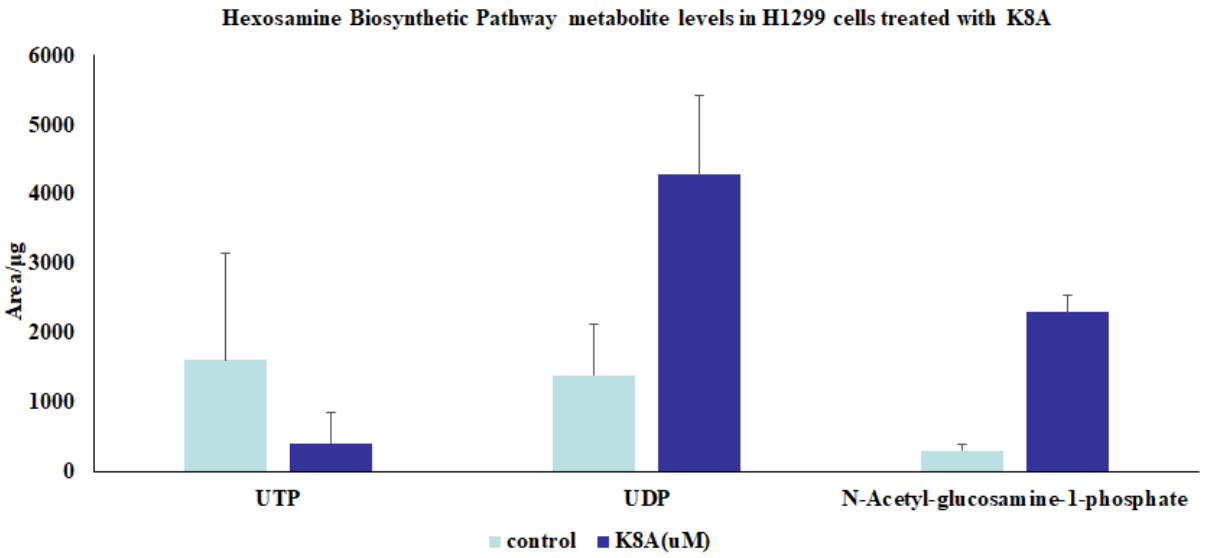

Figure 91-UTP, UDP and N-acetyl-glucosamine-1-phosphate levels in H1299 cells

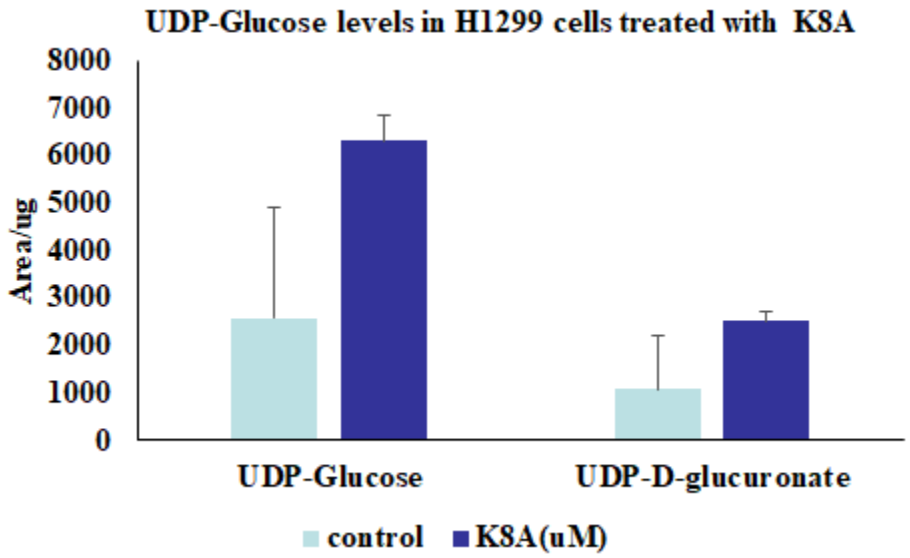

Figure 92-UDP-glucose and UDP-D-glucuronate levels in K8A-treated H1299 cells

4.3.6 Validation of HBP elevation by Western blot studies

Metabolomics revealed elevation of various HBP metabolites including UDP-glucose, UDP-glucuronate, N-acetyl glucosamine-1-phosphate and UDP-N-acetyl glucosamine (UDP-GlcNAc). UDP-GlcNAc is used for O-GlcNAcylation of proteins by OGT enzyme. Validation of UDP-elevation was done in OGT transfected and non-transfected H1299 cells by O-GlcNAc specific antibody (CTD 110.6). An increase in O-GlcNAcylation was observed within 100 μM K8A that was further increased with OGT transfection. OGT levels were unchanged but were higher in 2-DG treated cells.

4.3.7 Tricarboxylic Acid metabolite levels in H1299 cells treated with K8A

The TCA cycle is directly involved in cellular energetics. TCA cycle is a series of chemical reactions that release energy by oxidation of acetyl CoA. In the TCA cycle, three equivalents of NAD^+ are converted into three equivalents of NADH. One equivalent of GDP converts to GTP and then to ATP. Additionally, one equivalent of FAD produces one equivalent of $FADH_2$.

Importantly, NADH and $FADH_2$ are used as reducing agents in oxidative phosphorylation to generate ATP. Levels of NAD^+ and NADH were determined in this metabolomics analysis.

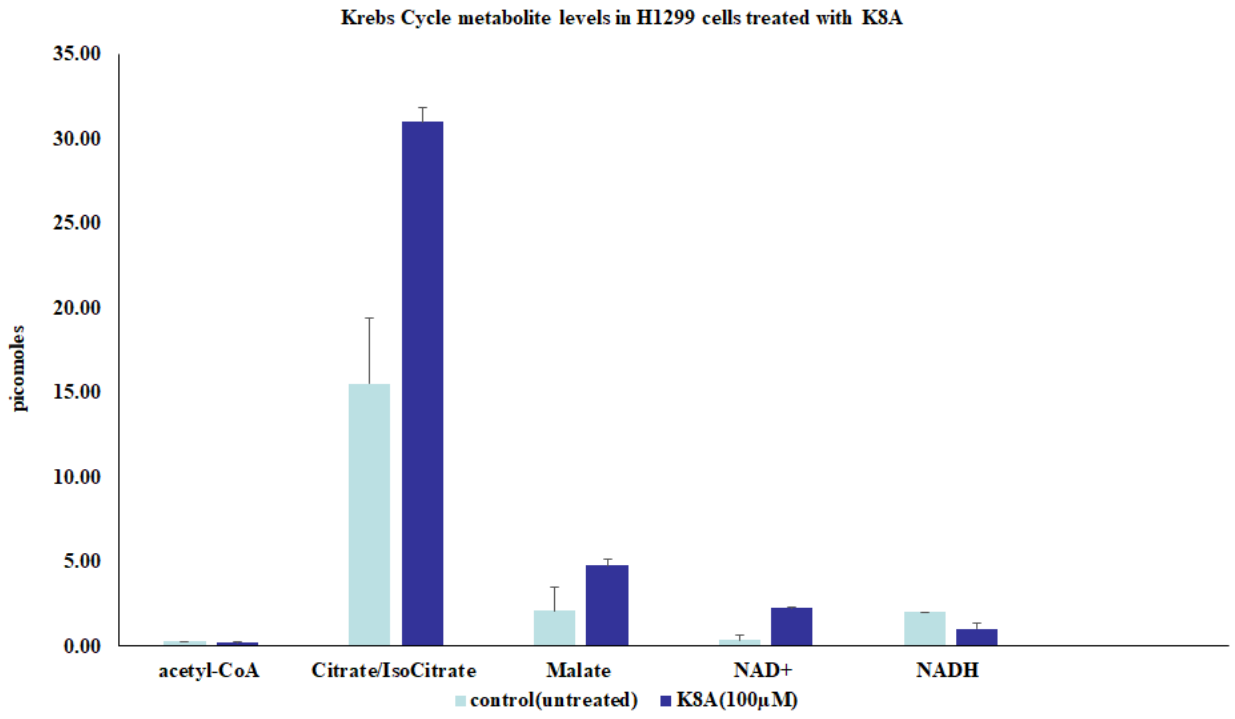

Figure 93-TCA metabolite levels in K8A-treated H1299 cells

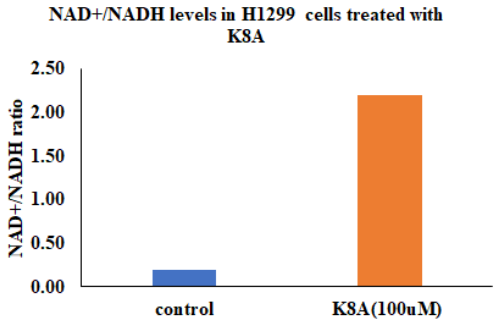

Figure 94-NAD^+/NADH levels in K8A-treated cells

Acetyl CoA levels remained unchanged with K8A treatment in H1299 cells consistent with recent metabolomics data on ROS induction[282]. Metabolomics analysis further revealed that citrate, isocitrate, and malate were increased 2-fold with 100 µM K8A treatment (Figure 93). Of note is the 4-fold increase of NAD^+ and 2-fold decrease of NADH (Figure 94). Notably, a ratio of

NAD^+ to NADH was increased 10-fold pointing to depletion of reducing equivalents necessary for ATP synthesis. Supporting AMPK activation shown by Western blot data in chapter 3, I observed an increase of ATP hydrolysis products, such as ADP and AMP (Figure 94). Other energy storage compounds such as UTP was equally decreased (Figure 95). Concomitantly, other cellular energy hydrolytic metabolites, such as UDP, UMP and GMP were disrupted.

AMP binds to energy sensing AMPK. AMPK consist of α, β, and γ subunits. Each of these subunits are involved in stabilization and activity of AMPK. Specifically, the γ subunit has ability to sense changes in the ratio of AMP to ATP. AMP binding to the γ subunit invokes a conformational change that exposes the phosphorylation site on the catalytic domain located on the α subunit. AMPK activation mitigates against dramatic losses of ATP in a cell[282]. K8A induced this activation at lower concentrations than 2-DG in HEK 293 and H1299 cells.

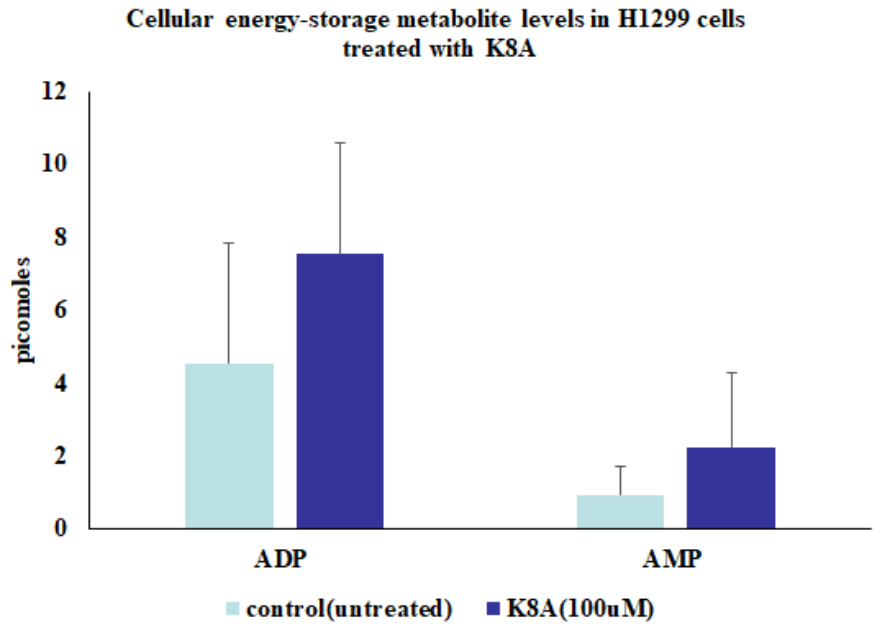

Figure 95-ADP and AMP levels in K8A-treated H1299 cells

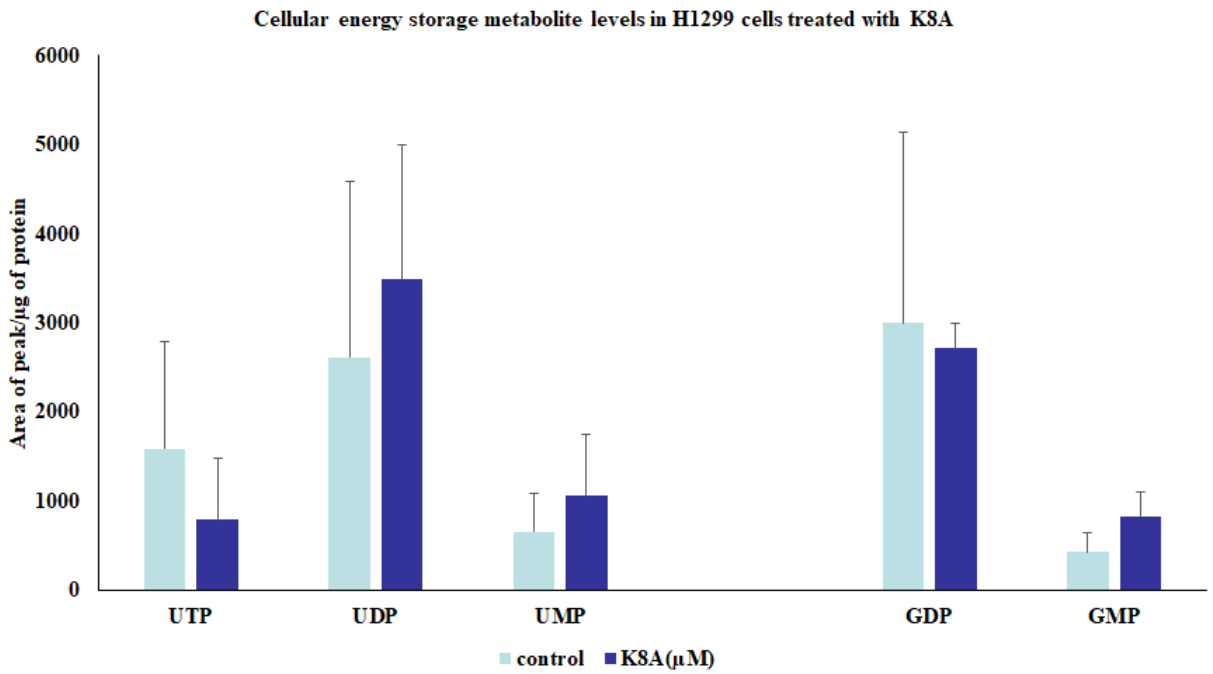

Figure 96-UTP, UDP, UMP, GDP and GMP levels in K8A-treated H1299 cells.

4.4 Amino acid levels in H1299 cells treated with K8A

Amino acid carbon backbones are generated from intermediates of glycolysis, PPP and TCA. Glycolytic 3-phosphoglycerate for example is the precursor for serine biosynthesis[287]. Serine is used in glycine, cysteine and NADPH biosynthesis that are important for glutathione homeostasis[288]. E4P from the PPP is used in synthesis of aromatic amino acids that include phenylalanine, tyrosine and tryptophan[289]. On the other hand, α-ketoglutarate from the TCA cycle is the precursor for many amino acids that include glutamate and glutamine[290]. We observed marginal (10%) increase of glutamate and glutamine with K8A incubation (Figure 99). Glutamine is required in HBP synthesis and ROS detoxification.

Conversely, there was a 2-fold increase in aspartate levels with K8A treatment at 100 µM (Figure 97). Aspartate may be used to generate oxaloacetate that is important in the TCA cycle. In addition, asparagine synthetase synthesizes asparagine from aspartate. This enzymatic reaction requires glutamine and ATP and generate glutamate. There was no significant difference in other

amino acid levels with K8A treatment in H1299 cells (Figure 96). Glycine and cysteine was not detected in this metabolomics study. Of note is the 2-fold increase of citrulline levels (Figure 99) with similar reduction of arginine which is the precursor molecule for citrulline biosynthesis. Nitric oxide synthase catalyzes this reaction that also require NADPH and oxygen to generate nitric oxide, $NADP^+$ and citrulline.

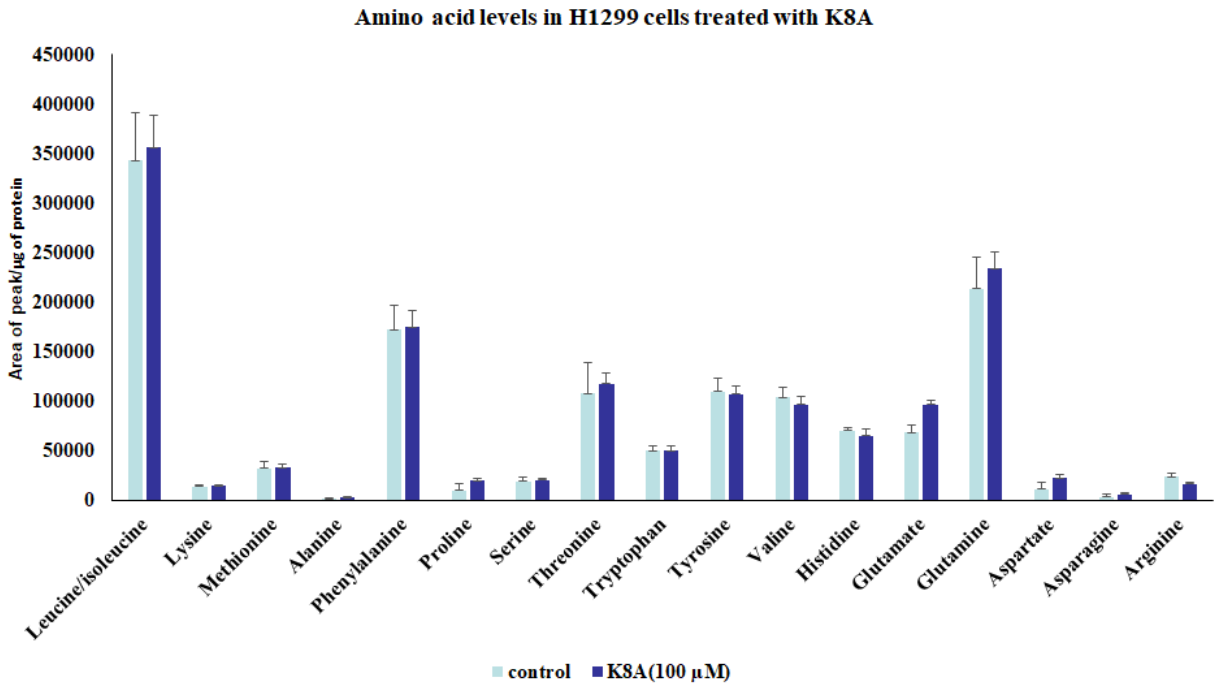

Figure 97-Amino acid levels in K8A-treated H1299 cells

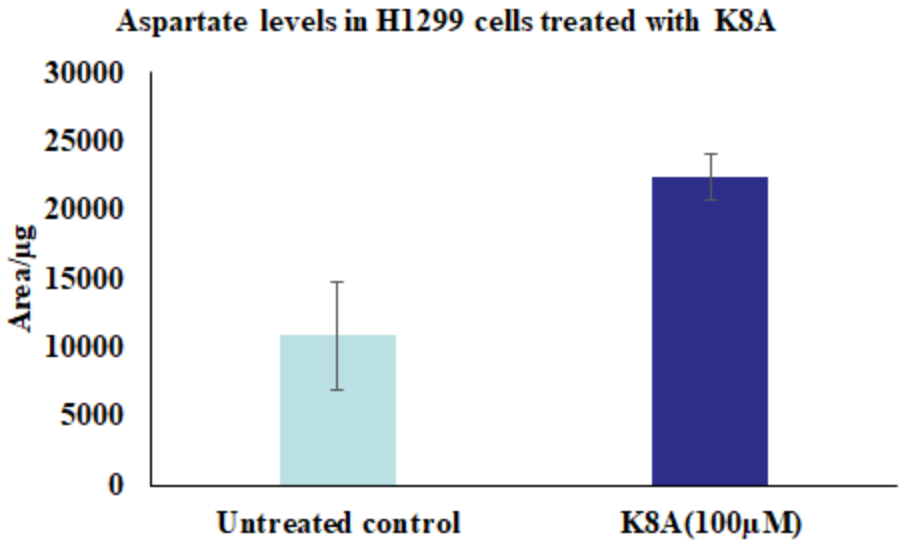

Figure 98-Aspartate levels in K8A-treated H1299 cells

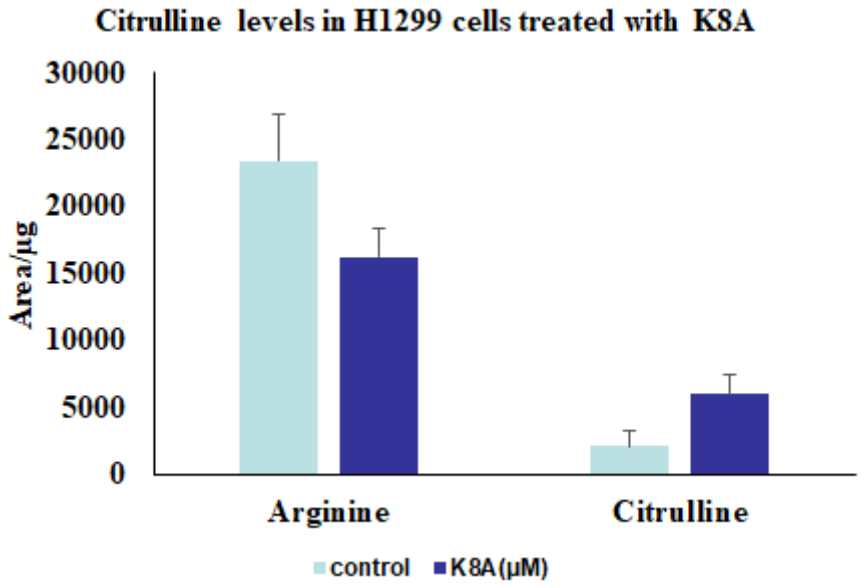

Figure 99-Arginine and citrulline levels in K8A-treated H1299 cells

4.5 Fatty acid levels in cells treated with K8A

Fatty acids are synthesized from acetyl CoA generated from glycolytic substrate pyruvate. Fatty acid synthesis also require NADPH generated from the PPP. Importantly, fatty acids are sources

of energy and a major component of cell membranes. Metabolomics revealed no change in levels of oleic acid, palmitic acid and stearic acid with treatment of K8A (Figure 99).

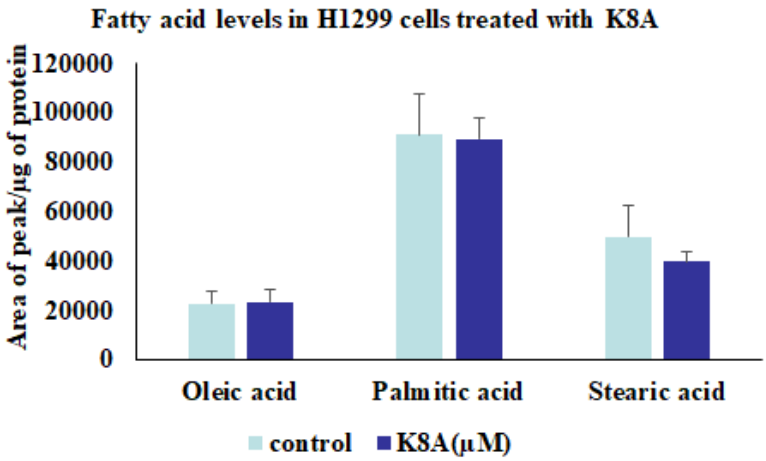

Figure 100-Oleic acid, palmitic acid and stearic acid levels in K8A-treated cells

4.6 Purine and Pyrimidine synthesis metabolite levels in H1299 cells treated with K8A

Purine and pyrimidine synthesis is important for generation of nucleotides, TCA metabolites such as fumarate and reducing equivalents such as NADH. IMP is a purine and a precursor for GMP and AMP synthesis. IMP levels were increased 2-fold upon K8A treatment in H1299 cells. Xanthine is a purine and an intermediate in the degradation of adenosine. Xanthine may be generated from hypoxanthine in a reaction catalyzed by xanthine oxidase that generate reactive oxygen species in form of the superoxide anion. In this metabolomics study, the levels of hypoxanthine and xanthine remained unchanged with treatment of 100 µM K8A in H1299 cells (Figure 101). Unchanged xanthine levels with unaltered Nrf2 expression warrants further study considering recent reports of coactivation of Nrf2-HKII complex in XOR expression[52].

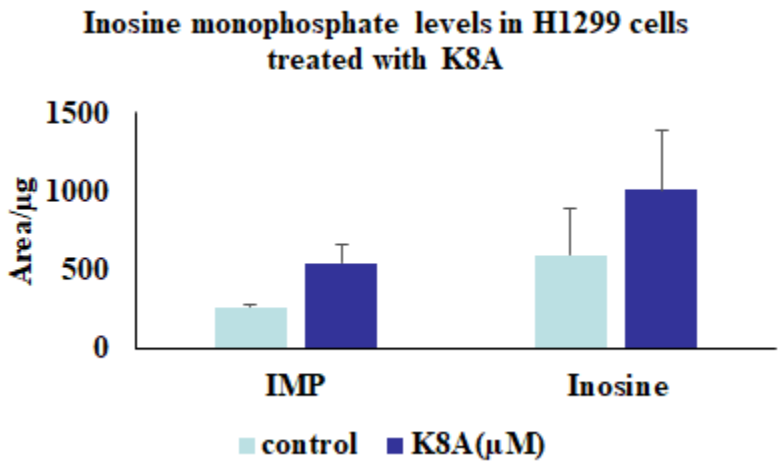

Figure 101-Inosine and IMP levels in H1299 cells

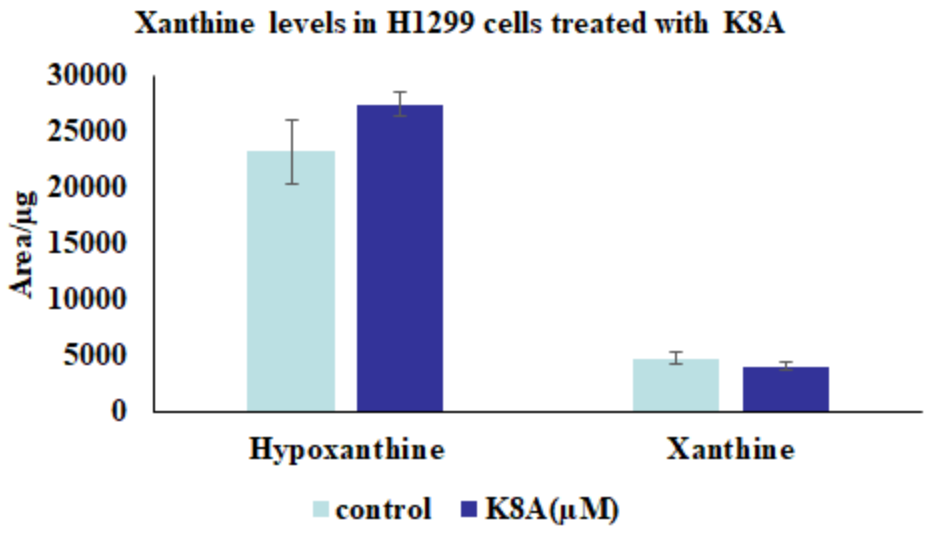

Figure 102-Hypoxanthine and xanthine levels in H1299 cells

4.7 Discussion

Glycolytic enzymes, such as hexokinase II (HKII), glyceraldehyde-3-phosphate dehydrogenase (GAPDH) and pyruvate kinase isoform (PKM2) are involved in redox homeostasis. Importantly, GAPDH acts as a reversible metabolic switch under oxidative stress. Additionally, mitochondrial superoxide overproduction inhibits GAPDH and activates the HBP to increase cellular O-GlcNAcylation. The activation of the HBP is presumably due to inhibition of GAPDH, thus

redirecting F6P from glycolysis to UDP-GlcNAc formation. We observed an increase in K8A-induced ROS production and G6P/F6P elevation in our metabolomics studies consistent with recent findings[282]. Hexose levels remained unaltered suggesting that the increased levels of G6P and F6P were due to activity of glycolytic enzymes.

Of note is the oxidation of one single cysteine residue in GAPDH catalytic site inactivates GAPDH to reverse glycolytic flux towards the PPP. Other ROS-sensitive glycolytic enzymes are PFK1 and PKM2 that redirect metabolites towards HBP and PPP. Additionally, metabolomics revealed a five-fold increase of PEP upon treatment of K8A to H1299 cells. Conversely, G6PD that catalyzes the rate limiting step in PPP is activated by O-GlcNAcylation at serine 84. G6PD converts G6P to 6-PG and NADPH[40]. Metabolic profiling showed the relative increase of 6-PG and R-5-P/X-5-P with K8A treatment in H1299 cells. Additionally, there was a dramatic increase of E-4-P which is a major indicator of elevated PPP and oxidative stress response induced by K8A. Of note, OGT overexpression increased NADPH and reduced glutathione levels (GSH) in A549 cells[291]. In this study, we observed elevated levels of O-GlcNAcylation, PPP and GSH upon treatment of H1299 cells with K8A. Overall, the NADPH/$NADP^+$ levels were attenuated, corroborating K8A-induced ROS increase in H1299 cells.

O-GlcNAcylation is a ubiquitous protein modification that occurs in over 4,000 nuclear, cytoplasmic, and mitochondrial proteins. Cycling of this carbohydrate modification regulates many cellular functions that include cellular stress response. Stress induced O-GlcNAcylation is involved in redox homeostasis by regulating activity of enzymes in various pathways that include glycolysis, fatty acid synthesis[292-293], PPP and TCA enzymes[30]. Importantly, O-GlcNAcylation responds to intracellular and extracellular changes that include glucose and glutamine deprivation, 2-DG treatment, and ROS induction by small molecules[249, 294]. For example, 2-DG increased O-

GlcNAcylation and disrupted cellular energetics in various cell lines[294-296]. Augmenting O-GlcNAc levels by OGT overexpression has been shown to attenuate oxidative stress.

O-GlcNAc precursor molecules, UDP-GlcNAc and N-acetyl-glucosamine-1-phosphate, were elevated by K8A with consumption of UTP. Additionally, K8A induced generation of UDP-glucose and UDP-D-glucuronate which are involved in detoxification[297-298]. UDP-D-glucuronic acid is involved in glucuronide conjugation with lipophilic xenobiotics in phase II drug metabolism. Glucuronide conjugation involves glycosidic bonds with thiol, amine and hydroxyl groups, or esterification with the hydroxyl and carboxyl groups[298].

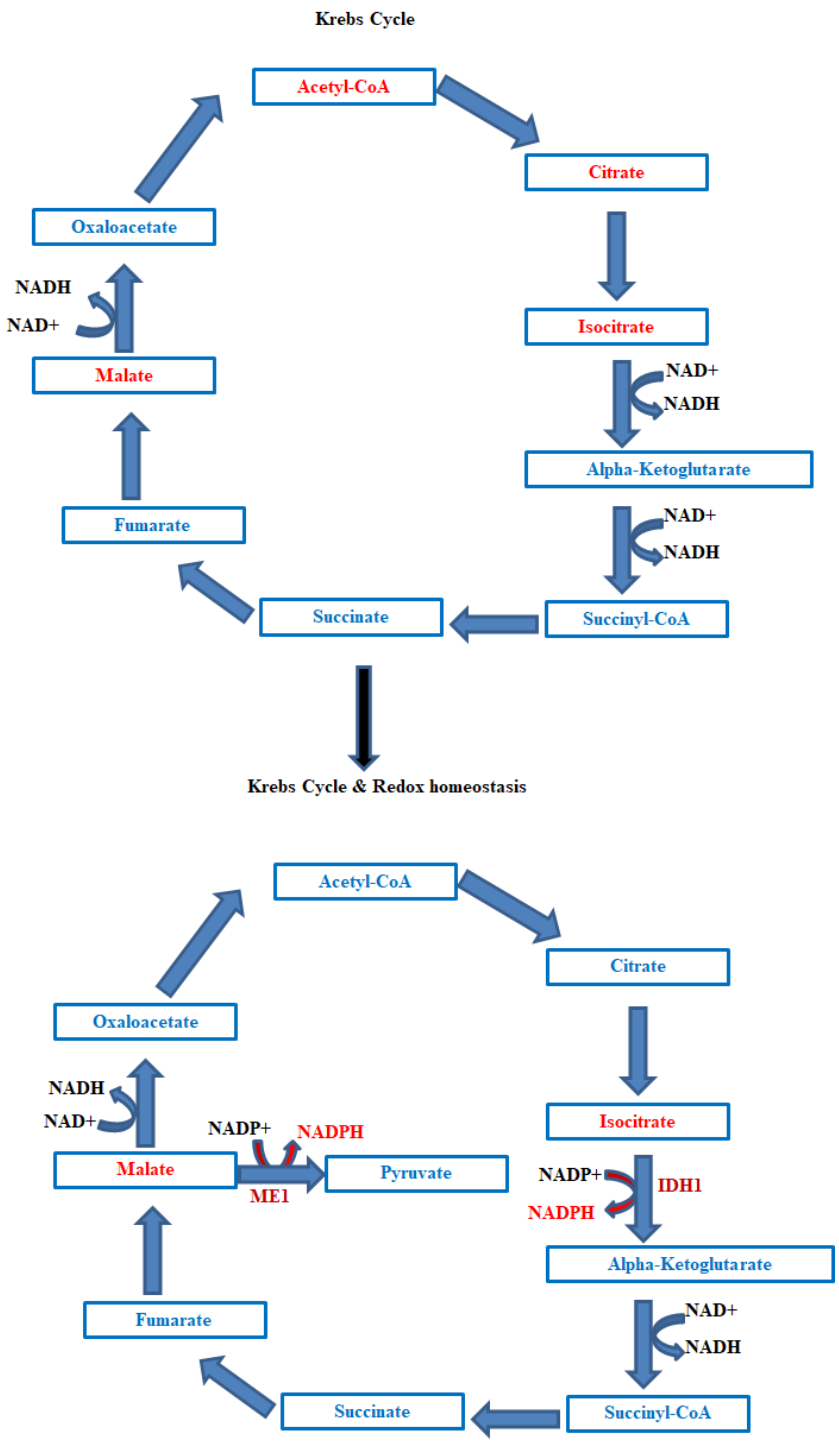

Figure 103-TCA cycle shift under oxidative stress conditions

The metabolomics study also revealed the relative increase of key metabolites that generate reducing equivalents, including citrate, isocitrate and malate. Under oxidative stress conditions, NADPH is generated by the TCA cycle from various metabolites that include isocitrate and malate. Isocitrate dehydrogenase 1 (IDH1)[184] catalyzes conversion of isocitrate to α-ketoglutarate. Malic enzyme 1 (ME1) catalyzes conversion of malate to pyruvate with production of NADPH[183] (Figure 102). In this way, ME1 contributes to the cytosolic NADPH pool and ROS detoxification. Of note is decreased cell growth in ME1-deficient cells in glucose-deprived cells[299]. Additionally, the NAD^+/NADH ratio was increased 10-fold with K8A treatment, suggesting deficiency in reducing equivalents necessary for ATP synthesis and ROS detoxification.

K8A had little interference on metabolism of other pathways that included amino acid, fatty acid, purine and pyrimidine synthesis. Minimal increase in glutamate levels was observed with K8A treatment and could be important in glutamine synthesis. Additionally, arginine levels decreased. Arginine is used by nitric oxide synthase to produce citrulline and nitric oxide[300-301]. Notably, this could potentially be the source of K8A-induced ROS.

The metabolomics studies also revealed that fatty acid synthesis of oleic, stearic and palmitic acid was halted. On lipid synthesis, AMPK activation observed in this study may lead to inhibition of the sterol regulatory element binding protein 1 (SREBP-1), which is a major regulator of fatty acid synthesis. Additionally, K8A-induced increase in AMP, ADP, UDP, and UMP and decrease in UTP levels corroborated our AMPK activation Western blot findings. UTP is consumed in the HBP in UDP-GlcNAc synthesis. Overall, K8A disrupted glycolysis, PPP and TCA with implications in variations in metabolite levels that affected cellular energetics and redox homeostasis in H1299 cancer cells.

4.8 Experimental procedure

4.8.1 Sample preparation and metabolic profiling

The H1299 adherent cells were cultured in 10 cm dishes in 5% CO_2 and 37 ^{o}C in DMEM to about 80% confluency before treatment with 100 μM K8A for 20 hours in triplicate dishes with separate triplicate controls. The medium was then aspirated out. The cells were then quickly washed with 150 mM ammonium acetate. The cells were frozen by pouring liquid nitrogen over the cells and evaporation allowed to take place with dishes placed on ice. The cells were stored in -80°C freezer before metabolomics analysis. LCMS detection involved a one-step liquid-liquid organic solvent extraction (methanol: chloroform 9:1) of cultured H1299 cells and separation on a 1 mm x150 mm HILIC specific column in a 35-minute separation cycle. The quantitative multiple-reaction monitoring transition of each particular metabolite was as follows: *m/z* 259 to 97 for G6P/F6P, *m/z* 259 to 79 for F16BP, *m/z* 169 to 97 for DHAP/GAPDH, *m/z* 185 to 79 for 2PG/3PG, *m/z* 167 to 79 for PEP, *m/z* 808 to 79 for acetyl-CoA, *m/z* 191 to 111 for citrate/Isocitrate, *m/z* 117 to 73 for succinate, *m/z* 133 to 115 for malate, *m/z* 275 to 79 for 6-PG, *m/z* 229 to 97 for R-5-P/X5P, and *m/z* 199 to 97 for E4P. Data analyzed by Mass Lynx software and Graph pad Prism are presented as the mean ± standard deviation of triplicate cell culture experiments with and without treatment of K8A.

Conclusion and future directions

This study has provided insights to the potential use of carbohydrate-based small molecules in cancer therapeutics in comparison to clinically tested 2-deoxy-D-glucose. This work widened the scope of synthesis of N-aryl glycosides from unprotected monosaccharides and aniline derivatives with formation of mostly β-N-aryl glycosides in pure form. This work also developed a HPLC method of separating the α and β anomers. Characterization was done by LC-MS and NMR.

Reactive oxygen species levels induced by our molecules revealed correlation between ROS levels and cytotoxicity in H1299 lung cancer model. These ROS and cytotoxicity screening assays revealed two hit compounds H8 and K8. Acetylated form K8A had improved lipophilicity and cytotoxicity in several cancer cell lines that include lung, breast and prostate among others.

Preliminary mechanistic studies revealed that our hit compound K8A induces ROS and ER stress in similar fashion to 2-DG in H1299 cells. Additionally, K8A activates AMPK and p53 which are involved in tumor suppression. Importantly, K8A disrupts global protein glycosylation in cancer cells. Western blot studies revealed increase in O-GlcNAcylation known to activate p53 and modulate redox homeostasis and cellular energetics. Additionally, metabolic labelling and click chemistry revealed potential role of K8A to block N-glycosylation with Lectin pull down studies with biotinylated Concanavalin A revealing N-glycosylation inhibition as potential mechanism of action. Furthermore, the metabolomics study corroborated our initial findings of K8A role in cellular energy disruption with increase in AMP, indicative of decrease in ATP. Overall, I think K8A is disrupting the glucosome[33] and it will be interesting how future work will dissect this observation against a backdrop of O-GlcNAcylation of glycolytic enzymes. Remotely, K8 being a xyloside could also act as a precursor in proteoglycan synthesis which utilize xyloside residues attached to proteins as building blocks. I therefore propose a model based on my findings to act as a basis for future work in pursuit of finding a carbohydrate-based inducer of cellular stress for targeting cancer cell metabolism.

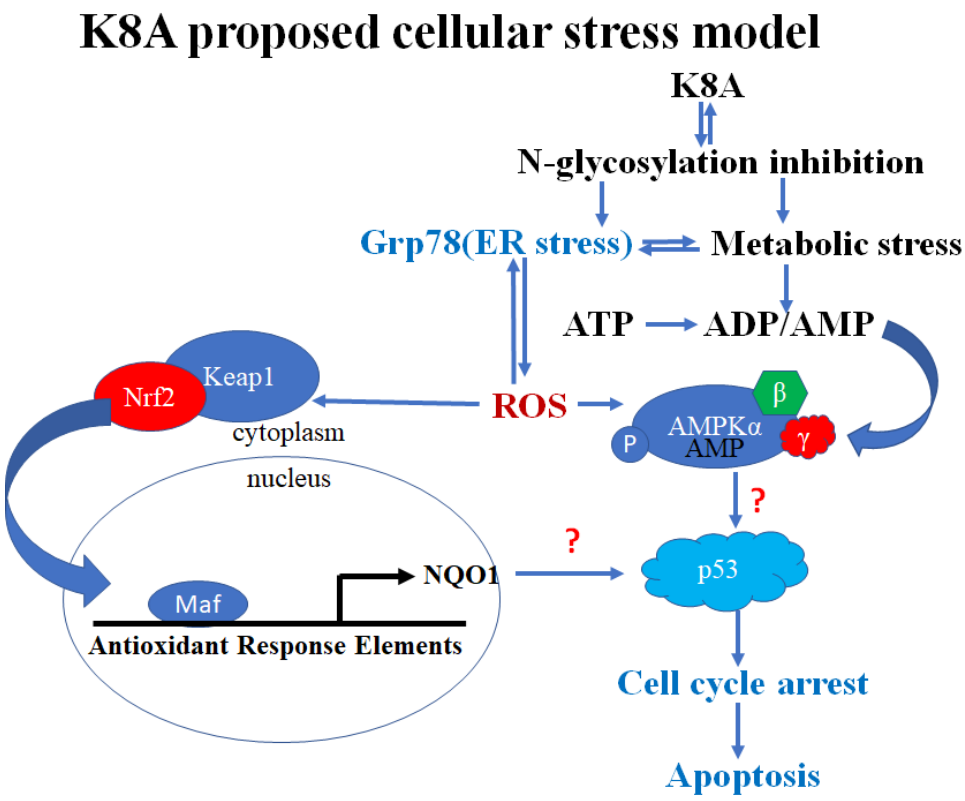

Figure 104-K8A mechanism of action model

Further studies are required to investigate upstream and downstream signaling effects of AMPK as well as a more elaborate biochemical and metabolomics study to delineate effects of K8A as an ER stress inducer, ROS modulator versus cellular energy disruptor. Of note is the possible role of K8A as an inhibitor of N-glycosylation as shown in this work in a pulldown study with lectins. The preliminary data of using biotinylated concanavalin A showed that K8A reduced N-glycosylation in H1299 cells (Figure in the appendix). Future work is likely to involve thorough investigation in comparison to N-glycosylation inhibitors such as tunicamycin. Furthermore, K8A selectivity of cancer versus normal cells is likely to provide greater insights on the mechanism of action that may be exploited in cancer therapeutics.

APPENDIX A: LC-MS Data

	N-aryl-glycoside	Purity (%)	Exact mass	Found mass
1	A1a	95	313.13	314.00
2	A1b	100	313.13	314.00
3	A3	100	337.11	338.00
4	A4	90	323.1	324.00
5	A5a	100	295.14	296.00
6	A5b	100	295.14	296.00
7	A6	100	307.12	308.00
8	A7	100	255.11	256.00
9	A8	95	305.13	306.00
10	B1	100	297.12	298.00
11	B2	100	273.08	274.00
12	B3a	90	321.13	322.00
13	B3b	100	321.13	322.00
14	B7a	100	239.12	240.00
15	B7b	100	239.12	240.00
16	B8	90	289.13	290.00
17	C1	90	283.11	284.00
18	C2	90	259.06	260.00
19	C4a	90	293.09	294.00
20	C4b	100	293.09	294.00
21	C5	100	265.13	266.00
22	C7	100	225.1	226.00
23	D1	100	355.13	356.00
24	D2	100	315.11	316.00
25	E1	90	267.11	268.00
26	E2	90	243.07	244.00
27	E5	90	249.14	250.00
28	E6	90	261.11	262.00
29	F1	90	354.14	355.00
30	F6	100	348.14	349.00
31	G5	90	295.14	296.00
32	G8	100	305.13	306.00
33	H1	90	283.11	284.00
34	H3	90	283.11	284.00
35	H5	90	265.13	266.00
36	H7a	90	225.11	250.00
37	H7b	90	225.11	250.00
38	H8	90	275.13	276.00
39	I4a	90	293.09	294.00
40	I4b	100	293.09	294.00
41	I7	100	225.1	226.00
42	I8	90	275.12	276.00
43	J5	100	295.14	296.00
44	J7	95	255.11	256.00
45	K8	98	275.13	276.00
46	L8	100	289.13	290.00

APPENDIX A (continued): LC-MS Data

	N-aryl-glycoside	Purity (%)	Exact mass	Found mass
47	K8A	100	401.15	402.00
48	K9A	100	401.15	402.00
49	K10A	~90	415.16	416.00
50	K11A	~90	436.10	437.00
51	K12A	~90	480.05	481.00
52	Q9A	100	415.16	416.00
53	Q8A	100	415.16	416.00
54	H9A	100	401.15	402.00
55	H8A	~90	401.15	402.00
56	C9A	100	401.15	402.00
57	C8A	100	401.15	402.00
58	L9A	95	473.17	474.00
59	L8A	100	473.17	474.00
60	2DGA	100	332.1	333.00
61	KA	~50	318.10	319.00
62	2DG8A	~90	415.16	416.00

APPENDIX B: HPLC CHROMATOGRAMS OF A1 & A2

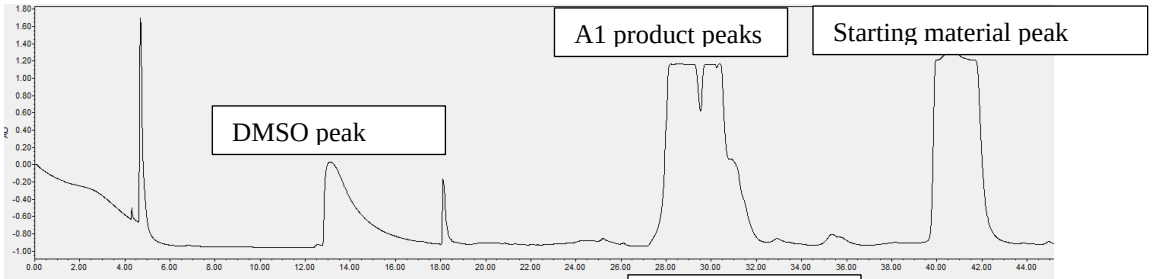

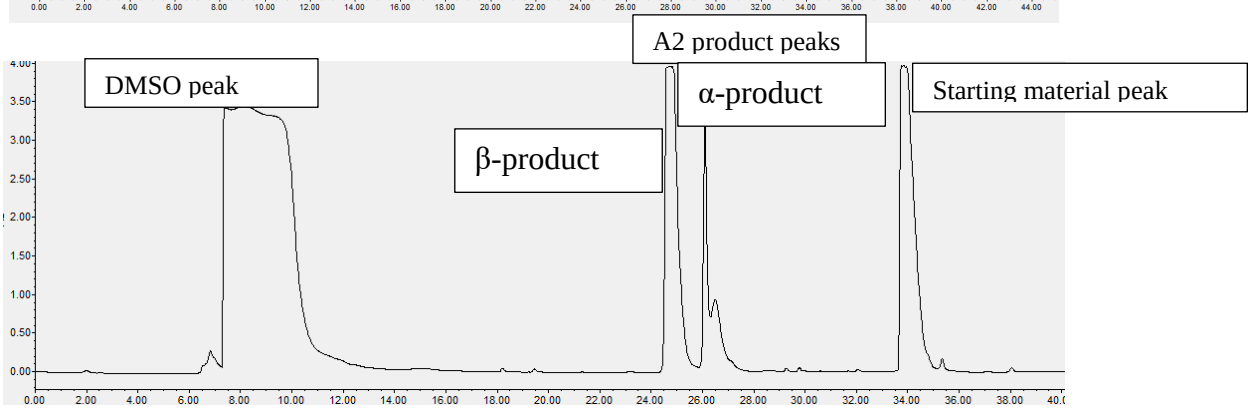

APPENDIX C: NMR Data

^{1}H-NMR of A8

^{1}H NMR (600 MHz, d_2o) δ 7.96 (dd, *J* = 6.3, 3.3 Hz, 1H), 7.78 (dd, *J* = 6.2, 3.2 Hz, 1H), 7.43 (dd, *J* = 6.3, 3.2 Hz, 2H), 7.37 – 7.27 (m, 2H), 6.87 (d, *J* = 7.3 Hz, 1H), 4.80 (d, *J* = 8.1 Hz, 1H), 3.78 (d, *J* = 10.5 Hz, 1H), 3.61 (dd, *J* = 12.2, 5.6 Hz, 1H), 3.56 – 3.49 (m, 2H), 3.41 – 3.34 (m, 1H).

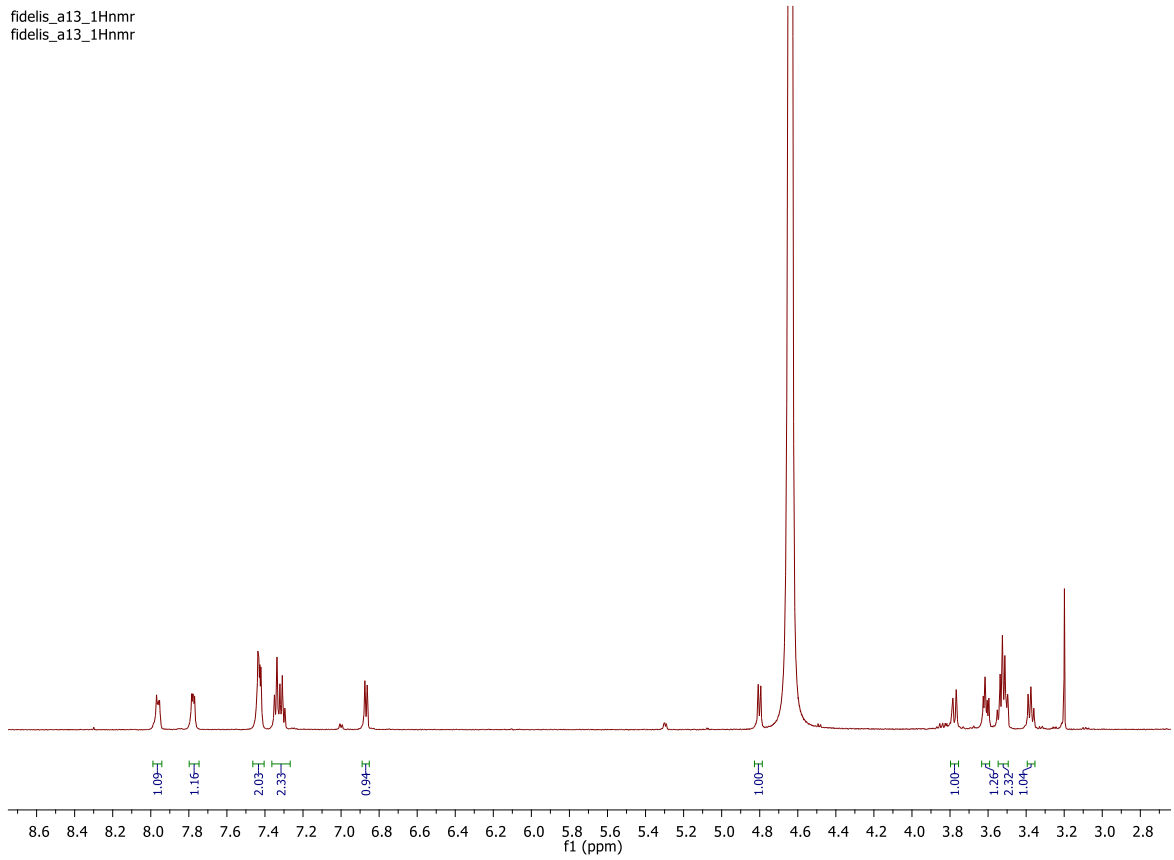

C8 ^{1}H NMR

^{1}H NMR (600 MHz, DMSO-d_6) δ 8.06 (d, J = 7.9 Hz, 1H), 7.80 – 7.74 (m, 1H), 7.47 – 7.38 (m, 3H), 7.31 – 7.25 (m, 1H), 7.19 (d, J = 8.1 Hz, 1H), 6.71 (d, J = 7.6 Hz, 1H), 6.62 (d, J = 7.7 Hz, 1H), 5.04 – 4.96 (m, 1H), 4.58 (t, J = 7.2 Hz, 2H), 3.79 (q, J = 7.2 Hz, 1H), 3.62 (dd, J = 11.7, 4.4 Hz, 1H), 3.57 (td, J = 9.1, 8.2, 2.6 Hz, 1H), 3.48 (dd, J = 11.9, 2.3 Hz, 1H).

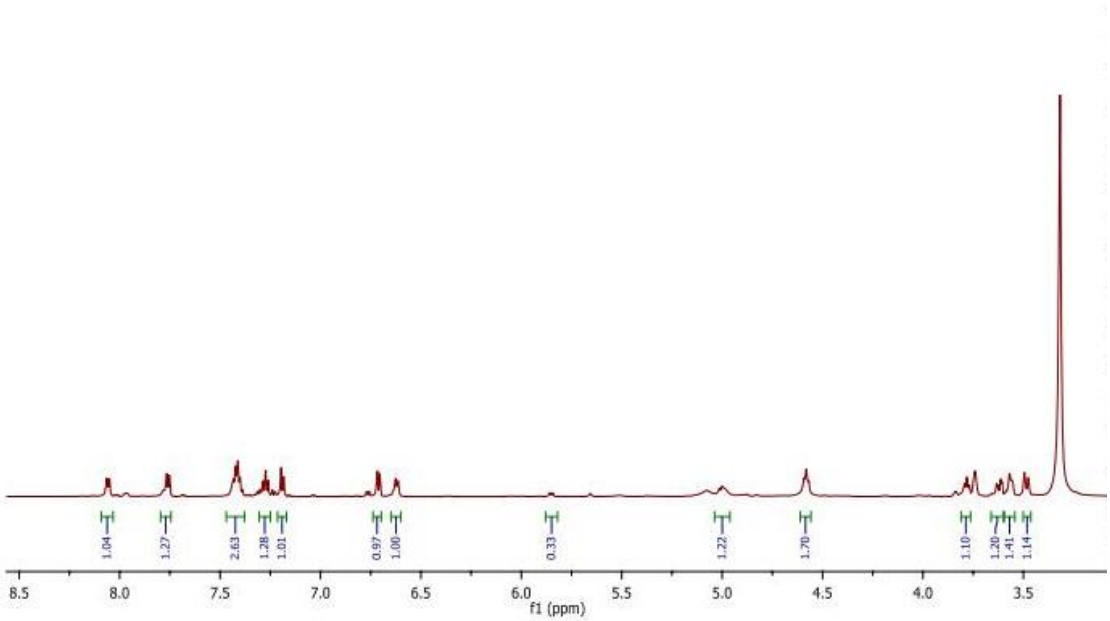

G8 ^{1}H NMR

^{1}H NMR (600 MHz, DMSO-d_6) δ 8.19 (dd, J = 8.4, 1.5 Hz, 1H), 7.80 – 7.72 (m, 1H), 7.46 – 7.35 (m, 2H), 7.32 – 7.24 (m, 1H), 7.18 (d, J = 8.1 Hz, 1H), 6.78 – 6.72 (m, 1H), 6.40 (d, J = 7.1 Hz, 1H), 4.84 (d, J = 5.2 Hz, 1H), 4.79 (d, J = 5.3 Hz, 1H), 4.56 (t, J = 5.2 Hz, 1H), 4.43 (s, 1H), 4.38 (d, J = 4.2 Hz, 1H), 3.76 – 3.70 (m, 2H), 3.55 – 3.49 (m, 2H), 3.46 – 3.39 (m, 2H).

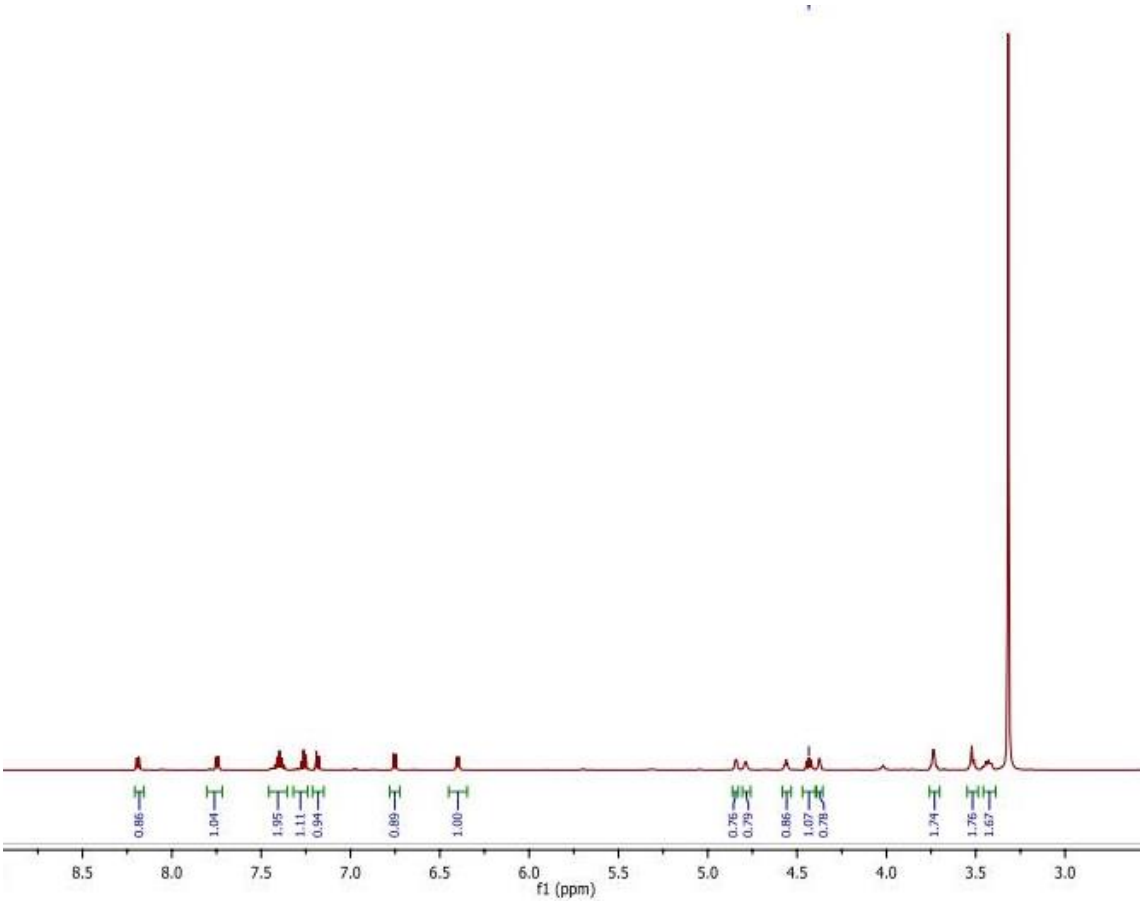

H8 ^{1}H NMR

^{1}H NMR (600 MHz, Chloroform-*d*) δ 7.91 – 7.86 (m, 1H), 7.85 – 7.76 (m, 2H), 7.47 – 7.43 (m, 3H), 7.37 – 7.33 (m, 2H), 5.32 (s, 2H), 4.70 (d, *J* = 8.0 Hz, 1H), 4.08 – 3.99 (m, 3H), 3.91 (t, *J* = 8.3 Hz, 1H), 3.81 (d, *J* = 8.6 Hz, 1H), 3.72 – 3.68 (m, 1H).

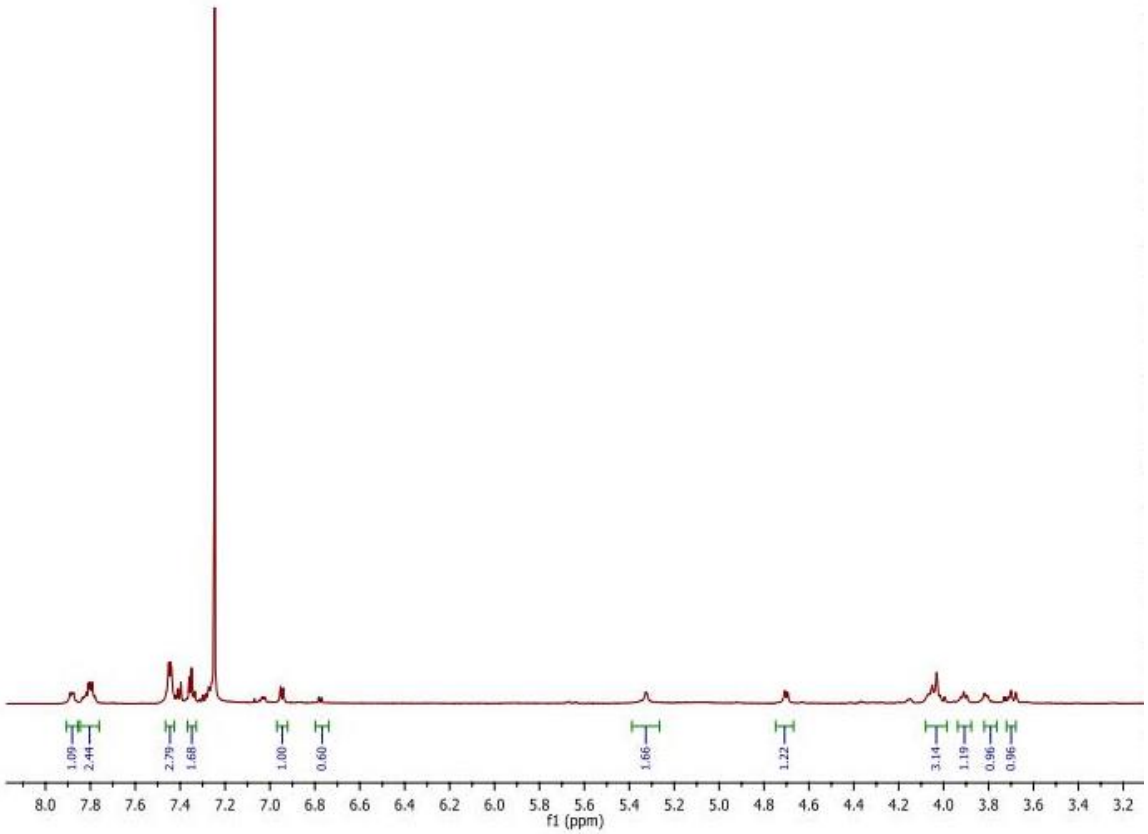

J8 ^{1}H NMR

^{1}H NMR (600 MHz, DMSO-d_6) δ 7.95 – 7.88 (m, 1H), 7.80 – 7.72 (m, 1H), 7.46 – 7.40 (m, 2H), 7.29 (t, J = 7.9 Hz, 1H), 7.24 (s, 1H), 6.80 (d, J = 7.5 Hz, 1H), 5.95 (d, J = 9.4 Hz, 1H), 5.22 (d, J = 4.9 Hz, 1H), 4.89 (d, J = 9.3 Hz, 1H), 4.75 (d, J = 5.0 Hz, 1H), 4.71 (d, J = 5.7 Hz, 1H), 4.34 (t, J = 5.8 Hz, 1H), 3.85 (t, J = 3.9 Hz, 1H), 3.46 – 3.36 (m, 2H), 3.20 (td, J = 6.1, 2.9 Hz, 1H).

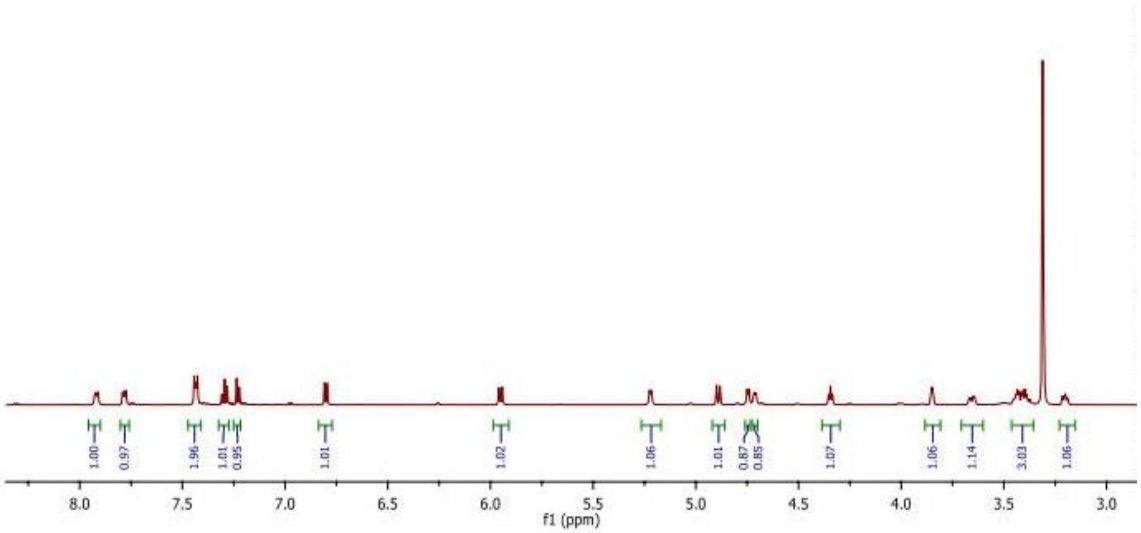

K8 ^{1}H NMR

^{1}H NMR (600 MHz, cd_3od) δ 8.07 (dd, *J* = 6.6, 2.9 Hz, 1H), 7.80 – 7.67 (m, 1H), 7.44 – 7.35 (m, 2H), 7.32 – 7.23 (m, *J* = 14.4, 7.9 Hz, 2H), 6.84 (d, *J* = 7.1 Hz, 1H), 4.67 (d, *J* = 8.2 Hz, 1H), 3.93 – 3.85 (m, 1H), 3.62 – 3.58 (m, 1H), 3.57 – 3.54 (m, 1H), 3.49 (t, *J* = 8.7 Hz, 1H), 3.39 (t, *J* = 10.7 Hz, 1H).

fc_p13_1hnmr
fc_p13_1hnmr

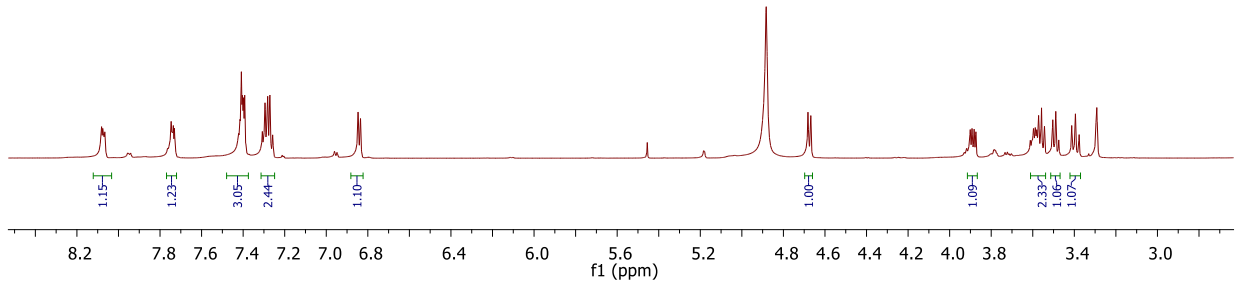

K9A ^{1}H NMR

^{1}H NMR (400 MHz, Methanol-d_4) δ 7.64 (q, J = 9.2, 8.4 Hz, 3H), 7.37 – 7.28 (m, 1H), 7.19 (ddd, J = 8.2, 6.8, 1.3 Hz, 1H), 7.12 – 6.97 (m, 2H), 5.49 – 5.21 (m, 3H), 5.05 (d, J = 5.9, 4.1 Hz, 1H), 4.04 – 3.74 (m, 2H), 2.15 – 2.12 (m, 3H), 2.06 – 1.91 (m, 6H).

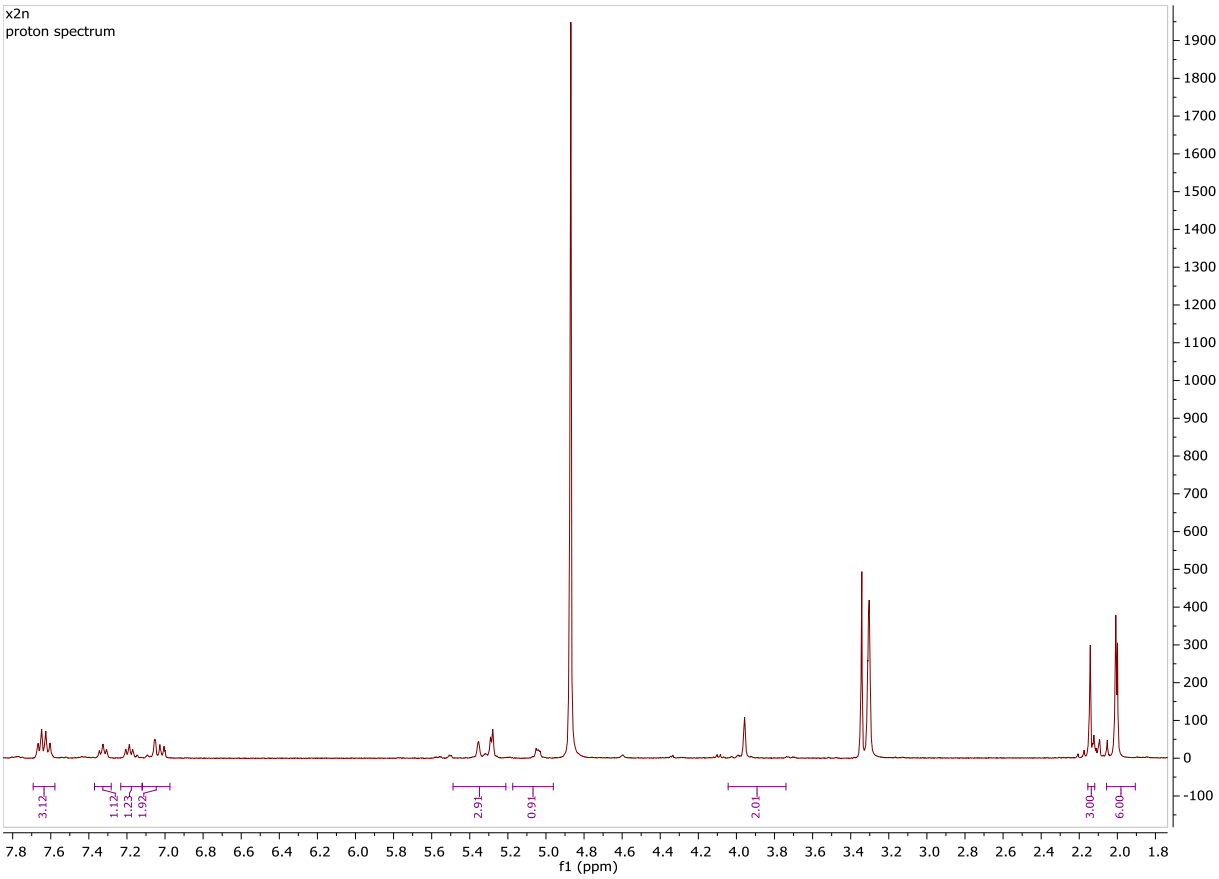

K9A ^{13}C NMR

^{13}C NMR (101 MHz, Methanol-d_4) δ 170.78, 170.55, 170.18, 143.37, 134.86, 128.43, 127.15, 125.87, 125.81,125.79,125.76, 122.19, 117.56, 106.86, 83.74, 71.54, 68.4, 64.25, 19.27, 19.34, 19.38.

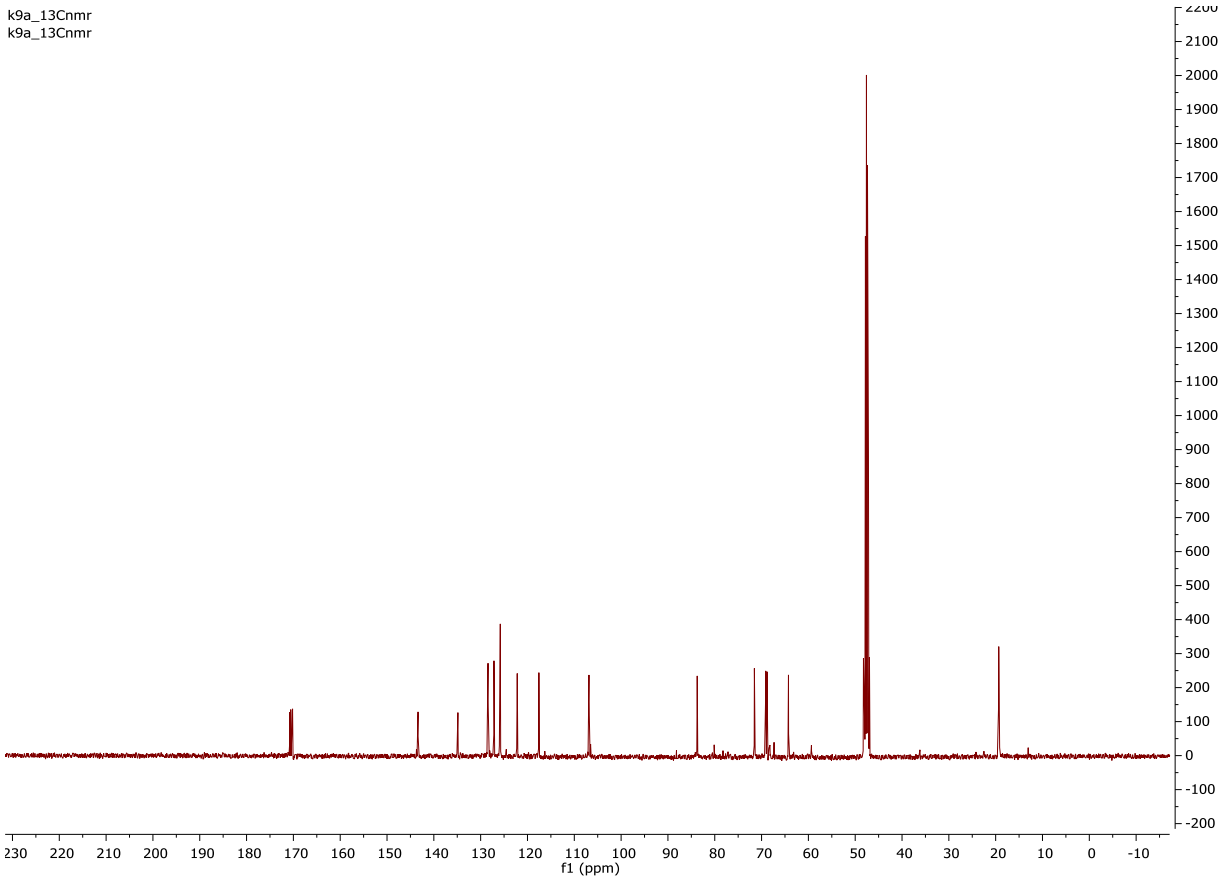

Q9A ^{1}H NMR

^{1}H NMR (400 MHz, Methanol-d_4) δ 7.64 (q, J = 8.1 Hz, 3H), 7.37 – 7.28 (m, 1H), 7.23 – 7.14 (m, 1H), 7.07 – 6.97 (m, 2H), 5.34 – 5.19 (m, 3H), 5.08 (d, J = 7.8 Hz, 1H), 4.13 – 4.08 (m, 1H), 2.19 – 2.15 (m, 3H), 2.01 – 1.97 (m, 6H), 1.19 – 1.15 (m, 3H).

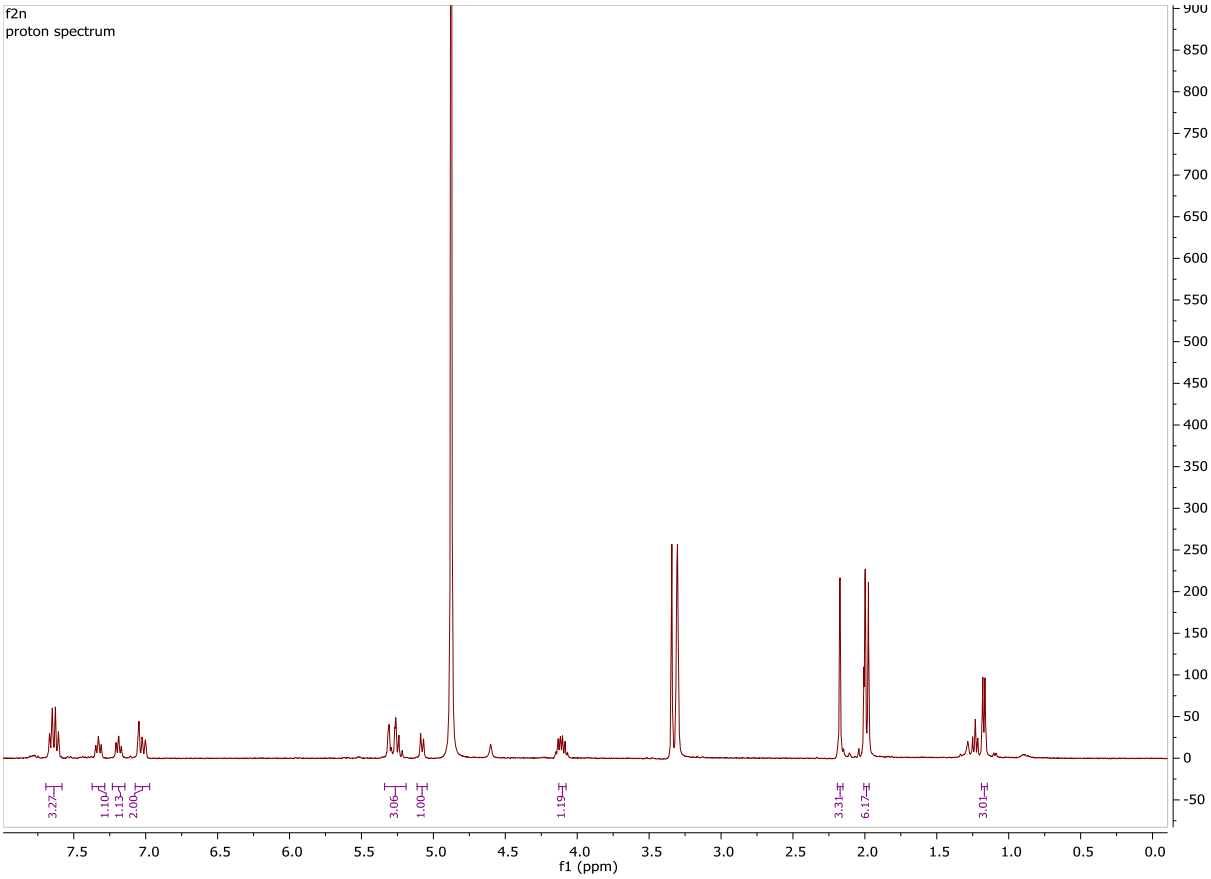

Q8A

^{1}H NMR (400 MHz, Methanol-d_4) δ 7.87 – 7.82 (m, 1H), 7.77 (t, *J* = 4.8 Hz, 1H), 7.46 – 7.39 (m, 2H), 7.32 (d, *J* = 3.9 Hz, 2H), 6.92 – 6.86 (m, 1H), 5.43 – 5.28 (m, 3H), 5.04 (d, *J* = 8.5 Hz, 1H), 4.16 (d, *J* = 6.5 Hz, 1H), 2.18 (s, 4H), 2.00 (t, *J* = 1.9 Hz, 6H), 1.21 (d, *J* = 6.4 Hz, 3H).

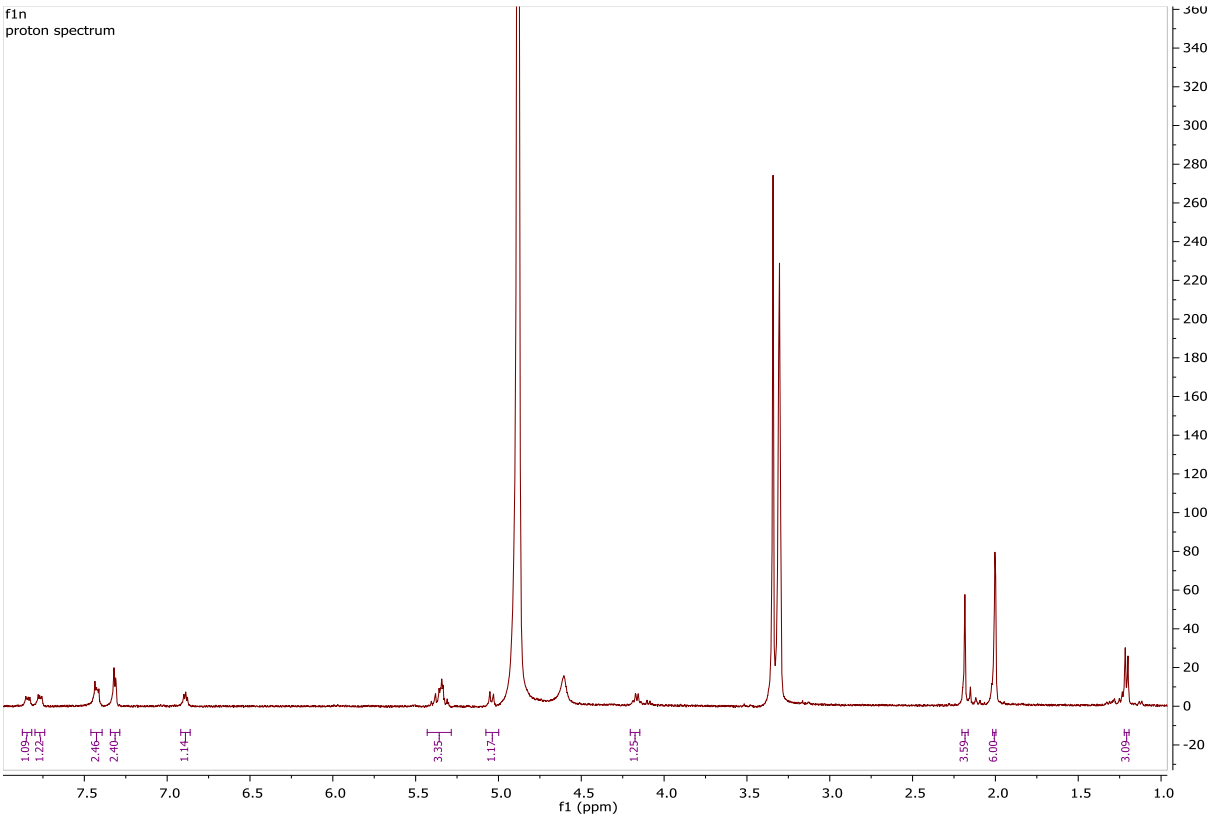

H9A ^{1}H NMR

^{1}H NMR (400 MHz, Methanol-d_4) δ 7.64 (q, J = 7.8 Hz, 3H), 7.33 (t, J = 7.7 Hz, 1H), 7.19 (t, J = 7.5 Hz, 1H), 7.06 – 6.96 (m, 2H), 5.39 (t, J = 8.7 Hz, 1H), 5.11 – 4.97 (m, 3H), 4.13 – 4.00 (m, 1H), 3.63 (t, J = 10.9 Hz, 1H), 2.03 – 1.80 (m, 9H).

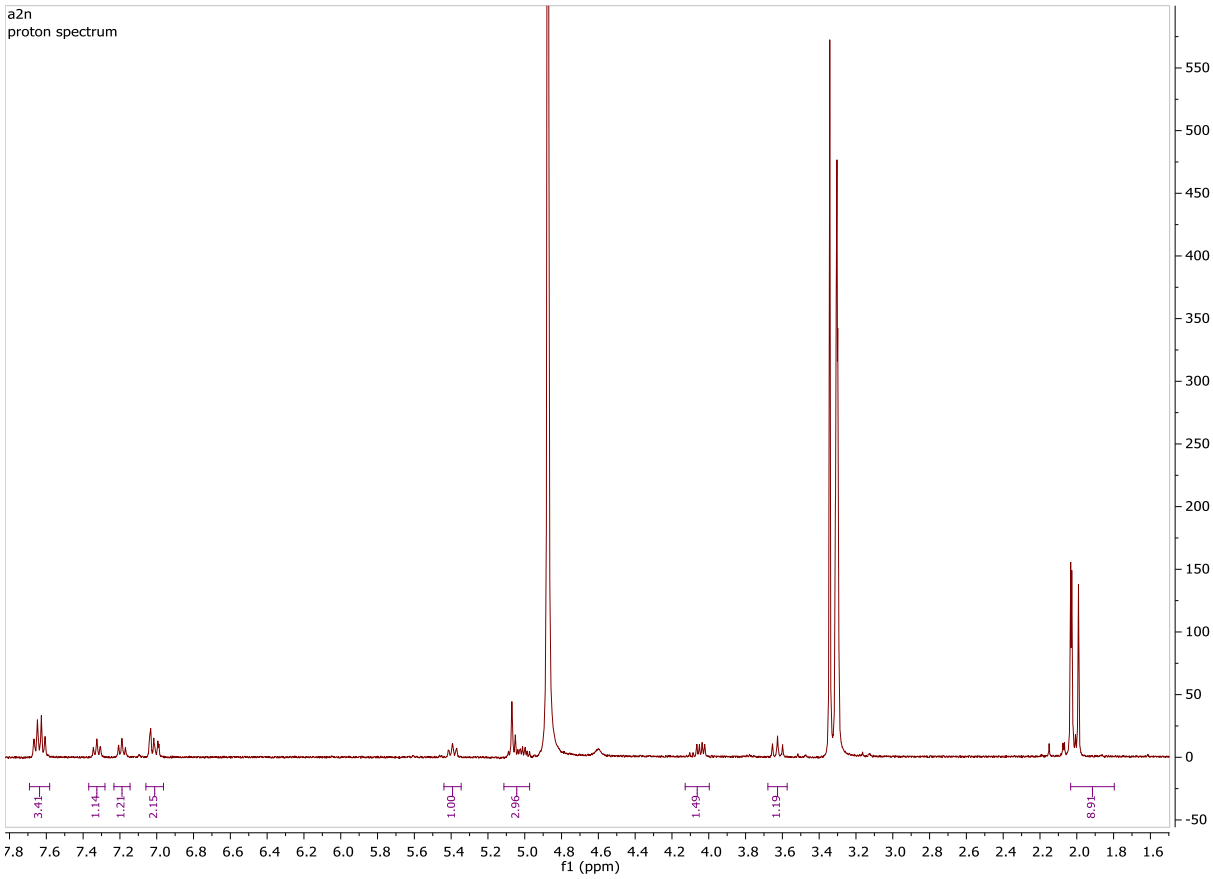

C9A ^{1}H NMR

^{1}H NMR (700 MHz, Methanol-d_4) δ 7.70 – 7.63 (m, 3H), 7.44 – 7.32 (m, 1H), 7.25 – 7.17 (m, 1H), 7.14 – 7.03 (m, 2H), 5.60 – 5.46 (m, 1H), 5.31 – 5.21 (m, 2H), 4.11 (dd, *J* = 14.5, 7.1 Hz, 1H), 4.08 – 3.81 (m, 1H), 2.18 – 2.13 (m, 3H), 2.10 – 2.00 (m, 6H).

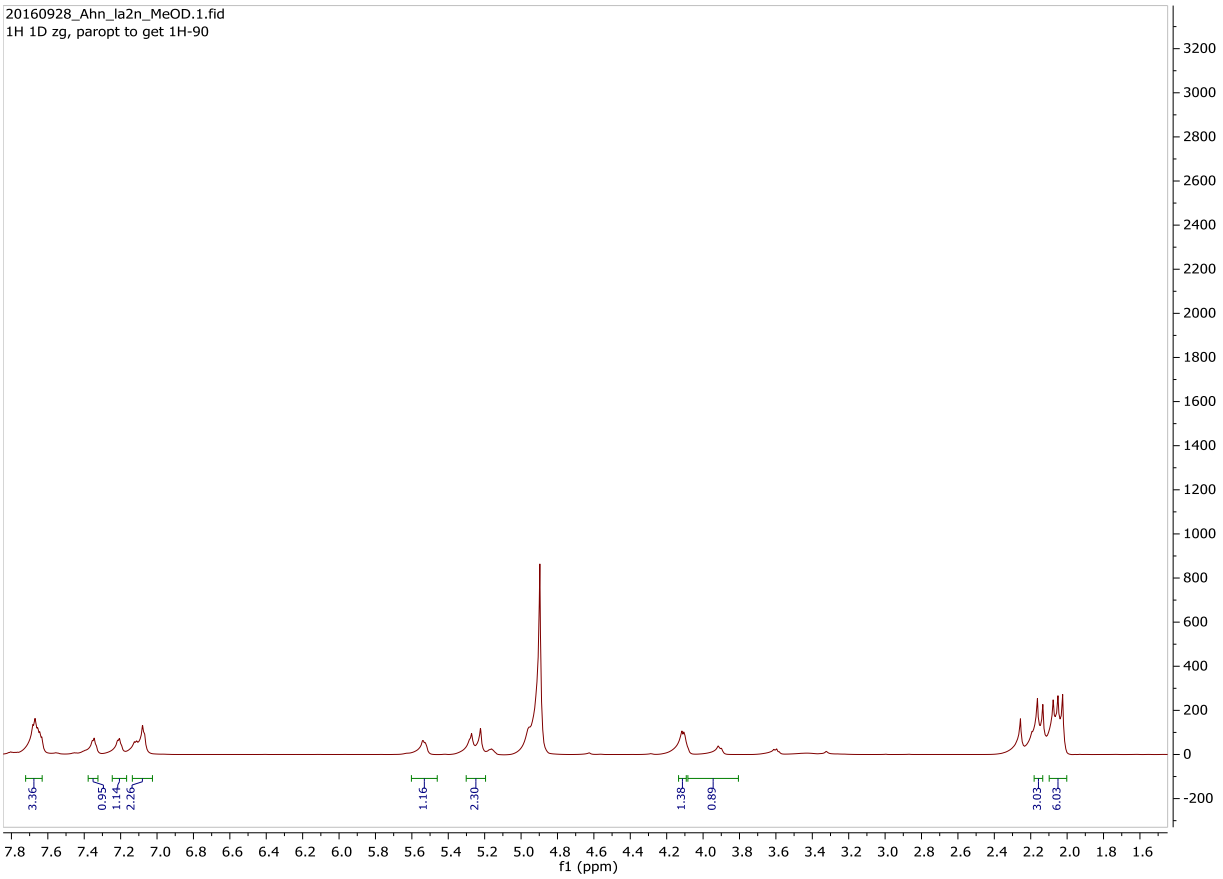

L9A

^{1}H NMR (400 MHz, Methanol-d_4) δ 7.80 – 7.75 (m, 1H), 7.69 – 7.61 (m, 2H), 7.47 – 7.29 (m, 2H), 7.23 – 7.16 (m, 1H), 7.02 (dd, J = 8.8, 2.3 Hz, 1H), 5.60 – 5.45 (m, 1H), 5.38 – 5.21 (m, 2H), 4.37 – 4.26 (m, 1H), 4.40 – 3.82 (m, 3H), 2.16 (d, J = 1.5 Hz, 3H), 2.03 – 1.92 (m, 9H).

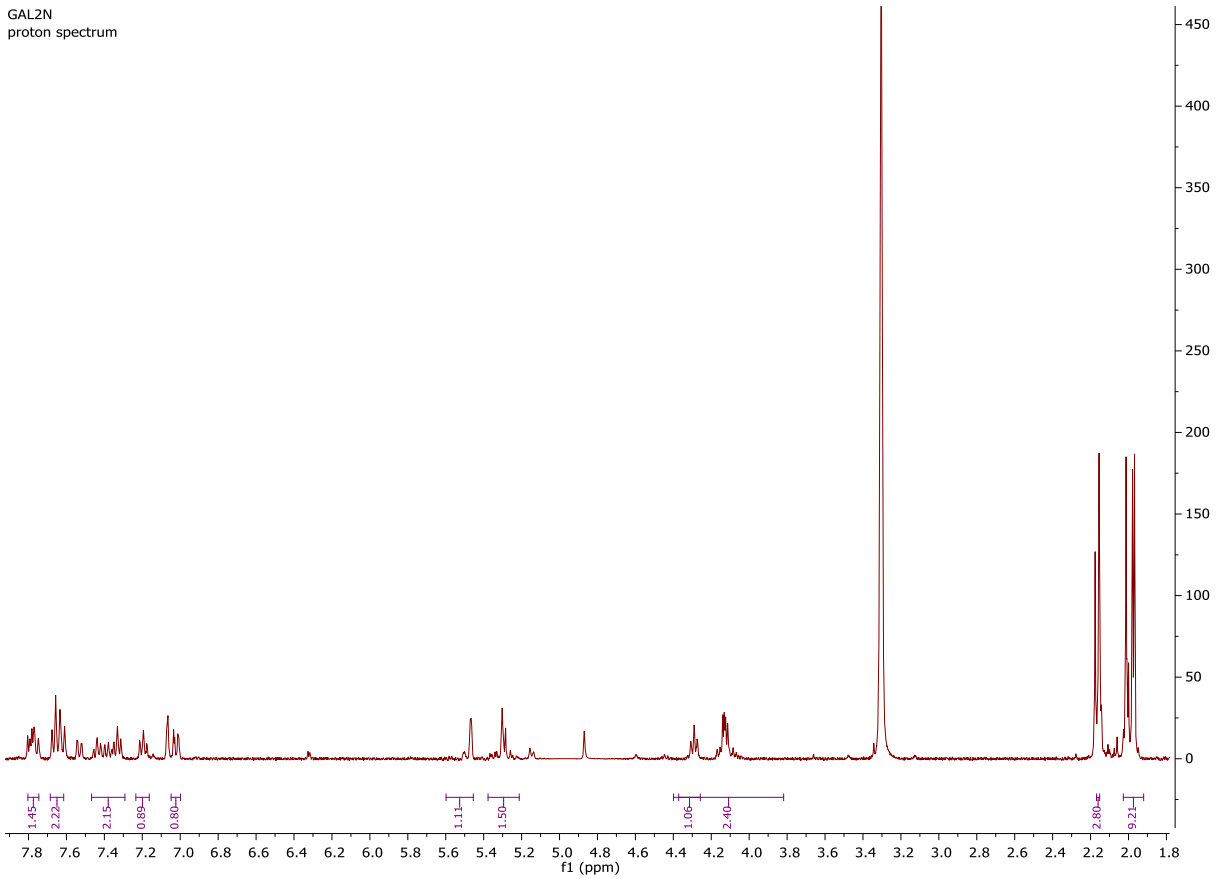

H8A

^{1}H NMR (400 MHz, Methanol-d_4) δ 7.45 – 7.39 (m, 3H), 7.30 (td, J = 6.3, 3.5 Hz, 3H), 6.86 (dt, J = 6.1, 2.7 Hz, 1H), 5.47 – 5.24 (m, 4H), 4.96 (dd, J = 8.8, 3.2 Hz, 1H), 4.12 – 4.04 (m, 1H), 2.06 – 1.96 (m, 9H).

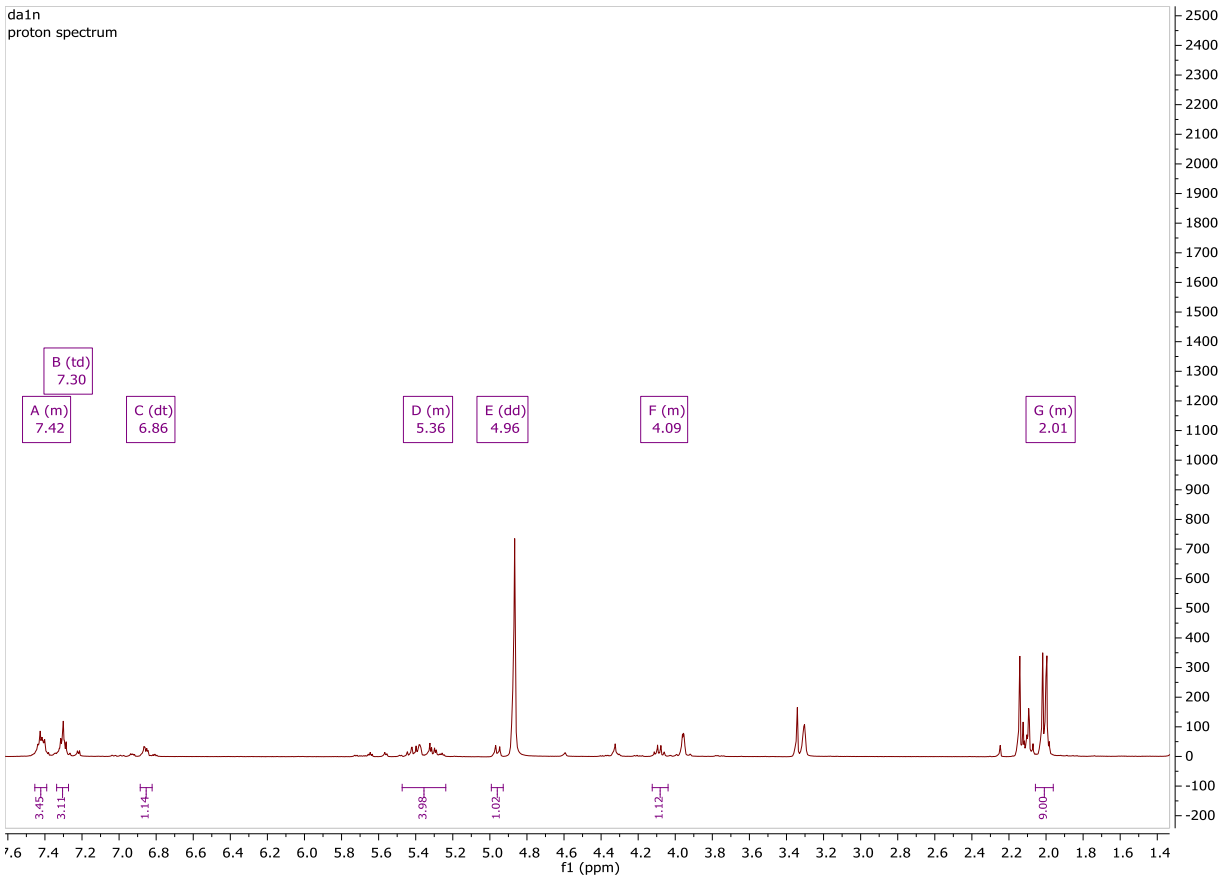

L8A ^{1}H NMR

^{1}H NMR (400 MHz, Methanol-d_4) δ 7.87 – 7.82 (m, 1H), 7.77 (t, J = 4.8 Hz, 1H), 7.46 – 7.39 (m, 2H), 7.32 (d, J = 3.9 Hz, 2H), 6.92 – 6.86 (m, 1H), 5.43 – 5.28 (m, 3H), 5.04 (d, J = 8.5 Hz, 1H), 4.16 (d, J = 6.5 Hz, 1H), 2.18 (s, 4H), 2.00 (t, J = 1.9 Hz, 6H), 1.21 (d, J = 6.4 Hz, 3H).

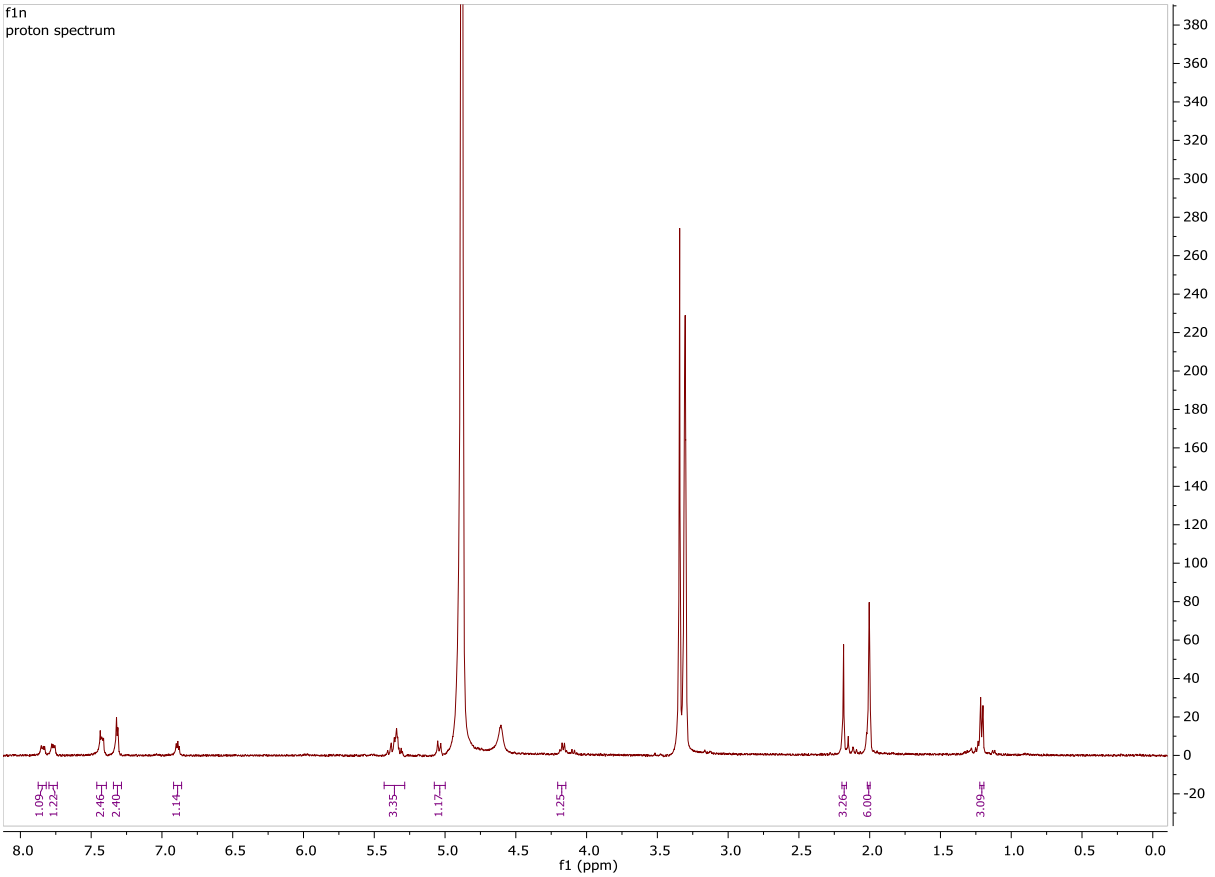

C8A ^{1}H NMR

^{1}H NMR (700 MHz, Methanol-d_4) δ 7.87 (s, 1H), 7.79 (s, 1H), 7.45 (s, 2H), 7.34 (s, 2H), 6.90 (s, 1H), 5.44 (s, 1H), 5.41 (s, 1H), 5.35 (s, 1H), 4.12 (s, 1H), 4.00 (s, 2H), 2.03 (d, J = 8.9 Hz, 9H).

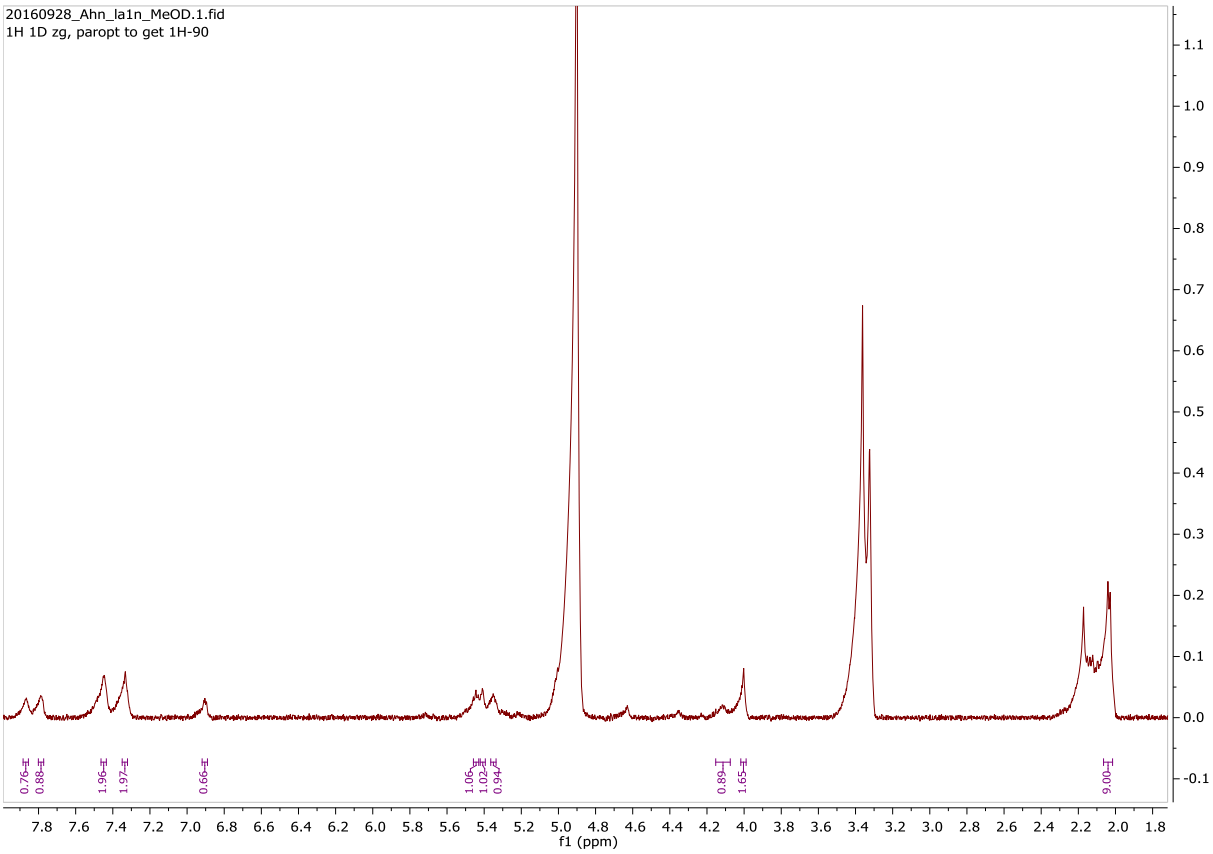

2DG8A ^{1}H NMR

^{1}H NMR (400 MHz, Methanol-d_4) δ 8.09 – 8.05 (m, 0H), 7.98 (d, J = 7.7 Hz, 1H), 7.89 (d, J = 7.6 Hz, 1H), 7.79 – 7.74 (m, 1H), 7.53 – 7.50 (m, 1H), 7.43 – 7.39 (m, 1H), 7.32 – 7.28 (m, 1H), 5.33 – 5.20 (m, 1H), 5.20 – 5.10 (m, 1H), 5.00 (dt, J = 19.3, 9.8 Hz, 1H), 4.36 – 4.23 (m, 1H), 4.11 – 4.04 (m, 1H), 2.28 (s, 1H), 2.12 (s, 1H), 2.02 (ddd, J = 12.4, 5.4, 3.1 Hz, 9H).

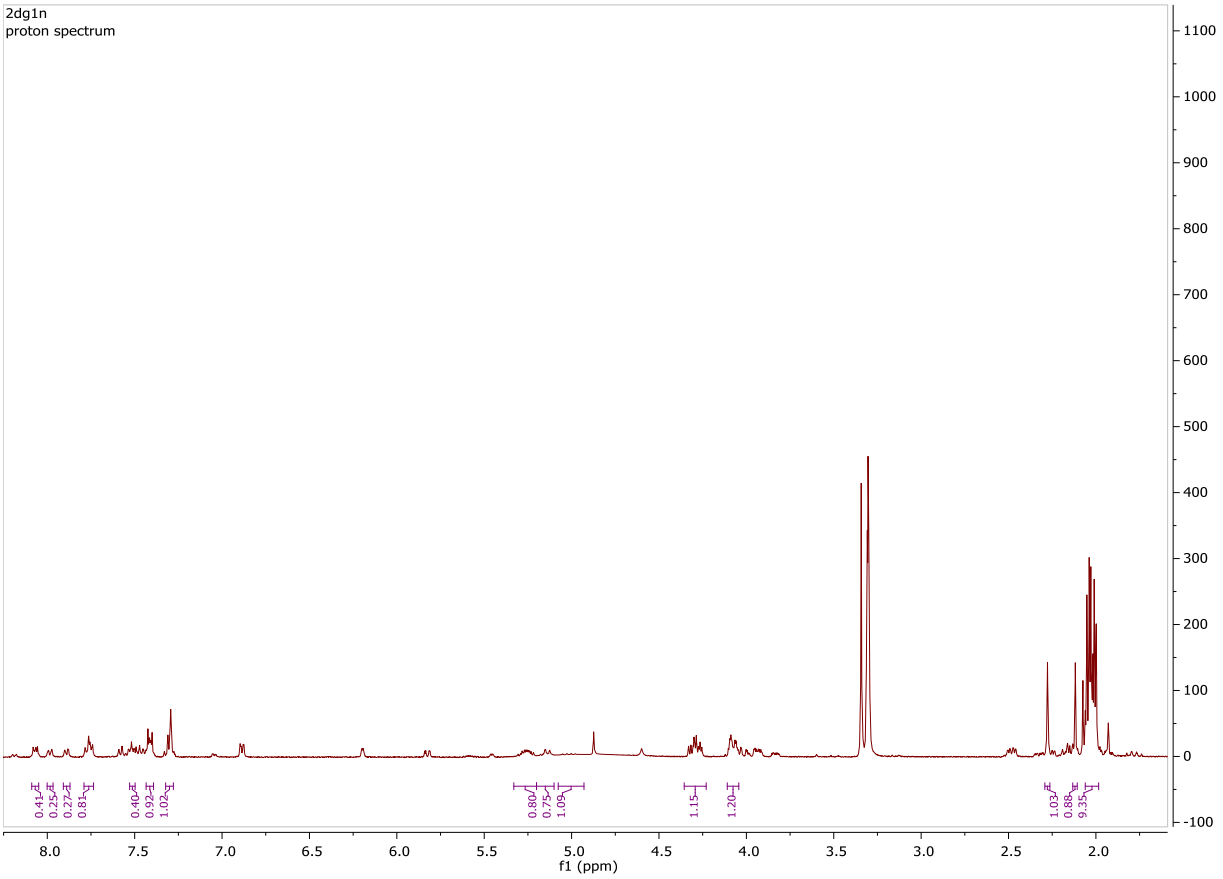

K10A ^{1}H NMR

^{1}H NMR (400 MHz, Methanol-d_4) δ 8.23 (d, J = 8.4 Hz, 1H), 7.76 (d, J = 9.2 Hz, 2H), 7.45 (s, 2H), 7.27 (d, J = 9.0 Hz, 1H), 5.27 (dt, J = 17.3, 9.0 Hz, 1H), 4.59 (d, J = 9.1 Hz, 1H), 4.09 (q, J = 7.2 Hz, 2H), 3.90 (s, 1H), 2.04 – 2.02 (m, 9H), 1.23 (t, J = 7.2 Hz, 3H).

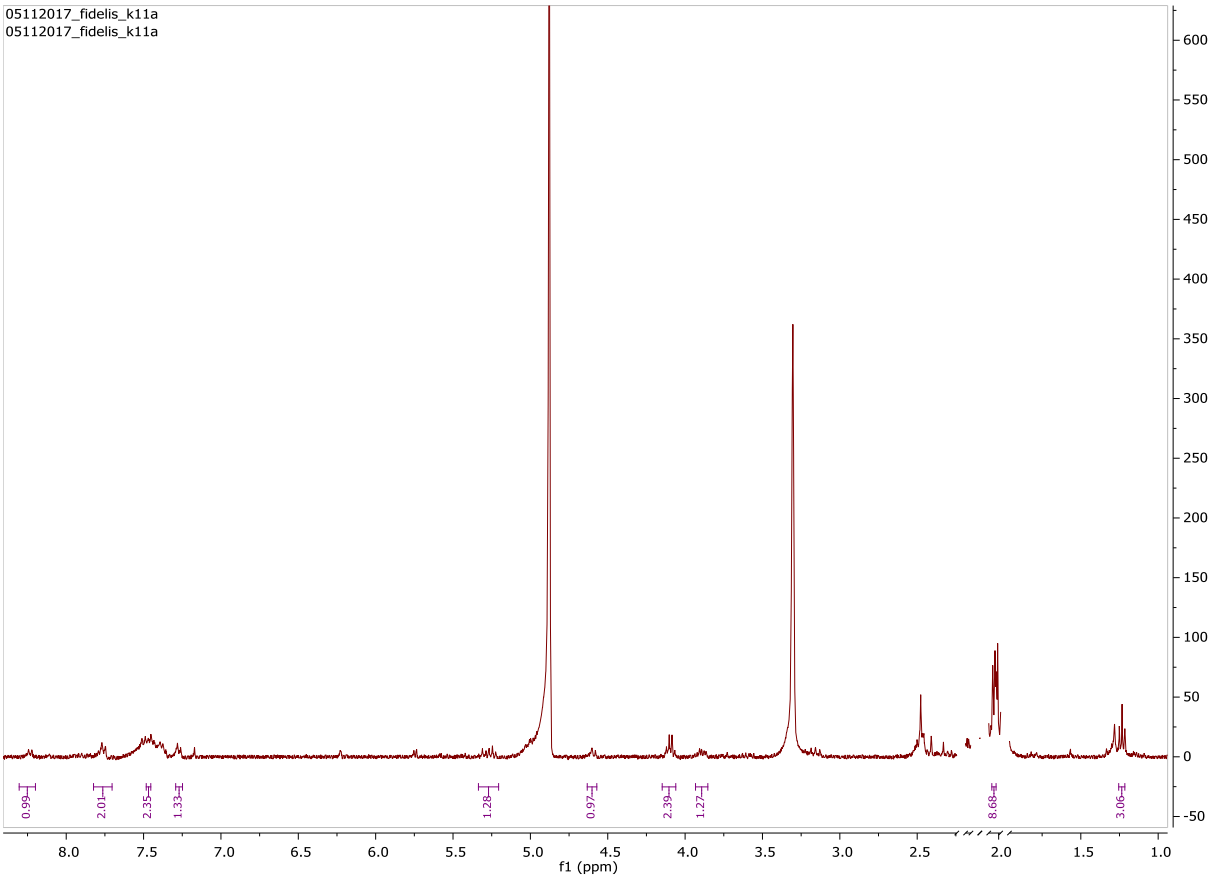

K12A ^{1}H NMR

^{1}H NMR (400 MHz, Methanol-d_4) δ 9.36 (s, 1H), 8.43 (d, J = 6.0 Hz, 1H), 8.18 – 7.99 (m, 1H), 7.96 – 7.83 (m, 1H), 7.81 – 7.64 (m, 1H), 5.26 (d, J = 8.4 Hz, 1H), 5.01 (dd, J = 9.9, 3.0 Hz, 1H), 4.10 (dd, J = 11.9, 5.0 Hz, 1H), 3.98 – 3.86 (m, 1H), 3.73 (s, 1H), 3.63 – 3.52 (m, 1H), 2.42 – 1.83 (m, 9H).

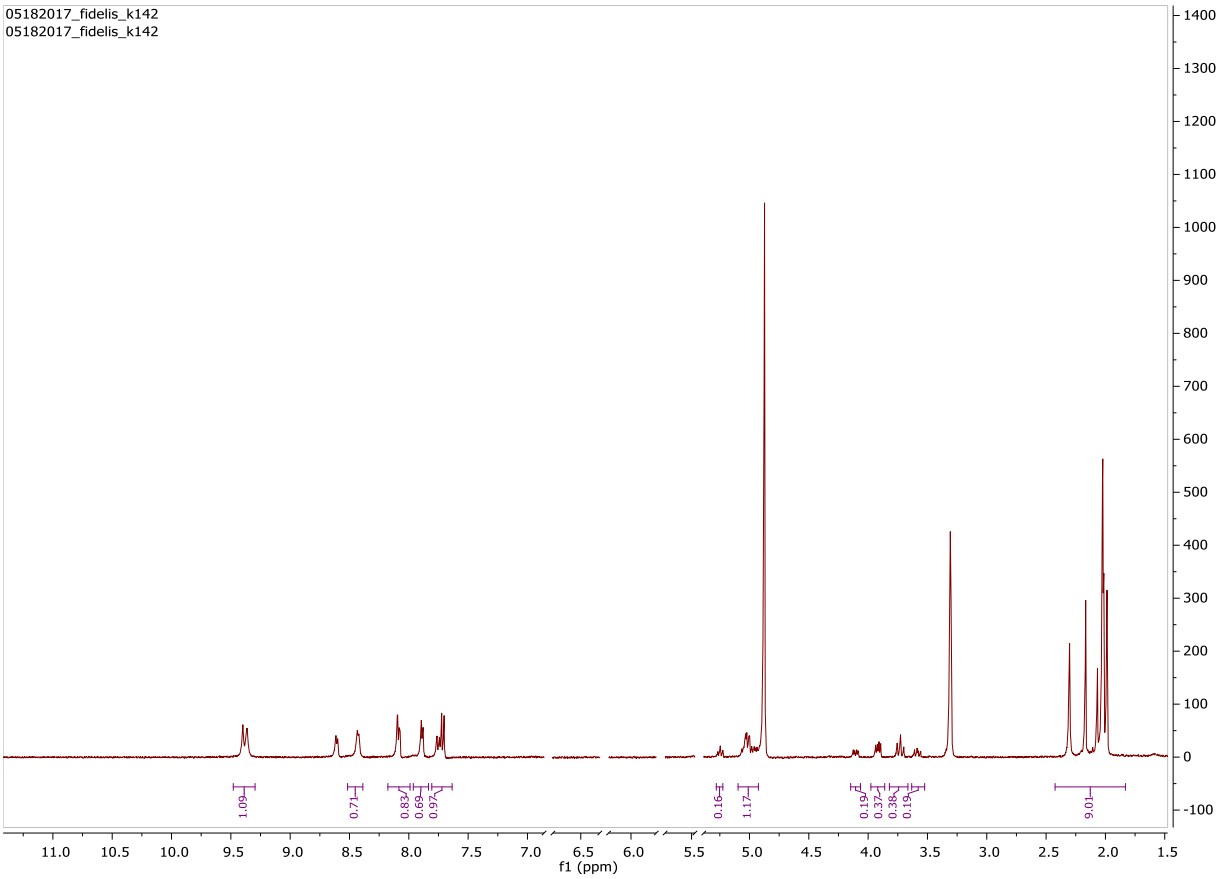

APPENDIX D: OGT Cloning and bacterial expression

Forward primer 5'-GCGCGGATCCATGTTTGCTGATGCCTACTC-3'

Reverse primer 5'-GAGAGCGGCCGCTGACTCAGTGACTTCAACAG-3'

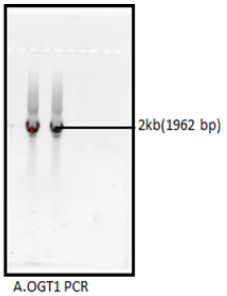

A.OGT1 PCR product

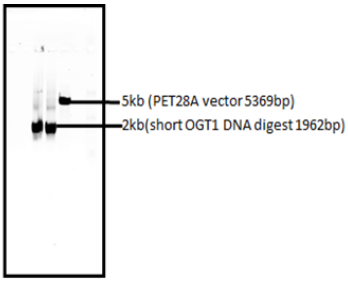

B. BamH1 and NOT1 digests of PET28a vector and OGT1 gene

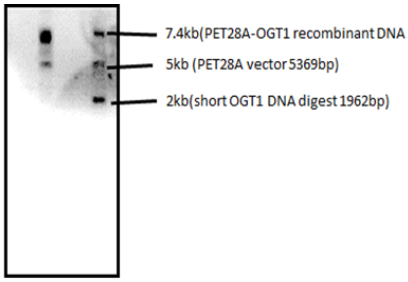

C. OGT1 recombinant DNA after ligation

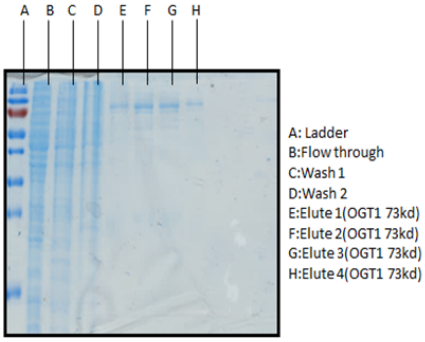

D. His-tagged OGT1 Nickel bead purification

E.Purified OGT1 after concentration with 30 kd MWC

APPENDIX E: K8A potentially blocks N-glycosylation of proteins

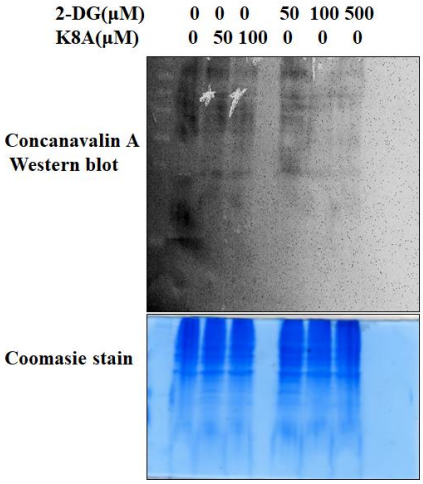

Cell lysate from H1299 cells pretreated with K8A and 2-DG were run on an SDS-PAGE gel. After protein transfer the PVDF membrane was incubated with Biotinylated Concanavalin A and probed with Streptavidin HRP. The SDS-PAGE gel after transfer was stained to monitor loading levels.

APPENDIX F: COPYRIGHT PERMISSIONS: NRF2-ARE PATHWAY

Copyright Clearance Center RightsLink

Home | Account Info | Help

ELSEVIER

Title: The Nrf2-ARE signaling pathway: An update on its regulation and possible role in cancer prevention and treatment
Author: Violetta Krajka-Kuźniak,Jarosław Paluszczak,Wanda Baer-Dubowska
Publication: Pharmacological Reports
Publisher: Elsevier
Date: June 2017
© 2016 Published by Elsevier Sp. z o.o. on behalf of Institute of Pharmacology, Polish Academy of Sciences.

Logged in as:
FIDELIS NDOMBERA
LOGOUT

Order Completed

Thank you for your order.

This Agreement between FIDELIS NDOMBERA ("You") and Elsevier ("Elsevier") consists of your license details and the terms and conditions provided by Elsevier and Copyright Clearance Center.

Your confirmation email will contain your order number for future reference.

printable details

License Number	4287100562592
License date	Feb 13, 2018
Licensed Content Publisher	Elsevier
Licensed Content Publication	Pharmacological Reports
Licensed Content Title	The Nrf2-ARE signaling pathway: An update on its regulation and possible role in cancer prevention and treatment
Licensed Content Author	Violetta Krajka-Kuźniak,Jarosław Paluszczak,Wanda Baer-Dubowska
Licensed Content Date	Jun 1, 2017
Licensed Content Volume	69
Licensed Content Issue	3
Licensed Content Pages	10
Type of Use	reuse in a thesis/dissertation
Portion	figures/tables/illustrations
Number of figures/tables/illustrations	1
Format	print
Are you the author of this Elsevier article?	No
Will you be translating?	No
Order reference number	1
Original figure numbers	Figure 2
Title of your thesis/dissertation	Carbohydrate-based inducers of cellular stress that target cancer cell metabolism
Expected completion date	May 2018
Estimated size (number of pages)	250
Attachment	
Requestor Location	FIDELIS NDOMBERA 950 FOREST WEST APT 1 DETROIT, MI 48201 United States Attn: FIDELIS NDOMBERA
Publisher Tax ID	98-0397604
Total	0.00 USD

ORDER MORE | CLOSE WINDOW

Copyright © 2018 Copyright Clearance Center, Inc. All Rights Reserved. Privacy statement. Terms and Conditions.
Comments? We would like to hear from you. E-mail us at customercare@copyright.com

APPENDIX G: COPYRIGHT PERMISSIONS: PENTOSE PHOSPHATE PATHWAY

Copyright Clearance Center RightsLink®

Home | Account Info | Help

Title: The pentose phosphate pathway and cancer
Author: Krushna C. Patra,Nissim Hay
Publication: Trends in Biochemical Sciences
Publisher: Elsevier
Date: August 2014
Copyright © 2014 Elsevier Ltd. All rights reserved.

Logged in as:
FIDELIS NDOMBERA
Account #: 3001249130
LOGOUT

Order Completed

Thank you for your order.

This Agreement between FIDELIS NDOMBERA ("You") and Elsevier ("Elsevier") consists of your license details and the terms and conditions provided by Elsevier and Copyright Clearance Center.

Your confirmation email will contain your order number for future reference.

printable details

License Number	4295440368492
License date	Feb 24, 2018
Licensed Content Publisher	Elsevier
Licensed Content Publication	Trends in Biochemical Sciences
Licensed Content Title	The pentose phosphate pathway and cancer
Licensed Content Author	Krushna C. Patra,Nissim Hay
Licensed Content Date	Aug 1, 2014
Licensed Content Volume	39
Licensed Content Issue	8
Licensed Content Pages	8
Type of Use	reuse in a thesis/dissertation
Portion	figures/tables/illustrations
Number of figures/tables/illustrations	1
Format	print
Are you the author of this Elsevier article?	No
Will you be translating?	No
Original figure numbers	Figure 1
Title of your thesis/dissertation	Carbohydrate-based inducers of cellular stress that target cancer cell metabolism
Expected completion date	May 2018
Estimated size (number of pages)	250
Attachment	
Requestor Location	FIDELIS NDOMBERA 950 FOREST WEST APT 1

APPENDIX H: COPYRIGHT PERMISSIONS: CANCER METABOLISM

REVIEW | ONCOLOGY

Fundamentals of cancer metabolism

Ralph J. DeBerardinis[1,*] and Navdeep S. Chandel[2,*]
+ See all authors and affiliations

Science Advances 27 May 2016:
Vol. 2, no. 5, e1600200
DOI: 10.1126/sciadv.1600200

Article | Figures & Data | Info & Metrics | eLetters | PDF

Article Information

vol. 2 no. 5

DOI: https://doi.org/10.1126/sciadv.1600200

Published By: American Association for the Advancement of Science

Online ISSN: 2375-2548

History: Received for publication February 1, 2016

Accepted for publication April 29, 2016

Copyright & Usage: Copyright © 2016, The Authors
This is an open-access article distributed under the terms of the **Creative Commons Attribution-NonCommercial license**, which permits use, distribution, and reproduction in any medium, so long as the resultant use is **not** for commercial advantage and provided the original work is properly cited.

APPENDIX F: COPYRIGHT PERMISSIONS: REDOX HOMEOSTASIS

Copyright Clearance Center RightsLink®

Home | Account Info | Help

SPRINGER NATURE

Title: Redox homeostasis: the linchpin in stem cell self-renewal and differentiation
Author: Kui Wang, Tao Zhang, Qiang Dong, Edouard Collins Nice, Canhua Huang et al.
Publication: Cell Death & Disease
Publisher: Springer Nature
Date: Mar 14, 2013
Copyright © 2013, Springer Nature

Logged in as:
FIDELIS NDOMBERA
Account #:
3001249130
LOGOUT

Creative Commons

The request you have made is considered to be non-commercial/educational. As the article you have requested has been distributed under a Creative Commons license (Attribution-Noncommercial), you may reuse this material for non-commercial/educational purposes without obtaining additional permission from Springer Nature, providing that the author and the original source of publication are fully acknowledged (please see the article itself for the license version number). You may reuse this material without obtaining permission from Springer Nature, providing that the author and the original source of publication are fully acknowledged, as per the terms of the license. For license terms, please see http://creativecommons.org/

BACK | CLOSE WINDOW

Copyright © 2018 Copyright Clearance Center, Inc. All Rights Reserved. Privacy statement. Terms and Conditions.
Comments? We would like to hear from you. E-mail us at customercare@copyright.com

REFERENCES

1. Kong, H.; Chandel, N. S., Regulation of redox balance in cancer and T cells. *The Journal of Biological Chemistry* **2017**.

2. Kumari, S.; Badana, A. K.; G, M. M.; G, S.; Malla, R., Reactive Oxygen Species: A Key Constituent in Cancer Survival. *Biomarker insights* **2018,** *13*, 1177271918755391.

3. Chang, C. W.; Chen, Y. S.; Tsay, Y. G.; Han, C. L.; Chen, Y. J.; Yang, C. C.; Hung, K. F.; Lin, C. H.; Huang, T. Y.; Kao, S. Y.; Lee, T. C.; Lo, J. F., ROS-independent ER stress-mediated NRF2 activation promotes warburg effect to maintain stemness-associated properties of cancer-initiating cells. *Cell death & disease* **2018,** *9* (2), 194.

4. Panieri, E.; Santoro, M. M., ROS homeostasis and metabolism: a dangerous liason in cancer cells. *Cell death & disease* **2016,** *7* (6), e2253-.

5. Luo, B.; Lee, A. S., The critical roles of endoplasmic reticulum chaperones and unfolded protein response in tumorigenesis and anti-cancer therapies. *Oncogene* **2013,** *32* (7).

6. Dai, C., Proteotoxic stress of cancer: implication of the heat-shock response in oncogenesis. **2012,** *227* (8), 2982-7.

7. Kim, S. M.; Roy, S. G.; Chen, B.; Nguyen, T. M.; McMonigle, R. J.; McCracken, A. N.; Zhang, Y.; Kofuji, S.; Hou, J.; Selwan, E.; Finicle, B. T.; Nguyen, T. T.; Ravi, A.; Ramirez, M. U.; Wiher, T.; Guenther, G. G.; Kono, M.; Sasaki, A. T.; Weisman, L. S.; Potma, E. O.; Tromberg, B. J.; Edwards, R. A.; Hanessian, S.; Edinger, A. L., Targeting cancer metabolism by simultaneously disrupting parallel nutrient access pathways. *The Journal of Clinical Investigation* **2016,** *126* (11), 4088-102.

8. Li, P.; Zhang, D.; Shen, L.; Dong, K.; Wu, M.; Ou, Z.; Shi, D., Redox homeostasis protects mitochondria through accelerating ROS conversion to enhance hypoxia resistance in cancer cells. *Scientific Reports* **2016,** *6*.

9. Hetz, C.; Papa, F. R., The Unfolded Protein Response and Cell Fate Control. *Molecular cell* **2018,** *69* (2), 169-181.

10. Zhao, D.; Badur, M. G.; Luebeck, J.; Magana, J. H.; Birmingham, A.; Sasik, R.; Ahn, C. S.; Ideker, T.; Metallo, C. M.; Mali, P., Combinatorial CRISPR-Cas9 Metabolic Screens Reveal Critical Redox Control Points Dependent on the KEAP1-NRF2 Regulatory Axis. *Molecular cell* **2018,** *69* (4), 699-708.e7.

11. Tseng, P. L.; Wu, W. H.; Hu, T. H.; Chen, C. W.; Cheng, H. C.; Li, C. F.; Tsai, W. H.; Tsai, H. J.; Hsieh, M. C.; Chuang, J. H.; Chang, W. T., Decreased succinate dehydrogenase B in human hepatocellular carcinoma accelerates tumor malignancy by inducing the Warburg effect. *Scientific Reports* **2018,** *8* (1), 3081.

12. Vander Heiden, M. G., Targeting cancer metabolism: a therapeutic window opens. *Nature Reviews Drug Discovery* **2011,** *10*, 671.

13. Ciccarese, F.; Ciminale, V., Escaping Death: Mitochondrial Redox Homeostasis in Cancer Cells. *Frontiers in Oncology* **2017,** *7*.

14. Liberti, M. V.; Locasale, J. W., The Warburg Effect: How Does it Benefit Cancer Cells? *Trends in biochemical sciences* **2016,** *41* (3), 211-8.

15. Bravo, R.; Parra, V.; Gatica, D.; Rodriguez, A. E.; Torrealba, N.; Paredes, F.; Wang, Z. V.; Zorzano, A.; Hill, J. A.; Jaimovich, E.; Quest, A. F. G.; Lavandero, S., Endoplasmic Reticulum and the Unfolded Protein Response: Dynamics and Metabolic Integration. *International review of cell and molecular biology* **2013,** *301*, 215-90.

16. Zhang, C.; Liu, J.; Liang, Y.; Wu, R.; Zhao, Y.; Hong, X.; Lin, M.; Yu, H.; Liu, L.; Levine, A. J.; Hu, W.; Feng, Z., Tumor-Associated Mutant p53 Drives the Warburg Effect. *Nature communications* **2013,** *4*, 2935.

17. Altman, B. J.; Rathmell, J. C., Metabolic Stress in Autophagy and Cell Death Pathways. *Cold Spring Harbor perspectives in biology 4* (9), a008763.

18. Kim, C. H.; Jeon, H. M.; Lee, S. Y.; Ju, M. K.; Moon, J. Y.; Park, H. G.; Yoo, M. A.; Choi, B. T.; Yook, J. I.; Lim, S. C.; Han, S. I.; Kang, H. S., Implication of Snail in Metabolic Stress-Induced Necrosis. *PLoS ONE* **2011,** *6* (3).

19. Circu, M. L.; Aw, T. Y., REACTIVE OXYGEN SPECIES, CELLULAR REDOX SYSTEMS AND APOPTOSIS. *Free radical biology & medicine* **2010,** *48* (6), 749-62.

20. Folger, O.; Jerby, L.; Frezza, C.; Gottlieb, E.; Ruppin, E.; Shlomi, T., Predicting selective drug targets in cancer through metabolic networks. *Molecular Systems Biology* **2011,** *7*, 501.

21. Zhu, C.; Hu, W.; Wu, H.; Hu, X., No evident dose-response relationship between cellular ROS level and its cytotoxicity – a paradoxical issue in ROS-based cancer therapy. *Scientific Reports* **2014,** *4*.

22. Hong, Y. H.; Uddin, M. H.; Jo, U.; Kim, B.; Song, J.; Suh, D. H.; Kim, H. S.; Song, Y. S., ROS Accumulation by PEITC Selectively Kills Ovarian Cancer Cells via UPR-Mediated Apoptosis. *Frontiers in Oncology* **2015,** *5*.

23. Wang, J.; Luo, B.; Li, X.; Lu, W.; Yang, J.; Hu, Y.; Huang, P.; Wen, S., Inhibition of cancer growth in vitro and in vivo by a novel ROS-modulating agent with ability to eliminate stem-like cancer cells. *Cell death & disease* **2017,** *8* (6), e2887-.

24. Lee, H. Y., Reactive Oxygen Species Synergize to Potently and Selectively Induce Cancer Cell Death. **2017,** *12* (5), 1416-24.

25. Xiong, X.; Liu, J.; Qiu, X.; Pan, F.; Yu, S.; Chen, X., Piperlongumine induces apoptotic and autophagic death of the primary myeloid leukemia cells from patients via activation of ROS-p38/JNK pathways. *Acta Pharmacologica Sinica* **2015,** *36* (3), 362-74.

26. Wang, Q.; Liang, B.; Shirwany, N. A.; Zou, M. H., 2-Deoxy-D-Glucose Treatment of Endothelial Cells Induces Autophagy by Reactive Oxygen Species-Mediated Activation of the AMP-Activated Protein Kinase. *PLoS ONE* **2011,** *6* (2).

27. Nicco, C.; Batteux, F., ROS Modulator Molecules with Therapeutic Potential in Cancers Treatments. *Molecules (Basel, Switzerland)* **2017,** *23* (1).

28. Robey, R. B.; Weisz, J.; Kuemmerle, N.; Salzberg, A. C.; Berg, A.; Brown, D. G.; Kubik, L.; Palorini, R.; Al-Mulla, F.; Al-Temaimi, R.; Colacci, A.; Mondello, C.; Raju, J.; Woodrick, J.; Scovassi, A. I.; Singh, N.; Vaccari, M.; Roy, R.; Forte, S.; Memeo, L.; Salem, H. K.; Amedei, A.; Hamid, R. A.; Williams, G. P.; Lowe, L.; Meyer, J.; Martin, F. L.; Bisson, W. H.; Chiaradonna, F.; Ryan, E. P., Metabolic reprogramming and dysregulated metabolism: cause, consequence and/or enabler of environmental carcinogenesis? *Carcinogenesis* **2015,** *36* (Suppl 1), S203-31.

29. Ferrer, C. M.; Sodi, V. L.; Reginato, M. J., O-GlcNAcylation in Cancer Biology: Linking Metabolism and Signaling. *Journal of molecular biology* **2016,** *428* (16), 3282-94.

30. Ma, Z.; Vosseller, K., Cancer Metabolism and Elevated O-GlcNAc in Oncogenic Signaling. *The Journal of Biological Chemistry* **2014,** *289* (50), 34457-65.

31. Groves, J. A.; Lee, A.; Yildirir, G.; Zachara, N. E., Dynamic O-GlcNAcylation and its roles in the cellular stress response and homeostasis. *Cell Stress & Chaperones* **2013,** *18* (5), 535-58.

32. Muñoz-Pinedo, C.; El Mjiyad, N.; Ricci, J., Cancer metabolism: current perspectives and future directions. *Cell death & disease* **2012,** *3* (1), e248-.

33. Jeon, M.; Kang, H.-W.; An, S., A Mathematical Model for Enzyme Clustering in Glucose Metabolism. *Scientific Reports* **2018,** *8* (1), 2696.

34. Vernieri, C.; Casola, S.; Foiani, M.; Pietrantonio, F.; de Braud, F.; Longo, V., Targeting Cancer Metabolism: Dietary and Pharmacologic Interventions. *Cancer discovery* **2016,** *6* (12), 1315-1333.

35. Tran, Q.; Lee, H.; Park, J.; Kim, S. H.; Park, J., Targeting Cancer Metabolism - Revisiting the Warburg Effects. *Toxicological research* **2016,** *32* (3), 177-93.

36. Kim, S. M.; Roy, S. G.; Chen, B.; Nguyen, T. M.; McMonigle, R. J.; McCracken, A. N.; Zhang, Y.; Kofuji, S.; Hou, J.; Selwan, E.; Finicle, B. T.; Nguyen, T. T.; Ravi, A.; Ramirez, M. U.; Wiher, T.; Guenther, G. G.; Kono, M.; Sasaki, A. T.; Weisman, L. S.; Potma, E. O.; Tromberg, B. J.; Edwards, R. A.; Hanessian, S.; Edinger, A. L., Targeting cancer metabolism by simultaneously disrupting parallel nutrient access pathways. *The Journal of Clinical Investigation* **2016,** *126* (11), 4088-4102.

37. Gu, L.; Yi, Z.; Zhang, Y.; Ma, Z.; Zhu, Y.; Gao, J., Low dose of 2-deoxy-D-glucose kills acute lymphoblastic leukemia cells and reverses glucocorticoid resistance via N-linked glycosylation inhibition under normoxia. *Oncotarget* **2017,** *8* (19), 30978-30991.

38. Le Pogam, P.; Doue, M.; Le Page, Y.; Habauzit, D.; Zhadobov, M.; Sauleau, R.; Le Drean, Y.; Rondeau, D., Untargeted Metabolomics Reveal Lipid Alterations upon 2-Deoxyglucose Treatment in Human HaCaT Keratinocytes. *Journal of proteome research* **2018**.

39. Xu, Y.; Wang, Q.; Zhang, L.; Zheng, M., 2-Deoxy-D-glucose enhances TRAIL-induced apoptosis in human gastric cancer cells through downregulating JNK-mediated cytoprotective autophagy. *Cancer chemotherapy and pharmacology* **2018**.

40. Rao, X.; Duan, X.; Mao, W.; Li, X.; Li, Z.; Li, Q.; Zheng, Z.; Xu, H.; Chen, M.; Wang, P. G.; Wang, Y.; Shen, B.; Yi, W., O-GlcNAcylation of G6PD promotes the pentose phosphate pathway and tumor growth. *Nature communications* **2015,** *6*.

41. Boroughs, L. K.; DeBerardinis, R. J., Metabolic pathways promoting cancer cell survival and growth. *Nature cell biology* **2015,** *17* (4), 351-9.

42. d'Amico, A., Review of clinical practice utility of positron emission tomography with 18F-fluorodeoxyglucose in assessing tumour response to therapy. *La Radiologia Medica* **2015,** *120* (4), 345-51.

43. Jones, T.; Rabiner, E. A., The development, past achievements, and future directions of brain PET. *Journal of Cerebral Blood Flow & Metabolism* **2012,** *32* (7), 1426-54.

44. Yu, L.; Chen, X.; Wang, L.; Chen, S., The sweet trap in tumors: aerobic glycolysis and potential targets for therapy. *Oncotarget* **2016,** *7* (25), 38908-26.

45. Li, X.; Deng, S.; Liu, M.; Jin, Y.; Zhu, S.; Deng, S.; Chen, J.; He, C.; Qin, Q.; Wang, C.; Zhao, G., The responsively decreased PKM2 facilitates the survival of pancreatic cancer cells in hypoglucose. *Cell death & disease* **2018,** *9* (2), 133.

46. Roberts, D. J.; Miyamoto, S., Hexokinase II integrates energy metabolism and cellular protection: Akting on mitochondria and TORCing to autophagy. *Cell Death and Differentiation* **2015,** *22* (2), 248-57.

47. Zhang, J. Y.; Zhang, F.; Hong, C. Q.; Giuliano, A. E.; Cui, X. J.; Zhou, G. J.; Zhang, G. J.; Cui, Y. K., Critical protein GAPDH and its regulatory mechanisms in cancer cells. *Cancer Biology & Medicine* **2015,** *12* (1), 10-22.

48. Liang, J.; Cao, R.; Wang, X.; Zhang, Y.; Wang, P.; Gao, H.; Li, C.; Yang, F.; Zeng, R.; Wei, P.; Li, D.; Li, W.; Yang, W., Mitochondrial PKM2 regulates oxidative stress-induced apoptosis by stabilizing Bcl2. *Cell Research* **2017,** *27* (3), 329-51.

49. Das, M. R.; Bag, A. K.; Saha, S.; Ghosh, A.; Dey, S. K.; Das, P.; Mandal, C.; Ray, S.; Chakrabarti, S.; Ray, M.; Jana, S. S., Molecular association of glucose-6-phosphate isomerase and pyruvate kinase M2 with glyceraldehyde-3-phosphate dehydrogenase in cancer cells. *BMC Cancer* **2016,** *16*.

50. Yi, W., PFK1 Glycosylation Is a Key Regulator of Cancer Cell Growth and Central Metabolic Pathways. **2012,** *337* (6097), 975-80.

51. DeWaal, D.; Nogueira, V.; Terry, A. R.; Patra, K. C.; Jeon, S. M.; Guzman, G.; Au, J.; Long, C. P.; Antoniewicz, M. R.; Hay, N., Hexokinase-2 depletion inhibits glycolysis and induces oxidative phosphorylation in hepatocellular carcinoma and sensitizes to metformin. *Nature communications* **2018,** *9* (1), 446.

52. Sheikh, T.; Gupta, P.; Gowda, P.; Patrick, S.; Sen, E., Hexokinase 2 and nuclear factor erythroid 2-related factor 2 transcriptionally coactivate xanthine oxidoreductase expression in stressed glioma cells. *The Journal of Biological Chemistry* **2018**.

53. Otto, A. M., Warburg effect(s)—a biographical sketch of Otto Warburg and his impacts on tumor metabolism. *Cancer & Metabolism* **2016,** *4*.

54. Pérez-Escuredo, J.; Van Hée, V. F.; Sboarina, M.; Falces, J.; Payen, V. L.; Pellerin, L.; Sonveaux, P., Monocarboxylate transporters in the brain and in cancer(). *Biochimica et Biophysica Acta* **2016,** *1863* (10), 2481-97.

55. Pivovarova, A. I.; MacGregor, G. G., Glucose-dependent growth arrest of leukemia cells by MCT1 inhibition: Feeding Warburg's sweet tooth and blocking acid export as an anticancer

strategy. *Biomedicine & pharmacotherapy = Biomedecine & pharmacotherapie* **2018,** *98*, 173-179.

56. Bola, B. M., Inhibition of Monocarboxylate transporter-1 (MCT1) by AZD3965 enhances radiosensitivity by reducing lactate transport. **2014,** *13* (12), 2805-16.

57. Boland, M. L.; Chourasia, A. H.; Macleod, K. F., Mitochondrial Dysfunction in Cancer. *Frontiers in Oncology* **2013,** *3*.

58. LeBleu, V. S.; O'Connell, J. T.; Herrera, K. N. G.; Wikman-Kocher, H.; Pantel, K.; Haigis, M. C.; de Carvalho, F. M.; Damascena, A.; Chinen, L. T. D.; Rocha, R. M.; Asara, J. M.; Kalluri, R., PGC-1α mediates mitochondrial biogenesis and oxidative phosphorylation to promote metastasis. *Nature cell biology* **2014,** *16* (10), 992-15.

59. Hay, N., Reprogramming glucose metabolism in cancer: can it be exploited for cancer therapy? *Nature reviews. Cancer* **2016,** *16* (10), 635-49.

60. Cantó, C.; Menzies, K.; Auwerx, J., NAD(+) metabolism and the control of energy homeostasis - a balancing act between mitochondria and the nucleus. *Cell metabolism* **2015,** *22* (1), 31-53.

61. Xie, J.; Wu, H.; Dai, C.; Pan, Q.; Ding, Z.; Hu, D.; Ji, B.; Luo, Y.; Hu, X., Beyond Warburg effect – dual metabolic nature of cancer cells. *Scientific Reports* **2014,** *4*.

62. Patra, K. C.; Hay, N., The pentose phosphate pathway and cancer. *Trends in biochemical sciences 39* (8), 347-354.

63. Stincone, A.; Prigione, A.; Cramer, T.; Wamelink, M. M. C.; Campbell, K.; Cheung, E.; Olin-Sandoval, V.; Grüning, N. M.; Krüger, A.; Alam, M. T.; Keller, M. A.; Breitenbach, M.; Brindle, K. M.; Rabinowitz, J. D.; Ralser, M., The return of metabolism: biochemistry and

physiology of the pentose phosphate pathway. *Biological reviews of the Cambridge Philosophical Society* **2015,** *90* (3), 927-63.

64. Lin, R.; Elf, S.; Shan, C.; Kang, H. B.; Ji, Q.; Zhou, L.; Hitosugi, T.; Zhang, L.; Zhang, S.; Ho Seo, J.; Xie, J.; Tucker, M.; Gu, T. L.; Sudderth, J.; Jiang, L.; Mitsche, M.; DeBerardinis, R. J.; Wu, S.; Li, Y.; Mao, H.; Chen, P. R.; Wang, D.; Chen, G. Z.; Hurwitz, S. J.; Lonial, S.; Khoury, H. J.; Arellano, M. L.; Khoury, H. J.; Khuri, F. R.; Lee, B. H.; Lei, Q.; Brat, D. J.; Ye, K.; Boggon, T. J.; He, C.; Kang, S.; Fan, J.; Chen, J., 6-phosphogluconate dehydrogenase links oxidative PPP, lipogenesis and tumor growth by inhibiting LKB1-AMPK signaling. *Nature cell biology* **2015,** *17* (11), 1484-96.

65. Benito, A.; Polat, I. H.; Noe, V.; Ciudad, C. J.; Marin, S.; Cascante, M., Glucose-6-phosphate dehydrogenase and transketolase modulate breast cancer cell metabolic reprogramming and correlate with poor patient outcome. *Oncotarget* **2017,** *8* (63), 106693-106706.

66. Xu, I. M. J.; Lai, R. K. H.; Lin, S. H.; Tse, A. P. W.; Chiu, D. K. C.; Koh, H. Y.; Law, C. T.; Wong, C. M.; Cai, Z.; Wong, C. C. L.; Ng, I. O. L., Transketolase counteracts oxidative stress to drive cancer development. *Proceedings of the National Academy of Sciences of the United States of America* **2016,** *113* (6), E725-34.

67. Perl, A.; Hanczko, R.; Telarico, T.; Oaks, Z.; Landas, S., Oxidative stress, inflammation and carcinogenesis are controlled through the pentose phosphate pathway by transaldolase. *Trends in molecular medicine* **2011,** *17* (7), 395-403.

68. Marin-Valencia, I., Glucose Metabolism via the Pentose Phosphate Pathway, Glycolysis and Krebs Cycle in an Orthotopic Mouse Model of Human Brain Tumors. **2012,** *25* (10), 1177-86.

69. Raimundo, N., Revisiting the TCA cycle: signaling to tumor formation. **2011,** *17* (11), 641-9.

70. Filipp, F. V.; Scott, D. A.; Ronai Z', A.; Osterman, A. L.; Smith, J. W., Reverse TCA cycle flux through isocitrate dehydrogenases 1 and 2 is required for lipogenesis in hypoxic melanoma cells. *Pigment cell & melanoma research* **2012,** *25* (3), 375-83.

71. Flöter, J.; Kaymak, I.; Schulze, A., Regulation of Metabolic Activity by p53. *Metabolites* **2017,** *7* (2).

72. Liang, Y.; Liu, J.; Feng, Z., The regulation of cellular metabolism by tumor suppressor p53. *Cell & Bioscience* **2013,** *3*, 9.

73. Altman, B. J., From Krebs to Clinic: Glutamine Metabolism to Cancer. **2016,** *16* (10), 619-34.

74. DeBerardinis, R. J.; Chandel, N. S., Fundamentals of cancer metabolism. *Science Advances* **2016,** *2* (5).

75. Murai, S.; Ando, A.; Ebara, S.; Hirayama, M.; Satomi, Y.; Hara, T., Inhibition of malic enzyme 1 disrupts cellular metabolism and leads to vulnerability in cancer cells in glucose-restricted conditions. *Oncogenesis* **2017,** *6* (5), e329-.

76. Ferrer, C. M.; Lynch, T. P.; Sodi, V. L.; Falcone, J. N.; Schwab, L. P.; Peacock, D. L.; Vocadlo, D. J.; Seagroves, T. N.; Reginato, M. J., O-GlcNAcylation regulates cancer metabolism and survival stress signaling via regulation of HIF-1 pathway. *Molecular cell* **2014,** *54* (5), 820-31.

77. Yi, W.; Clark, P. M.; Mason, D. E.; Keenan, M. C.; Hill, C.; Goddard, W. A., 3rd; Peters, E. C.; Driggers, E. M.; Hsieh-Wilson, L. C., Phosphofructokinase 1 glycosylation regulates cell growth and metabolism. *Science (New York, N.Y.)* **2012,** *337* (6097), 975-80.

78. Chaiyawat, P.; Chokchaichamnankit, D.; Lirdprapamongkol, K.; Srisomsap, C.; Svasti, J.; Champattanachai, V., Alteration of O-GlcNAcylation affects serine phosphorylation and regulates

gene expression and activity of pyruvate kinase M2 in colorectal cancer cells. *Oncology reports* **2015,** *34* (4), 1933-42.

79. Wang, Y.; Liu, J.; Jin, X.; Zhang, D.; Li, D.; Hao, F.; Feng, Y.; Gu, S.; Meng, F.; Tian, M.; Zheng, Y.; Xin, L.; Zhang, X.; Han, X.; Aravind, L.; Wei, M., O-GlcNAcylation destabilizes the active tetrameric PKM2 to promote the Warburg effect. *Proceedings of the National Academy of Sciences* **2017,** *114* (52), 13732-13737.

80. Jóźwiak, P.; Forma, E.; Bryś, M.; Krześlak, A., O-GlcNAcylation and Metabolic Reprograming in Cancer. *Frontiers in Endocrinology* **2014,** *5*, 145.

81. Zeeshan, H.; Lee, G.; Kim, H.-R.; Chae, H.-J., Endoplasmic Reticulum Stress and Associated ROS. *International journal of molecular sciences* **2016,** *17* (3), 327.

82. Gilbert, H. F., Protein disulfide isomerase and assisted protein folding. *The Journal of Biological Chemistry* **1997,** *272* (47), 29399-402.

83. Zito, E., ERO1: A protein disulfide oxidase and H2O2 producer. *Free radical biology & medicine* **2015,** *83*, 299-304.

84. Nisimoto, Y.; Ogawa, H.; Kadokawa, Y.; Qiao, S., NADPH Oxidase 4 Function as a Hydrogen Peroxide Sensor. *Journal of biochemistry* **2018**.

85. Cook, K. L.; Soto-Pantoja, D. R.; Clarke, P. A. G.; Cruz, M. I.; Zwart, A.; Wärri, A.; Hilakivi-Clarke, L.; Roberts, D. D.; Clarke, R., Endoplasmic reticulum stress protein GRP78 modulates lipid metabolism to control drug sensitivity and anti-tumor immunity in breast cancer. *Cancer research* **2016,** *76* (19), 5657-70.

86. Ni, M.; Zhang, Y.; Lee, A. S., Beyond the endoplasmic reticulum: atypical GRP78 in cell viability, signaling and therapeutic targeting. *Biochemical Journal* **2011,** *434* (2), 181-8.

87. Lee, A. S., Glucose regulated proteins in cancer: molecular mechanisms and therapeutic potential. *Nature reviews. Cancer* **2014,** *14* (4), 263-76.

88. Bu, Y.; Diehl, J. A., PERK integrates oncogenic signaling and cell survival during cancer development. *Journal of cellular physiology* **2016,** *231* (10), 2088-96.

89. Gu, S.; Chen, C.; Jiang, X.; Zhang, Z., ROS-mediated endoplasmic reticulum stress and mitochondrial dysfunction underlie apoptosis induced by resveratrol and arsenic trioxide in A549 cells. *Chemico-biological interactions* **2016,** *245*, 100-9.

90. Hattori, K.; Naguro, I.; Runchel, C.; Ichijo, H., The roles of ASK family proteins in stress responses and diseases. *Cell Communication and Signaling : CCS* **2009,** *7*, 9.

91. Brown, M.; Strudwick, N.; Suwara, M.; Sutcliffe, L. K.; Mihai, A. D.; Ali, A. A.; Watson, J. N.; Schröder, M., An initial phase of JNK activation inhibits cell death early in the endoplasmic reticulum stress response. *Journal of cell science* **2016,** *129* (12), 2317-28.

92. Bubici, C.; Papa, S., JNK signalling in cancer: in need of new, smarter therapeutic targets. *British Journal of Pharmacology* **2014,** *171* (1), 24-37.

93. Lei, Y.; Wang, S.; Ren, B.; Wang, J.; Chen, J.; Lu, J.; Zhan, S.; Fu, Y.; Huang, L.; Tan, J., CHOP favors endoplasmic reticulum stress-induced apoptosis in hepatocellular carcinoma cells via inhibition of autophagy. *PLoS ONE* **2017,** *12* (8).

94. Pytel, D.; Majsterek, I.; Diehl, J. A., Tumor progression and the Different Faces of the PERK kinase. *Oncogene* **2016,** *35* (10), 1207-15.

95. Chatham, J. C.; Marchase, R. B., Protein O-GlcNAcylation: A critical regulator of the cellular response to stress. *Current signal transduction therapy* **2010,** *5* (1), 49-59.

96. Jang, I.; Kim, H. B.; Seo, H.; Kim, J. Y.; Choi, H.; Yoo, J. S.; Kim, J. W.; Cho, J. W., O-GlcNAcylation of eIF2alpha regulates the phospho-eIF2alpha-mediated ER stress response. *Biochimica et Biophysica Acta* **2015,** *1853* (8), 1860-9.

97. Aft, R. L.; Zhang, F. W.; Gius, D., Evaluation of 2-deoxy-D-glucose as a chemotherapeutic agent: mechanism of cell death. *British Journal of Cancer* **2002,** *87* (7), 805-12.

98. Shutt, D. C.; O'Dorisio, M. S.; Aykin-Burns, N.; Spitz, D. R., 2-deoxy-D-glucose induces oxidative stress and cell killing in human neuroblastoma cells. *Cancer biology & therapy* **2010,** *9* (11), 853-61.

99. Zhang, X. D.; Deslandes, E.; Villedieu, M.; Poulain, L.; Duval, M.; Gauduchon, P.; Schwartz, L.; Icard, P., Effect of 2-deoxy-D-glucose on various malignant cell lines in vitro. *Anticancer research* **2006,** *26* (5a), 3561-6.

100. Calvaresi, E. C.; Hergenrother, P. J., Glucose conjugation for the specific targeting and treatment of cancer. *Chemical science (Royal Society of Chemistry : 2010)* **2013,** *4* (6), 2319-33.

101. Lee, H. Y.; Itahana, Y.; Schuechner, S.; Fukuda, M.; Je, H. S.; Ogris, E.; Virshup, D. M.; Itahana, K., Ca²⁺-dependent demethylation of phosphatase PP2Ac promotes glucose deprivation–induced cell death independently of inhibiting glycolysis. *Science Signaling* **2018,** *11* (512).

102. Kim, J.; Kim, J.; Bae, J. S., ROS homeostasis and metabolism: a critical liaison for cancer therapy. *Experimental & Molecular Medicine* **2016,** *48* (11), e269-.

103. Poprac, P.; Jomova, K.; Simunkova, M.; Kollar, V.; Rhodes, C. J.; Valko, M., Targeting Free Radicals in Oxidative Stress-Related Human Diseases. *Trends in pharmacological sciences* **2017,** *38* (7), 592-607.

104. Rahal, A.; Kumar, A.; Singh, V.; Yadav, B.; Tiwari, R.; Chakraborty, S.; Dhama, K., Oxidative Stress, Prooxidants, and Antioxidants: The Interplay. *BioMed Research International* **2014,** *2014*.

105. Di Meo, S.; Reed, T. T.; Venditti, P.; Victor, V. M., Role of ROS and RNS Sources in Physiological and Pathological Conditions. *Oxidative Medicine and Cellular Longevity* **2016,** *2016*.

106. Meitzler, J. L.; Antony, S.; Wu, Y.; Juhasz, A.; Liu, H.; Jiang, G.; Lu, J.; Roy, K.; Doroshow, J. H., NADPH Oxidases: A Perspective on Reactive Oxygen Species Production in Tumor Biology. *Antioxidants & Redox Signaling* **2014,** *20* (17), 2873-89.

107. Dan Dunn, J.; Alvarez, L. A. J.; Zhang, X.; Soldati, T., Reactive oxygen species and mitochondria: A nexus of cellular homeostasis. *Redox Biology* **2015,** *6*, 472-85.

108. Wang, K.; Zhang, T.; Dong, Q.; Nice, E. C.; Huang, C.; Wei, Y., Redox homeostasis: the linchpin in stem cell self-renewal and differentiation. *Cell Death &Amp; Disease* **2013,** *4*, e537.

109. McLain, A. L.; Szweda, P. A.; Szweda, L. I., α-Ketoglutarate dehydrogenase: A mitochondrial redox sensor. *Free radical research* **2011,** *45* (1), 29-36.

110. Li, X.; Fang, P.; Mai, J.; Choi, E. T.; Wang, H.; Yang, X.-f., Targeting mitochondrial reactive oxygen species as novel therapy for inflammatory diseases and cancers. *Journal of Hematology & Oncology* **2013,** *6* (1), 19.

111. Jo, M. J.; Kim, H. J.; Lee, S.-Y.; Lee, D.-H.; Oh, S. C., Abstract 2254: Reactive oxygen species modulator 1 (Romo1) predicts unfavorable prognosis in colorectal cancer patients. *Cancer research* **2017,** *77* (13 Supplement), 2254-2254.

112. Lee, S. H.; Choi, S. I.; Lee, J. S.; Kim, C. H.; Jung, W. J.; Lee, E. J.; Min, K. H.; Hur, G. Y.; Lee, S. H.; Lee, S. Y.; Kim, J. H.; Lee, S. Y.; Shin, C.; Shim, J. J.; Kang, K. H.; In, K. H.,

Reactive Oxygen Species Modulator 1 (Romo1) Predicts Poor Outcomes in Advanced Non-small Cell Lung Cancer Patients Treated with Platinum-Based Chemotherapy. *Cancer research and treatment : official journal of Korean Cancer Association* **2017,** *49* (1), 141-149.

113. Zeke, A.; Misheva, M.; Reményi, A.; Bogoyevitch, M. A., JNK Signaling: Regulation and Functions Based on Complex Protein-Protein Partnerships. *Microbiology and Molecular Biology Reviews : MMBR* **2016,** *80* (3), 793-835.

114. Yang, H.; Xie, Y.; Yang, D.; Ren, D., Oxidative stress-induced apoptosis in granulosa cells involves JNK, p53 and Puma. *Oncotarget* **2017,** *8* (15), 25310-22.

115. Yang, L.; Wu, D.; Wang, X.; Cederbaum, A. I., Depletion of cytosolic or mitochondrial thioredoxin increases CYP2E1 induced oxidative stress via an ASK-1-JNK1 pathway in HepG2 cells. *Free radical biology & medicine* **2011,** *51* (1), 185-96.

116. Xu, H. G.; Zhai, Y. X.; Chen, J.; Lu, Y.; Wang, J. W.; Quan, C. S.; Zhao, R. X.; Xiao, X.; He, Q.; Werle, K. D.; Kim, H. G.; Lopez, R.; Cui, R.; Liang, J.; Li, Y. L.; Xu, Z. X., LKB1 reduces ROS-mediated cell damage via activation of p38. *Oncogene* **2015,** *34* (29), 3848-59.

117. Arvidsson, Y.; Hamazaki, T. S.; Ichijo, H.; Funa, K., ASK1 resistant neuroblastoma is deficient in activation of p38 kinase. *Cell Death and Differentiation* **2001,** *8*, 1029.

118. Zhuang, S.; Demirs, J. T.; Kochevar, I. E., p38 mitogen-activated protein kinase mediates bid cleavage, mitochondrial dysfunction, and caspase-3 activation during apoptosis induced by singlet oxygen but not by hydrogen peroxide. *The Journal of Biological Chemistry* **2000,** *275* (34), 25939-48.

119. Zawacka-Pankau, J.; Grinkevich, V. V.; Hünten, S.; Nikulenkov, F.; Gluch, A.; Li, H.; Enge, M.; Kel, A.; Selivanova, G., Inhibition of Glycolytic Enzymes Mediated by

Pharmacologically Activated p53: TARGETING WARBURG EFFECT TO FIGHT CANCER. *The Journal of Biological Chemistry* **2011,** *286* (48), 41600-15.

120. Jiang, P.; Du, W.; Wang, X.; Mancuso, A.; Gao, X.; Wu, M.; Yang, X., p53 regulates biosynthesis through direct inactivation of glucose-6-phosphate dehydrogenase. *Nature cell biology* **2011,** *13* (3), 310-6.

121. Polyak, K.; Xia, Y.; Zweier, J. L.; Kinzler, K. W.; Vogelstein, B., A model for p53-induced apoptosis. *Nature* **1997,** *389* (6648), 300-5.

122. Drane, P.; Bravard, A.; Bouvard, V.; May, E., Reciprocal down-regulation of p53 and SOD2 gene expression-implication in p53 mediated apoptosis. *Oncogene* **2001,** *20* (4), 430-9.

123. Yang, W. H.; Kim, J. E.; Nam, H. W.; Ju, J. W.; Kim, H. S.; Kim, Y. S.; Cho, J. W., Modification of p53 with O-linked N-acetylglucosamine regulates p53 activity and stability. *Nature cell biology* **2006,** *8* (10), 1074-83.

124. de Queiroz, R. M.; Madan, R.; Chien, J.; Dias, W. B.; Slawson, C., Changes in O-Linked N-Acetylglucosamine (O-GlcNAc) Homeostasis Activate the p53 Pathway in Ovarian Cancer Cells. *The Journal of Biological Chemistry* **2016,** *291* (36), 18897-914.

125. Hsieh, A. L.; Walton, Z. E.; Altman, B. J.; Stine, Z. E.; Dang, C. V., MYC and metabolism on the path to cancer. *Seminars in cell & developmental biology* **2015,** *43*, 11-21.

126. Collins, M. A.; Pasca di Magliano, M., Kras as a key oncogene and therapeutic target in pancreatic cancer. *Frontiers in Physiology* **2013,** *4*.

127. Yu, C.; Wang, X.; Huang, L.; Tong, Y.; Chen, L.; Wu, H.; Xia, Q.; Kong, X., Deciphering the spectrum of Mitochondrial DNA Mutations in Hepatocellular Carcinoma using High throughput Sequencing ----Mitochondrial DNA in Hepatocellular Carcinoma. *Gene expression* **2018**.

128. Schumacker, Paul T., Reactive Oxygen Species in Cancer: A Dance with the Devil. *Cancer Cell 27* (2), 156-157.

129. Schumacker, P. T., Reactive oxygen species in cancer cells: Live by the sword, die by the sword. *Cancer Cell* **2006,** *10* (3), 175-176.

130. Masgras, I.; Carrera, S.; de Verdier, P. J.; Brennan, P.; Majid, A.; Makhtar, W.; Tulchinsky, E.; Jones, G. D.; Roninson, I. B.; Macip, S., Reactive oxygen species and mitochondrial sensitivity to oxidative stress determine induction of cancer cell death by p21. *The Journal of Biological Chemistry* **2012,** *287* (13), 9845-54.

131. Nilsson, R.; Jain, M.; Madhusudhan, N.; Sheppard, N. G.; Strittmatter, L.; Kampf, C.; Huang, J.; Asplund, A.; Mootha, V. K., Metabolic enzyme expression highlights a key role for MTHFD2 and the mitochondrial folate pathway in cancer. *Nature communications* **2014,** *5*, 3128.

132. Wang, N.; Wu, Y.; Bian, J.; Qian, X.; Lin, H.; Sun, H.; You, Q.; Zhang, X., Current Development of ROS-Modulating Agents as Novel Antitumor Therapy. *Current cancer drug targets* **2017,** *17* (2), 122-136.

133. Ribas, J.; Mattiolo, P.; Boix, J., Pharmacological modulation of reactive oxygen species in cancer treatment. *Current drug targets* **2015,** *16* (1), 31-7.

134. Peng, X.; Gandhi, V., ROS-activated anticancer prodrugs: a new strategy for tumor-specific damage. *Therapeutic delivery* **2012,** *3* (7), 823-33.

135. Gupta, S. C.; Hevia, D.; Patchva, S.; Park, B.; Koh, W.; Aggarwal, B. B., Upsides and Downsides of Reactive Oxygen Species for Cancer: The Roles of Reactive Oxygen Species in Tumorigenesis, Prevention, and Therapy. *Antioxidants & Redox Signaling* **2012,** *16* (11), 1295-322.

136. Kasherman, Y.; Sturup, S.; Gibson, D., Is Glutathione the Major Cellular Target of Cisplatin? A Study of the Interactions of Cisplatin with Cancer Cell Extracts. *Journal of medicinal chemistry* **2009,** *52* (14), 4319-4328.

137. Choi, Y. M.; Kim, H. K.; Shim, W.; Anwar, M. A.; Kwon, J. W.; Kwon, H. K.; Kim, H. J.; Jeong, H.; Kim, H. M.; Hwang, D.; Kim, H. S.; Choi, S., Mechanism of Cisplatin-Induced Cytotoxicity Is Correlated to Impaired Metabolism Due to Mitochondrial ROS Generation. *PLoS ONE* **2015,** *10* (8).

138. Wang, S. Y.; Wei, Y. H.; Shieh, D. B.; Lin, L. L.; Cheng, S. P.; Wang, P. W.; Chuang, J. H., 2-Deoxy-d-Glucose Can Complement Doxorubicin and Sorafenib to Suppress the Growth of Papillary Thyroid Carcinoma Cells. *PLoS ONE* **2015,** *10* (7).

139. Zhang, D.; Fei, Q.; Li, J.; Zhang, C.; Sun, Y.; Zhu, C.; Wang, F.; Sun, Y., 2-Deoxyglucose Reverses the Promoting Effect of Insulin on Colorectal Cancer Cells In Vitro. *PLoS ONE* **2016,** *11* (3).

140. Jeon, J. Y.; Kim, S. W.; Park, K. C.; Yun, M., The bifunctional autophagic flux by 2-deoxyglucose to control survival or growth of prostate cancer cells. *BMC Cancer* **2015,** *15*.

141. Bizjak, M.; Malavašič, P.; Dolinar, K.; Pohar, J.; Pirkmajer, S.; Pavlin, M., Combined treatment with Metformin and 2-deoxy glucose induces detachment of viable MDA-MB-231 breast cancer cells in vitro. *Scientific Reports* **2017,** *7*.

142. Kovács, K., 2-DEOXY-GLUCOSE DOWN REGULATES ENDOTHELIAL AKT AND ERK VIA INTERFERENCE WITH N-LINKED GLYCOSYLATION, INDUCTION OF ENDOPLASMIC RETICULUM STRESS AND GSK-3β ACTIVATION. **2016,** *15* (2), 264-75.

143. Merchan, J. R.; Kovács, K.; Railsback, J. W.; Kurtoglu, M.; Jing, Y.; Piña, Y.; Gao, N.; Murray, T. G.; Lehrman, M. A.; Lampidis, T. J., Antiangiogenic Activity of 2-Deoxy-D-Glucose. *PLoS ONE* **2010,** *5* (10), e13699.

144. Datema, R.; Schwarz, R. T., Interference with glycosylation of glycoproteins. Inhibition of formation of lipid-linked oligosaccharides <em>in vivo</em&gt. *Biochemical Journal* **1979,** *184* (1), 113.

145. Simons, A. L.; Ahmad, I. M.; Mattson, D. M.; Dornfeld, K. J.; Spitz, D. R., 2-Deoxy-d-Glucose Combined with Cisplatin Enhances Cytotoxicity via Metabolic Oxidative Stress in Human Head and Neck Cancer Cells. *Cancer research* **2007,** *67* (7).

146. Agerholm, M.; Dall, M.; Jensen, B. A. H.; Prats, C.; Madsen, S.; Basse, A. L.; Graae, A. S.; Risis, S.; Goldenbaum, J.; Quistorff, B.; Larsen, S.; Vienberg, S. G.; Treebak, J. T., Perturbations of NAD salvage systems impact mitochondrial function and energy homeostasis in mouse myoblasts and intact skeletal muscle. *American journal of physiology. Endocrinology and metabolism* **2017**.

147. Ralser, M.; Wamelink, M. M.; Struys, E. A.; Joppich, C.; Krobitsch, S.; Jakobs, C.; Lehrach, H., A catabolic block does not sufficiently explain how 2-deoxy-d-glucose inhibits cell growth. *Proceedings of the National Academy of Sciences* **2008,** *105* (46), 17807-17811.

148. Kurtoglu, M.; Gao, N.; Shang, J.; Maher, J. C.; Lehrman, M. A.; Wangpaichitr, M.; Savaraj, N.; Lane, A. N.; Lampidis, T. J., Under normoxia, 2-deoxy-D-glucose elicits cell death in select tumor types not by inhibition of glycolysis but by interfering with N-linked glycosylation. *Molecular cancer therapeutics* **2007,** *6* (11), 3049-58.

149. Mühlenberg, T.; Grunewald, S.; Treckmann, J.; Podleska, L.; Schuler, M.; Fletcher, J. A.; Bauer, S., Inhibition of KIT-Glycosylation by 2-Deoxyglucose Abrogates KIT-Signaling and Combination with ABT-263 Synergistically Induces Apoptosis in Gastrointestinal Stromal Tumor. *PLoS ONE* **2015,** *10* (3).

150. Leung, H. J.; Duran, E. M.; Kurtoglu, M.; Andreansky, S.; Lampidis, T. J.; Mesri, E. A., Activation of the Unfolded Protein Response by 2-Deoxy-d-Glucose Inhibits Kaposi's Sarcoma-Associated Herpesvirus Replication and Gene Expression. *Antimicrobial Agents and Chemotherapy* **2012,** *56* (11), 5794-803.

151. Xi, H.; Kurtoglu, M.; Liu, H.; Wangpaichitr, M.; You, M.; Liu, X.; Savaraj, N.; Lampidis, T. J., 2-Deoxy-D-glucose activates autophagy via endoplasmic reticulum stress rather than ATP depletion. *Cancer chemotherapy and pharmacology* **2011,** *67* (4), 899-910.

152. Zagorodna, O.; Martin, S. M.; Rutkowski, D. T.; Kuwana, T.; Spitz, D. R.; Knudson, C. M., 2-Deoxyglucose-induced toxicity is regulated by Bcl-2 family members and is enhanced by antagonizing Bcl-2 in lymphoma cell lines. *Oncogene* **2012,** *31* (22), 2738-49.

153. Stein, M.; Lin, H.; Jeyamohan, C.; Dvorzhinski, D.; Gounder, M.; Bray, K.; Eddy, S.; Goodin, S.; White, E.; DiPaola, R. S., TargetingTumor MetabolismWith 2-Deoxyglucose in Patients With Castrate-Resistant Prostate Cancer and Advanced Malignancies. *The Prostate* **2010,** *70* (13), 1388-94.

154. Andrade-Vieira, R.; Goguen, D.; Bentley, H. A.; Bowen, C. V.; Marignani, P. A., Pre-clinical study of drug combinations that reduce breast cancer burden due to aberrant mTOR and metabolism promoted by LKB1 loss. *Oncotarget* **2014,** *5* (24), 12738-52.

155. Zhong, D.; Xiong, L.; Liu, T.; Liu, X.; Liu, X.; Chen, J.; Sun, S. Y.; Khuri, F. R.; Zong, Y.; Zhou, Q.; Zhou, W., The Glycolytic Inhibitor 2-Deoxyglucose Activates Multiple Prosurvival Pathways through IGF1R. *The Journal of Biological Chemistry* **2009,** *284* (35), 23225-33.

156. Trincone, A., Uncommon Glycosidases for the Enzymatic Preparation of Glycosides. *Biomolecules* **2015,** *5* (4), 2160-83.

157. Bridiau, N.; Benmansour, M.; Legoy, M. D.; Maugard, T., One-pot stereoselective synthesis of β-N-aryl-glycosides by N-glycosylation of aromatic amines: application to the synthesis of tumor-associated carbohydrate antigen building blocks. *Tetrahedron* **2007,** *63* (19), 4178-4183.

158. Isono, T.; Chano, T.; Kitamura, A.; Yuasa, T., Glucose Deprivation Induces G2/M Transition-Arrest and Cell Death in N-GlcNAc(2)-Modified Protein-Producing Renal Carcinoma Cells. *PLoS ONE* **2014,** *9* (5).

159. Graham, N. A.; Tahmasian, M.; Kohli, B.; Komisopoulou, E.; Zhu, M.; Vivanco, I.; Teitell, M. A.; Wu, H.; Ribas, A.; Lo, R. S.; Mellinghoff, I. K.; Mischel, P. S.; Graeber, T. G., Glucose deprivation activates a metabolic and signaling amplification loop leading to cell death. *Molecular Systems Biology* **2012,** *8*, 589.

160. Yang, J.; Zhao, X.; Tang, M.; Li, L.; Lei, Y.; Cheng, P.; Guo, W.; Zheng, Y.; Wang, W.; Luo, N.; Peng, Y.; Tong, A.; Wei, Y.; Nie, C.; Yuan, Z., The role of ROS and subsequent DNA-damage response in PUMA-induced apoptosis of ovarian cancer cells. *Oncotarget* **2017,** *8* (14), 23492-506.

161. Granchi, C., Anticancer agents interacting with membrane glucose transporters(). **2016,** *7* (9), 1716-29.

162. Thorens, B.; Mueckler, M., Glucose transporters in the 21st Century. *American journal of physiology. Endocrinology and metabolism* **2010,** *298* (2), E141-5.

163. Krivohlava, R.; Grobarova, V.; Neuhoferova, E.; Fiserova, A.; Benson, V., Interaction of colon cancer cells with glycoconjugates triggers complex changes in gene expression, glucose transporters and cell invasion. *Molecular medicine reports* **2018**.

164. Ndombera, F. T.; VanHecke, G. C.; Nagi, S.; Ahn, Y.-H., Carbohydrate-based inducers of cellular stress for targeting cancer cells. *Bioorganic & Medicinal Chemistry Letters* **2016,** *26* (5), 1452-1456.

165. Grynkiewicz, G.; Szeja, W.; Boryski, J., Synthetic analogs of natural glycosides in drug discovery and development. *Acta poloniae pharmaceutica* **2008,** *65* (6), 655-76.

166. Hricovíni, M.; Malkina, O. L.; Bízik, F.; Nagy, L. T.; Malkin, V. G., Calculation of NMR Chemical Shifts and Spin−Spin Coupling Constants in the Monosaccharide Methyl-β-d-xylopyranoside Using a Density Functional Theory Approach. *The Journal of Physical Chemistry A* **1997,** *101* (50), 9756-9762.

167. Allen, H. J.; Kisailus, E. C., *Glycoconjugates: Composition: Structure, and Function*. Taylor & Francis: 1992.

168. Govindaraju, V.; Young, K.; Maudsley, A. A., Proton NMR chemical shifts and coupling constants for brain metabolites. *NMR in biomedicine* **2000,** *13* (3), 129-53.

169. Bubb, W. A., NMR spectroscopy in the study of carbohydrates: Characterizing the structural complexity. *Concepts in magnetic resonance* **2003,** *19A* (1), 1-19.

170. Siegbahn, A.; Aili, U.; Ochocinska, A.; Olofsson, M.; Rönnols, J.; Mani, K.; Widmalm, G.; Ellervik, U., Synthesis, conformation and biology of naphthoxylosides. *Bioorganic & medicinal chemistry* **2011,** *19* (13), 4114-4126.

171. Gasparovic, A. C.; Jaganjac, M.; Mihaljevic, B.; Sunjic, S. B.; Zarkovic, N., Assays for the measurement of lipid peroxidation. *Methods in molecular biology (Clifton, N.J.)* **2013,** *965*, 283-96.

172. Augustyniak, E.; Adam, A.; Wojdyla, K.; Rogowska-Wrzesinska, A.; Willetts, R.; Korkmaz, A.; Atalay, M.; Weber, D.; Grune, T.; Borsa, C.; Gradinaru, D.; Chand Bollineni, R.; Fedorova, M.; Griffiths, H. R., Validation of protein carbonyl measurement: A multi-centre study. *Redox Biology* **2015,** *4*, 149-57.

173. Brown, K., Methods for the detection of DNA adducts. *Methods in molecular biology (Clifton, N.J.)* **2012,** *817*, 207-30.

174. Comini, M. A., Measurement and meaning of cellular thiol:disufhide redox status. *Free radical research* **2016,** *50* (2), 246-71.

175. Banerjee, P. S.; Hart, G. W.; Cho, J. W., Chemical approaches to study O-GlcNAcylation. *Chemical Society reviews* **2013,** *42* (10), 4345-57.

176. Wang, X.; Roper, M. G., Measurement of DCF fluorescence as a measure of reactive oxygen species in murine islets of Langerhans. *Analytical methods : advancing methods and applications* **2014,** *6* (9), 3019-24.

177. Tetz, L. M.; Kamau, P. W.; Cheng, A. A.; Meeker, J. D.; Loch-Caruso, R., Troubleshooting the dichlorofluorescein assay to avoid artifacts in measurement of toxicant-stimulated cellular production of reactive oxidant species. *Journal of pharmacological and toxicological methods* **2013,** *67* (2), 56-60.

178. Northoff, H.; Flegel, W. A., Fetal Calf Serum A2 - Delves, Peter J. In *Encyclopedia of Immunology (Second Edition)*, Elsevier: Oxford, 1998; pp 896-897.

179. Brunner, D.; Frank, J.; Appl, H.; Schoffl, H.; Pfaller, W.; Gstraunthaler, G., Serum-free cell culture: the serum-free media interactive online database. *Altex* **2010,** *27* (1), 53-62.

180. Shen, W.-J.; Hsieh, C.-Y.; Chen, C.-L.; Yang, K.-C.; Ma, C.-T.; Choi, P.-C.; Lin, C.-F., A modified fixed staining method for the simultaneous measurement of reactive oxygen species and oxidative responses. *Biochemical and Biophysical Research Communications* **2013,** *430* (1), 442-447.

181. Chen, C. L.; Chan, P. C.; Wang, S. H.; Pan, Y. R.; Chen, H. C., Elevated expression of protein kinase C delta induces cell scattering upon serum deprivation. *Journal of cell science* **2010,** *123* (Pt 17), 2901-13.

182. Tsachaki, M.; Mladenovic, N.; Stambergova, H.; Birk, J.; Odermatt, A., Hexose-6-phosphate dehydrogenase controls cancer cell proliferation and migration through pleiotropic effects on the unfolded-protein response, calcium homeostasis, and redox balance. *FASEB journal : official publication of the Federation of American Societies for Experimental Biology* **2018**, fj201700870RR.

183. Murai, S.; Ando, A.; Ebara, S.; Hirayama, M.; Satomi, Y.; Hara, T., Inhibition of malic enzyme 1 disrupts cellular metabolism and leads to vulnerability in cancer cells in glucose-restricted conditions. *Oncogenesis* **2017,** *6* (5), e329.

184. Gelman, S. J.; Naser, F.; Mahieu, N. G.; McKenzie, L. D.; Dunn, G. P.; Chheda, M. G.; Patti, G. J., Consumption of NADPH for 2-HG Synthesis Increases Pentose Phosphate Pathway Flux and Sensitizes Cells to Oxidative Stress. *Cell reports* **2018,** *22* (2), 512-522.

185. Yu, T.; Robotham, J. L.; Yoon, Y., Increased production of reactive oxygen species in hyperglycemic conditions requires dynamic change of mitochondrial morphology. *Proceedings of the National Academy of Sciences of the United States of America* **2006,** *103* (8), 2653-2658.

186. Liu, Y.; Song, X.-D.; Liu, W.; Zhang, T.-Y.; Zuo, J., Glucose deprivation induces mitochondrial dysfunction and oxidative stress in PC12 cell line. *Journal of Cellular and Molecular Medicine* **2003,** *7* (1), 49-56.

187. Ceriello, A.; Russo, P. d.; Amstad, P.; Cerutti, P., High Glucose Induces Antioxidant Enzymes in Human Endothelial Cells in Culture: Evidence Linking Hyperglycemia and Oxidative Stress. *Diabetes* **1996,** *45* (4), 471-477.

188. Prabst, K.; Engelhardt, H.; Ringgeler, S.; Hubner, H., Basic Colorimetric Proliferation Assays: MTT, WST, and Resazurin. *Methods in molecular biology (Clifton, N.J.)* **2017,** *1601*, 1-17.

189. Adan, A.; Kiraz, Y.; Baran, Y., Cell Proliferation and Cytotoxicity Assays. *Current pharmaceutical biotechnology* **2016,** *17* (14), 1213-1221.

190. Altman, S. A.; Randers, L.; Rao, G., Comparison of trypan blue dye exclusion and fluorometric assays for mammalian cell viability determinations. *Biotechnology Progress* **1993,** *9* (6), 671-674.

191. Pei, X. Y.; Dai, Y.; Rahmani, M.; Li, W.; Dent, P.; Grant, S., The farnesyltransferase inhibitor L744832 potentiates UCN-01-induced apoptosis in human multiple myeloma cells. *Clinical cancer research : an official journal of the American Association for Cancer Research* **2005,** *11* (12), 4589-600.

192. Allen, L. F.; Sebolt-Leopold, J.; Meyer, M. B., CI-1040 (PD184352), a targeted signal transduction inhibitor of MEK (MAPKK). *Seminars in Oncology* **2003,** *30*, 105-116.

193. Arcidiacono, P.; Stabile, A. M.; Ragonese, F.; Pistilli, A.; Calvieri, S.; Bottoni, U.; Crisanti, A.; Spaccapelo, R.; Rende, M., Anticarcinogenic activities of sulforaphane are influenced by

Nerve Growth Factor in human melanoma A375 cells. *Food and chemical toxicology : an international journal published for the British Industrial Biological Research Association* **2018**.

194. Wang, A.; Zhao, C.; Liu, X.; Su, W.; Duan, G.; Xie, Z.; Chu, S.; Gao, Y., Knockdown of TBRG4 affects tumorigenesis in human H1299 lung cancer cells by regulating DDIT3, CAV1 and RRM2. *Oncology letters* **2018,** *15* (1), 121-128.

195. Zhou, W.; Ma, H.; Deng, G.; Tang, L.; Lu, J.; Chen, X., Clinical significance and biological function of fucosyltransferase 2 in lung adenocarcinoma. *Oncotarget* **2017,** *8* (57), 97246-97259.

196. Wang, D. X.; Zou, Y. J.; Zhuang, X. B.; Chen, S. X.; Lin, Y.; Li, W. L.; Lin, J. J.; Lin, Z. Q., Sulforaphane suppresses EMT and metastasis in human lung cancer through miR-616-5p-mediated GSK3beta/beta-catenin signaling pathways. *Acta Pharmacologica Sinica* **2017,** *38* (2), 241-251.

197. Chen, C.-Y.; Yu, Z.-Y.; Chuang, Y.-S.; Huang, R.-M.; Wang, T.-C. V., Sulforaphane attenuates EGFR signaling in NSCLC cells. *Journal of Biomedical Science* **2015,** *22* (1), 38.

198. Li, Q. Q.; Xie, Y. K.; Wu, Y.; Li, L. L.; Liu, Y.; Miao, X. B.; Liu, Q. Z.; Yao, K. T.; Xiao, G. H., Sulforaphane inhibits cancer stem-like cell properties and cisplatin resistance through miR-214-mediated downregulation of c-MYC in non-small cell lung cancer. *Oncotarget* **2017,** *8* (7), 12067-12080.

199. Park, W. H., MAPK inhibitors, particularly the JNK inhibitor, increase cell death effects in H2O2-treated lung cancer cells via increased superoxide anion and glutathione depletion. *Oncology reports* **2018,** *39* (2), 860-870.

200. Seo, M.; Nam, H. J.; Kim, S. Y.; Juhnn, Y. S., Inhibitory heterotrimeric GTP-binding proteins inhibit hydrogen peroxide-induced apoptosis by up-regulation of Bcl-2 via NF-kappaB in H1299 human lung cancer cells. *Biochem Biophys Res Commun* **2009,** *381* (2), 153-8.

201. Korotkov, S. M.; Konovalova, S. A.; Brailovskaya, I. V., Diamide accelerates opening of the Tl(+)-induced permeability transition pore in Ca(2+)-loaded rat liver mitochondria. *Biochem Biophys Res Commun* **2015,** *468* (1-2), 360-4.

202. Kosower, N. S.; Kosower, E. M.; Wertheim, B.; Correa, W. S., Diamide, a new reagent for the intracellular oxidation of glutathione to the disulfide. *Biochemical and Biophysical Research Communications* **1969,** *37* (4), 593-596.

203. Xiao, H.; Wang, J.; Yan, W.; Cui, Y.; Chen, Z.; Gao, X.; Wen, X.; Chen, J., GLUT1 regulates cell glycolysis and proliferation in prostate cancer. *The Prostate* **2018,** *78* (2), 86-94.

204. Dai, J.; Zhou, J.; Liu, H.; Huang, K., Selenite and ebselen supplementation attenuates D-galactose-induced oxidative stress and increases expression of SELR and SEP15 in rat lens. *Journal of biological inorganic chemistry : JBIC : a publication of the Society of Biological Inorganic Chemistry* **2016,** *21* (8), 1037-1046.

205. Xu, Y.; Li, Y.; Ma, L.; Xin, G.; Wei, Z.; Zeng, Z.; Xing, Z.; Li, S.; Niu, H.; Huang, W., d-Galactose induces premature senescence of lens epithelial cells by disturbing autophagy flux and mitochondrial functions. *Toxicology letters* **2018**.

206. Singh, D.; Banerji, A. K.; Dwarakanath, B. S.; Tripathi, R. P.; Gupta, J. P.; Mathew, T. L.; Ravindranath, T.; Jain, V., Optimizing cancer radiotherapy with 2-deoxy-d-glucose dose escalation studies in patients with glioblastoma multiforme. *Strahlentherapie und Onkologie : Organ der Deutschen Rontgengesellschaft ... [et al]* **2005,** *181* (8), 507-14.

207. Dwarakanath, B. S.; Singh, D.; Banerji, A. K.; Sarin, R.; Venkataramana, N. K.; Jalali, R.; Vishwanath, P. N.; Mohanti, B. K.; Tripathi, R. P.; Kalia, V. K.; Jain, V., Clinical studies for improving radiotherapy with 2-deoxy-D-glucose: present status and future prospects. *Journal of cancer research and therapeutics* **2009,** *5 Suppl 1*, S21-6.

208. Mohanti, B. K.; Rath, G. K.; Anantha, N.; Kannan, V.; Das, B. S.; Chandramouli, B. A.; Banerjee, A. K.; Das, S.; Jena, A.; Ravichandran, R.; Sahi, U. P.; Kumar, R.; Kapoor, N.; Kalia, V. K.; Dwarakanath, B. S.; Jain, V., Improving cancer radiotherapy with 2-deoxy-D-glucose: phase I/II clinical trials on human cerebral gliomas. *International journal of radiation oncology, biology, physics* **1996,** *35* (1), 103-11.

209. Raez, L. E.; Papadopoulos, K.; Ricart, A. D.; Chiorean, E. G.; Dipaola, R. S.; Stein, M. N.; Rocha Lima, C. M.; Schlesselman, J. J.; Tolba, K.; Langmuir, V. K.; Kroll, S.; Jung, D. T.; Kurtoglu, M.; Rosenblatt, J.; Lampidis, T. J., A phase I dose-escalation trial of 2-deoxy-D-glucose alone or combined with docetaxel in patients with advanced solid tumors. *Cancer chemotherapy and pharmacology* **2013,** *71* (2), 523-30.

210. Mohanti, B. K.; Rath, G. K.; Anantha, N.; Kannan, V.; Das, B. S.; Chandramouli, B. A. R.; Banerjee, A. K.; Das, S.; Jena, A.; Ravichandran, R.; Sahi, U. P.; Kumar, R.; Kapoor, N.; Kalia, V. K.; Dwarakanath, B. S.; Jain, V., Improving cancer radiotherapy with 2-deoxy-d-glucose: phase I/II clinical trials on human cerebral gliomas. *International Journal of Radiation Oncology*Biology*Physics* **1996,** *35* (1), 103-111.

211. Purchase, I. F.; Kalinowski, A. E.; Ishmael, J.; Wilson, J.; Gore, C. W.; Chart, I. S., Lifetime carcinogenicity study of 1- and 2-naphthylamine in dogs. *British Journal of Cancer* **1981,** *44* (6), 892-901.

212. Chua, J. S.; Kuberan, B., Synthetic Xylosides: Probing the Glycosaminoglycan Biosynthetic Machinery for Biomedical Applications. *Accounts of Chemical Research* **2017,** *50* (11), 2693-2705.

213. Yoon, J. W.; Lee, J. S.; Kim, B. M.; Ahn, J.; Yang, K. M., Catechin-7-O-xyloside induces apoptosis via endoplasmic reticulum stress and mitochondrial dysfunction in human non-small cell lung carcinoma H1299 cells. *Oncology reports* **2014,** *31* (1), 314-20.

214. Mani, K.; Belting, M.; Ellervik, U.; Falk, N.; Svensson, G.; Sandgren, S.; Cheng, F.; Fransson, L. A., Tumor attenuation by 2(6-hydroxynaphthyl)-beta-D-xylopyranoside requires priming of heparan sulfate and nuclear targeting of the products. *Glycobiology* **2004,** *14* (5), 387-97.

215. Crowley, L. C.; Marfell, B. J.; Christensen, M. E.; Waterhouse, N. J., Measuring Cell Death by Trypan Blue Uptake and Light Microscopy. *Cold Spring Harbor protocols* **2016,** *2016* (7), pdb.prot087155.

216. Voigt, W., Sulforhodamine B assay and chemosensitivity. *Methods in molecular medicine* **2005,** *110*, 39-48.

217. Krajka-Kuzniak, V.; Paluszczak, J.; Baer-Dubowska, W., The Nrf2-ARE signaling pathway: An update on its regulation and possible role in cancer prevention and treatment. *Pharmacological reports : PR* **2017,** *69* (3), 393-402.

218. Nomura, K.; Lee, M.; Banks, C.; Lee, G.; Morris, B. J., An ASK1-p38 signalling pathway mediates hydrogen peroxide-induced toxicity in NG108-15 neuronal cells. *Neuroscience letters* **2013,** *549*, 163-7.

219. Beyfuss, K.; Hood, D. A., A systematic review of p53 regulation of oxidative stress in skeletal muscle. *Redox report : communications in free radical research* **2018,** *23* (1), 100-117.

220. Tan, E. P.; McGreal, S. R.; Graw, S.; Tessman, R.; Koppel, S. J.; Dhakal, P.; Zhang, Z.; Machacek, M.; Zachara, N. E.; Koestler, D. C.; Peterson, K. R.; Thyfault, J. P.; Swerdlow, R. H.; Krishnamurthy, P.; DiTacchio, L.; Apte, U.; Slawson, C., Sustained O-GlcNAcylation reprograms

mitochondrial function to regulate energy metabolism. *The Journal of Biological Chemistry* **2017,** *292* (36), 14940-14962.

221. Holst, S.; Belo, A. I.; Giovannetti, E.; van Die, I.; Wuhrer, M., Profiling of different pancreatic cancer cells used as models for metastatic behaviour shows large variation in their N-glycosylation. *Scientific Reports* **2017,** *7* (1), 16623.

222. Dong, X.; Luo, Z.; Wang, Y.; Meng, L.; Duan, Q.; Qiu, L.; Peng, F.; Shen, L., Altered O-glycosylation is associated with inherent radioresistance and malignancy of human laryngeal carcinoma. *Experimental cell research* **2018,** *362* (2), 302-310.

223. Lee, S.; Lim, M. J.; Kim, M. H.; Yu, C. H.; Yun, Y. S.; Ahn, J.; Song, J. Y., An effective strategy for increasing the radiosensitivity of Human lung Cancer cells by blocking Nrf2-dependent antioxidant responses. *Free radical biology & medicine* **2012,** *53* (4), 807-16.

224. Yun, H. S.; Baek, J. H.; Yim, J. H.; Lee, S. J.; Lee, C. W.; Song, J. Y.; Um, H. D.; Park, J. K.; Park, I. C.; Hwang, S. G., Knockdown of hepatoma-derived growth factor-related protein-3 induces apoptosis of H1299 cells via ROS-dependent and p53-independent NF-kappaB activation. *Biochem Biophys Res Commun* **2014,** *449* (4), 471-6.

225. Sun, X.; Wang, Q.; Wang, Y.; Du, L.; Xu, C.; Liu, Q., Brusatol Enhances the Radiosensitivity of A549 Cells by Promoting ROS Production and Enhancing DNA Damage. *International journal of molecular sciences* **2016,** *17* (7).

226. Pool-Zobel, B.; Veeriah, S.; Bohmer, F. D., Modulation of xenobiotic metabolising enzymes by anticarcinogens -- focus on glutathione S-transferases and their role as targets of dietary chemoprevention in colorectal carcinogenesis. *Mutation research* **2005,** *591* (1-2), 74-92.

227. Langer, S.; Singer, C. F.; Hudelist, G.; Dampier, B.; Kaserer, K.; Vinatzer, U.; Pehamberger, H.; Zielinski, C.; Kubista, E.; Schreibner, M., Jun and Fos family protein expression

in human breast cancer: correlation of protein expression and clinicopathological parameters. *European journal of gynaecological oncology* **2006,** *27* (4), 345-52.

228. Satoh, T.; McKercher, S. R.; Lipton, S. A., Nrf2/ARE-mediated antioxidant actions of pro-electrophilic drugs. *Free radical biology & medicine* **2013,** *65*, 645-57.

229. Tong, Y. H.; Zhang, B.; Yan, Y. Y.; Fan, Y.; Yu, J. W.; Kong, S. S.; Zhang, D.; Fang, L.; Su, D.; Lin, N. M., Dual-negative expression of Nrf2 and NQO1 predicts superior outcomes in patients with non-small cell lung cancer. *Oncotarget* **2017,** *8* (28), 45750-45758.

230. King, C. D.; Rios, G. R.; Green, M. D.; Tephly, T. R., UDP-glucuronosyltransferases. *Current drug metabolism* **2000,** *1* (2), 143-61.

231. Sayin, V. I.; LeBoeuf, S. E.; Singh, S. X.; Davidson, S. M.; Biancur, D.; Guzelhan, B. S.; Alvarez, S. W.; Wu, W. L.; Karakousi, T. R.; Zavitsanou, A. M.; Ubriaco, J.; Muir, A.; Karagiannis, D.; Morris, P. J.; Thomas, C. J.; Possemato, R.; Vander Heiden, M. G.; Papagiannakopoulos, T., Activation of the NRF2 antioxidant program generates an imbalance in central carbon metabolism in cancer. *eLife* **2017,** *6*.

232. Xu, I. M.; Lai, R. K.; Lin, S. H.; Tse, A. P.; Chiu, D. K.; Koh, H. Y.; Law, C. T.; Wong, C. M.; Cai, Z.; Wong, C. C.; Ng, I. O., Transketolase counteracts oxidative stress to drive cancer development. *Proceedings of the National Academy of Sciences of the United States of America* **2016,** *113* (6), E725-34.

233. Ichimura, Y.; Waguri, S.; Sou, Y.-s.; Kageyama, S.; Hasegawa, J.; Ishimura, R.; Saito, T.; Yang, Y.; Kouno, T.; Fukutomi, T.; Hoshii, T.; Hirao, A.; Takagi, K.; Mizushima, T.; Motohashi, H.; Lee, M.-S.; Yoshimori, T.; Tanaka, K.; Yamamoto, M.; Komatsu, M., Phosphorylation of p62 Activates the Keap1-Nrf2 Pathway during Selective Autophagy. *Molecular cell 51* (5), 618-631.

234. Bolton, J. L.; Dunlap, T., Formation and Biological Targets of Quinones: Cytotoxic versus Cytoprotective Effects. *Chemical research in toxicology* **2017,** *30* (1), 13-37.

235. Nadeau, P. J.; Charette, S. J.; Landry, J., REDOX reaction at ASK1-Cys250 is essential for activation of JNK and induction of apoptosis. *Molecular biology of the cell* **2009,** *20* (16), 3628-37.

236. Olivier, S.; Foretz, M.; Viollet, B., Promise and challenges for direct small molecule AMPK activators. *Biochemical pharmacology* **2018**.

237. Lin, S.-C.; Hardie, D. G., AMPK: Sensing Glucose as well as Cellular Energy Status. *Cell metabolism* **2018,** *27* (2), 299-313.

238. Rabinovitch, R. C.; Samborska, B.; Faubert, B.; Ma, E. H.; Gravel, S.-P.; Andrzejewski, S.; Raissi, T. C.; Pause, A.; St.-Pierre, J.; Jones, R. G., AMPK Maintains Cellular Metabolic Homeostasis through Regulation of Mitochondrial Reactive Oxygen Species. *Cell reports 21* (1), 1-9.

239. Corazzari, M.; Gagliardi, M.; Fimia, G. M.; Piacentini, M., Endoplasmic Reticulum Stress, Unfolded Protein Response, and Cancer Cell Fate. *Frontiers in Oncology* **2017,** *7*.

240. Kranz, P.; Neumann, F.; Wolf, A.; Classen, F.; Pompsch, M.; Ocklenburg, T.; Baumann, J.; Janke, K.; Baumann, M.; Goepelt, K.; Riffkin, H.; Metzen, E.; Brockmeier, U., PDI is an essential redox-sensitive activator of PERK during the unfolded protein response (UPR). *Cell death & disease* **2017,** *8* (8), e2986.

241. Kanemura, S.; Okumura, M.; Yutani, K.; Ramming, T.; Hikima, T.; Appenzeller-Herzog, C.; Akiyama, S.; Inaba, K., Human ER Oxidoreductin-1alpha (Ero1alpha) Undergoes Dual Regulation through Complementary Redox Interactions with Protein-Disulfide Isomerase. *The Journal of Biological Chemistry* **2016,** *291* (46), 23952-23964.

242. Kamil, M.; Haque, E.; Irfan, S.; Sheikh, S.; Hasan, A.; Nazir, A.; Lohani, M.; Mir, S. S., ER chaperone GRP78 regulates autophagy by modulation of p53 localization. *Frontiers in bioscience (Elite edition)* **2017,** *9*, 54-66.

243. Wang, J.; Sevier, C. S., Formation and Reversibility of BiP Protein Cysteine Oxidation Facilitate Cell Survival during and post Oxidative Stress. *The Journal of Biological Chemistry* **2016,** *291* (14), 7541-57.

244. Peanne, R.; Vanbeselaere, J.; Vicogne, D.; Mir, A. M.; Biot, C.; Matthijs, G.; Guerardel, Y.; Foulquier, F., Assessing ER and Golgi N-glycosylation process using metabolic labeling in mammalian cultured cells. *Methods in cell biology* **2013,** *118*, 157-76.

245. Wang, Y.; Zhu, J.; Zhang, L., Discovery of Cell-Permeable O-GlcNAc Transferase Inhibitors via Tethering in Situ Click Chemistry. *Journal of medicinal chemistry* **2017,** *60* (1), 263-272.

246. Hahne, H.; Sobotzki, N.; Nyberg, T.; Helm, D.; Borodkin, V. S.; van Aalten, D. M.; Agnew, B.; Kuster, B., Proteome wide purification and identification of O-GlcNAc-modified proteins using click chemistry and mass spectrometry. *Journal of proteome research* **2013,** *12* (2), 927-36.

247. Thompson, J. W.; Griffin, M. E.; Hsieh-Wilson, L. C., Methods for the Detection, Study, and Dynamic Profiling of O-GlcNAc Glycosylation. *Methods in enzymology* **2018,** *598*, 101-135.

248. Vocadlo, D. J.; Hang, H. C.; Kim, E.-J.; Hanover, J. A.; Bertozzi, C. R., A chemical approach for identifying O-GlcNAc-modified proteins in cells. *Proceedings of the National Academy of Sciences* **2003,** *100* (16), 9116-9121.

249. Ortiz-Meoz, R. F.; Jiang, J.; Lazarus, M. B.; Orman, M.; Janetzko, J.; Fan, C.; Duveau, D. Y.; Tan, Z. W.; Thomas, C. J.; Walker, S., A small molecule that inhibits OGT activity in cells. *ACS chemical biology* **2015,** *10* (6), 1392-7.

250. Shen, D. L.; Gloster, T. M.; Yuzwa, S. A.; Vocadlo, D. J., Insights into O-linked N-acetylglucosamine ([0-9]O-GlcNAc) processing and dynamics through kinetic analysis of O-GlcNAc transferase and O-GlcNAcase activity on protein substrates. *The Journal of Biological Chemistry* **2012,** *287* (19), 15395-408.

251. Liu, X.; Li, L.; Wang, Y.; Yan, H.; Ma, X.; Wang, P. G.; Zhang, L., A peptide panel investigation reveals the acceptor specificity of O-GlcNAc transferase. *FASEB journal : official publication of the Federation of American Societies for Experimental Biology* **2014,** *28* (8), 3362-72.

252. Overath, T.; Kuckelkorn, U.; Henklein, P.; Strehl, B.; Bonar, D.; Kloss, A.; Siele, D.; Kloetzel, P. M.; Janek, K., Mapping of O-GlcNAc sites of 20 S proteasome subunits and Hsp90 by a novel biotin-cystamine tag. *Molecular & cellular proteomics : MCP* **2012,** *11* (8), 467-77.

253. Haltiwanger, R. S.; Holt, G. D.; Hart, G. W., Enzymatic addition of O-GlcNAc to nuclear and cytoplasmic proteins. Identification of a uridine diphospho-N-acetylglucosamine:peptide beta-N-acetylglucosaminyltransferase. *The Journal of Biological Chemistry* **1990,** *265* (5), 2563-8.

254. Li, B.; Kohler, J. J., Glycosylation of the Nuclear Pore. *Traffic* **2014,** *15* (4), 347-361.

255. Ma, X.; Liu, P.; Yan, H.; Sun, H.; Liu, X.; Zhou, F.; Li, L.; Chen, Y.; Muthana, M. M.; Chen, X.; Wang, P. G.; Zhang, L., Substrate specificity provides insights into the sugar donor recognition mechanism of O-GlcNAc transferase (OGT). *PLoS ONE* **2013,** *8* (5), e63452.

256. Okuda, T., Western blot data using two distinct anti-O-GlcNAc monoclonal antibodies showing unique glycosylation status on cellular proteins under 2-deoxy-d-glucose treatment. *Data in brief* **2017,** *10*, 449-453.

257. Jaradat, D. M. M., Thirteen decades of peptide synthesis: key developments in solid phase peptide synthesis and amide bond formation utilized in peptide ligation. *Amino acids* **2018,** *50* (1), 39-68.

258. Zhang, B.; Zhou, P.; Li, X.; Shi, Q.; Li, D.; Ju, X., Bitterness in sugar: O-GlcNAcylation aggravates pre-B acute lymphocytic leukemia through glycolysis via the PI3K/Akt/c-Myc pathway. *American journal of cancer research* **2017,** *7* (6), 1337-1349.

259. Chen, P.-H.; Smith, T. J.; Wu, J.; Siesser, P. F.; Bisnett, B. J.; Khan, F.; Hogue, M.; Soderblom, E.; Tang, F.; Marks, J. R.; Major, M. B.; Swarts, B. M.; Boyce, M.; Chi, J.-T., Glycosylation of KEAP1 links nutrient sensing to redox stress signaling. *The EMBO Journal* **2017,** *36* (15), 2233-2250.

260. He, G.; Troberg, J.; Lv, X.; Xia, Y. L.; Zhu, L. L.; Ning, J.; Ge, G. B.; Finel, M.; Yang, L., Identification and characterization of human UDP-glucuronosyltransferases responsible for xanthotoxol glucuronidation. *Xenobiotica; the fate of foreign compounds in biological systems* **2018,** *48* (2), 109-116.

261. Yang, N.; Sun, R.; Liao, X.; Aa, J.; Wang, G., UDP-glucuronosyltransferases (UGTs) and their related metabolic cross-talk with internal homeostasis: A systematic review of UGT isoforms for precision medicine. *Pharmacological research* **2017,** *121*, 169-183.

262. Liu, K.; Jin, B.; Wu, C.; Yang, J.; Zhan, X.; Wang, L.; Shen, X.; Chen, J.; Chen, H.; Mao, Z., NQO1 Stabilizes p53 in Response to Oncogene-Induced Senescence. *International journal of biological sciences* **2015,** *11* (7), 762-71.

263. Bey, E. A.; Bentle, M. S.; Reinicke, K. E.; Dong, Y.; Yang, C. R.; Girard, L.; Minna, J. D.; Bornmann, W. G.; Gao, J.; Boothman, D. A., An NQO1- and PARP-1-mediated cell death pathway induced in non-small-cell lung cancer cells by beta-lapachone. *Proceedings of the National Academy of Sciences of the United States of America* **2007,** *104* (28), 11832-7.

264. Donald, S. P.; Sun, X. Y.; Hu, C. A.; Yu, J.; Mei, J. M.; Valle, D.; Phang, J. M., Proline oxidase, encoded by p53-induced gene-6, catalyzes the generation of proline-dependent reactive oxygen species. *Cancer research* **2001,** *61* (5), 1810-5.

265. Liu, B.; Chen, Y.; St Clair, D. K., ROS and p53: a versatile partnership. *Free radical biology & medicine* **2008,** *44* (8), 1529-35.

266. He, G., AMP-Activated Protein Kinase Induces p53 by Phosphorylating MDMX and Inhibiting Its Activity. **2014,** *34* (2), 148-57.

267. Zmijewski, J. W.; Banerjee, S.; Bae, H.; Friggeri, A.; Lazarowski, E. R.; Abraham, E., Exposure to hydrogen peroxide induces oxidation and activation of AMP-activated protein kinase. *The Journal of Biological Chemistry* **2010,** *285* (43), 33154-64.

268. Chaube, B.; Malvi, P.; Singh, S. V.; Mohammad, N.; Viollet, B.; Bhat, M. K., AMPK maintains energy homeostasis and survival in cancer cells via regulating p38/PGC-1alpha-mediated mitochondrial biogenesis. *Cell death discovery* **2015,** *1*, 15063.

269. Shi, Y.; Tomic, J.; Wen, F.; Shaha, S.; Bahlo, A.; Harrison, R.; Dennis, J. W.; Williams, R.; Gross, B. J.; Walker, S.; Zuccolo, J.; Deans, J. P.; Hart, G. W.; Spaner, D. E., Aberrant O-GlcNAcylation characterizes chronic lymphocytic leukemia. *Leukemia* **2010,** *24* (9), 1588-1598.

270. Villanueva-Paz, M.; Cotan, D.; Garrido-Maraver, J.; Oropesa-Avila, M.; de la Mata, M.; Delgado-Pavon, A.; de Lavera, I.; Alcocer-Gomez, E.; Alvarez-Cordoba, M.; Sanchez-Alcazar, J.

A., AMPK Regulation of Cell Growth, Apoptosis, Autophagy, and Bioenergetics. *Exs* **2016,** *107*, 45-71.

271. Chaveroux, C.; Sarcinelli, C.; Barbet, V.; Belfeki, S.; Barthelaix, A.; Ferraro-Peyret, C.; Lebecque, S.; Renno, T.; Bruhat, A.; Fafournoux, P.; Manie, S. N., Nutrient shortage triggers the hexosamine biosynthetic pathway via the GCN2-ATF4 signalling pathway. *Scientific Reports* **2016,** *6*, 27278.

272. Wang, Y.; Liu, J.; Jin, X.; Zhang, D.; Li, D.; Hao, F.; Feng, Y.; Gu, S.; Meng, F.; Tian, M.; Zheng, Y.; Xin, L.; Zhang, X.; Han, X.; Aravind, L.; Wei, M., O-GlcNAcylation destabilizes the active tetrameric PKM2 to promote the Warburg effect. *Proceedings of the National Academy of Sciences of the United States of America* **2017,** *114* (52), 13732-13737.

273. Yi, W.; Clark, P. M.; Mason, D. E.; Keenan, M. C.; Hill, C.; Goddard, W. A.; Peters, E. C.; Driggers, E. M.; Hsieh-Wilson, L. C., PFK1 Glycosylation Is a Key Regulator of Cancer Cell Growth and Central Metabolic Pathways. *Science (New York, N.Y.)* **2012,** *337* (6097), 975-980.

274. Bacigalupa, Z. A.; Bhadiadra, C. H.; Reginato, M. J., O-GlcNAcylation: key regulator of glycolytic pathways. *Journal of bioenergetics and biomembranes* **2018**.

275. Lazarus, M. B.; Nam, Y.; Jiang, J.; Sliz, P.; Walker, S., Structure of human O-GlcNAc transferase and its complex with a peptide substrate. *Nature* **2011,** *469*, 564.

276. Lea, M. A.; Qureshi, M. S.; Buxhoeveden, M.; Gengel, N.; Kleinschmit, J.; desBordes, C., Regulation of the Proliferation of Colon Cancer Cells by Compounds that Affect Glycolysis, Including 3-Bromopyruvate, 2-Deoxyglucose and Biguanides. *Anticancer research* **2013,** *33* (2), 401-7.

277. Nath, K.; Guo, L.; Nancolas, B.; Nelson, D. S.; Shestov, A. A.; Lee, S. C.; Roman, J.; Zhou, R.; Leeper, D. B.; Halestrap, A. P.; Blair, I. A.; Glickson, J. D., Mechanism of Antineoplastic Activity of Lonidamine. *Biochimica et Biophysica Acta* **2016,** *1866* (2), 151-62.

278. Sinthupibulyakit, C.; Ittarat, W.; St. Clair, W. H.; St. Clair, D. K., p53 protects lung cancer cells against metabolic stress. *International journal of oncology* **2010,** *37* (6), 1575-81.

279. Wang, J.; Pareja, K. A.; Kaiser, C. A.; Sevier, C. S., Redox signaling via the molecular chaperone BiP protects cells against endoplasmic reticulum-derived oxidative stress. *eLife* **2014,** *3*, e03496.

280. Hetz, C.; Papa, F. R., The Unfolded Protein Response and Cell Fate Control. *Molecular cell* **2018,** *69* (2), 169-181.

281. Yu, L.; Li, K.; Zhang, X., Next-generation metabolomics in lung cancer diagnosis, treatment and precision medicine: mini review. *Oncotarget* **2017,** *8* (70), 115774-115786.

282. Weckmann, K.; Diefenthaler, P.; Baeken, M. W.; Yusifli, K.; Turck, C. W.; Asara, J. M.; Behl, C.; Hajieva, P., Metabolomics profiling reveals differential adaptation of major energy metabolism pathways associated with autophagy upon oxygen and glucose reduction. *Scientific Reports* **2018,** *8* (1), 2337.

283. Lorenz, M. A.; Burant, C. F.; Kennedy, R. T., Reducing Time and Increasing Sensitivity in Sample Preparation for Adherent Mammalian Cell Metabolomics. *Analytical chemistry* **2011,** *83* (9), 3406-3414.

284. Masson, P.; Alves, A. C.; Ebbels, T. M. D.; Nicholson, J. K.; Want, E. J., Optimization and Evaluation of Metabolite Extraction Protocols for Untargeted Metabolic Profiling of Liver Samples by UPLC-MS. *Analytical chemistry* **2010,** *82* (18), 7779-7786.

285. Canelas, A. B.; ten Pierick, A.; Ras, C.; Seifar, R. M.; van Dam, J. C.; van Gulik, W. M.; Heijnen, J. J., Quantitative Evaluation of Intracellular Metabolite Extraction Techniques for Yeast Metabolomics. *Analytical chemistry* **2009,** *81* (17), 7379-7389.

286. Sreedhar, A.; Zhao, Y., Dysregulated metabolic enzymes and metabolic reprogramming in cancer cells. *Biomedical reports* **2018,** *8* (1), 3-10.

287. Zhang, T.; Gillies, M. C.; Madigan, M. C.; Shen, W.; Du, J.; Grunert, U.; Zhou, F.; Yam, M.; Zhu, L., Disruption of De Novo Serine Synthesis in Muller Cells Induced Mitochondrial Dysfunction and Aggravated Oxidative Damage. *Molecular neurobiology* **2018**.

288. Vucetic, M.; Cormerais, Y.; Parks, S. K.; Pouyssegur, J., The Central Role of Amino Acids in Cancer Redox Homeostasis: Vulnerability Points of the Cancer Redox Code. *Frontiers in Oncology* **2017,** *7*, 319.

289. Bender, D. A., The Aromatic Amino Acids: Phenylalanine, Tyrosine and Tryptophan. In *Amino Acid Metabolism*, John Wiley & Sons, Ltd: 2012; pp 323-376.

290. Bender, D. A., Amino Acids Synthesized from Glutamate: Glutamine, Proline, Ornithine, Citrulline and Arginine. In *Amino Acid Metabolism*, John Wiley & Sons, Ltd: 2012; pp 157-223.

291. Kang, J. G.; Park, S. Y.; Ji, S.; Jang, I.; Park, S.; Kim, H. S.; Kim, S. M.; Yook, J. I.; Park, Y. I.; Roth, J.; Cho, J. W., O-GlcNAc protein modification in cancer cells increases in response to glucose deprivation through glycogen degradation. *The Journal of Biological Chemistry* **2009,** *284* (50), 34777-84.

292. Sodi, V. L.; Bacigalupa, Z. A.; Ferrer, C. M.; Lee, J. V.; Gocal, W. A.; Mukhopadhyay, D.; Wellen, K. E.; Ivan, M.; Reginato, M. J., Nutrient sensor O-GlcNAc transferase controls cancer lipid metabolism via SREBP-1 regulation. *Oncogene* **2018,** *37* (7), 924-934.

293. Groves, J. A.; Maduka, A. O.; O'Meally, R. N.; Cole, R. N.; Zachara, N. E., Fatty acid synthase inhibits the O-GlcNAcase during oxidative stress. *The Journal of Biological Chemistry* **2017,** *292* (16), 6493-6511.

294. Hong, S. Y.; Hagen, T., 2-Deoxyglucose induces the expression of thioredoxin interacting protein (TXNIP) by increasing O-GlcNAcylation - Implications for targeting the Warburg effect in cancer cells. *Biochem Biophys Res Commun* **2015,** *465* (4), 838-44.

295. Kang, H. T.; Hwang, E. S., 2-Deoxyglucose: An anticancer and antiviral therapeutic, but not any more a low glucose mimetic. *Life Sciences* **2006,** *78* (12), 1392-1399.

296. Dwarkanath, B. S.; Zolzer, F.; Chandana, S.; Bauch, T.; Adhikari, J. S.; Muller, W. U.; Streffer, C.; Jain, V., Heterogeneity in 2-deoxy-D-glucose–induced modifications in energetics and radiation responses of human tumor cell lines. *International Journal of Radiation Oncology*Biology*Physics* **2001,** *50* (4), 1051-1061.

297. Oikari, S.; Kettunen, T.; Tiainen, S.; Hayrinen, J.; Masarwah, A.; Sudah, M.; Sutela, A.; Vanninen, R.; Tammi, M.; Auvinen, P., UDP-sugar accumulation drives hyaluronan synthesis in breast cancer. *Matrix biology : journal of the International Society for Matrix Biology* **2018**.

298. Grant, D. J.; Chen, Z.; Howard, L. E.; Wiggins, E.; De Hoedt, A.; Vidal, A. C.; Carney, S. T.; Squires, J.; Magyar, C. E.; Huang, J.; Freedland, S. J., UDP-glucuronosyltransferases and biochemical recurrence in prostate cancer progression. *BMC Cancer* **2017,** *17* (1), 463.

299. Zheng, F. J.; Ye, H. B.; Wu, M. S.; Lian, Y. F.; Qian, C. N.; Zeng, Y. X., Repressing malic enzyme 1 redirects glucose metabolism, unbalances the redox state, and attenuates migratory and invasive abilities in nasopharyngeal carcinoma cell lines. *Chinese journal of cancer* **2012,** *31* (11), 519-31.

300. Shafran, Y.; Zurgil, N.; Ravid-Hermesh, O.; Sobolev, M.; Afrimzon, E.; Hakuk, Y.; Shainberg, A.; Deutsch, M., Nitric oxide is cytoprotective to breast cancer spheroids vulnerable to estrogen-induced apoptosis. *Oncotarget* **2017,** *8* (65), 108890-108911.

ABSTRACT

CARBOHYDRATE-BASED INDUCERS OF CELLULAR STRESS FOR TARGETING CANCER CELL METABOLISM

by

FIDELIS TOLOYI NDOMBERA

May 2018

Advisor: Dr. Young-Hoon Ahn

Major: Chemistry (Biochemistry)

Degree: Doctor of Philosophy

Metabolic reprogramming and redox control of cancer cells is vital for their proliferation, but also provides selective strategies for treating cancer. Increased generation of reactive oxygen species (ROS) and an intricate control of redox status in cancer cells relative to normal cells provide a basis for designing ROS-inducing anticancer agents. In my work, I designed, synthesized and evaluated carbohydrate-based small molecules for ROS-generation, cytotoxicity and redox signaling and stress response. Our data from assays, including cell viability assays, enzyme inhibition studies, Western blot studies, click chemistry, and metabolomics, reveal that our compound (K8A) is more potent than 2-DG, a well-known carbohydrate-derived inhibitor of glycolysis. We reported discovery of carbohydrate-based small molecules with the property of blocking altered metabolic activity and enhancing ROS with potential therapeutic benefits for targeting cancer cells. Importantly, we investigated the mechanism of action of our potent compound that involve disruption of protein glycosylation in cancer with downstream effects on cancer metabolism.

AUTOBIOGRAPHICAL STATEMENT

FIDELIS TOLOYI NDOMBERA

EDUCATION

PhD., Chemistry (Biochemistry Major).
Department of Chemistry, Wayne State University, Detroit, Michigan, USA
Advisor: Prof. Young-Hoon Ahn
Master of Education Administration (Course work), Maseno University, Kenya
P.G.D.E, Kenyatta University, Nairobi, Kenya
Bachelor of Science (Biochemistry), Department of Biochemistry, Kenyatta University, Nairobi, Kenya.

AWARDS & FELLOWSHIPS

1. Travel grant: 33rd Annual Chemistry Graduate Symposium, State University of New York at Buffalo, 2015.
2. Wayne State University/Chemistry Department Travel grant, 2016.
3. Advancing Science Career Travel Award, NOBCChE 2016.
4. Lodging Award, NExM Conference, NOBCChE 2017.
5. GRC Carl Storm Underrepresented Minority Fellowship, 2017.
6. Advancing Science Career Travel Award, NOBCChE 2017.
7. Midwest Graduate Symposium, 2017
8. Graduate Student Research Day, Wayne State University School of Medicine, Honors Mention Award, 2017.
9. Graduate Employees Organization Committee 2017 Travel Award.
10. NOBCChE National Conference 2017, 3-Minute Thesis Award.

PUBLICATIONS

1. **Fidelis T. Ndombera**, Garret Van-Hecke, Nagi, Shima and Ahn, Young-Hoon. Carbohydrate-based inducers of cellular stress for targeting cancer cells. ***Biorg. Med. Chem. Lett***. **26**, 1452 (**2016**).
2. Kusal T. G. Samarasinghe, Dhanushka N. P. Munkanatta Godage, Yani Zhou, **Fidelis T. Ndombera**, Eranthie Weerapana, Young-Hoon Ahn. Clickable Glutathione Approach for Identification of Protein Glutathionylation in Response to Glucose Metabolism. ***Mol. BioSyst.***, 2016,**12**, 2471-2480 (**2016**).
3. **Fidelis T. Ndombera** and Young-Hoon Ahn. N-aryl xyloside inhibits N-glycosylation and altered metabolism in cancer cells. (**2018**) Manuscript